School of Pharmacy

DEVELOPMENT AND EVALUATION OF AN INTRANASAL NANOPARTICULATE FORMULATION FOR ENHANCED TRANSPORT OF RIVASTIGMINE INTO THE BRAIN

Bhawna Gauri

This thesis is presented for the Degree of
Doctor of Philosophy
of
Curtin University

May 2017

Declaration

To the best of my knowledge and belief this thesis contains no material previously published by any other person except where due acknowledgment has been made. This thesis contains no material which has been accepted for the award of any other degree or diploma in any university.

The research presented and reported in this thesis was conducted in compliance with the National Health and Medical Research Council Australian code for the care and use of animals for scientific purposes 8th edition (2013). The proposed research study received animal ethics approval from the Curtin University Animal Ethics Committee, Approval Number AEC_2015_37.

Signature....Bhawna.....

Date.....16-05-2017.....

Acknowledgment

First and foremost, I would like to express my sincere gratitude to my supervisor, **Dr. Yan Chen** for giving her invaluable and wholehearted continuous support during the accomplishment of my Ph.D. I am very grateful for all her brilliant intellectual ideas, patience, dedication for work, motivation and motherly attitude towards me. I am very grateful to her for being a tremendous mentor and for providing me her research funding that allowed me to complete my Ph.D.

I would also like to express my profound gratitude to **Associate Professor Heather AE Benson,** co-supervisor, for guiding me during various stages of my research. It became easy to cross tough hurdles with her brilliant suggestions, recommendations, and continuous support. Her insightful guidance and comments helped me to shape my research project within the given time frame.

I would also like to thank my associate supervisor, **Dr. Anton Dolzhenko** for providing me his valuable intellectual research expertise while synthesizing different chemical molecules during my Ph.D. His vast in-depth knowledge allowed me to gain experience in synthesis and an edge in analytical techniques. I also appreciate his patient support while going through my thesis, despite being off-shore.

I would like to thank Curtin University for providing me with Curtin International Postgraduate Research Scholarship (CIPRS) which gives me an opportunity to do the Ph.D. in a field of my choice and allow me to grow as a researcher. My sincere thanks to Curtin Health Innovation Research Institute for allowing me to use their Lab facilities for my research. I would like to thank Ching Goh and Department of Chemistry for assisting me to use the NMR facilities in Department of Chemistry and associated research centers for my research. My sincere acknowledgment to Elaine Miller and John deLaeter Centre, Facility of Science and Engineering for providing the technical assistance into using FE-SEM microscopy facility. I would like to thank Dr. Beng Chua, Kodee King, Tara and Yanjing Ng for their timely support for conducting my animal studies, without their kind co-operation, my animal work would not have been successful. I will also express my

sincere thanks to all academic, technical and administrative staff of the School of Pharmacy, Curtin University.

My sincere and heartfelt appreciation and thanks to the senior lab technician, Giuseppe in the school of Pharmacy who helped me for setting up a chemical reaction, providing me assistance for analyzing NMR and HPLC data. My lab work would not have been possible without the timely help of Mr. Jorge Martinez, Ms. Angela Samec and Ms. Sonia for giving their invaluable time for training me on various instruments. I am thankful to Dr. Madu Pagesharp for providing me a few chemicals during my Ph.D. I would also like to thank Charmaine D'costa for timely processing of our chemical orders in an emergency. My sincere thanks to Ganga Senarathna, for helping me in the analysis of pharmacokinetic data. I'd like to thank Nazhasan Huda for providing me his chemical molecule for my research and for several discussions. I would like to thank all my lab colleagues and my friends Aparna and Adnan for giving their support.

Last, but not least a special thanks to my whole family and my husband for their continuous motivation, unbelievable support and effort to keep me up during my tough days. They are the most important people in my life and I dedicate my thesis to them.

BHAWNA GAURI

Table of Contents

List of Figures

List of Tables

List of Abbreviation

Symbol used	Full explanation
µg	microgram
Aβ peptide	Amyloid beta peptide
AUC	Area under the curve
AD	Alzheimer's disease
BBB	Blood-brain barrier
C-6	Coumarin-6
Conc.	Concentration
CNS	Central nervous System
CPP	Cell penetrating peptides
CSF	Cerebrospinal fluid
DMF	Dimethyl formamide
DMSO	Dimethyl sulphoxide
DTNB	5,5'-dithio-bis-2-nitrobenzoic acid (Ellman's Reagent)
EC	Endothelial cells
EDC	1-Ethyl-3-(3-dimethylamino) propyl carbodiimide
EE	Encapsulation efficiency
FT-IR	Fourier Transform-Infrared
GC	Glycol chitosan
GIT	Gastrointestinal tract
gm	Gram
h	Hour
HPLC	High-Performance Liquid Chromatography
IGF-1	Insulin-like Growth Factor-1
IN	Intranasal
IS	Internal standard

Symbol used	Full explanation
IV	Intravenous
$KMnO_4$	Potassium permanganate
KOH	Potassium hydroxide
LOD	Limit of Detection
LOQ	Limit of Quantification
mAU	milli Absorption units
M or mM	Molar or millimolar
min	minutes
mmol	millimole
mPEG	methoxy Polyethylene Glycol
mPEG-COOH	methoxy Polyethylene Glycol carboxylate polymer
mPEG-PLA	methoxy Polyethylene Glycol-Polylactic acid
NDs	Neurodegenerative disorders
NHS	N-Hydroxysucciniimide
nm	nanometre
NPs	Nanoparticles
PD	Parkinson's disease
PEG	Polyethylene glycol
PLGA	Poly-lactic-co-glycolic acid
PLA	Polylactic acid
RP-HPLC-FLD	Reverse phase- High-Performance Liquid Chromatography-Fluorescent Light Detector
RSD	relative standard deviation
RV	Rivastigmine
SA-ODA	Sialic acid-Octadecylamine
SD	Standard deviation
SLNs	Solid-lipid nanoliposomes

Symbol used	Full explanation
TAT peptide	Transcriptional Activator Peptide
TFA	Trifluoroacetic acid
THF	Tetrahydrofuran
TGC	Thiolated glycol chitosan
TPGS	d-α-tocopheryl polyethylene glycol 1000 succinate
UV-VIS	Ultraviolet-visible
US-FDA	United States Food and Drug Administration
VIP	Vasoactive Intestinal Peptide
WGA	Wheat germ agglutinin

Abstract

Neurodegenerative disorders (NDs) are causes for a growing concern among health professionals and health care agencies, especially for the lack of effective treatments for these devastating disorders. One of the most common forms of the NDs is Alzheimer's disease (AD) which involves extracellular deposition of Amyloid-β peptide and intracellular accumulation of neurofibrillary tangles of hyperphosphorylated tau protein, resulting in gradually decline in memory, cognitive functions and behaviour. Rivastigmine (RV) is a reversible acetylcholinesterase inhibitor drug which has been approved by FDA for treatment the cognitive problems of AD and Parkinson disease. It acts by reversibly inhibiting acetylcholinesterases in the brain thereby, retard the rate at which acetylcholine (ACh) is broken down. RV has a restricted entry into the brain due to its hydrophilic nature, therefore, requires increased dosing to promote drug penetration into the brain. Consequently, it results in the cholinergic adverse effects. It is a challenge to deliver a high enough concentration of drug across the blood-brain barrier (BBB) without causing side effects. Intranasal (IN) drug delivery provides advantages over the intravenous (IV) route for drug delivery into the brain as it can bypass the BBB. It allows the drug molecule to pass from nose to various brain compartments via the olfactory and trigeminal pathway, therefore, enhance brain uptake of the drug. Use of nanoparticles (NPs) especially biodegradable NPs in conjunction with IN route administration have demonstrated further benefits because of increased transport of drug via nano-carriers. Evidence showed that surface modification of NPs with targeting ligand(s) enhanced NPs transport from nose to the brain and close to the neuronal cells.

The objective of this thesis was to develop an effective nanoparticulate drug delivery system which can enhance the delivery of therapeutic molecules like RV into the brain through IN route. A biodegradable and biocompatible RV-loaded-polylactic-co-glycolic acid (PLGA) NPs functionalized with single ligand (sialic acid-octadecyl amine, SA-ODA) and dual ligands (SA-ODA and thiolated glycol chitosan, TGC) were developed. The developed NPs were loaded with RV and coumarin 6 (C-6), the latter a fluorescent

marker which can also represent the diagnostic agent or a hydrophobic drug for various purposes including tracking and easy detection.

The two different targeting ligands: TGC (targeting ligand-1) and SA-ODA (targeting ligand-2) was synthesized. The latter was by another member of the research group. TGC was selected as ligand-1 because of its ability to promote the interaction of NPs with nasal mucosa membrane. For the synthesis of TGC, Glycol chitosan (GC) was chemically modified using thioglycolic acid via a selective carbodiimide reaction in the presence of EDC and NHS. The presence of the thiol group on the surface of GC was determined by both FT-IR spectroscopy analysis and quantitative assay using Ellman's reagent. The thiol group content of 881.1 ± 21.3 µmol thiol groups/gm of synthesized polymer was detected. To achieve the prolonged residence time of NPs in the brain and enhance its interaction with neuron cells, Sialic acid (SA) was chosen as ligand-2. SA was incorporated as SA-ODA for its easy formulation of NPs. RV and C-6 loaded dual ligand PLGA NPs were prepared by double emulsion (w/o/w) solvent evaporation method using 0.3% d-α-tocopheryl polyethylene glycol 1000 succinate (TPGS) as a stabilizer and 0.2% TGC as a coating solution after investigating various formulation variables such as polymer molecular weight, stabilizer type and its concentration, method of preparation, and coating polymer concentration to produce the NPs with smallest possible particle size and highest possible drug loading.

The most suitable formulation conditions produced the mean particle size of single ligand PLGA-SA-ODA NPs and dual ligand PLGA-SA-ODA NPs coated with TGC being 168.4 ± 10.3 nm and 236.0 ± 9.8 nm respectively with low polydispersity index (PDI). The zeta potential of single ligand and dual ligand NPs was -32.4 ± 4.1 mV and +10.4 ± 3.3 mV respectively. The drug loading of developed single ligand and dual ligand NPs were 3.7 ± 0.7 % and 3.6 ± 0.1% of RV respectively and the entrapment efficiency is 23.1 ± 0.7 and 22.8 ± 0.7, analysed using a validated RP-HPLC method. The increase in the particle size and positive zeta potential of dual ligand modified NPs indicated the presence of cationic TGC polymer on the nanoparticle surface. In addition, the presence of thiol group on the surface of the NPs was confirmed by its reaction with Ellman's reagent (a thiol group specific agent), suggesting the successful attachment of TGC polymer on PLGA-SA-ODA

NPs. The number of thiol groups present on the surface of each NP was 533.67 ± 94.7 calculated using a formula reported in the literature. The stability study data revealed that single ligand NPs were stable for a period up to seven days whereas dual ligand NPs were stable only for 24 h. Therefore, dual ligands NPs should be freshly prepared and used within 24 h. The *in-vitro* release study of single ligand and dual ligand NPs showed a biphasic release pattern with an initial burst release of 13% RV in one hour followed by a relatively constant release of RV from NPs over 24 h.

The developed single ligand and dual ligand modified PLGA NPs were evaluated for their effectiveness in enhancing RV and C-6 transport into the brain using Sprague-Dawley rats by IN route at the dose of 1mg/kg of free RV base and 80 µg/kg of C-6. Both RV and C6 pharmacokinetic profiles, when delivered by NPs, were determined and their brain concentrations were analyzed against control solutions of RV administered by IV and IN route over a period of 8 h. The data indicated the area under curve (AUC) of plasma concentration-time profile of RV from dual ligand PLGA-SA-ODA NPs coated with TGC was greater than that of single ligand NPs; and both dual and single ligand NPs were 2.6 and 1.8 times greater than that of IN solution of RV respectively over 8h period, providing more drug for transport across the BBB. At 2 h post administration, dual ligand NPs showed 6.5 times and 3.3 times higher RV concentration in the brain than that of IV and IN drug solutions respectively whereas, single ligand NPs enhanced 4.5 times and 2.2 times brain RV concentration when compared to IV and IN administered control solutions. In addition, the brain uptake efficiency of C-6 from dual ligand NPs was 1.25 times, at 2 h, and reached 2 times of that of single ligand NPs at 8 h. In comparison to those reported in the literature, our developed system displayed stronger brain transport ability with versatility for delivery of both hydrophilic and hydrophobic drugs.

This increase in the brain drug concentration of RV and C-6 was attributed to the presence of the targeting ligands viz TGC and SA-ODA. These two targeting ligands 1) allowed the NPs to have better interaction with the nasal mucosal membrane; 2) transported NPs more effectively into the brain from the nose; 3) prolonged NPs residence time in the brain by remaining closely to the neuronal cells and released drug locally. Moreover, both single and dual ligand PLGA-SA-ODA NPs showed sustained release properties which

also permitted high plasma concentration of RV, which promoted drug permeation through the BBB at the same time. All of these effects contributed to the high brain RV concentration.

It was concluded that our dual ligand NPs showed better brain targeting ability compared to single ligand NPs via IN route, possibly via their strong mucoadhesive interaction. The use of single SA ligand, which allowed NP to stay in the brain longer has also demonstrated improved brain targeting compared to the control IN solution. All these indicated the importance influence of the targeting ligands in drug delivery into the brain via IN route. Furthermore, the differences in plasma profile and RV brain concentrations produced by IN and IV solutions, as well as IN NPs support the presence of the direct transport pathway from nose to the brain which is far more effective than the IV route. The indirect comparison of our developed NPs with that reported in the literature supports the conclusion that dual ligand NPs developed in this project are effective brain drug carriers and they have potential to become a platform technology for brain delivery of a wide range of molecules, from diagnostic agents to therapeutic molecules. However, these formulations still require further development to improve their drug encapsulation efficiency and stability during storage conditions.

1. Chapter-1 General Introduction and Literature Review

1.1 Introduction

A growing interest in neurodegenerative disorders (NDs) has been seen in the last few decades by researchers and health experts. A variety of NDs including Alzheimer's disease (AD) and Parkinson's diseases (PD) are thought to be caused by or related to the persistent loss of neuronal activity (Sahni et al., 2011). This group of diseases is interlinked with progressing age, change in environmental factors and immunological alterations (Kabanov & Gendelman, 2007). The most devastating ND is AD, which is the most predominant form of dementia, associated with a decline in cognitive and behavioral skills in an individual. The term Alzheimer is coined by Alois Alzheimer, a German physician, in 1906. It is characterized by extracellular deposition of senile plaques (mainly known as a β-amyloid peptide) and intracellular aggregation as well as accumulation of hyperphosphorylated tau proteins in the brain (Alistair & Steve, 2009). This neuropathological condition is lead to a cognitive decline (learning, abstraction, judgment etc.) and memory dysfunction such as depression, aggression, hallucination, anger, delusion and agitation (Brambilla et al., 2011; A. Nazem & Mansoori, 2008).

Today, millions of people have this neurological disorder bearing a high burden on the families and society around the world. According to one report published by Alzheimer's Association in the USA, AD is the sixth leading cause of death in the United States of America (Alzheimer's-Association, 2016). More than 5.4 million Americans are suffering from this disease and 90% of the mentioned figures are above the age of 65 or older. In 2017 report, dementia including AD is formed to be the second leading cause of death in Australia after cardiovascular heart disease (Alzheimer's-Australia, 2017). At present, AD/ dementia is predicted to cause heavy economic, medical and social burdens all over the world in the next few decades as world population ages, because there is no specific treatment for stopping this progressive disease yet.

In the recent decades, growing efforts has been devoted to finding new treatments for this devastating disorder. However, the success is limited. It was reported that between 1998 and 2014 only four new drugs were approved by US-FDA for the treatment of AD while 123 investigated drugs failed (Robert-Egge, 2015). Though the cost of the bringing the

new drug for AD treatment in the market is so high. Therefore, it is become very important to maximize the effect of existing and new drug via drug delivery system.

Currently, there are two main therapies are approved by US-FDA for the treatment of AD, which includes acetylcholinesterase inhibitors (Folch et al., 2016; Mehta et al., 2012), and N-methyl-D-Aspartate (NMDA) receptor antagonist (Table 1.1). These drugs have been regarded as safe and first line therapy in the treatment of AD.

Table 1.1: Drugs approved by US-FDA for the treatment of Alzheimer's disease

Drug name	Marketed name	Mechanism of action	Approved treatments	FDA approval year
Donepezil	Aricept	Prevents the breakdown of acetylcholine	All stages	1996
Rivastigmine	Exelon	Prevents the breakdown of acetylcholine	Mild to moderate	2000
Memantine	Namenda	Regulates glutamate activity by binding NMDA glutamate receptor	Moderate to severe	2003
Galantamine	Razadyne	Prevents the breakdown of acetylcholine	Mild to moderate	2004

The cholinesterase inhibitors class of drugs are the first line of drugs, includes rivastigmine, donepezil, and galantamine. These drugs act by inhibiting the acetylcholinesterase enzyme, thus prolong the action of acetylcholine in the synapse. All currently available cholinesterase inhibitors only used to limit disease progression after AD has occurred rather than they do target on the underlying causes of AD. Although many of cholinesterase inhibitor drugs have the ability to improve cognitive functions of patients in mild to moderate AD, the effectiveness of these therapies can be affected by variable degrees of drug bioavailability and pharmacokinetics profiles. Hence, it is expected that AD treatment demands multiple drug therapy because of various responsible underlying factors.

A few reports have been published comparing the efficacy of cholinesterase inhibitors and they have had contradicting results. They measured the decline in cognitive function on the AD assessment scale (Birks, 2006; Gill et al., 2009; Kobayashi et al., 2016). J Birks (Birks, 2006) compared the results of controlled clinical trials of donepezil, rivastigmine, and galantamine on 13 randomized, double-blind placebos. His study indicated that the AD assessment scale score improved cognitive function in patients with mild to moderate AD. However, there were increased risks of adverse effects and enhanced rate of withdrawal symptoms in patients treated with cholinesterase inhibitors. Gill and his colleagues (Gill et al., 2009) also reported that the use of cholinesterase inhibitors enhanced increased risks of syncope and bradycardia in older patients. Kobayashi and his colleagues (Kobayashi et al., 2016) conducted a meta-analysis on various published reviews for determination of overall benefit of rivastigmine, donepezil, and galantamine on improved cognition, function, and behavior. All these reports indicated the increased incidence of adverse effects of existing cholinesterase inhibitor drugs along with their beneficial effects.

Later in 2003, US-FDA approved the NMDA receptor antagonist drug (Memantine) for the treatment of patients with moderate to severe AD (US-FDA, 2003). This lead to the transformation of the treatment of AD, using a combination of cholinesterase inhibitors and memantine. Memantine is uncompetitive drug having a moderate affinity which acts by binding to NMDA-type glutamate receptor surface of neuronal cells thus blocking the activity of glutamate neurotransmitter and ameliorating cognitive and memory loss. These drugs are used to decrease symptoms in patients with moderate to severe AD by targeting on cholinergic and glutaminergic receptors, however; there is no supporting evidence of disease-modifying effects.

In addition, several reports have been published regarding clinical outcomes of active immunization and vaccination against amyloid aggregates that may demonstrate useful in designing new generation vaccines (Hock et al., 2002; Hock et al., 2003; Nicoll et al., 2003). These scientific findings led to the development of the amyloid vaccines such as AN-1792 and ACC-001. However, all these active immunization improvements have been on the grounds because of some adverse events such as vasculitis (Wilcock & Colton,

2008) and meningoencephalitis (Gilman et al., 2005). So, endeavors were turned onto the advancement of existing approved therapy to reduce adverse effects with total benefits.

One of the insurmountable hurdles while attempting the delivery of neurotherapeutic drug molecules is blood brain barrier (BBB) which limits the access of drug to the brain parenchyma. BBB is structurally formed by a complex system of cerebrovascular endothelial cells lining cerebral microvessels which separate blood circulation in the brain and the neuronal tissue or its fluid space. It is protecting the brain against unwanted microscopic objects (e.g. bacteria) and large molecules and possibly as a most challenging dynamic barrier for *in-vivo* therapeutic drug delivery (Doggui et al., 2012; S.-S. Feng & Chien, 2003). The principal role of the BBB is to maintain brain homeostasis for neuronal functions (Fernandes et al., 2010).

However, BBB is not merely a mechanical fence but more a gate, selectively permitting the transcellular uptake of essential nutrients (glucose, amino acids and ketone bodies), vitamins and hormones, through the brain endothelium via a large number of receptor transporters. It was found that more than 98% of small-molecular-weight drugs and nearly 100% large therapeutic molecules are unable to cross the BBB because of poor brain penetration (Bodor et al., 1992; Pardridge, 2007). The most challenging task for many treatments is to deliver a sufficient amount of therapeutic molecule across the BBB to the central nervous system (CNS) for the treatment of NDs (Khawli & Prabhu, 2013). In the grassland of this research, many scientific communities are trying to develop a new effective delivery system to improve the drug delivery to the brain by both invasive and non-invasive methods. The invasive approach includes the temporary disruption of the BBB, allowing the entry of drug molecule into the brain or of a direct delivery by means of intracerebral or intraventricular administration (Tosi et al., 2007). While, non-invasive approaches employ the systemic administration of colloidal drug carriers with targeting ligands which promote the receptor or absorptive-mediated transcytosis mechanisms, or bypassing the BBB via intranasal (IN) route (Xia et al., 2011).

Nose to brain delivery provides the various advantages over IV route such as it is a non-invasive and painless delivery which helps in the direct drug delivery to the brain bypassing the BBB. It allows the drug molecule to pass from nose to various brain

compartments via the olfactory and trigeminal pathway, therefore, enhanced brain uptake of the drug. Unlike the other routes of administration, it reduces the systemic drug exposure thereby reducing the relevant side effects, first pass effect and enzymatic degradation (Quintana et al., 2016). This route of administration provides an alternative method to injectable formulations with better patient compliance (D. Sharma et al., 2015).

1.2 Biology of the human nose

The human nose is the most protruding part of the face which extends approximately 3-5 cm in height externally and 10 cm long nasal cavity internally (Sforza et al., 2011). Human nasal cavity starts from external nares (nostrils) to the nasopharynx (the upper section of the throat) which is equally divided by the nasal septum into 2 similar non-connected halves i.e., left and right nasal cavity. Anatomically, the human nasal cavity is subdivided into three main regions that can be easily recognized based on anatomical and histological characteristics. (i) Nasal vestibule and atrium (ii) Respiratory region and mucocilliary clearance (iii) Olfactory region

Nasal vestibule comprises an outermost part of nasal cavity bears nasal cartilages having an area of about 0.6 cm^2. Nasal vestibule bears small hairs, also known as vibrissae. These small hairs are lined by a thin layer of mucus which maintains the filtration of air, dust and other deleterious matters that are breathed in (Pires et al., 2009). The atrium is the middle portion of the nasal meatus which interconnects the vestibule and respiratory region. Both the region possesses low vascularity attributable to its low permeability nature and small surface area and therefore, they are of the low interest of area for drug delivery applications.

The respiratory region is also called as conchae, is considered as the primary site of interest because it represents the major role in the drug absorption into the systemic blood circulation. The nasal mucosa present in the respiratory region is enclosed with a thin layer of mucus to facilitate mucociliary clearance. Mucus (nasal secretion) layer consisting of 95% of water, 2-3% of mucin, 2% of electrolytes, protein, lipids, enzymes and lysozymes (Kaliner et al., 1986; Mistry et al., 2009). The subsequent pH of the mucus layer in the

basal cavity is close to marginal acidic or neutral pH (5.5-6.5). This mucus is mainly secreted by goblet cells having 2-4µm in thickness overlies a basement membrane.

Olfactory region mainly lies between the nasal septum and the lateral wall of each of the two nasal cavities. Anatomically, it is situated beneath the cribriform plate of the ethmoid bone. Olfactory epithelium plays a functional role in the detection of smells by enhancing the accessibility of air to olfactory neuronal cells bearing odorant detectors. It predominantly includes three primary types of cells: the olfactory neural cells, basal cells and supporting cells (also known as sustentacular cells). Basal cells are the small, conical-shaped cells, mainly progenitor cells of supporting cells which usually provide the mechanical strength to other cells. The olfactory neural cells are originated in the olfactory bulb and terminate in the apical surface of the olfactory epithelium mucosa. These cells are unmyelinated and intercalated between the supporting cells (Pardeshi & Belgamwar, 2013). Sustentacular cells are elongated columnar cells which are resting upon the basement membrane and bears numerous long microvilli entangled with cilia of the receptor cells. The functions of the sustentacular cells are not clearly understood but rather they are intended to provide the mechanical support to the other receptor cells (L. Illum, 2000).

1.3 Nose to brain pathways and mechanisms

Once the drug formulation is administered intranasally, it reaches to the brain and CSF via olfactory receptor neurons and systemic circulation via respiratory epithelium. While the precise underlying mechanism of transport of the drug from nose to the brain is not entirely understood yet, however, recent developments have highlighted the conceivable pathways of direct transport of drugs to the cerebrum through the nasal route in man. An accumulated evidence of the literature demonstrated that nerves emerging from the brain and spinal cord are associated with the nasal cavity, are mainly responsible for the transport of the drug molecule from nose to brain (Quintana et al., 2016). A combination of one or two pathways responsible for transportation (Figure 1.1), albeit one mechanism may prevail contingent on the delivery device employed, characteristics of neurotherapeutics and formulation characteristics.

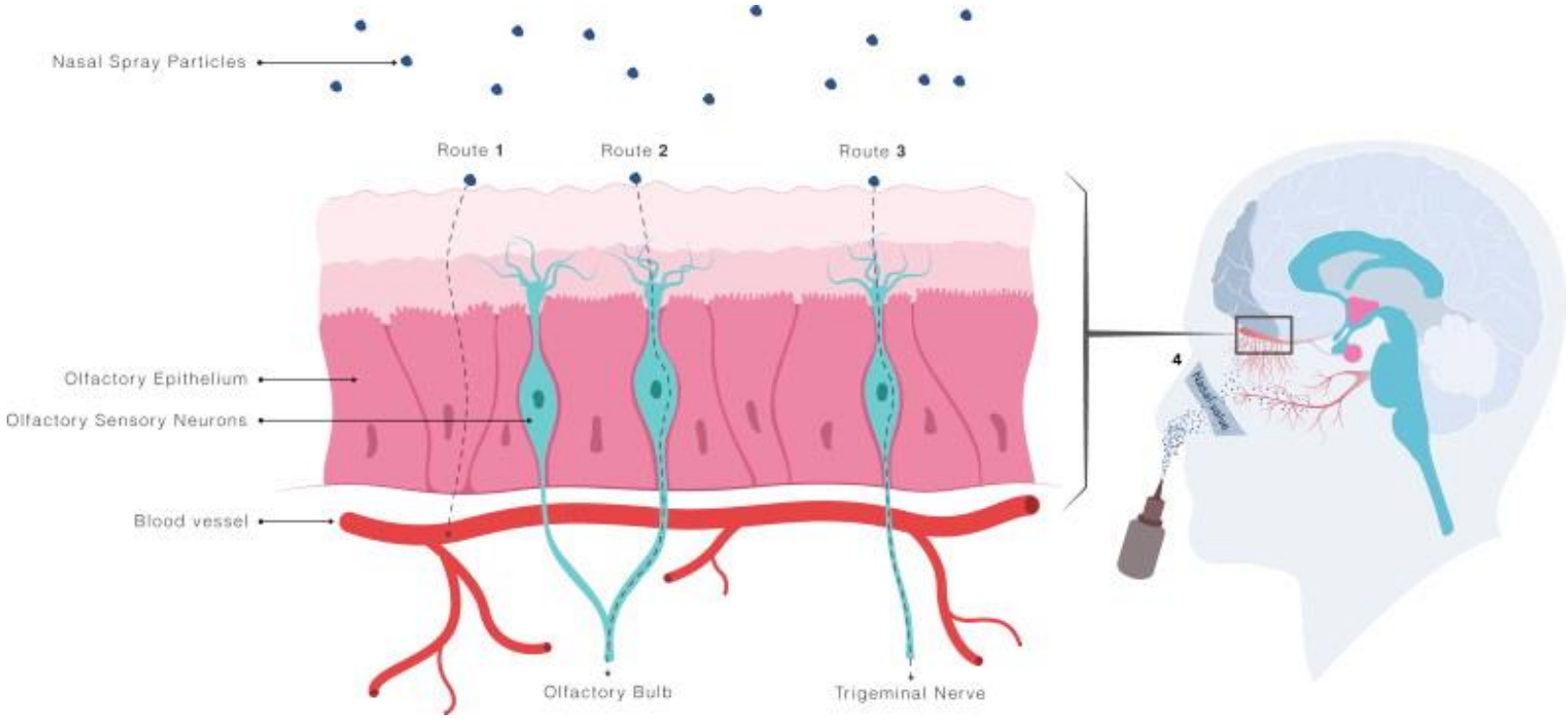

Figure 1.1: Representation of three major pathways of drug transportation to the brain via the nasal route.
Route-1 is transportation via blood capillaries. Route-2 is direct brain transportation via olfactory pathway. Route-3 is the transportation of therapeutics molecules to the brain via a trigeminal pathway. Figure adapted with permission from Elsevier Publisher (Quintana. et al., 2015).

1.3.1 Olfactory nerve pathway

The olfactory region is mostly present in the roof of the nasal cavity which is modified form of respiratory epithelium. Although olfactory epithelium consists just 3% of the nasal epithelium but this pathway serves as a most direct drug transport route to the brain and CSF, bypassing the BBB (Lisbeth Illum, 2003). It is the simplest and a slow pathway through three different pathways across the olfactory epithelium (i) transcellular pathway involving receptor-mediated endocytosis, fluid phase endocytosis or by passive diffusion. This pathway is mainly responsible for the transport of the lipophilic drugs and rate of their transport relies on their lipophilicity. (ii) the paracellular pathway is appropriate for the transport of the hydrophilic drugs most presumably occur by passive diffusion via tight junctions between sustentacular cells and olfactory neurons or open clefts in the membrane. The rate of drug transportation through this pathway mainly depends on the molecular weight of the drug. Drugs having a molecular weight less than 1000 Da easily transport through this mechanism and give greater bioavailability without any absorption enhancer. (iii) Olfactory nerve pathway; where the drug is mainly transported by means of intraneuronal (axonal transport) or extraneuronal pathway through perineural channels. The intraneuronal pathway is slow and takes hours to days for drug transportation to the distinctive brain region. Extraneuronal pathways allow the drug transportation within minutes (Pardeshi & Belgamwar, 2013). Drugs can cross the olfactory epithelium by using one or a combination of different mechanism depending upon their characteristic features.

1.3.2 Trigeminal nerve pathway

The Trigeminal nerve is the largest nerve amongst all the cranial nerve (fifth nerve) innervates in the nasal respiratory epithelium and olfactory epithelium of the nasal cavity. It comprises of three main branches (i) ophthalmic nerve V1, (ii) maxillary division V2, (iii) mandibular division V3. The former two nerves of the trigeminal nerve are important for the nose to brain delivery as they are directly associated with the nasal mucosa (Pardeshi & Belgamwar, 2013). The sheer number of proof proposes that there is direct

pathway connecting the nasal passages to the cerebrum involving trigeminal nerve (Quintana. et al., 2015; Ross et al., 2004; Yasir & Sara, 2014). Evidence suggests that IN administered drugs reach to the brain through trigeminal nerve and perineural space present in the permeable respiratory and olfactory epithelium since they are innervated by trigeminal nerves (Johnson et al., 2010). Furthermore, trigeminal nerve is also present in the maxillary sinus which is lined by a pseudo epithelium and associated with the nasal cavity. Thorne and his colleagues (Thorne et al., 2004) have studied the possible trigeminal neural pathway and mechanism for the CNS delivering of insulin-like growth factor-1 (IGF-1), a protein neurotrophic factor, following IN administration. The evidence showed an increase in the concentration of IGF-1 in the three major branches of the trigeminal nerve and in the brain by observing the high level of radioactive [I^{125}] IGF-1 in trigeminal branches, pons, and olfactory bulb. Later, the same group of researchers has recognized the significant contribution of the trigeminal nerve to the IN delivery, particularly to the caudal brain and the spinal cord (Lochhead & Thorne, 2012). This study proposes that trigeminal nerve pathway act as a conduit to transport drugs to the brain stem after IN administration.

1.3.3 Nasal lymphatic system pathway and cerebrospinal fluid

Several studies suggest the pathways connecting the nasal lymphatics and CNS may involve the transport of the drug to the cerebrospinal fluid (CSF) after IN administration followed by subsequent distribution to the brain (Dhuria et al., 2010; Johnston et al., 2004; Kida et al., 1993; Walter et al., 2006). Johnson and his colleagues (Johnston et al., 2004) investigated the existence of a connection between CSF and nasal lymphatic system pathway in humans, non-human primates, and other species. For their studies, they introduced yellow microfibrils into the CSF. The presence of yellow microfibrils in the nasal lymphatic network in the submucosal region associated with the olfactory and respiratory region evidenced the fact that there is a direct association between CSF and nasal lymphatic pathway. Walter and his colleagues (Walter et al., 2006) administered antigen into the subarachnoid space of the rat brain and their experimental evidence showed the presence of the antigen in the cervical lymph nodes and nasal mucosa owing

to the drainage of the antigen from subarachnoid space to nasal lymphatic vessels which provided the direct relationship between CSF and nasal lymphatics. These possible pathways are significant predominant in a number of animal species (rats, rabbits, and sheep) accounting for 50% of CSF clearance (Boulton et al., 1999; Boulton et al., 1996). However, in the case of human drug therapeutics are essentially transported into the blood because of the pressure difference at the arachnoid granulations present on the blood capillaries in the subarachnoid space. These pathways are evidenced by the fact that therapeutics can be specifically delivered to the CSF following intranasal administration (Born et al., 2002).

Experimentally it is hard to determine the contribution of a pathway followed by a drug molecule for the transportation into the cerebrum after IN administration. Still, it is possible, however, more than one pathway involved for nasally administered drug to be transported to the brain tissue. The possible pathways are depicted in Figure 1.2.

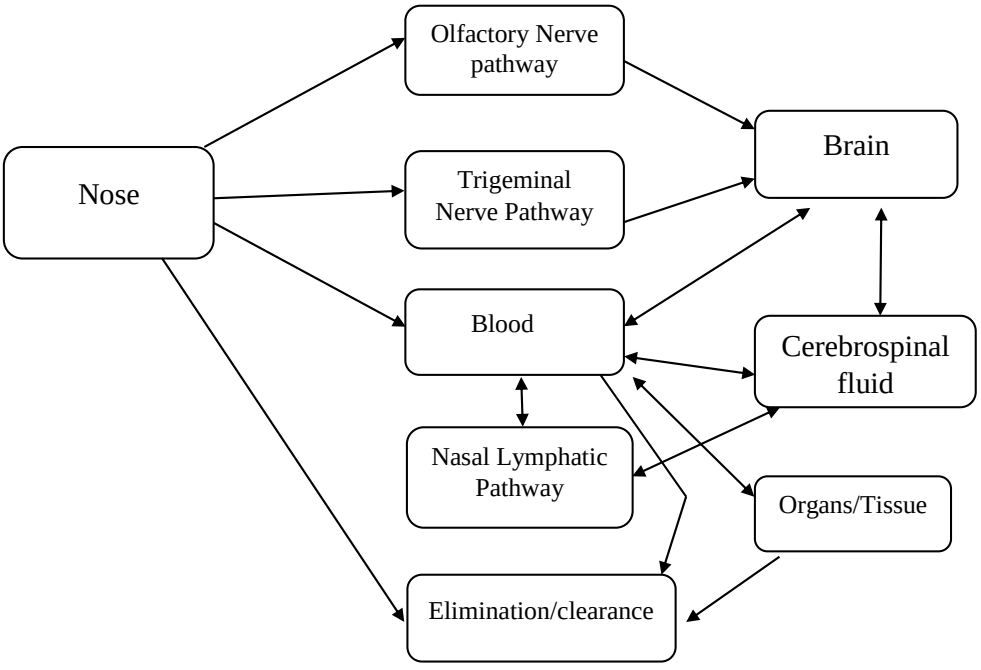

Figure 1.2: Proposed pathways of drug molecule from nose to the brain in human after IN administration

1.4 Nose to Brain drug delivery

In spite of the various advantages mentioned earlier, nose to brain delivery possess some challenges such as the rapid elimination of drugs due to increased nasal mucociliary clearance, reduced nasal permeability of high molecular weight drugs across nasal mucosa, and damage to the nasal mucosa due to frequent use of drug (Pardeshi & Belgamwar, 2013). These limitations lead to the development of modified formulation such as NPs which has attracted great interest in the drug delivery into the brain. NPs can be used as a platform technology for delivery of an extensive range of hydrophilic drugs, hydrophobic drugs, peptides & proteins, vaccines, biological macromolecules etc. (Wilson et al., 2008). In addition, NPs retard drug release at the peripheral site and reduce local and peripheral toxicity by means of altering their surface properties which make them attractive carriers for brain transport (Cheng et al., 2013; J. P. Rao & Geckeler, 2011). Additionally, higher surface/volume ratio of NPs subsequently bring about a reduction in dose as well as the frequency of administration of the drug.

During the last two decades, numerous systems have been developed to target the drugs from nose to the brain which include polymer based NPs (Al-Ghananeem et al., 2010; Md et al., 2012; Wang et al., 2008), lipid-based NPs (Kumar et al., 2008) and liposomes (Li et al., 2012). Among the various targeted drug delivery systems for the brain, polymeric NPs have demonstrated the promising potential for the treatment of AD and other NDs (Brambilla et al., 2011; Amir Nazem & Mansoori, 2011). This is due to their capability of site-specific targeting nature and ability to deliver a wide range of therapeutics molecules in a controlled release manner to the brain (Fazil et al., 2012) for example estradiol (G. Mittal et al., 2011), rivastigmine (Wilson et al., 2008) and curcumin (Cheng et al., 2013; La Porte et al., 2012).

1.4.1 Polymeric nanoparticles

Polymeric NPs possess controlled and sustained release properties due to their solid matrix. Those particulate carriers also protect the drug molecule from degradation. Due to their polymeric nature, they can be used to further enhance bioavailability and even

permeability of many drugs. Although they are very simple to formulate, still physicochemical properties of a drug such as molecular mass, lipophilic nature, and its ability to cross mucous membrane are needed to be considered while designing polymeric NPs for IN delivery. Additional issues such as protection against systematic enzymatic attack and minimizing clearance rate of drugs in the brain are also to be concerned in designing polymeric NPs (Modi et al., 2009).

A wide variety of natural to semi-synthetic polymers has been used in the preparation of polymeric NPs. These include chitosan, gelatin, sodium alginate, albumin, guar gum and xanthan gum etc. However, in last decades, biodegradable polymers are attracting more attention in medical and pharmaceutical applications. Most popular ones are Polylactides (PLA), Polyglycolides (PGA), Poly (lactide-co-glycolides) (PLGA), Polyanhydrides, Polyorthoesters, Polycyanoacrylates, and Polycaprolactone (PCL).

There has been increased interest in the development of bioadhesive/mucoadhesive polymer pertaining to nasal drug delivery in recent years. These types of mucoadhesive polymers are certainly not only needed for enhancing the residence time in the nasal cavity and increasing drug transport across nasal barrier but also, pertaining to reducing the drug clearance by increasing the viscosity of formulation as well as enhancing the uptake by the nasal epithelium. Over the recent decades, several synthetic and natural biodegradable mucoadhesive polymers have been studied and showed substantially prolonged residence time through the nasal epithelium and reduced drug clearance (Ugwoke et al., 1999; Zaki et al., 2007). These polymers primarily consist of derivatives of cellulose, polyacrylates, starch and chitosan derivatives (Chaturvedi et al., 2011). Various designed polymeric nanoparticulate formulations for the nose to brain targeting with and without targeting ligands, mentioned in literature are tabulated in Table 1.2.

Table 1.2: Overview of the various polymeric NP formulations that enhance the drug transport to the brain via IN administration

Core polymer in NP Formulation	Targeting ligand used / surface modification	Name of the drug loaded	Animal study	Findings	Reference
Polylactic acid (PLA)	PEG-20000 Polysorbate-80 chitosan Borneol Mentholum	Aniracetam	*In-vivo* brain targeting efficiency was determined by administering multi-coated PLA NPs and control solution of Aniracetam in Sprague-Dawley rats.	Multi-coated PLA NPs showed 5 times higher drug concentration and AUC in the brain as compared to control drug solution.	(Bian et al., 2016)
PLGA	Glutathione	Paclitaxel	*In vivo* study was performed in Wistar rats by administering both glutathione conjugated and unconjugated PLGA NPs and their brain targeting efficiency were determined against control (paclitaxel solution).	Glutathione conjugated NPs and unconjugated NPs showed 388% and 225% respectively higher brain targeting efficiency compared to paclitaxel solution.	(Acharya & Reddy, 2016)

Core polymer in NP Formulation	Targeting ligand used / surface modification	Name of the drug loaded	Animal study	Findings	Reference
Chitosan, and its thiolated derivative	Thiolation using thioglycolic acid	Selegiline	*In vivo* study was performed in Wistar rats by administering both thiolated chitosan NPs and chitosan NPs and their brain uptake study was compared against control selegiline solution.	Their brain uptake study results indicated that thiolated NPs enhanced ~2 times and 3 times higher brain drug concentration than that to chitosan NPs and selegiline drug solution.	(Singh et al, 2016)
Chitosan Glutamate	-	Rasagiline	Biodistribution study was carried out in Swiss albino mice (male) after IN and IV administration of rasagiline loaded chitosan glutamate NPs.	Brain targeting efficiency of the IN administered rasagiline loaded NPs was higher (69%) than that of IV administered chitosan glutamate NPs (66%).	(Mittal et al., 2016)
PEG-PLGA	Lactoferrin	Rotigotine	Brain targeting efficiency of Rotigotine was determined by IN administration of lactoferrin modified and unmodified PEG-PLGA NPs in male Kunming mice.	*In-vivo* results revealed that Lactoferrin modified NPs showed higher drug concentration in the brain as compared to unmodified NPs.	(Bi et al., 2016)
Thiolated Chitosan	Thiolation on chitosan polymer using thioglycolic acid	Buspirone hydrochloride	*In vivo* study was performed on Albino Wistar rats by IN administered Thiolated chitosan NPs and their brain targeting efficiency were	Buspirone loaded thiolated chitosan NPs showed 2 times higher drug concentration in the brain when compared	(Bari et al., 2015)

Core polymer in NP Formulation	Targeting ligand used / surface modification	Name of the drug loaded	Animal study	Findings	Reference
			determined against control (buspirone solution).	with IN administered buspirone solution.	
PLGA	-	Diazepam	^{99m}Tc-Labelled Diazepam loaded PLGA NPs were compared with ^{99m}Tc-labelled Diazepam suspension in Sprague-Dawley rats.	Results indicated that ^{99m}Tc-Labelled Diazepam loaded PLGA NPs showed 60% higher drug transport from nose to brain as compared to ^{99m}Tc-labelled diazepam suspension post-IN administration.	(D. Sharma et al., 2015)
PLGA	TAT peptide (11 amino acid)	Insulin	Both unmodified and TAT-modified PLGA NPs loaded with Fluorescein were administered to KM Mice via IN route to determine the brain uptake efficiency.	TAT-modified PLGA NPs showed 3 times higher drug concentration in the olfactory bulb as compared to unmodified PLGA NPs.	(L. Yan et al., 2013)
Chitosan	-	Venlafaxine	Venlafaxine loaded chitosan NPs were administered to Wistar rats by IN route and compared against IN and IV administered control drug solution.	IN administered Venlafaxine loaded NPs showed two times higher drug concentration in the brain as compared to IN administered drug solution.	(Haque et al., 2012)

Core polymer in NP Formulation	Targeting ligand used / surface modification	Name of the drug loaded	Animal study	Findings	Reference
PLGA	-	Olanzapine	Olanzapine loaded PLGA NPs were administered IN to Albino rats and compared with IN and IV administered drug solution.	The *in-vivo* study revealed that IN administered Olanzapine loaded PLGA NPs enhanced 6.4 and 10.9 times higher brain drug concentration as compared to IV and IN administered Olanzapine drug solution.	(Seju et al., 2011)
PEG-PLA	low molecular weight Protamine	Coumarin-6 (C-6)	Both uncoated and protamine coated PEG-PLA NPs were administered via IN route to Sprague-Dawley rats.	The pharmacokinetic data also showed 2.03, 2.55, 2.68 and 2.82 folds higher C-6 concentration in rat cerebrum, cerebellum, olfactory tract and olfactory bulb respectively as compared to unmodified NPs.	(Xia. et al., 2011)

1.4.2 Sialic acid surface modification

Sialic acids (SA) are the most abundantly occurring acidic 9-carbon-sugar derivatives (Figure 1.3 (A)) present on the erythrocyte cell membrane (Murrey & Hsieh-Wilson, 2008; She et al., 2014). They constitute a group of more than 50 structurally distinct compounds, mostly derived from a 5-acetamido-D-glycero-D-galacto-2-nonulosonic acid (N-acetylneuraminic acid). N-acetylneuraminic acid (Neu5Ac) is one of the most abundantly available sialic acids, that have been used for neuronal targeting (Bondioli. et al., 2010; Tosi et al., 2010; Wielgat & Braszko, 2012). They are present in the brain close to the mammalian neuronal cell adhesion molecule (NCAM), a glycoprotein present on the glial cell surface and skeletal muscle cells. Sialic acids are preferably taken up by these protein molecules that play an important role in various neurological processes, such as maintenance of plasticity during neuron development (Bondioli et al., 2011). They also play an important role in evading the reticuloendothelial system (RES) thus prolonging the circulation of nano-systems without any uptake by the immune system (Bondioli et al., 2011).

(A)

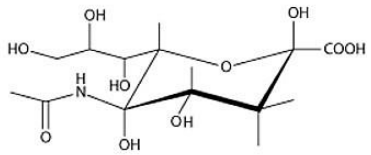

(B)

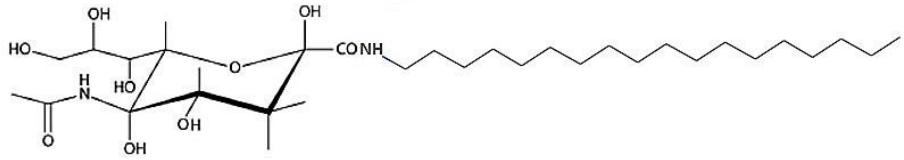

Figure 1.3: Chemical structure of (A) Sialic acid (B) Sialic acid-Octadecylamine conjugate

Using this principle, Tosi and his colleagues (Tosi et al., 2010) developed a Neu5Ac (SA) and glycopeptide (G7) tagged PLGA NPs for CNS localization to achieve significant levels of brain delivery of the loperamide. Their results indicated the increased drug concentration of loperamide in the brain along with extended time period of 24 h, after an administration of PLGA-SA-G7 NPs. The increased brain drug concentration was thought owing to the interaction of the SA present on the NPs with neuronal cells present in the brain and also resist the NPs efflux, ultimately prolonged brain drug concentration.

Based on this concept that SA could enhance and maintain the brain drug concentration for an extended time, we choose Neu5Ac as our choice of the targeting ligand aiming to deliver and then increase retention of RV close to neuronal cells in the CNS. As SA is hydrophilic in nature, therefore, it was conjugated with a hydrophobic moiety (octadecylamine) to form sialic acid-octadecylamine (SA-ODA) to incorporate the sialic acid into the NPs matrix phase [Figure 1.3 (B)].

1.4.3 Chitosan modification

A widely used mucoadhesive polymer, chitosan, a biodegradable and biocompatible polymer, is naturally occurring and abundantly available [Figure 1.4(A)]. It is derived from alkaline deacetylation of chitin, which can be obtained from crustacean shells. chitosan is composed of repeating units of D-glucosamine and N-acetyl-D-glucosamine residues coupled through a β (1→4) glycosidic linkage. It bears the positive charge owing to free amino groups, resulting in its pKa value 5.5-6.5. The actual mucoadhesion and permeation characteristics of chitosan are results of the ionic interaction between cationic amino group and anionic counterpart of the mucous membrane. Hence, it possesses mucoadhesive characteristics which in turn not only reduce mucociliary clearance but also transiently open up the tight junctions between epithelial cells thereby significantly improving drug transportation across the nasal membrane to the brain by paracellular route (Md et al., 2012). This unique property is favorable in retaining the particulate formulations for the extended time period inside the nasal cavity and also simultaneously helping in translocation of the drug molecule across the membrane (Casettari & Illum, 2014). It has been widely used in the development of advanced formulation because of its desirable biological properties such as biodegradability, good stability, non-toxicity, biocompatibility, mucoadhesive

and permeation enhancing ability (Jayakumar et al., 2010; Md et al., 2012; Wilson et al., 2011; Wilson et al., 2010).

Wang and his colleagues (Wang et al., 2008) formulated Estradiol loaded chitosan NPs by using ionic gelation method with an average size of 269.3±31.6 nm, +25.4mV zeta potential and estradiol loading capacity of 1.9 mg/mL with an entrapment efficiency of 64.7%. Subsequently, they targeted Estradiol in CSF via IN and IV administration of Estradiol loaded chitosan NPs. The CSF drug concentration was substantially higher when they compared IN administration (76.4±14 ng/mL) with IV administration (29.5 ±7.4 ng/mL) of NPs. It was concluded that Estradiol loaded chitosan NPs transported through nasal cavity into cerebrospinal fluid improving the levels of Estradiol into the brain thereby providing neuroprotection.

A similar study was also performed by Al-Ghananeem and his colleagues (Al-Ghananeem et al., 2010) for investigating the IN route as a potential route for drug targeting to the brain. They formulated didanosine loaded chitosan NPs using ionic gelation method. Brain targeting efficiency of didanosine loaded chitosan NPs was determined and compared against drug solution of didanosine IN and IV via the nose. It is reported that drug concentration in the brain, olfactory bulb, and CSF was higher in the case of didanosine loaded chitosan NPs than that of drug solutions.

Another set of similar results were also reported by Fazil and his colleagues (Fazil et al., 2012). They encapsulated Rivastigmine (RV) into chitosan NPs for brain targeting via IN delivery, with an average size of 185.0±8 nm and zeta potential of +38.9 ±2.85 mV. They also studied nose to brain delivery pathway using confocal laser scanning microscopy technique via administering blank NPs loaded with rhodamine-123 as a fluorescent marker. Confocal studies indicated the higher concentration of rhodamine in the brain after IN administration compared to IV administration. Further pharmacokinetic studies indicated that area under the curve (AUC) of RV was 2 times higher in the brain in RV loaded chitosan NPs as compared to RV drug solution after IN administration. These results suggest that there is a direct nose to brain pathway for the drug administered in the form of chitosan NPs via IN route. All these studies suggest that the combination of polymeric NPs with IN route is an effective strategy to enhance the drug delivery into the brain.

Despite many superior properties, chitosan has a major disadvantage, that could lead to loss of its permeability enhancing property and absorption nature *in vivo,* its poor solubility at physiological pH which may cause it to precipitate out from solution *in-vivo* (Kotze et al., 1999). Thus, various chemical modifications have been introduced in order to improve chitosan solubility at physiological pH (Cho et al., 1999; Kubota et al., 2000; Mourya & Inamdar, 2008).

The synthesis of water-soluble chitosan derivatives has led to the introduction of glycol chitosan (GC), [Figure 1.4 (B)] a water-soluble derivative which maintains its free amino group and favorable mucoadhesive property. GC is hydrophilic in nature at all neutral/acidic pH owing to its hydrophilic ethylene glycol side chain thus provides steric stabilization. It was produced by reacting the chitin with ethylene oxide followed by its deacetylation (Trapani et al., 2009).

Pawar and his colleagues (Pawar & Jaganathan, 2016) introduced the Hepatitis B surface antigen loaded GC NPs via IN route to evaluate the systemic and mucosal response. Both chitosan and GC NPs were prepared using polyelectrolyte complex method with an average size below 200 nm and positive surface charge. *In vivo* nasal clearance study was performed in male New Zealand white rabbits by administering separately ^{99m}Tc-labelled chitosan and GC NPs. Their results indicated that mucoadhesive polymer showed less nasal clearance from nasal mucosa as compared to control ^{99m}Tc-labelled lactose solution and ^{99m}Tc-labelled Hepatitis surface antigen solution. GC NPs showed significantly ($p<0.05$) less nasal clearance and even better mucosal uptake than that of chitosan NPs. These results attributed to less nasal clearance of NPs and the better mucoadhesive nature of GC. Considering the better mucoadhesive property and reduced nasal clearance of the GC, we decided to use GC as a polymer coat to target to the nasal mucosa membrane.

(A) (B)

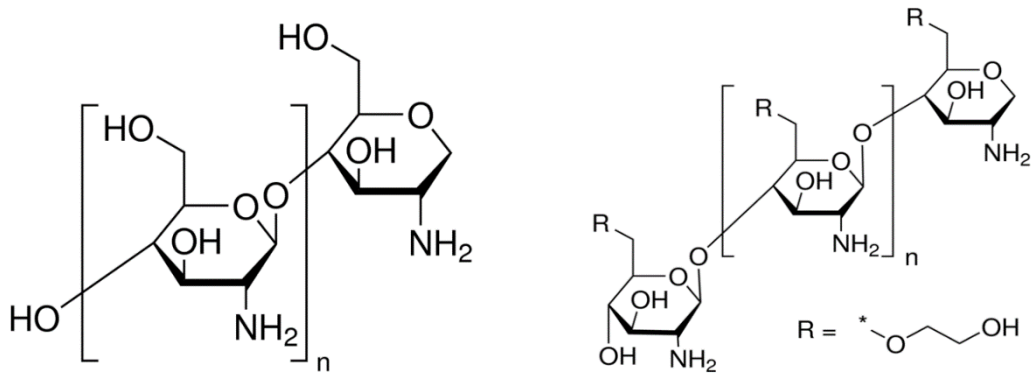

Figure 1.4: Chemical structure of (A) Chitosan (B) Glycol Chitosan

Lately, it has been reported that chitosan showed stronger mucoadhesive property when sulfhydryl groups were conjugated to the polycation amino group (Bernkop-Schnürch et al., 2004). This thiolated chitosan is also known as "Thiomers". Bernkop-Schnurch and his colleagues (Bernkop-Schnürch et al., 2004) compared the mucoadhesive properties of thiolated chitosan with native chitosan. Their study indicated that mucoadhesive property was augmented by 6-100 folds in thiolated chitosan depending upon the degree of thiolation. It was suggested that the underlying mechanism behind the enhanced mucoadhesion is the formation of the strong disulfide bond between thiol groups of the polymer and cysteine-rich domain of mucus layer (Bernkop-Schnürch et al., 2004).

Furthermore, Shahnaz and her colleagues (Shahnaz et al., 2012) compared pharmacokinetic profiles of Leuprolide from thiolated chitosan NPs, unmodified chitosan NPs and IN Leuprolide solutions in Sprague-Dawley rats via IN administration. Their results indicated that the thiolated chitosan NPs has enhanced the AUC and increased mean residence time of leuprolide in plasma as compared to unmodified NPs and control drug solution which led to an increase in plasma bioavailability of leuprolide. In another study, Bari and his colleagues (Bari et al., 2015) evaluated the brain delivery of buspirone hydrochloride after administration of thiolated chitosan NPs and control drug solution into Wistar rats through IN route. Their results provide the evidence of enhanced brain concentration (797.3 ± 35.7 ng/mL) of the thiolated chitosan NPs as compared to IV administered buspirone drug

solution (384.5 ± 13.4 ng/mL) and IN administered buspirone drug solution (417.7 ± 19.2 ng/mL).

Recently, Singh and his colleagues (Singh et al., 2016) investigated the increase in the brain delivery of selegiline hydrochloride to improve the depression symptoms. For this, they formulated selegiline loaded chitosan and thiolated chitosan NPs and evaluated their pharmacological effects against IN administered control selegiline solution. Their brain uptake study revealed the thiolated chitosan NPs has attained 2 times and 3 times higher brain drug concentration as compared to chitosan NPs and control drug solution respectively.

All the above-mentioned studies indicate that thiolation of the chitosan helps to increase the brain drug concentration via IN route and it is expected to see the same principle will work for the GC. Because this chemical modified GC would not alter the fundamental skeleton of chitosan, would maintain its original biochemical and physiochemical properties and finally would bring the new better-targeted delivery system. Till date, the author is not aware of the any published literature involving the use of the thiolated glycol chitosan (TGC) for improved brain drug delivery via IN route. Therefore, using this principle, we proposed a novel nanoparticulate formulation using TGC as a polymer coat to improve the brain uptake efficiency of the drug.

1.4.4 Polyethylene Glycol surface modification

Not only the chitosan NPs used for the nose to brain drug targeting, but also there are a number of other polymers which substantially prolong the residence time through the nasal epithelium and reduced drug clearance, has been employed. For example, Polyethylene glycol (PEG), a polyether compound along with versatile applications, biodegradable nature, and low toxicity profile. Surface modification of NPs with PEG progresses the diffusion of the NPs across the mucus layer by improving their physiochemical properties.

Zhang and his colleagues (Q.-Z. Zhang et al., 2006) investigated the use of methoxy Polyethylene Glycol-Polylactic acid (mPEG-PLA) NPs to enhance the brain uptake of nimodipine following IN administration. Nimodipine loaded NPs were prepared by using emulsion/solvent evaporation technique bearing size 76.5±7.4 nm and a negative

surface zeta potential with 5.2% drug loading. CSF/plasma and olfactory bulb/plasma concentration were significantly higher after an IN administration of NPs as compared to control drug solution. Thus, it has indicated that mPEG-PLA NPs demonstrated improved targeting efficacy from direct nose to brain transport of drugs.

1.4.5 Peptide surface modification

Despite the direct route from nose to brain, a drug needs to be penetrated through various heterogeneous compartments before reaching the brain. To overcome the multiple bio-barriers a versatile drug carrier is necessary. Cell penetrating peptides (CPP) are one of the best carrier systems for the delivery of the drugs into the brain. They are short chain cationic peptides that have drawn much attention due to their ability to enhance the permeability of hydrophilic drug cargoes into cells.

The research work led by Xia and his colleagues (Xia et al., 2011) used low molecular weight protamine as a CPP for enhanced drug delivery into the brain. Protamine possesses various advantages such as high cell translocation potency, being neither antigenic nor mutagenic and showed reduced toxicity. This protamine has high arginine content and can act as an efficient carrier for delivering cargoes across the brain. Considering all these known facts, they developed a PEG-PLA NPs functionalized with protamine using emulsion/evaporation techniques to enhance brain delivery following IN administration. C-6 was used as a fluorescent molecular probe to study brain targeting efficiency of modified nanoparticulate system. Modified protamine NPs showed significantly better cellular internalization compared to that of unmodified NPs yet, without detectable cytotoxicity on a Human Bronchial Epithelial cells line. The pharmacokinetic data showed 2.0, 2.5, 2.7 and 2.8 folds higher C-6 concentration in rat cerebrum, cerebellum, olfactory tract and olfactory bulb respectively for a modified NPs than that of unmodified NPs.

Trans-activated transcriptional (TAT) peptide is one type of CPP, obtained from the protein transduction domain of the human immunodeficiency virus (HIV). It has been successfully used to deliver small and large macromolecules such as Insulin across the biological membrane for their biological action. Yan and his colleagues (L. Yan et al., 2013) studied the effect of the TAT peptide modified PLGA NPs for enhanced nose to brain delivery of macromolecule agents via olfactory pathways. Insulin-loaded TAT-

conjugated-PLGA NPs were formulated by a modified double emulsion solvent evaporation method for the delivery of Insulin to the brain. The intracellular uptake efficiency was 4-5 folds higher in *Caco-2* cells with TAT modification as compared to unmodified PLGA NPs. *In-vivo* experiments were conducted in mice revealed that there is only 0.4% of insulin disposition in olfactory bulb from uncoated NPs compared to 2.6% insulin disposition of TAT-modified PLGA NPs. A similar pattern of drug concentration (3.4% vs. 0.9%) for modified NPs vs. unmodified was detected in the cerebrum. A total brain delivery of Insulin reached 6.0% which provided a proof-of-concept of using TAT to enhance IN delivery of macromolecular drugs such as insulin to the brain.

The literature suggests that the basic domain of TAT peptide should be rich with arginine content with at least 9 amino acid sequence for enhanced cellular uptake of various types of cargoes molecules (Brooks et al., 2005). The removal of this arginine content leads to the non-translocation property. The most common sequence of TAT peptide used for cellular interaction is GRKKRRQRRR sequence. Later, Torchilin and his colleagues (Torchilin, 2008) used TAT peptide with lysine and arginine amino acid residues for increased cell adhesion with the energy dependent mechanism. Therefore, we decided to use the basic domain of TAT peptide (NH_2-RKKRRQRRR-COOH) to enhance the translocation of NPs across the biological membrane further.

All these findings clearly suggested that there is a direct nose-to-brain drug transport and the use of positively charged functionalized groups such as TAT, chitosan, thiolated chitosan or protamine on NPs surface can enhance the drug delivery into the brain.

1.4.6 Dual and multi targeted ligands modified NPs

NPs functionalized with dual targeted and multi-targeted ligands is a new innovative technology which mainly implies the use of various ligands targeting to the variety of different receptor cells to improve the targeting efficiency and residence time of the NPs or drug at the target.

Using this principle, Bian and his colleagues (Bian et al., 2016) formulated an Aniracetam loaded PLA NPs. Aniracetam is a racetam chemical class compound. It is

currently being tried in the animal's treatment and human for treatment of senile cognitive disorder and memory impairment. Bian's group formulated a multi-component coated PLA NPs. The various ligands used are PEG 20000, Polysorbate-80, chitosan, borneol, and mentholum were added during the various stages of NPs formulation and by coating processes. The formulated multi-coated aniracetam loaded PLA NPs were administered intranasally and their brain targeting efficiency was determined and compared against IN administered aniracetam solution (control). Their results indicated five-time enhanced brain drug concentration by multicoated PLA NPs as compared to control drug solution. The various targeting ligands viz., chitosan and borneol/mentholum mixture support in enhancing the brain uptake of aniracetam by acting as a permeation enhancing agents. Whereas tween-80 allowed to maintain the constant drug concentration in the brain for longer duration via inhibiting the P-glycoprotein in the brain endothelial cells, ultimately inhibiting the drug efflux. The coating of mPEG-20,000 polymer allowed the multi-coated PLA NPs to escape from reticuloendothelial cells, resulting in the longer circulation of the NPs for a prolonged time. Therefore, these all targeting ligands not only helped to maintain a higher drug concentration in the brain but also contribute to maintaining a constant drug level for a prolonged time. Further, the drug concentration in the brain was maintained for an extended period compared to control which gives the direct evidence of the significance of the multiple ligands loaded NPs. However, Bian and his colleagues have not included the comparison of control PLA NPs without any targeting ligands or using single or double targeting ligands, therefore it is difficult to assess the contribution of the individual targeting ligand in order to enhance the drug level in the brain (Bian et al., 2016).

Hence, to evaluate the impact of the individual targeting ligands for attaining higher brain drug concentration, a concept of NP with single ligand and dual ligands was designed. Till date, the available literature suggests the dual ligands modified NPs for promoting brain targeting via IV route (Cui et al., 2016; Huile et al., 2011; Tosi et al., 2010; C. Zhang et al., 2014), whereas, author is not aware of any dual targeting ligand modified NPs for targeting from nose to brain bypassing the BBB. Therefore, using the same concept, we also aimed to enhance the brain drug concentration of RV by formulating dual targeting ligands associated PLGA NPs.

.

1.5 Rivastigmine

1.5.1 Physicochemical properties of Rivastigmine

Rivastigmine (RV), (S)- N-Ethyl-N-methyl-3-[1-(dimethylamino)ethyl]-phenyl carbamate is a parasympathomimetic agent, belongs to a cholinergic class of drug. It is a carbamate derivative structurally related to physostigmine. Its molecular formula is $C_{14}H_{22}N_2O_2$ with a molecular weight of 250.33 Dalton. It is available in tartrate form having a molecular formula $C_{184}H_{28}N_2O_8$ with a molecular weight of 400.42 Dalton. The detailed structure of rivastigmine and rivastigmine hydrogen tartrate is represented in Figure 1.5. It is available under generic name as rivastigmine and marketed under brand name mainly as Exelon (Novartis).

(A)

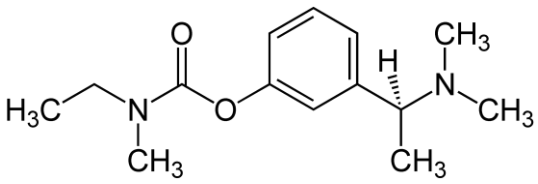

(B)

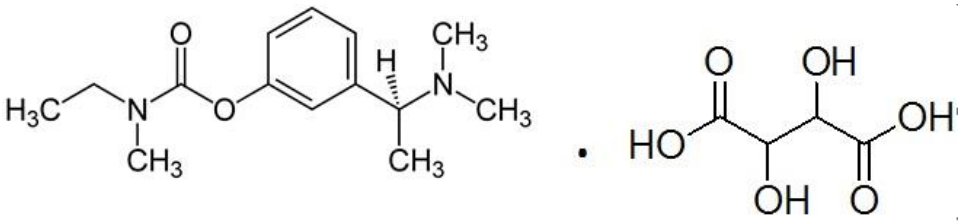

Figure 1.5: Chemical structure of (A) Rivastigmine (B) Rivastigmine hydrogen tartrate

Its melting point varies from 123.0 to 127.0°C. RV is both hydrophilic and lipophilic in nature. Due to this, it has a certain solubility in water (2.04 mg/mL), slightly soluble in n-octanol and slightly soluble in ethyl acetate (Human Metabolome Database NIH, 2012). It is stable and its shelf life is more than 5 years if stored below 30°C. RV is a weak base and its pKa is 8.89 and Log P is 2.41 (US-National-Library-of-Medicine). As indicated by its Log P, RV can cross the BBB to a certain degree. Although it can permeate the BBB but it has restricted entry in the brain due to its hydrophilic nature, therefore, requires frequent dosing administration. The frequent dosing ultimately producing cholinergic adverse effects such as anorexia, bradycardia, vomiting nausea etc. (Nagpal et al., 2013).

The literature indicated that RV is stable under various conditions such as heat (37°C and 60°C), 0.5N hydrochloric acid except for basic conditions (Rao et al., 2005; Temussi et al., 2012). RV produces degradation products under alkaline conditions (0.5 M sodium hydroxide) however, these degradation conditions were milder than ours' degradations conditions. The literature study indicated that RV and its active metabolite NAP-226-90 is stable in human plasma at various storage conditions such as storage at -18°C, room temperature and after three freeze-thaw cycles (Pommier & Frigola, 2003).

1.5.2 Mechanism of action of Rivastigmine

RV is most commonly employed in the treatment of AD with mild to moderate dementia (Joshi et al., 2010). It is a reversible dual cholinesterase inhibitor (IC_{50}= 5.5 µM), that reversibly inhibits both brain butyrylcholinesterase and acetylcholinesterase enzyme, thereby, retard the rate at which acetylcholine (ACh) is broken down. (Yang et al., 2013). While the precise mechanism of RV action is unknown, it is postulated to exert its therapeutic effect by enhancing the amount of acetylcholine in the brain, which may help to reduce the progression of dementia in patients with AD. RV is structurally similar to acetylcholine so it occupies the enzyme's active site, after the administration, in a similar fashion to acetylcholine which results in a "flattening" of an active site producing prolonged inhibition of acetylcholine esterase enzyme (Jann, 2000). Ultimately prolong the action of acetylcholine in the CNS.

1.5.3 Rivastigmine dosage and administration

RV is available in its hydrogen tartrate form which is known as Rivastigmine hydrogen tartrate. The initial dose for Rivastigmine hydrogen tartrate is 3.0 mg/day (1.5 mg b.i.d). If this initial dose is well tolerated, after a minimum of 2 weeks the dose may be increased to 3 mg b.i.d. (6 mg/day, up to maximum 12 mg/day). The usual maintenance dose of Rivastigmine hydrogen tartrate is 6-12 mg/day. It may cause the dose-related side effects in human such as weight loss, nausea, vomiting, diarrhea, increased saliva sweating, slow heartbeat, dizziness, etc. (Gottwald & Rozanski, 1999).

1.5.4 Pharmacokinetic profile of Rivastigmine

RV is well absorbed and approximately 40% bound to plasma proteins over a concentration range of 1 to 400 ng/mL after oral administration. Its peak plasma concentration is attained in approximately within 1 h of administration and can also be detected in CSF, brain within 1-4 hours of peak plasma concentration (Polinsky, 1998). The absolute oral bioavailability of RV ranges from nearly 35% at 3 mg/day to 71.7% at 6 mg/day after oral dosing (Amini & Ahmadiani, 2010). The estimated oral LD_{50} values in rats are 8.1 mg/kg (males) and 13.8 mg/kg (females). These dose levels are more than 20 times the maximum recommended a human dose of 12 mg/day (assuming a normal healthy adults' weight). The apparent volume of distribution of RV is 5±3 L/Kg.

RV extensively undergoes first pass metabolism primarily via acetylcholinesterase enzyme-mediated hydrolysis to a decarbamylated phenolic metabolite (NAP 226-90). RV is also metabolized into its principal metabolite, NAP 226-90 in CNS by cholinesterase enzyme, therefore, bypassing the hepatic metabolic pathways. It has an approximately 10% activity and 2.5 to 4 h plasma half-life compared to the parent compound. Further, NAP 226-90 is metabolized in the liver into N-demethylated conjugate and sulfate conjugate (Jann, 2000). This sulfate conjugate predominantly accounts for 40% of the dose. Approximately 7% of this decarbamylated phenolic derivative excreted through the kidney within 24 h (Gottwald & Rozanski, 1999).

As RV has and short biological half-life (~1.5 h) and undergoes extensive metabolism. Furthermore, its hydrophilic nature limits its entry into the brain. Due to all these above-mentioned reasons, it needs to be administered frequently to maintain constant brain drug level. The frequent dosing increases its bioavailability along with increased incidence of dose-related adverse effects. Hence all these determinants provide an opportunity for the development of targeted drug delivery system especially NPs to provide the better targeting and sustained release.

1.6 Significance of research

The most outstanding feature of this project is the use of functionalized NPs with two targeting ligands, SA derivative (N-acetylneuraminic acid) and GC modified polymer, to deliver RV loaded PLGA NPs into the brain and to extend the drug residence time there.

The first targeting ligand chosen was employed as a modified mucoadhesive TGC polymer to coat the surface of the PLGA-SA-ODA NPs. The target ligand-1 (TGC polymer) will target to the nasal mucosal membrane which will reduce the nasal clearance of NPs owing to its mucoadhesive nature and enhance the uptake of the NPs via nose to the brain via olfactory pathway.

The second targeting ligand chosen was SA-ODA which is coupled with PLGA NPs. The targeting ligand-2 (SA-ODA) will interact with the SA residue receptor cells expressed on neuronal cells present inside the brain (Bondioli et al., 2011). This interaction will allow the NPs to stay longer inside the brain region close to neuronal cells, thereby, helps to increase the drug concentration in the brain.

Thus, a novel formulation with dual targeting ligands was developed to enhance the drug concentration in the brain for the treatment of brain disorders. RV was selected as a model drug for the development and evaluation of nanoparticulate formulations for the nose to brain targeting. The developed NPs was also loaded with C-6 along with the RV because C-6 is used as a diagnostic model drug for the various studies and a fluorescent marker which can be easily detected.

The nasal route of administration of dual ligand NPs will provide an alternate and efficient route for CNS delivery of RV to improve brain bioavailability and minimize the cholinergic side effects. A novel nasal delivery also offers significant advantages in terms of ease of delivery, pain-free administration, ability to bypass the BBB, and reduce the systemic drug metabolism which limits the drug concentration in the brain. Thus, the synthesis and development of this novel nanoparticulate technology is not limited to this drug but represents a platform technology potentially applicable for delivery of therapeutic molecules targeting other neurodegenerative disorders.

1.7 Overall objectives

The overall aim of this project was to develop an effective nanoparticulate based platform technology which can promote the delivery of therapeutics molecules like RV into the brain through IN administration. This system was aimed to enhance the drug delivery into the brain and possible to extend the drug retention in the brain to maximize the therapeutic effects and minimize the drug distribution to non-targeted areas, thereby reducing peripheral adverse effects. The objective was achieved via following steps:

- Synthesis and characterisation of various functionalised polymeric ligands such as
  - TGC via conjugating thioglycolic acid to GC using selective carbodiimide reaction
  - TAT-conjugated mPEG polymer
- Development and validation of a suitable RP-HPLC method for analytical determination of both RV and C-6 concentration *in-vitro* and in biological samples.
- Design, development, and formulation of various types of polymeric PLGA NPs using single ligand or dual ligand such as
  - RV+C-6 loaded PLGA-SA-ODA NPs (single ligand)
  - RV+ C-6 loaded PLGA-SA-ODA NPs coated with GC (dual ligand)
  - RV+ C-6 loaded PLGA-SA-ODA NPs coated with TGC (dual ligand)
- *In-vitro* evaluation of designed PLGA polymeric nanoformulations to determine the encapsulation efficiency, drug loading, release profile and stability characteristics.
- *In-vivo* evaluation of the developed PLGA nanoformulation modified with one and two targeting ligands for brain targeting via nose to the brain pathway. The *in-vivo* studies were conducted to evaluate:
  - Pharmacokinetic profile of the developed nanoformulation against control drug solutions administered by IV and IN routes.
  - Brain targeting efficacy of the developed NPs administered via IN.

1.8 Thesis overview

This project is focused on the development and evaluation of a novel nanoparticle formulation for enhancement of RV delivery into the brain via IN administration. The whole thesis is divided into four main chapter followed by general discussion and conclusion. The summary of rest of the chapters are as follows:

- The second chapter describes the synthesis and characterisation of two modified polymeric ligands: TGC and mPEG-CONH-TAT. The TGC was eventually employed to physically coat the nanoparticulate formulations whereas, synthesized mPEG-TAT was not used further due to its low yield.
- The third chapter deals with the development and validation of various analytical methods that has been employed for analysis of RV and C-6 during various stages of this project.
- The fourth chapter explained the formulation, development, and evaluation of PLGA NPs coupled with various synthesized targeting ligands. Various parameters have been studied and optimized for the successful development of single ligand and dual ligand functionalized PLGA NPs.
- The fifth chapter reports the *in-vivo* evaluation of the developed PLGA based nano-formulations and assesses the potential use of single ligand and dual ligands PLGA NPs for its brain targeting efficacy via nose to the brain pathway. The NPs were loaded with both RV and C-6 for determination of their pharmacokinetic profile and brain uptake.

2. Chapter-2 Synthesis and Characterisation of Functionalised Targeting Ligands

2.1 Introduction

There is extensive use of natural or semi-synthetic polysaccharides in the pharmaceutical and biomedical industries due to their biodegradability, non-toxicity, low immunogenicity, biocompatibility and ease production by living organisms (Wilson et al., 2011; Zalipsky, 1995). These polysaccharides are abundant in nature and have the capacity to form physical and chemical bonds with a wide variety of therapeutically active drug molecules. GC is water soluble chitosan derivative with the mucoadhesive property itself and its chemical modifications of chitosan do not alter the fundamental skeleton of chitosan and amino groups would maintain its original biochemical properties while mean time with enhanced solubility which leads to potentially better targeting (Figure 1.4). We have selected GC, a base polymer for the synthesis of TGC which will be further employed as a targeting ligand-1 for the surface coating of the developed NPs. All the properties of GC and TGC have been already discussed in section 1.4.3.

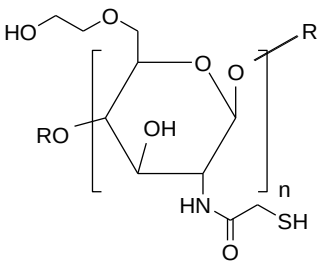

Thiolated Glycol Chitosan

Figure 2.1: Chemical structure of Thiolated glycol chitosan

PEGs are another established polymer of interest with varying molecular weight. They are gaining a lot of interest in biological fields due to their hydrophilic, non-toxic and biodegradable nature. Furthermore, pegylation, which is an attachment of the PEG molecule to a protein/peptide or therapeutic drug molecule, does further enhance the pharmacokinetics and pharmacodynamics properties and protects the cargoes from removal by RES, enzymatic degradation and renal clearance. Due to this property, it leads to increased blood circulation and reduced cytotoxicity (Malhotra et al., 2013). Despite of the fact that PEGylation enhances the hydrophilic nature of the polymer

which leads to biocompatibility and extension of the NPs' residence time *in-vivo*, increasing the success of the drug targeting, however, PEGylation of NPs also has been reported to be related to a pronounced reduction of cellular uptake in comparison to bare NPs (Pelaz et al., 2015). Hence, incorporating a cationic cell penetrating peptide into the NPs may encourage NPs interaction with negatively charged cell surface in order to enhance the cellular uptake of NPs. For this purpose, conjugate the basic domain of TAT peptide (Arg-Lys-Lys-Arg-Arg-Gln-Arg-Arg-Arg) with mPEG to increase the translocation of NPs across the biological membrane.

2.2 Objectives

The primary objectives of this study were to synthesis biodegradable targeting ligands which can be used for providing the NPs with strong interaction with mucosa membrane and or olfactory epithelium in the nasal cavity and capable of enhancing NPs transport into the brain. This is achieved by using selective synthetic approaches with the following steps:

1. Synthesis and characterisation of TGC polymer.
2. Synthesis of TAT peptide conjugated mPEG polymer
    a. Synthesis and characterisation of mPEG carboxyl derivative (mPEG-COOH) from the mPEG polymer.
    b. The conjugation of mPEG-COOH polymer with TAT peptide
    c. The optimization of the PEG grafting conditions which enables successful conjugation of TAT peptide onto the mPEG derivative and exploration of suitable purification methods to extract TAT peptide tagged PEGylated derivative from the reaction mixture.

2.3 Materials

Methoxy Polyethylene Glycol (mPEG) (Average Mw: 2000, 202509-500 gm), Fluorescamine (>98%, F9015-100 mg), N-Hydroxysucciniimide (NHS) (98%, 130672-25 gm), Chloroacetic acid (>99.0%, 402923), Thioglycolic acid (>98%, T3758-250 mL), GC, (Mw 250 kDa: G7753-5g), 5,5′-Dithiobis(2-nitrobenzoic acid) (DTNB or Ellman's Reagent), Potassium permanganate ($KMnO_4$) and Potassium hydroxide (KOH), Sodium Chloride, Sodium Hydroxide, Dichloromethane and sodium hydride were purchased from Sigma-Aldrich Company (Castle Hill, NSW, Australia). A TAT peptide (Arg-Lys-Lys-Arg-Arg-Gln-Arg-Arg-Arg) having a molecular weight of 1339.63 g/mole (pI 12.81) and 1-Ethyl-3-(3-dimethylamino) propyl carbodiimide (EDC), was purchased from GL Biochem Ltd, (Shanghai) China.

Dialysis bag (cellophane membrane, the various molecular weight cut off) was purchased from Spectrum Laboratories Inc (Rancho Dominguez, USA). Tetrahydrofuran (THF), Dimethyl sulphoxide (DMSO), Dimethylformamide (DMF) and Dichloromethane (DCM) was purchased from Thermo Fischer Scientific Company (Australia) and stored over the molecular sieves (4A°). Ultrapure Milli-Q water was used throughout all the procedures and experiments. All other chemicals used for analysis was of HPLC grade unless otherwise specified.

2.4 Methods

2.4.1 Synthesis of TGC

The amino group of GC was chemically modified via selective acylation with thioglycolic acid using carbodiimide crosslinker approach *i.e.* activation of the carboxylate group of thioglycolic acid with EDC and NHS and conjugation with GC by following a method of Makhlof and his colleagues (Makhlof et al., 2010).

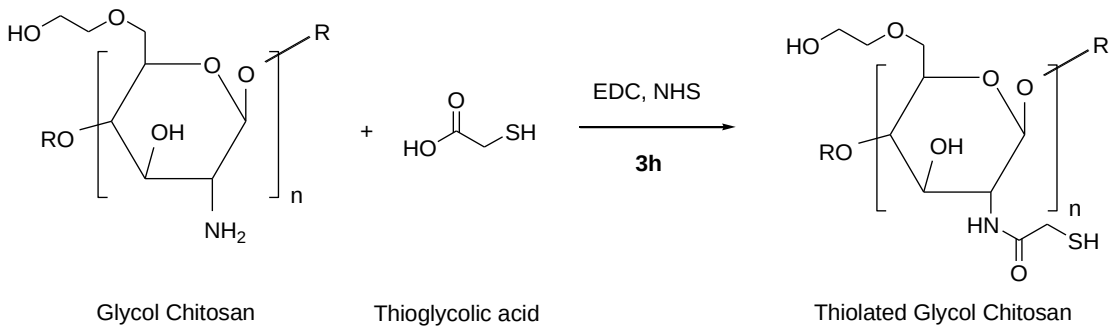

Figure 2.2: Synthesis of TGC from GC using selective carbodiimide-mediated acylation

Initially, GC (0.002 mmol, 500 mg) was dissolved in 50 mL of 0.1% acetic acid solution. Further, 30 mL of thioglycolic acid, EDC (0.645 mmol, 100 mg) and NHS (0.52 mmol, 60 mg) were dissolved in above reaction mixture and pH was adjusted to 5.0 using 3N sodium hydroxide solution. The reaction mixture was stirred for 3 h in the dark at room temperature to achieve maximum thiolation. The modified TGC was purified using a dialysis tube (molecular weight cut-off 12KDa). The dialysis medium was changed 5 times, initially replacing 3 times with 5.0 mM HCl followed by 2 times with 1 mM HCl containing 1% sodium chloride for 3 days at 8°C in the dark followed by freeze drying and dried product stored at -20°C until use. Sodium Chloride was added to reduce the ionic interaction between the positively charged polymer and a negatively charged sulfhydryl group. HCl was added for complete removal of unreacted thioglycolic acid (Anitha et al., 2011). It is very unlikely that sodium

chloride remains in the samples in significant amount after dialysis. To ensure this, a simple flame test was conducted for the presence of sodium ion traces.

2.4.2 Characterisation of TGC

2.4.2.1 FT-IR characterization

Thiolation of GC leading to the formation of an amide bond between a carboxylic group of thioglycolic acid and the amino group of GC was confirmed by FT-IR spectroscopy. All FT-IR spectrum analysis was performed using 5 mg of the sample on a Perkin-Elmer UTAR TWO, FTIR Spectrophotometer (Perkin Elmer, Massachusetts, USA).

2.4.2.2 Thiol group quantification

Quantitative determination of free thiol group substitutions on GC was performed spectrophotometrically using Ellman's reagent (5,5'-dithio-bis-2-nitrobenzoic acid, DTNB) as described in the literature (Anitha et al., 2011; Bravo-Osuna et al., 2007; Hornof et al., 2003). DTNB is a water-soluble compound specifically reacting with the free sulfhydryl group present in the polymer producing a yellow colored complex with absorbance at 412 nm. Ellman's reagent was prepared by dissolving 3.0 mg of DTNB in 10 mL of 0.5 M phosphate buffer, pH 8.0.

Derivatization procedure for thiol group determination

Briefly, 2 mg/mL of TGC polymer solution was prepared in milli-Q water. To 1.0 mL of the TGC solution (containing 2.0 mg of TGC polymer), 1.0 mL of phosphate buffer saline (pH 8.0) and 2.0 mL of Ellman's reagent was added. The mixture was incubated for 3 h at 37°C in dark to allow the reaction of free sulfhydryl groups with Ellman's reagent and absorbance was measured at 412 nm. A control sample (GC) was also incubated using the same procedure with similar concentration (2 mg/mL GC solution in milli-Q water).

The number of thiol groups present in the synthesized TGC polymer was determined from a standard curve constructed from 0.20 to 2.0 mM of thioglycolic acid in water after subtracting absorbance of the control samples (Anitha et al., 2011). The various

concentration of thioglycolic acid was prepared and derivatized similarly as that of the unknown sample.

2.4.3 Synthesis of mPEG carboxylate polymer

Functionalisation of a polymer with acid terminal groups is essential for attaching targeting ligands such as TAT peptide for drug targeting. The hydroxyl group of mPEG was converted into the carboxylic group. This carboxyl group was further adjoined with the amino group of the TAT peptide using a selective carbodiimide-mediated coupling. To convert the hydroxyl group into the carboxylic group we compared two methods (i) the carboxylic group was introduced by the nucleophilic substitution reaction of chloroacetic acid with mPEG (ii) direct oxidation of terminal hydroxyl group in mPEG.

2.4.3.1 Nucleophilic substitution reaction

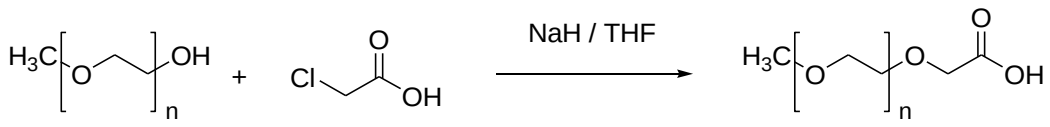

mPEG-2000 Chloroacetic acid mPEG-carboxylate polymer

Figure 2.3: Synthesis of mPEG-carboxylate polymer using nucleophilic substitution reaction (Scheme I)

In Scheme-I, mPEG with acid terminal was synthesized by grafting chloroacetic acid to a mPEG molecule in the presence of sodium hydride in THF. Briefly, mPEG (1.0 mmol, 2.0 g) was dissolved in 10 mL of THF, then a suspension of sodium hydride (10 mmol; 240 mg) in THF was added dropwise and the reaction mixture was stirred at 40°C under a nitrogen atmosphere for 4 h. After 4 h, chloroacetic acid (5 mmol; 472.5 mg) was added and the reaction mixture was stirred at 60°C for 48 h. After 48 h, the reaction mixture was washed with 30 mL of ultrapure milli-Q water to decompose the excess of sodium hydride and then extracted with dichloromethane. The organic layer was mixed with anhydrous sodium sulfate for overnight to remove residual water, then filtered and concentrated under reduced pressure using a rotary

evaporator (Buchi Rotavapor, R-200, Flawfil Switzerland). mPEG-Carboxylate (mPEG-COOH) was then dried in a vacuum oven overnight. The purified mPEG-COOH was stored in an air-tight container at -20°C and was characterized by FT-IR and ^{1}H-NMR spectroscopy. The ^{1}H-NMR analysis was performed on a Bruker Avance III AVN 400 spectrometer (400.1 MHz for ^{1}H-NMR, Bruker, USA).

2.4.3.2 Direct oxidation method

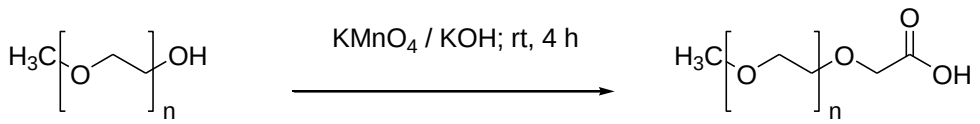

mPEG-2000 mPEG-carboxylate polymer

Figure 2.4: Synthesis of mPEG-carboxylate polymer using direct oxidation method (Scheme II)

The mPEG-COOH was also prepared using direct oxidation via a modification of the method reported by (Heimann & Vögtle, 1980). Briefly, mPEG (5 mmol; 10.0 g) and KOH (10 mmol; 560 mg ;) was dissolved in 50 mL of water. An aqueous solution of $KMnO_4$ (10 mmol; 1.6 g in 20 mL) was added dropwise and the reaction mixture was stirred on ice bath for 4 h. After 4h, pH of the reaction mixture was adjusted to 2 or lesser and the product was extracted with dichloromethane. The organic layers were combined and dried over anhydrous sodium sulfate in order to remove the residual water, then filtered and concentrated under reduced pressure using a rotary evaporator. The mPEG-COOH was then dried in a vacuum oven at 40°C overnight. The purified mPEG-COOH was stored in an airtight container at -20°C and was characterized by FT-IR and ^{1}H-NMR spectroscopy.

2.4.4 Synthesis of mPEG-CONH-TAT polymer

The conjugation of mPEG-COOH to TAT peptide was achieved by selective carbodiimide coupling reaction, using EDC and NHS. This reaction involves the formation of the unstable reactive intermediate ester derivative. The detailed mechanism of amide bond formation between TAT and mPEG is represented in Figure 2.5.

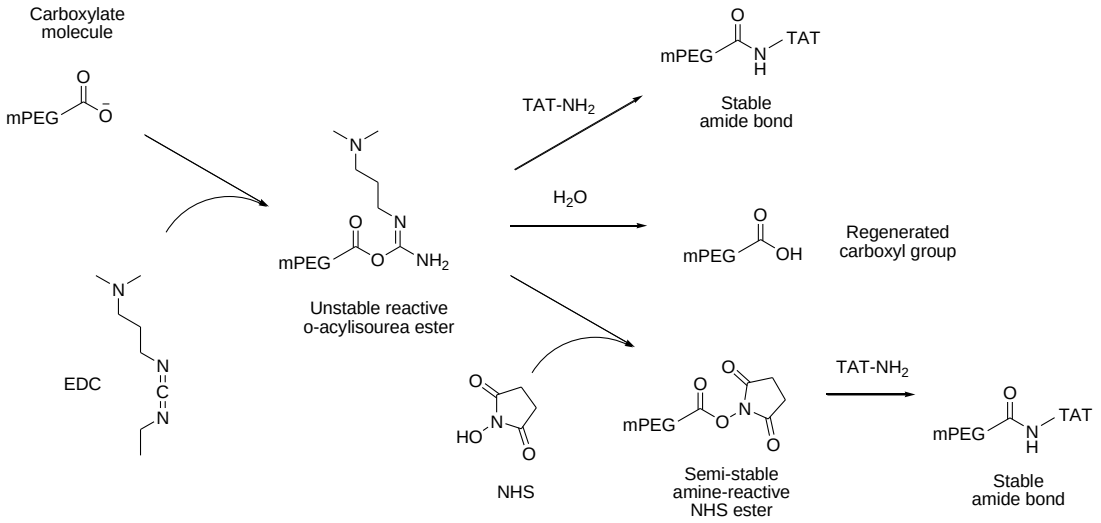

Figure 2.5: Reaction mechanism of mPEG with EDC, NHS and TAT peptide
mPEG carboxylate molecule reacts with EDC produces intermediary an unstable urea derivative which couples with NHS generating semi-stable highly reactive ester derivative that further reacts with amine nucleophile and forms a stable amide bond.

2.4.4.1 General procedure used for TAT conjugation to mPEG

The coupling reaction of the mPEG-COOH polymer with TAT peptide was performed in a single pot system following the Malhotra and her colleague's procedure (Malhotra et al., 2013). The conjugation reaction was carried out in a single step reaction, the carboxyl group of the functionalized PEG molecule was activated in situ using EDC and NHS and reacted with an amino group of a peptide molecule, which is also present in the reaction mixture.

To the synthesized mPEG-COOH (0.02 mmol; 40 mg) in 2 mL of water, EDC (0.1 mmol; 19.2 mg) and NHS (0.5 mmol; 57.5 mg) were added and the reaction mixture was stirred for 2 h for the activation of carboxylic group. After 2 h, the pH of the reaction mixture was raised to 10.0 (near to the isoelectric point of TAT peptide). TAT peptide (0.02 mmol; 26.7 mg), previously dissolved in the water was added to the reaction mixture and mixture was stirred for 24 h at room temperature to form a mPEG-TAT-conjugated polymer. The conjugated polymer was purified using dialysis technique (Spectra/Por Dialysis membrane, molecular weight cut-off 2000 Da, Diameter: 11.5 mm, volume: 1.1 mL/cm, length 5 m, Rancho Dominguez, USA) at room temperature to remove the unreacted polymer and its by-products. The conjugated mPEG-CONH-TAT polymer was dried using freeze dryer. The purified dried product was stored in airtight container at -20°C and was characterized by fluorescamine assay method described in section 2.4.6.1.

To conjugate mPEG-COOH with TAT peptide, various reaction conditions were optimized which are explained below.

(a) Effect of type of reaction solvent on TAT conjugation

The selection of solvents for chemical reaction often plays a critical role in the success and efficiency of the reaction. In order to determine the effect of reaction medium on the conjugation reaction of TAT peptide with the mPEG-COOH molecule and reaction feasibility, various solvents such as DMSO, DMF+DMSO, water and MES buffer (pH 6.0) were employed. Four different sets of reactions were conducted following the general procedure and similar amount of the reaction components as mentioned in section 2.4.4.1. The effect of the reaction solvent on TAT conjugation was determined by analyzing the dried product using fluorescamine assay method.

(b) Effect of EDC molar ratio on TAT conjugation

EDC required to activate the carboxylic group of the mPEG-COOH polymer. The molar ratio of the EDC was optimized to accomplish better TAT conjugation efficiency to the mPEG polymer. Experiments were performed utilizing five and ten mmol excess of EDC with respect to the mPEG-COOH amount used in the reaction to ensure a sufficient degree of mPEG-COOH activation. The TAT conjugation chemical reaction was performed in water using similar conditions and general procedure was followed as described in section 2.4.4.1. The reactions were performed using water as a reaction medium with 2 h of pre-activation time and 24 h of reaction stirring time at room temperature. The synthesized conjugated products were analyzed using fluorescamine assay method to determine the effect of the molar ratio of EDC on the level of the TAT conjugation on the mPEG polymer.

(c) Effect of coupling reaction time on TAT conjugation

Optimization of reaction time was very crucial for the extent of TAT conjugation on the mPEG-COOH polymer. Therefore, we investigated the effect of the conjugation reaction time on the effectiveness of TAT grafting on the mPEG-COOH molecule. Three different types of conjugation reaction were performed at different time intervals viz. 4 h, 24 h, and 48 h.

For this, the synthesized mPEG-COOH (0.02 mmol; 40 mg) in 2 mL of water, EDC (0.2 mmol; 39 mg) and NHS (0.5 mmol; 57.5 mg) were added and the reaction mixture was stirred for 2 h for the activation of carboxylic group. After 2 h, the pH of the reaction mixture was raised to 10.0 (near to the isoelectric point of TAT peptide) and TAT peptide solution (0.02 mmol; 26.7 mg dissolved in the 1 mL of water) was added to the reaction mixture. All the three different set of reaction mixtures were stirred for three different time intervals viz. 4 h, 24 h and 48 h at room temperature to optimize the coupling reaction time to form a mPEG-TAT conjugated polymer. The conjugated polymer was purified using dialysis, freeze dried and analyzed using fluorescamine assay method.

(d) Effect of pre-activation time on TAT conjugation

The influence of pre-activation time of carboxyl group of mPEG-COOH polymer on conjugation efficiency was studied in two sets of reactions. The pre-activation time of the carboxyl group of mPEG-COOH was carried out with 20 min and 40 min followed by the 4 h stirring time after adding the TAT peptide. All the set of reaction parameters were similar as mentioned in section 2.4.4.1 (c) except the pre-activation time. After pre-activation of mPEG-COOH, the reaction mixture was stirred for 4 h for TAT conjugation with activated mPEG-COOH polymer. The conjugated product was purified using dialysis of the reaction mixture in milli-Q water for 24 h and freeze dried. The extent of TAT conjugation over mPEG molecule was monitored by analyzing the dried conjugated products using fluorescamine assay.

(e) Effect of Temperature on the TAT conjugation

To determine the effect of temperature on the conjugation reaction, we performed three different set of reactions. The three different sets of TAT conjugation reaction was carried out at room temperature (25°C), 40°C and 48°C with equimolar concentrations of reactants. Briefly, all the three sets of reactions were conducted in water with an initial activation of the mPEG-COOH at room temperature for 20 min and, after addition pH of reaction mixture was raised to 10.0. TAT peptide (previously dissolved in water) was added to the reaction mixture and the temperature was further increased to 40°C and 48°C for sets II and III, respectively. The conjugated polymer was purified by using dialysis technique against milli-Q water for 24 h and freeze dried further. The dried products were analysed using fluorescamine assay method to evaluate the effect of the temperature on the TAT conjugation onto mPEG molecule.

The summary of all the parameters optimized during the reaction optimization is represented in Table 2.1.

Table 2.1: Optimization parameters studies during mPEG-CONH-TAT conjugation reaction

Optimization step	**Factors Optimized**					**Optimized conditions**
	Reaction solvent	**Activating agent**	**Conjugation Reaction time**	**Temperature**	**Purification**	
Aqueous vs non-aqueous	Water/DMSO/DMF+ DMSO/ MES buffer (pH 4.5)	EDC (0.1 mmol)	24 h	25°C	Dialysis	Aqueous Medium
EDC Molar ratio	Water	EDC 0.1 mmol or 0.2 mmole	24 h	25°C	Dialysis	0.2 mmol (10 times higher as compared to mPEG amount)
Coupling reaction time	Water	EDC (0.2 mmol)	4 h/ 24 h/ 48 h	25°C	Dialysis	4 h
Pre-activation time	Water	EDC (0.2 mmol)	20 min/40 min pre-activation time with 4 h total reaction time	25°C	Dialysis	20 min pre-activation time with 4 h total reaction time
Reaction Temperature	Water	EDC (0.2 mmol)	40 min pre-activation time with 4 h total reaction time	25°C/40°C/48°C	Dialysis	25°C
Product purification	Water	EDC (0.2 mmol)	40 min pre-activation time with 4 h total reaction time	25°C	Dialysis/ Size exclusion chromatography	Size exclusion chromatography

2.4.4.2 Optimized procedure for mPEG-CONH-TAT synthesis

After optimization of several reaction parameters, we used the following final procedure for the synthesis of the mPEG-CONH-TAT peptide. To synthesized mPEG-COOH (0.02 mmol; 40 mg) dissolve in 10 mL of 0.1M MES buffer (pH-6.0), EDC (0.2 mmol; 38.3 mg) and NHS (0.5 mmol; 57.5 mg) were added and the reaction mixture was stirred for 20 min for the activation of carboxylic group. After 20 min, excess EDC was neutralized by adding 2-mercaptoethanol (14 µL) and the pH of the reaction mixture was raised to 10.0 (near to the isoelectric point of TAT peptide) using sodium bicarbonate-carbonate buffer. TAT peptide (0.02 mmol; 26.7 mg), previously dissolved in sodium bicarbonate-carbonate buffer, was added to the reaction mixture and stirred for 4 h to form mPEG-TAT conjugated polymer. The conjugated polymer was purified using dialysis technique (Spectra/Por Dialysis membrane, molecular weight cut-off 2000 Da, Diameter: 11.5 mm, volume: 1.1 mL/cm, length 5 m) at room temperature for 24 h or size exclusion chromatographic technique to remove the unreacted polymer, and its by-products. The conjugated mPEG-CONH-TAT polymer was dried using freeze dryer. The purified dried product was stored in airtight container at -20°C and was characterized by fluorescamine assay method.

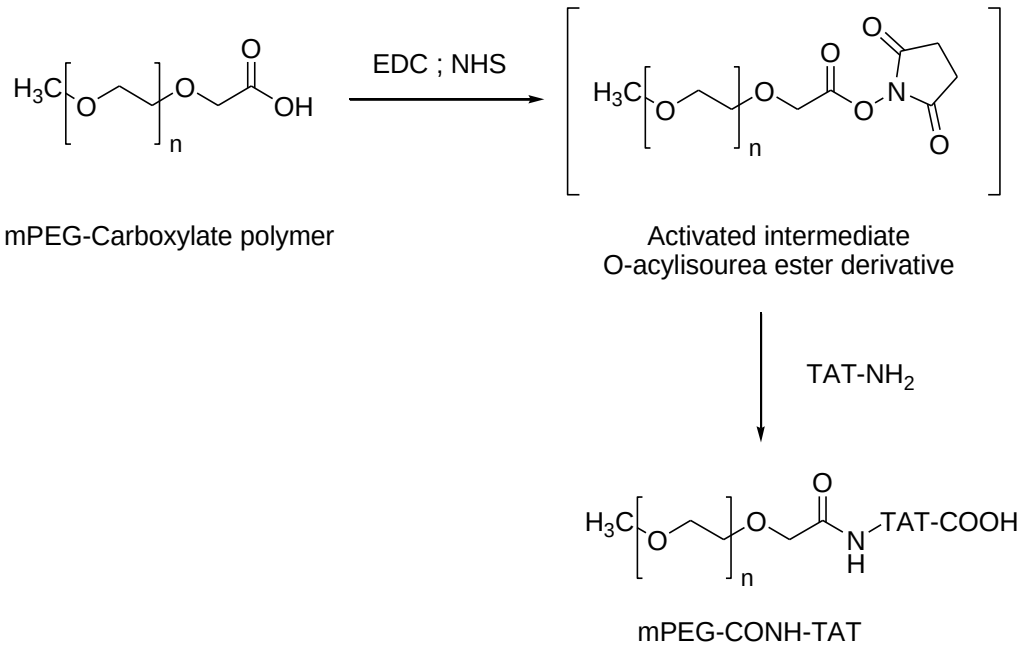

Figure 2.6: Synthesis of mPEG-TAT polymer via amide bond formation

2.4.5 Purification of mPEG-CONH-TAT conjugate

Purification of the functionally modified mPEG-TAT conjugated polymer should be performed under mild conditions to avoid modifying its nature and to provide acceptable quality and quantity of the material. Due to the high cost of TAT peptide, isolation of mPEG-TAT from the reaction mixture was employed in a small volume to optimize the in-process purification parameters. Two different methods of purification of mPEG-TAT conjugate were carried out to separate it out from the remaining reaction mixture.

2.4.5.1 Dialysis technique

It was expected to get an increase in the molecular weight of mPEG polymer after tethering it with TAT peptide. Thus, the isolation of conjugate polymer was accomplished by using dialysis membrane owing to its increased molecular weight. For this, mPEG-TAT complex was purified using dialysis membrane to remove unreacted polymer and its by-products (Spectra/Por Dialysis membrane, molecular weight cut-off 2000 Da, Diameter: 11.5 mm, volume: 1.1 mL/cm, length 5 m, Rancho Dominguez, USA) at room temperature. Purification was performed using 1 L of water as a medium for the removal of unreacted reaction material. During first 8 h, water was changed after every 2 h to avoid the saturation conditions and dialysis was performed for 24 h.

2.4.5.2 Purification by Size exclusion

Size exclusion technique was another technique used to purify the mPEG-TAT conjugated polymer from the reaction mixture. Samples were purified using a Bio Scale^{TM} Mini Bio-Gel® P-6 Desalting column (Bio-Rad laboratories Inc., Australia) connected to size exclusion chromatography (AKTA explorer 10XT (GE Healthcare Technologies, Australia)). Purification of PEGylyated TAT peptide was performed using degassed 50mM PBS buffer (pH 7.2) at flow rate 0.5 mL/min. Various components of the reaction mixture were separated based on their molecular sizes and their elution profiles were monitored by following UV spectroscopy measuring absorbance at 200, 205 and 210 nm.

2.4.6 Analytical method for TAT characterisation

2.4.6.1 Fluorescamine assay

The fluorescamine assay method was used for the determination of TAT conjugated to the mPEG polymer and free TAT peptide released into the dialysis medium. Fluorescamine interacts with primary amino groups of TAT peptide in the picomole range to yield fluorophores in a fraction of seconds (Figure 2.7). The intensity of fluorophores was used as a marker to determine the TAT content, while the excess of fluorescamine rapidly hydrolysed to give non-fluorescent products.

The fluorescamine derivatization method used in this study was adapted from the method described by Bae and his colleague (Bae et al., 2000). A standard solution of TAT at 20 µg/mL was prepared in water, derivatized with fluorescamine and scanned for excitation and emission using Varian Cary Eclipse spectrofluorometer (Varian Technologies, Australia). Based on these results, excitation and emission wavelengths for the fluorescence analysis were adjusted at 390 nm and 485 nm, respectively.

Derivatization method for fluorescamine assay

To each 500 µL of TAT peptide solution, 500 µL of 0.05% w/v fluorescamine dissolved in acetone and 1.5 mL of 60 mM boric acid buffer pH 9.0 were added. The solution was incubated for 5 min at room temperature before its fluorescence was measured using Varian Cary Eclipse spectrofluorometer. Blank solutions consisting of water, boric acid buffer and fluorescamine in acetone were used to correct for fluorescence background. The degree of fluorescence was recorded after subtracting the blank. The amount of peptide content in the unknown samples was then determined using a calibration curve prepared from the TAT standard concentration.

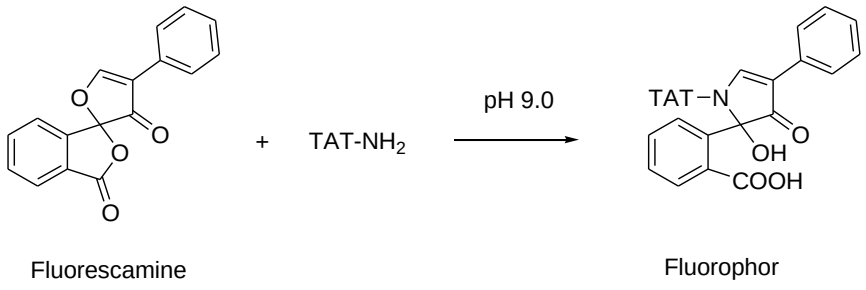

Figure 2.7: Derivatization reaction between fluorescamine and TAT peptide

2.5 Results and Discussion

2.5.1 Synthesis and characterisation of TGC

TGC was synthesized successfully by the amide bond formation between carboxylic group of thioglycolic acid and the amino group of GC as shown in Figure 2.2. The product obtained was 82.0% in yield, white in color, fibrous in structure, and odorless.

2.5.1.1 FT-IR Characterisation

Both GC and TGC showed a broad band around 3343 cm^{-1} due to stretching vibration of NH_2 and OH group involved into the inter and intramolecular hydrogen bonding (i.e., $\nu_{(O-H)}$ and $\nu_{(N-H)}$) and 2868 cm^{-1} due to $\nu_{(C-H)}$ stretching vibrations. The peaks at 1057 cm^{-1} represented the pyranose ring. The peaks at 1651 cm^{-1} and 1586 cm^{-1} were attributed to the presence of $\delta_{(N-H)}$ vibrations in GC spectra which represent the peak of the amino group present in the GC [Figure-2.8 (A)].

Considering FT-IR spectra of TGC, [Figure-2.8 (B)] all peaks were present except the amino group peaks corresponding 1651 cm^{-1} and 1586 cm^{-1}, as the GC amino group reacted with the carboxylic group of the thioglycolic acid successively forming an amide bond. The appearance of the amide bond formation can be seen at 1627 cm^{-1} (Amide-I band) and 1519 cm^{-1} (Amide-II band). The disappearance of the peak at 1651 cm^{-1} and the appearance of the amide bands indicates the successful conjugation of the thiol moiety with GC. The weak peak at 2323 cm^{-1} corresponded to SH group thus confirming the conjugation between thioglycolic acid and a primary amino group of GC (Anitha et al., 2011). It is expected that FT-IR is not sensitive enough to detect SH group tagged to the GC moiety. It is, therefore, another method which involves the use of the Ellman's reagent was employed for the analysis of the thiol groups attached to GC molecule.

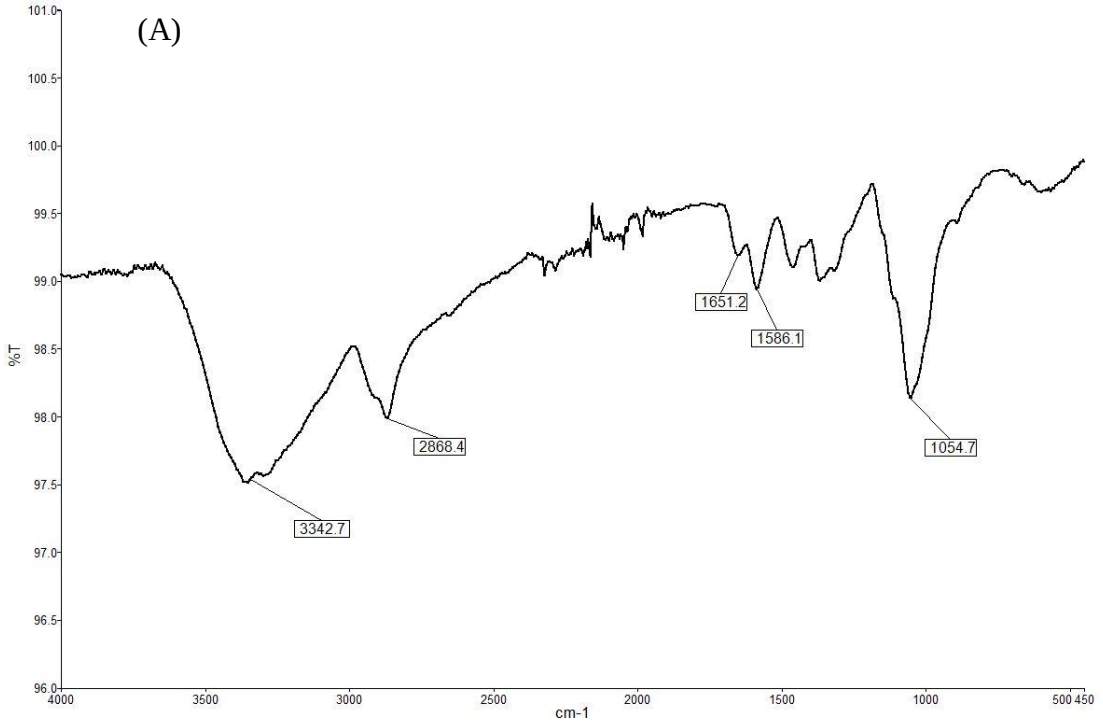

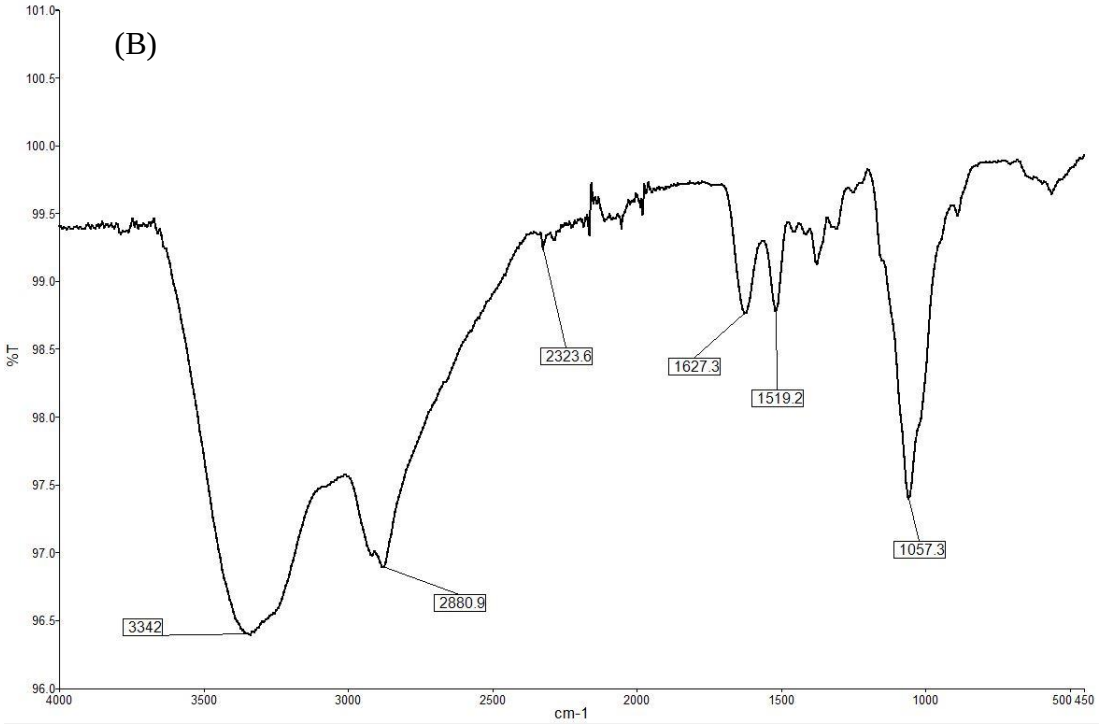

Figure 2.8: FT-IR spectrum of (A) GC (B) TGC

2.5.1.2 Thiol group quantification by Ellman's reagent

Ellman's reagent is very selective towards the -SH groups present in the polymer. It is highly sensitive in nature and can detect from 50 µM -1000 µM concentration. It produces the yellow colored complex which can be detected in the visible range (412 nm). The standard curve of thioglycolic acid was employed for the determination of the free thiol groups concentration conjugated on GC using Ellman's reagent (Anitha et al., 2011). The determined amount of micro mole of thiol group present per gram of polymer is represented in Table 2.2 and Appendix 8 (section 8.2).

Table 2.2: Determination of amount of thiol group content on synthesized TGC polymer

Sample name	Amount of –SH group content (µmol/g of TGC polymer)	Amount of -SH group Content (g/g of TGC polymer (% w/w))
TGC	881.8 ± 21.3	8.25 ± 0.19

TGC: Thiolated Glycol chitosan

2.5.2 Synthesis and characterisation of mPEG-COOH for TAT conjugation

To convert the hydroxyl group of mPEG 2000 to the carboxyl group, we attempted two different routes. According to Scheme-I, we performed nucleophilic substitution reaction using chloroacetic acid and mPEG in the presence of sodium hydride using THF as the reaction medium. In Scheme II, a straightforward direct oxidation of terminal primary alcohol functional group of mPEG with potassium permanganate in the presence of potassium hydroxide was used for the preparation of carboxylic acid functionalised mPEG. Scheme-II produced the functionalised polymer in almost 98% yield, whereas, Scheme-I produced the desired product in 65-70% of yield. The high level of purity was confirmed by FT-IR and ^{1}H-NMR spectroscopy with their characteristic signals. The FT-IR spectrum of the starting material mPEG and mPEG-COOH is shown in Figure 2.9 (A).

The FT-IR spectrum of mPEG did not show any characteristic peak in the range of 1,700-1,750 cm^{-1} indicating the absence of the carbonyl functional moiety, while the presence of a peak at 1,744 cm^{-1} in the spectra of mPEG-COOH [Figure 2.9 (B)] confirms oxidation of the terminal $–CH_2OH$ group to –COOH group. Both spectra showed a broad peak at about 2,883 cm^{-1} corresponding to $–CH_2$ stretching vibrations of mPEG backbone.

^1H NMR spectrum of mPEG in $CDCl_3$ (Figure 2.10) showed a singlet at 3.37 ppm corresponding to $–OCH_3$ group and a broad singlet at 3.63 ppm corresponding to $(−CH_2–CH_2–O)_n$ of the PEG chain. The conversion of mPEG to mPEG-COOH polymer led to the appearance of the new peak with a singlet at 4.13 ppm for $–CH_2$ group vicinal to $–O–CH_2–COOH$ and other corresponding peaks of the PEG chain remained same (Figure 2.11). The ratios of the methoxy group and a carboxyl moiety of the modified mPEG polymer samples were identified using ^1H NMR spectra by comparing integration values of signals for the methoxy group on the one side of the polymer and methylene protons on the carbon adjacent to the carboxylic acid group at the other end of the polymer.

In comparison, the direct oxidation of the terminal alcohol (Scheme II) was found to be a simpler and more effective method for the introduction of the carboxylic group to the mPEG. The success of the direct oxidation of PEG using less toxic and more environmentally friendly solvents offers a better choice for the PEG functionalization. This has significant implications as carboxylic acid PEGs are important intermediates for polymeric drug delivery systems and other fields.

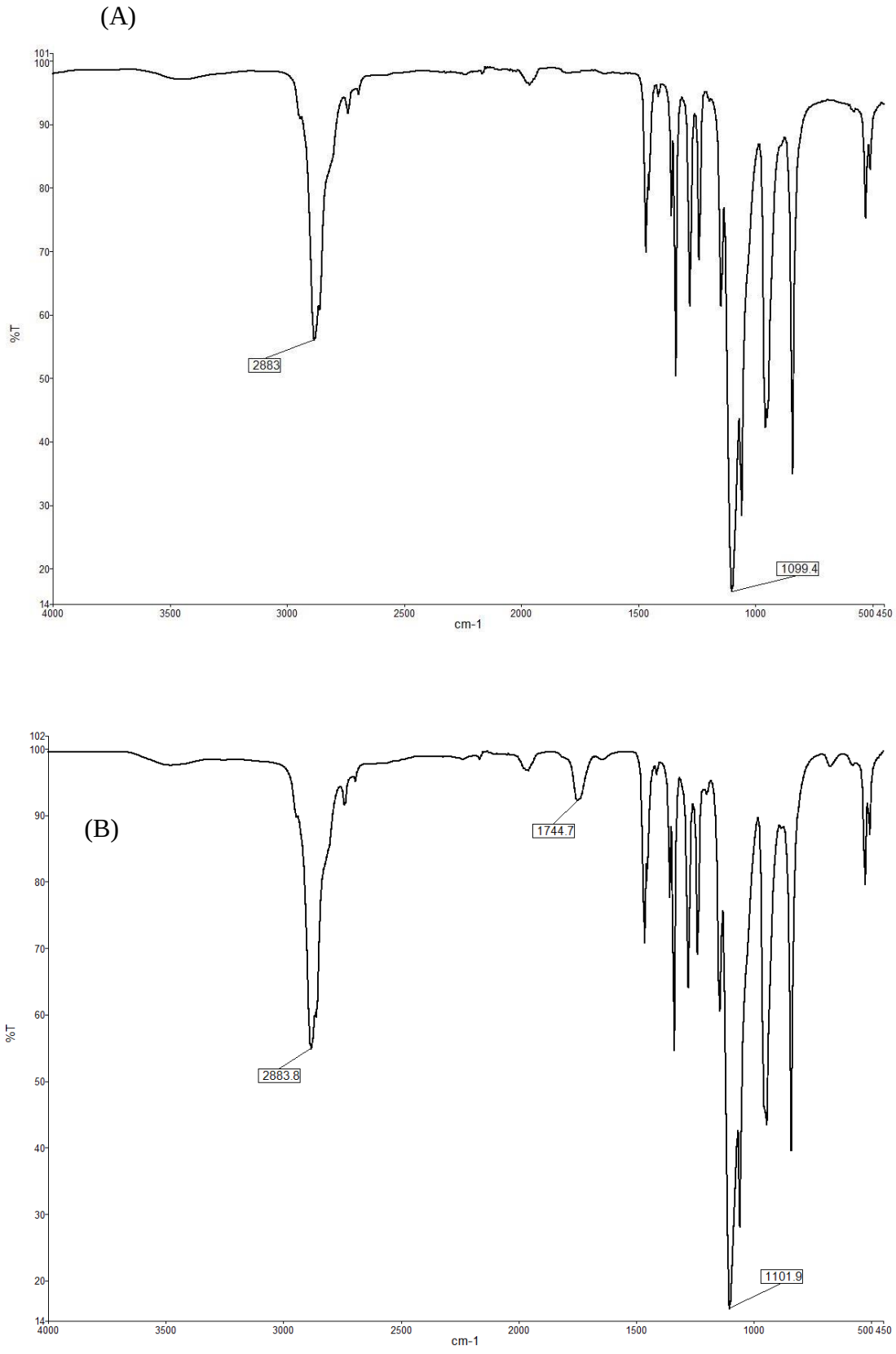

Figure 2.9: FT-IR spectra of (a) mPEG and (b) mPEG-COOH polymer

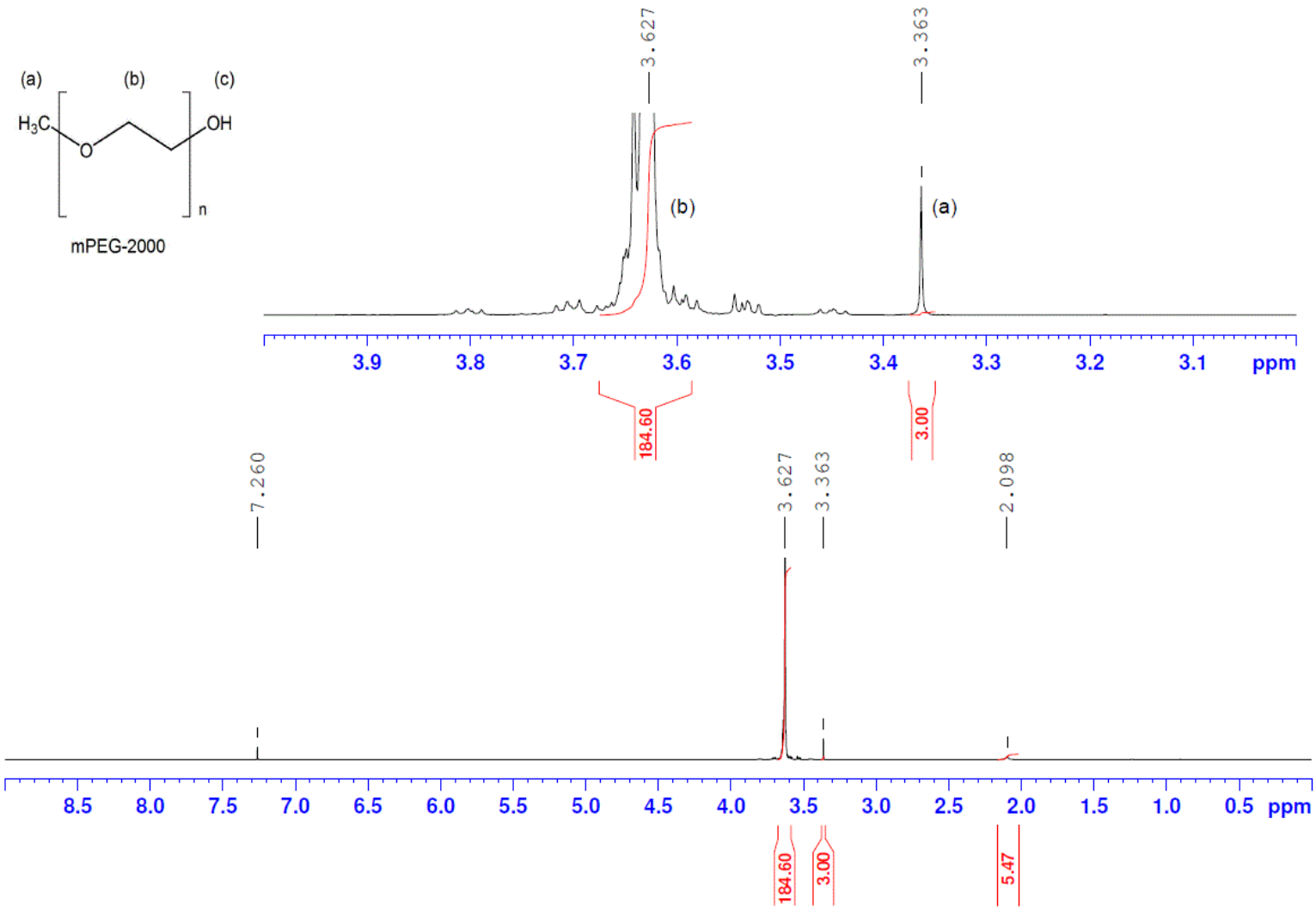

Figure 2.10: ^{1}H-NMR spectra of mPEG-2000 in deuterated chloroform

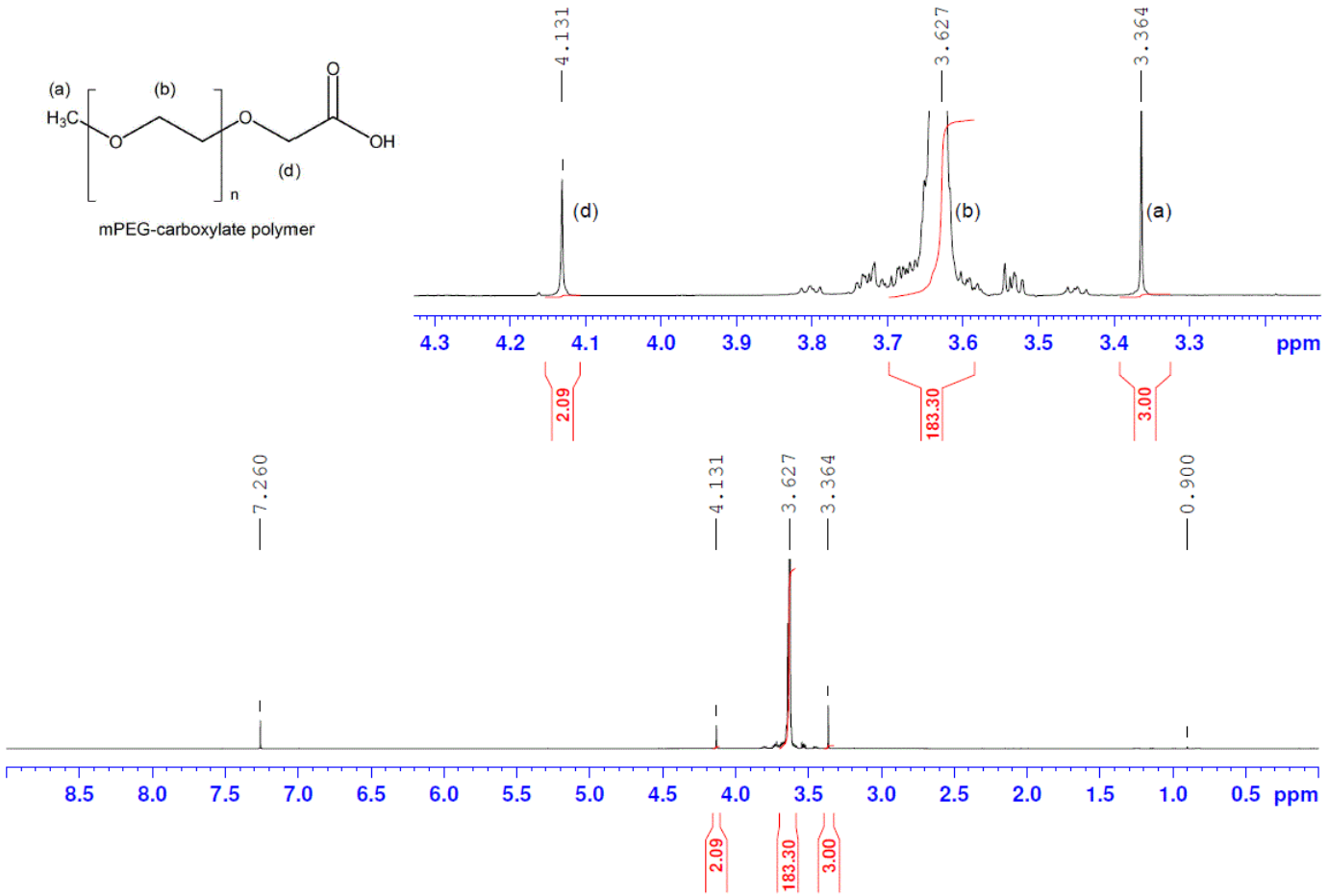

Figure 2.11: ^{1}H-NMR spectra of mPEG-COOH in deuterated chloroform obtained by a reaction of mPEG with KOH and $KMnO_4$.

2.5.3 Synthesis and characterisation of mPEG-CONH-TAT conjugate

2.5.3.1 TAT peptide fluorescamine assay method

The fluorescamine assay method was successfully developed to determine the concentration of TAT peptide in the conjugated polymer and free TAT released in the dialysis medium during the product purification. This assay method was simple, efficient and economical but it will detect both free and conjugated TAT peptide.

To ensure that only conjugated TAT peptide was analyzed in synthesized product, we determined the time required to remove all free TAT peptide from conjugated polymer by dialysis. For this, dialysis of a physical mixture of mPEG polymer and TAT peptide (in equimolar concentration to mimic the actual concentration in the reaction mixture) was performed against milli-Q water. It was found that all free TAT peptide (100 %) was released from the bag over a period of 17 hours (Figure 2.12).

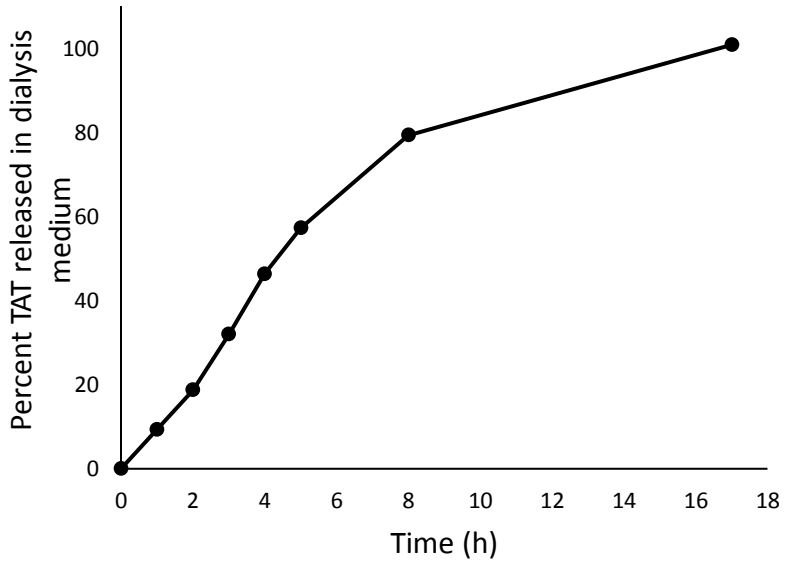

Figure 2.12: Determination of release of free TAT peptide during dialysis. Samples were taken after every hour and derivatized using fluorescamine assay method to determine the release of free TAT peptide over a time frame. Dialysis medium was changed after every hour for initial five h to avoid the saturated conditions. Data represents the percent of TAT peptide released in the dialysis medium with respect to time (n=1).

The results indicated that the presence of free unreacted mPEG-COOH polymer does not alter the release of free TAT peptide from the dialysis of physical mixture. However, dialysis of only mPEG-COOH polymer did not show any fluorescent intensity in fluorescamine assay method which further signifies that fluorescamine method is also selective to the amine group of TAT peptide. Therefore, it can be anticipated that the presence of mPEG does not affect the release of free TAT peptide. It was also confirmed that unreacted TAT peptide can be removed from the dialysis bag after dialysis over a period of 17 h. Thus, all the synthesized products were purified by dialysis against water for 24 h and characterized by using fluorescamine assay method.

2.5.3.2 Effect of type of reaction solvent on TAT conjugation

Researchers have reported the use of selective carbodiimide reaction in the presence of water/non-amine buffers for the conjugating PEG carboxylates and peptide molecule (Barrera et al., 2009; Hong et al., 2007; Wazawa et al., 2006). When water used as a reaction solvent for the conjugation of TAT peptide with mPEG-COOH polymer, we found that the degree of conjugation efficiency was enhanced significantly compared to the non-aqueous solvent systems. A similar pattern was detected when the reaction was carried out in the water/ MES buffer (pH 6.0) with a pH adjustment using sodium bicarbonate-carbonate buffer (Figure 2.13).

The TAT peptide coupled with mPEG-COOH polymer was negligible in DMF+DMSO and DMSO. Conjugation was increased significantly to 0.527 mmol of TAT peptide/mmole of conjugated polymer in presence of water as the reaction medium. The use of MES buffer (pH 6.0) didn't improve the conjugation efficiency. A similar conjugation trend was observed by Van Delden and his colleagues (Van Delden et al., 1997). Therefore, the aqueous medium was selected as a medium to perform the conjugation reaction.

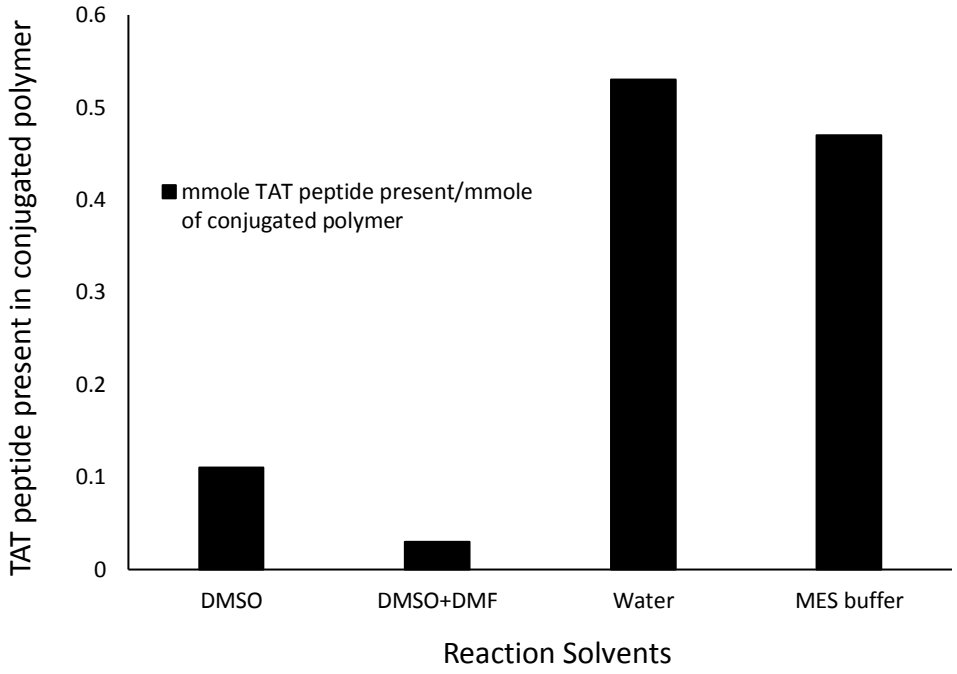

Figure 2.13: Effect of type of reaction solvent on the level of conjugation of TAT peptide onto mPEG molecule

The chemical reactions were performed in different solvents in order to determine the effect of reaction medium on TAT conjugation level onto the mPEG polymer (n=1). All the reaction parameters were similar except the change of the reaction medium.

2.5.3.3 Effect of EDC molar ratio on TAT conjugation

As demonstrated in Figure 2.14, 10 mmol equivalents of EDC showed 1.5 times better TAT conjugation level than that of 5 mmol equivalents because of maximum NHS activated ester available to conjugate with TAT peptide. Subsequently, further experiments were done using 10 mmol equivalents of EDC.

As per mentioned literature, the few millimolar concentration of EDC is sufficient to form the activated intermediate complex (Grabarek & Gergely, 1990). Since we employed ten times concentration of EDC for conducting the reaction in the one-pot system, the presence of the excess of EDC in the reaction mixture may react with the carboxyl group of the TAT peptide (NH_2-Arg-Lys-Lys-Arg-Arg-Glu-Arg-Arg-Arg-COOH). This could lead to the formation of an amide bond between TAT peptide molecules. The addition of β-mercaptoethanol or EDTA precludes the chances of cross-linking of TAT peptide by inactivating an excess of EDC (Grabarek & Gergely, 1990). For this reason, we employed β-mercaptoethanol to quench the excess of EDC before addition of TAT peptide.

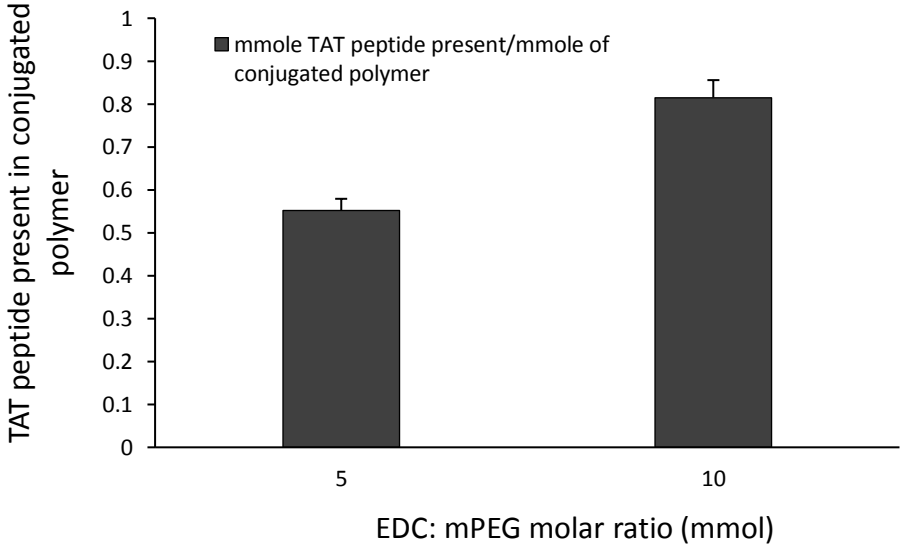

Figure 2.14: Effect of EDC: mPEG molar ratio on the level of TAT conjugation. X axis represents the two different mmol ratios of EDC were taken with respect to the mmol of mPEG-COOH used in the reaction. Data represents the mean TAT peptide present in the conjugated polymer ± SD (n=2).

2.5.3.4 Effect of reaction time on TAT conjugation

The extent of the conjugation efficiency was influenced by total reaction stirring time which is the sum of pre-activation time for carboxyl group and TAT coupling reaction time to the polymer. The conjugation efficiency of TAT peptide over mPEG-COOH molecule decreased with the increase of the coupling reaction time (Figure 2.15). The maximum TAT conjugation was achieved in 4 h, however, the presence of TAT peptide was decreased to 0.82 mmol of TAT peptide/mmol of conjugated polymer with an increase in the reaction time. The TAT peptide conjugation increased to the 0.90 mmol of TAT peptide/mmol of the conjugated polymer after increasing the reaction time from 24 h to 48 h. The possible reason could be the extent of saturation could be associated with an increase in the repulsive forces and steric hindrance caused by the already formed mPEG-TAT complex towards the TAT peptide approaching activated carbonyl group of mPEG-COOH and henceforth the conjugation becomes inhibited after a certain time-period.

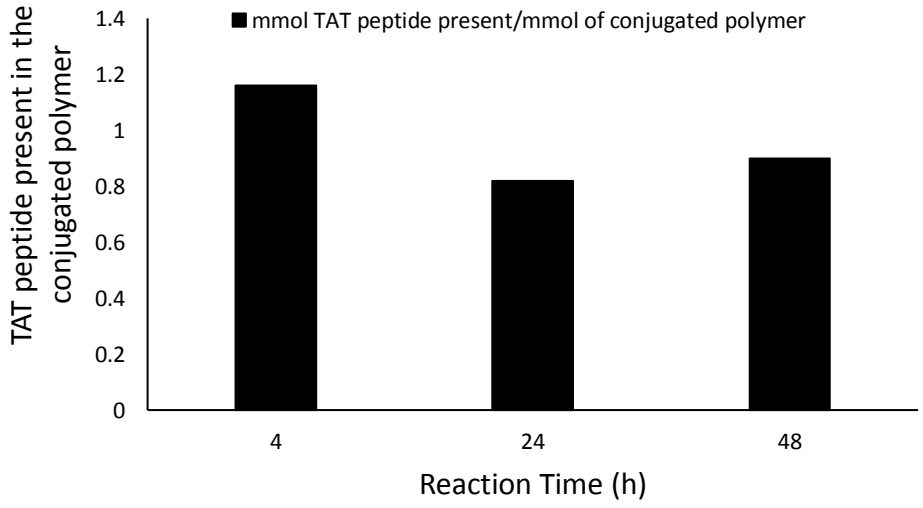

Figure 2.15: Effect of reaction coupling time on level of conjugation of TAT peptide onto mPEG molecule

All the three-different set of reactions were conducted using water as a reaction medium using similar reaction conditions except varying conjugation reaction time viz. 4, 24 and 48 h. The data represented is TAT peptide present in the conjugated polymer (n=1) for this reaction.

2.5.3.5 Effect of pre-activation time on coupling efficiency

Pre-activation time is an important parameter for the stability of the NHS ester formed. NHS-ester is optimally stable at neutral pH (half-life is 4-5 h), however, its stability fluctuates with a change of the reaction medium pH. Therefore, it is important to determine the optimal pre-activation time. It was observed in the fluorescamine assay that the product of the reaction with 20 min pre-activation contained 0.47 mmol of TAT peptide present/mmol of the polymer compared to 0.43 mmol of TAT peptide per/ mmol of the polymer for the reaction with 40 min pre-activation. Hence, it can be concluded that the reaction performed with 20 min pre-activation time gave better results compared to the reaction with the pre-activation time increased to 40 min.

2.5.3.6 Effect of temperature on conjugation efficiency

There was a significant increase in TAT conjugation after raising the temperature from room temperature to 40°C. Conjugation efficiency decreased with a further increase in temperature to 48°C (Figure 2.16). Emoto and his colleagues (Emoto et al., 1996) studied the impact of various factors, such as temperature and pH, on the grafting efficiency of polyethylene glycol oxide derivatives to amino-derivatized quartz. They envisaged that a change in temperature influences the grafting kinetics. Their results showed that 35°C is the optimum temperature for grafting. We obtained similar results for our conjugation process. Hence it can be concluded that optimal temperature of the conjugation reaction is 40°C at which the conjugation efficiency was accelerated. However, the increase in temperature can also cause the increase of side reactions such as hydrolysis which could here negative impact on the conjugation. This could be the reason for the reduced conjugation seen at 48°C.

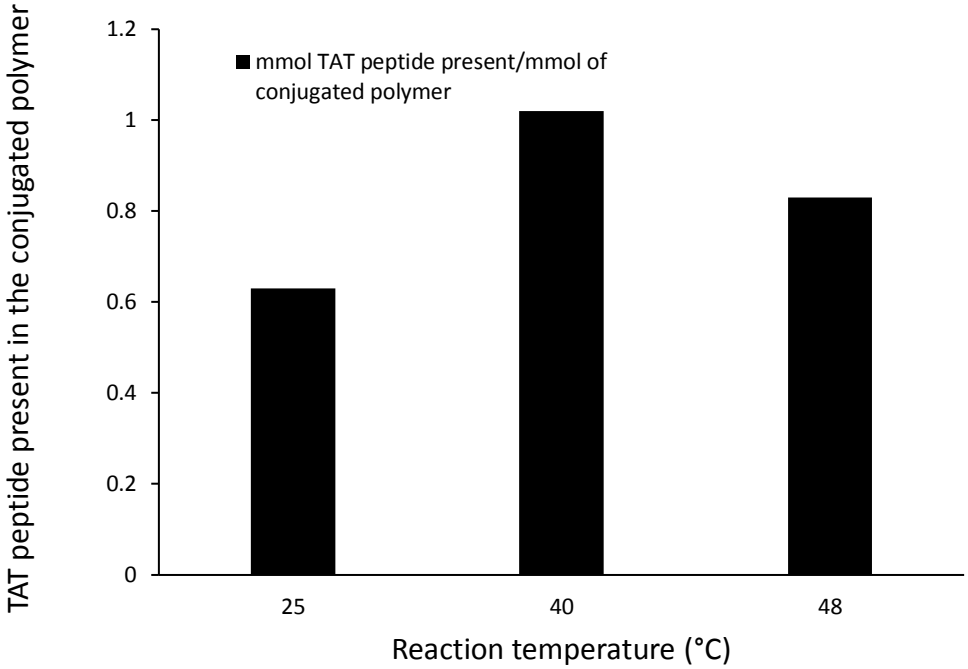

Figure 2.16: Effect of the reaction temperature on conjugation of TAT peptide on mPEG-COOH.

The TAT peptide conjugation reaction was conducted in presence of water with an initial activation of mPEG-COOH activation at room temperature for 2 h. After addition of TAT peptide, the reaction temperature was further raised to three different levels (25, 40, and 48 °C) to evaluate the effect of reaction temperature on TAT level conjugation. The data represented is TAT peptide present in the conjugate polymer for single set (n=1) of reaction.

2.5.4 Purification of mPEG-CONH-TAT conjugate

We utilized two commonly used purification methods for purifying the reaction mixtures: (i) dialysis technique and (ii) size exclusion chromatography.

Purification of the reaction mixture using dialysis membrane has several problems such as poor product yield, probably due to hydrolysis of the product. Dialysis was also unable to separate the mono-PEGylated peptide conjugate from peptides conjugated with more than one mPEG-COOH molecule. Due to the heterogeneity nature of the mixture of the native mPEG-COOH, mono-, di- and tri-PEGylated peptide conjugates, it was unacceptable to employ the product further as a therapeutic agent. Therefore, a downstream purification is necessary to overcome this issue and obtain a homogenous end-product.

SEC technique demonstrated that it is possible to remove mPEG-COOH and by-products from the desired PEGylated product using SEC technique. However, several factors such as buffer ionic strength of the elution buffer, flow rate, and injection volume need to be optimized for the complete separation of mono-PEGylated TAT peptide conjugate from the mixture of the multiple PEGylated peptide complexes. Although the smaller injection volume gives better resolution of the purified components, the complete purification of the large volume of the reaction mixture requires a larger column, which was unavailable due to budget constraints. Moreover, the use of small injection volumes produces a low amount of the purified product, which would be insufficient for subsequent application.

2.6 Conclusion

We synthesized and characterized two different types of modified cationic polymers: (i) TGC and (ii) mPEG-CONH-TAT polymer.

TGC was successfully synthesized using selective carbodiimide reaction. The developed method allowed the successful conjugation of thioglycolic acid onto GC. The formation of amide bond was confirmed qualitatively by FT-IR spectroscopy. The presence of thiol groups on GC was confirmed and quantitatively determined using Ellman's reagent. The appearance of the amide bond formation and presence of thiol group on GC confirms the successful attachment of thiolate moiety on GC polymer. This synthesized polymer was utilized as our first targeting ligand for coating of the developed nanoparticles.

The development of cationic mPEG-CONH-TAT polymer was also accomplished by using selective carbodiimide reaction. Two different approaches were employed to accomplish preparation of a key reagent for the PEGylation, mPEG-COOH. Use of an aqueous based solvent system makes this method a 'greener approach' compared to the nucleophilic substitution according to Scheme I. The reaction was optimized with pre-activation reaction as 20 min. In addition to this, the addition of β-mercaptoethanol to neutralize the excess of EDC in the reaction mixture, coupling reaction time as 4 h and optimum reaction pH for the conjugation being 10.0, using in aqueous conditions compared to the non-aqueous solvents.

The fluorescamine assay showed the presence of a total amount of the TAT peptide including both free and conjugated peptides. Unfortunately, we cannot use this analytical technique to produce uniform, reproducible results in complex reaction mixtures. Although we employed a various method of purification to extract out the mPEG-TAT conjugated polymer from the reaction mixture but to reproduce the accurate amount of conjugated polymer was a major difficulty throughout the process development. Hence, a suitable methodology for further improvement in synthesis and purification of mPEG-TAT is needed to be established. As there is no single analytical method to cover the detection of all different types of aggregates, it is recommended to use several complimentary methods based on different principles in order to examine conjugates from an orthogonal angle.

Furthermore, the prolonged reaction between reacting species leads to the formation of a heterogeneous mixture of mono, di- and tri-PEGylated peptide conjugate, and unreacted mPEG polymer. Therefore, complex and multistep downstream purification steps are required to isolate the desired product. Due to the time constrain and the high cost to obtain the required amount of the purified mPEG-TAT, we discontinued the approach of using mPEG-TAT for our future NPs.

3. Chapter-3 Analytical Method Development and Validation for Rivastigmine and Coumarin-6 Analysis

3.1 Introduction

One of the most important approach for the quantitative analysis of the drug and their metabolites present in the samples is the Reverse Phase-High Performance Liquid Chromatography (RP-HPLC). It is an efficient analytical tool which permits separation and quantification of the drug and its metabolites from other biological and chemical components present in the sample in a precise and reproducible manner. Therefore, the development of a suitable analytical method for RV is the focus of the study in this chapter to facilitate the analysis of RV concentration in clean *in-vitro* samples and biological samples during *in-vivo* animal studies.

A few RP-HPLC methods have been reported in the literature to determine the RV in the non-biological matrix using RP-HPLC (Kale, 2014; Simon et al., 2016). However, these methods used different kinds of buffers for RV analysis, which caused peak tailing. Therefore, a new RP-HPLC method was developed for the use of the acetonitrile/TFA and water/TFA mixture with an isocratic mode or gradient mode.

The developed RP-HPLC method used for *in-vitro* samples analysis was not able to produce neat chromatograms with good selectivity for RV analysis in biological samples. It was due to the low absorption wavelength of plasma interferences and resulting in the overlapping with the RV peak in chromatograms. Several methods have been reported for the estimation of RV in biological matrices using RP-HPLC chromatography using UV detector (Amini & Ahmadiani, 2010), fluorescence detector (Arumugam et al., 2011; Karthik et al., 2008). In addition, the few reported literatures (Bhatt et al., 2007; Enz et al., 2004; Frankfort et al., 2006; Parekh et al., 2014; Pommier & Frigola, 2003) also used LC-MS technique for RV quantification in biological samples which we were not able to use owing to the limited resources.

As RV is fluorescent in nature, therefore, can be easily detected using fluorescence detector. Hence a simple and suitable RP-HPLC method using fluorescence detector was developed and validated for the quantitative analysis of RV in biological matrices such as plasma or brain homogenate. Furthermore, there was a need to develop a sample preparation method to extract the RV from biological samples. There are reports on established sample preparation methods for the extraction of RV from biological matrix include liquid-liquid extraction (Amini & Ahmadiani, 2010; Enz et al., 2004), protein precipitation (Noetzli et al., 2012) and solid phase extraction (Bhatt

et al., 2007; Parekh et al., 2014). All these reported literature were used either liquid-liquid extraction method or protein precipitation method for the RV extraction from the sample. These reported methods were not efficient enough for complete recovery of RV and our chosen internal standard (venlafaxine) from biological matrices in our laboratory. The given sample preparations methods were either partial recovering the drug and internal standard or producing dirty chromatograms. Therefore, a novel extraction method involving the combination of liquid-liquid extraction and protein precipitation technique was developed to achieve high drug recovery with clean chromatograms.

In addition to RV, C-6 was also incorporated into our NPs as a marker, thus, a simple and sensitive RP-HPLC method using the fluorescent detector was developed for the analysis of C-6 *in-vitro* samples during various drug loading and leaching experiments. In addition, biological samples for C-6 analysis were determined using 96 well plate reader. The various developed analytical methods are represented in Figure 3.1

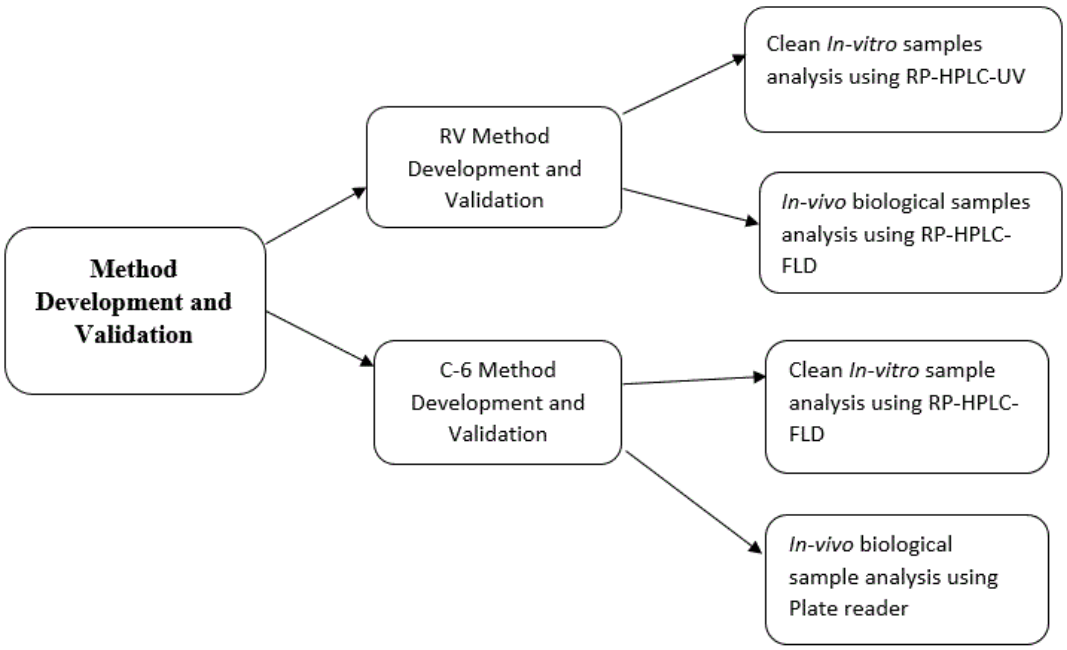

Figure 3.1: Flow diagram of various quantitative analytical method developed for analysis of RV and C-6

3.2 Objectives

The overall objective of this part of Ph.D. was to develop a simple, accurate, selective and sensitive RP-HPLC method for the analysis of RV during *in-vitro* release and *in-vivo* pharmacokinetics studies. The aim of this method development was to produce a selective, accurate and precise HPLC assay method. In addition, a simple clean-up procedure was developed to extract the drug from the biological samples. As a part of method development, a forced degradation study was conducted to ensure the HPLC method is a stability indicating assay method.

The present chapter also presented the work on the development of RP-HPLC method employed for the analysis of C-6 in clean samples. As C-6 is fluorescent in nature, therefore, a simple and sensitive plate reader method was also developed to determine the concentration of C-6 in plasma and brain samples.

3.3 Materials

Rivastigmine hydrogen tartrate (IC-CS-146-0-140108 99.2%) was purchased from Innochem (Beijing) Technology Co., Ltd. C-6 (442631-1G), Venlafaxine (V7264-10 mg), Tertbutyl methyl ether (306975-2L) and RIPA Buffer (R0278-500mL), Ethylenediaminetetraacetic acid, Acetonitrile, Methanol, Trifluoroacetic acid (solvents in HPLC grade) were purchased from Sigma-Aldrich (Castle Hill NSW, Australia) and stored as per mentioned storage conditions.

Drug-free blood was collected from healthy male Sprague-Dawley rats. Plasma was collected in blood collecting centrifuge tubes containing 20 µL of 10% EDTA solution and stored at -80°C after spinning down the blood at 11,370 g for 10 min.

RP-HPLC analysis of the various samples of this thesis work was performed on an Agilent Technologies chromatographic HPLC-1100 system with dual detectors (G1315B UV-DAD detector and G1321A fluorescence detector), G1316A column oven, G1329A autosampler, G1311A pump and chemstation B.04.02 software. A RP-HPLC C-18 column (150 mm X 4.6 ID, 5µm) serial no 215070077 (Grace Division Discovery Sciences, Alltech Australia, Catalogue No: 36505) was employed for analysis of various samples on RP-HPLC for this thesis work.

3.4 Methods

3.4.1 Conversion of Rivastigmine hydrogen tartrate to RV base

RV free base was prepared from rivastigmine hydrogen tartrate using 2M potassium carbonate solution (pH 10.0). A weighed amount of rivastigmine hydrogen tartrate was dissolved in 5 mL of milli-Q water and then treated with a 2M aqueous solution of potassium carbonate until the pH raised to 10.0 or above. The aqueous alkaline solution of rivastigmine hydrogen tartrate was further extracted 5 times with 5 mL of dichloromethane. The extracted organic layers were combined and dichloromethane was evaporated using rotary evaporator at 50°C. The RV base concentrate was dried overnight using vacuum oven at room temperature for complete removal of organic solvent. The % purity and conversion of rivastigmine hydrogen tartrate to RV base was confirmed by running ^{1}H-NMR spectrum.

3.4.2 UV and Fluorescence scanning

A stock solution of RV free base (2 mg/mL) was prepared in acetonitrile by dissolving 20 mg RV in 10 mL of acetonitrile in a volumetric flask and stored at -20°C. A standard solution of 20 µg/mL RV was prepared with dilution using water from the RV stock solution and scanned for excitation and emission wavelengths. A standard solution of C-6 (20 µg/mL) in methanol was prepared from C-6 stock solution (2 mg/mL in methanol) and scanned for excitation and emission wavelength.

UV absorption maxima were determined using Hewlett Packard 8452A UV-VIS spectrophotometer (Hewlett Packard, Germany) and fluorescence excitation and emission wavelengths determined using a Varian Cary Eclipse spectrofluorometer (Varian Technologies, Australia).

3.4.3 Method development and validation for *in-vitro* RV analysis

3.4.3.1 RV method development

A 20 µg/mL RV concentration was prepared in a mixture of acetonitrile and water (20: 80) from a stock solution of RV and used for method development and forced degradation study.

The mobile phase used for quantitative determination of RV was composed of acetonitrile: Milli-Q water in a ratio of 20: 80 respectively with 0.1% trifluoroacetic acid. The chromatographic elutant was detected by using a UV-Diode Array detector at a wavelength of 214 nm. The flow rate was 1.5 mL/min in isocratic mode. The temperature of the column oven was maintained at 50°C for faster elution of RV. The injection volume used for analysis and validation was 50µL.

3.4.3.2 Forced degradation study

The forced degradation study was performed to develop and validate the stability indicating HPLC method for analysis of RV. This study was mainly used to evaluate the selectivity of the developed method. This study was performed using various stress conditions to produce degradation products that are likely to be generated during storage conditions. The forced degradation studies typically involve the treatment of the samples with stress conditions under different pH, oxidative degradation, light and thermal degradation (Blessy et al., 2014).

(a) Hydrolytic degradation

Hydrolytic forced degradation involves the degradation of the chemical drug in presence of water under acidic/basic stress conditions.

Base Hydrolysis

Base hydrolysis was performed by treating 20 µg/mL of RV sample with 1M sodium hydroxide and pH of the sample was adjusted to 10.0. The base-treated sample was stored at 60°C. Samples were withdrawn at predetermined fixed time intervals and neutralized for analysis by HPLC to determine the degradation products.

Acid Hydrolysis

Acid hydrolysis was carried out by treating the samples with 1M HCL and pH of RV drug solution was adjusted to 2.0. The acid treated samples were further stored at 60°C and samples were withdrawn at predetermined fixed time intervals and neutralized for analysis by HPLC to determine the degradation products.

(b) Oxidative degradation

Oxidative degradation study was performed by treating the 20 µg/mL RV drug solutions with 5% hydrogen peroxide solutions further storing at 60°C. Samples were withdrawn at predetermined fixed time intervals to analyze by HPLC for the determination of oxidized degradation products.

(c) Thermal degradation

To evaluate the stability of RV in the presence of heat, a 20 µg/mL RV drug solution was prepared separately in mobile phase and PBS (10mM, pH 7.4) and exposed to 37°C and 60°C. Samples were withdrawn at predetermined fixed time intervals up to 72 h to analyze by HPLC to determine degradation products.

3.4.3.3 RV method validation

(a) Selectivity for analyzing *in-vitro* samples

The selectivity of the developed RP-HPLC method for RV analysis was determined by comparing the RV samples with various controls. These controls are:

(i) blank supernatants obtained from developed blank PLGA nanoparticulate formulations.

(ii) blank dialysis medium obtained after performing *in-vitro* release study of blank PLGA NPs in PBS.

These supernatants were diluted 100 times with the mobile phase and analyzed on HPLC to determine the method selectivity. The HPLC chromatograms were observed for the interference of the matrix with the retention time of RV.

The selectivity of the developed method was evaluated by analyzing the various RV samples against their respective blanks obtained during the various studies such as samples stored at a different temperature, stressed acidic and alkaline conditions and analysis in different solvents viz: water, mobile phase, PBS etc. All these sample selectivity studies had already described in section 3.4.3.2.

(b) Linearity

Assay linearity was evaluated in the two different solvents that are used for determination of RV drug loading and *in-vitro* release study.

(i) Drug loading solvent (20:80 v/v acetonitrile: water): 2 mg/mL RV stock solution was prepared in 0.3% TPGS (d-α-tocopheryl polyethylene glycol 1000 succinate) solution to mimic the actual conditions. A series of RV concentrations ranging from 0.1-20 µg/mL was further prepared by diluting the stock solution with the solvent.

(ii) *In-vitro* release study solvent (PBS; 10mM, pH 7.4); RV stock solution (2mg/mL in acetonitrile) was diluted with PBS at the concentration ranging from 0.1-20 µg/mL. All samples were injected on HPLC and analyzed with double injections. The peak area of chromatogram was measured by using UV-DAD detector at a wavelength of 214 nm. The standard curve was constructed using known standard RV concentrations versus peak area recorded.

(c) Sensitivity

The limit of detection (LOD) and limit of quantification (LOQ) were determined using noise level obtained after injecting blank supernatant solution diluted in the mobile phase and PBS. Each solvent was injected six times and the average noise level was determined and LOD and LOQ were calculated using following formula:

$$\mathrm{LOD} = \frac{3.0 \times \text{average noise level of six blank injection}}{\text{slope obtained from calibration curve of RV peak height against conc}}$$

$$\mathrm{LOQ} = \frac{10.0 \times \text{average noise level of six blank injection}}{\text{slope obtained from calibration curve of RV peak height against conc}}$$

(d) Recovery (Accuracy)

Accuracy or recovery is the closeness of the test result values with the standard true values. The recovery of the RV was carried out to determine the interference of the PLGA matrix formulation during RV analysis. RV recovery was performed by spiking with the blank supernatant obtained after centrifugation of blank PLGA nanoparticulate formulation with a known amount of RV. Three sets of different concentrations of 2, 4 and 8 µg/mL of RV were spiked in the blank supernatant and analyzed by HPLC. The accuracy of the developed method was determined by comparing the calculated spiked RV concentration with spiked concentrations.

(e) Precision

System precision was determined by six replicate injections of RV sample at three different concentrations. Two sets of RV samples were prepared separately in a mobile phase and PBS. The average area of the RV and %RSD was determined for all six injections.

(f) Intraday and interday repeatability

Intraday and interday repeatability were performed by analyzing triplicate samples of the two different concentrations of the RV. The two sets of RV concentrations were prepared separately in the acetonitrile/water (1 µg/mL and 4 µg/mL) and PBS (2µg/mL and 5 µg/mL) solutions. The prepared samples were analyzed at three different times during the same day and two consecutive days to determine intraday and interday variability respectively. The relative standard deviation was calculated in each case.

3.4.4 Development and validation of analytical method for analysis of biological samples containing RV

3.4.4.1 Preparation of biological samples for processing and extraction of biological samples containing RV

To analyse RV concentration from *in-vivo* animal samples, firstly, an extraction method was developed to extract RV from plasma and brain samples using a mixture of tertbutyl methyl ether, acetonitrile and RIPA buffer. Tertbutyl methyl ether and acetonitrile were employed to extract RV from biological samples and RIPA buffer was used for protein solubilization and cell lysis.

To develop a method, A known amount of RV and 15 µL of venlafaxine (1µg/mL in milli-Q water) as an internal standard was added to a 100 µL of blank plasma. The mixture was thoroughly mixed then extracted following the procedure described in Figure 3.2. To develop a method for extraction of RV from brain homogenate, 500 µL of blank brain homogenate sample was mixed with a known amount of the RV and 50 µL of venlafaxine (1.5 µg/mL in milli-Q water) as an internal standard. The mixture was extracted by following a procedure as described in Figure 3.3.

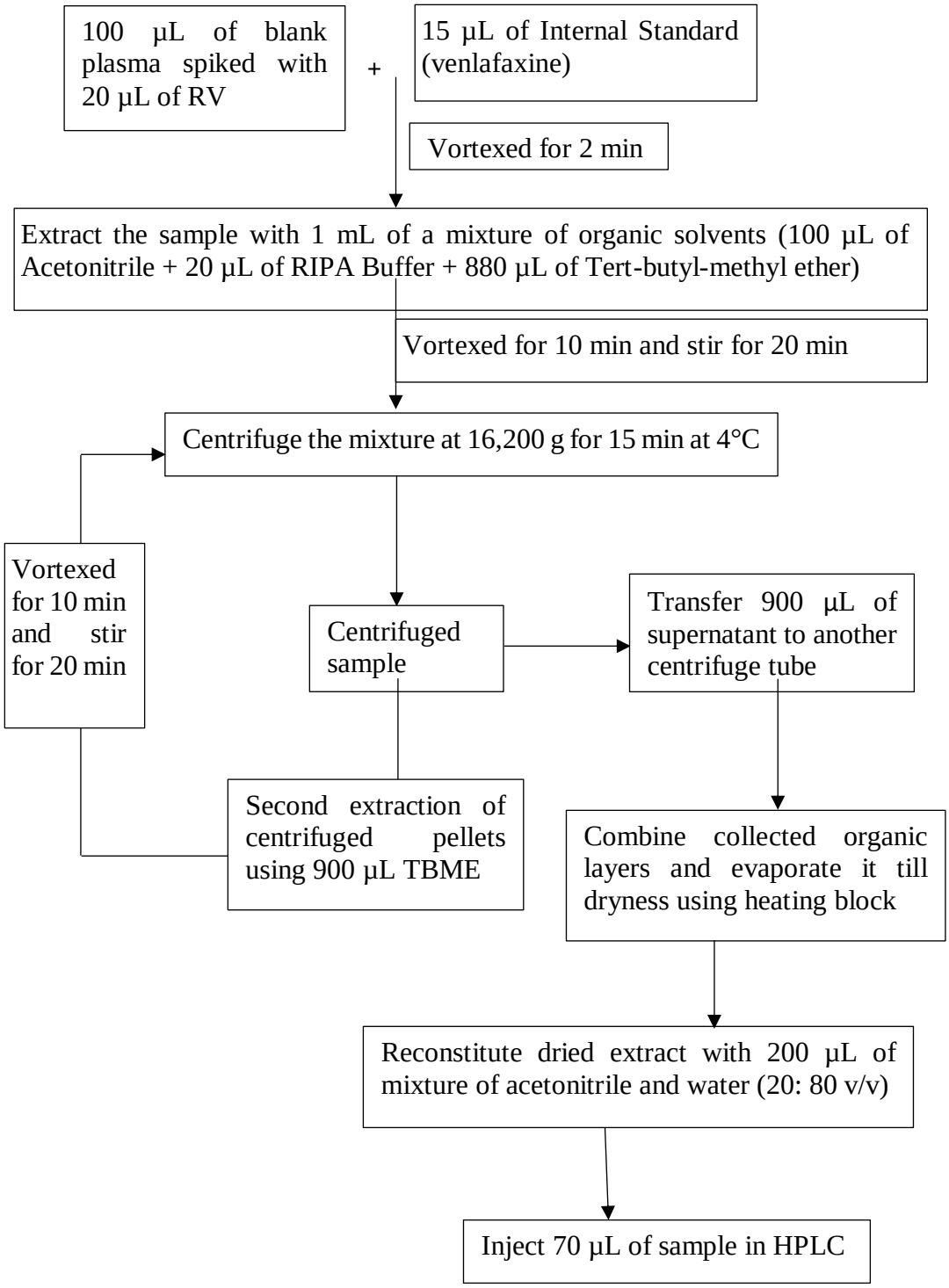

Figure 3.2: Method employed for extraction of RV and IS from plasma samples

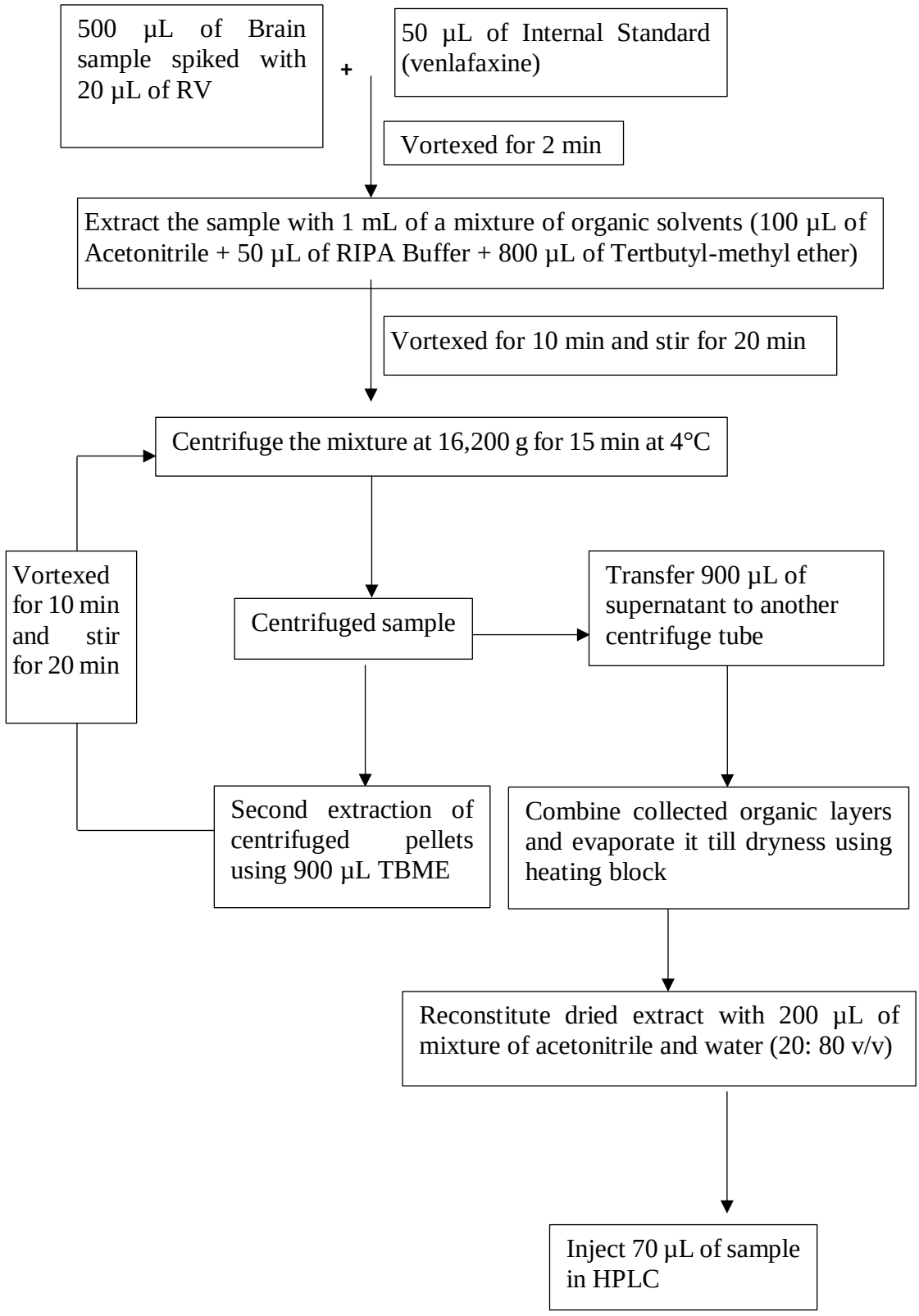

Figure 3.3: Method employed for extraction of RV and IS from the brain samples

3.4.4.2 HPLC method development

After extraction of RV from biological samples, processed samples was analysed by RP-HPLC to determine the drug concentration. For this, a RP-HPLC method was developed using fluorescence detector. The chromatographic elutant was detected by using fluorescence detector at an excitation and emission wavelength of 220 and 305 nm respectively. The temperature of the column oven was maintained at 50°C during the analysis. The injection volume used for RV analysis and validation was 70µL.

The mobile phase used for the analysis of RV in biological samples consisted of two different solvents. Solvent A was acetonitrile with 0.1% trifluoroacetic acid and solvent B was Milli-Q water with 0.1% trifluoroacetic acid. The flow rate employed was 1.0 mL/min with a gradient elution mode. The run time was programmed to 30 min with the gradient system as follows:

Time (min)	% acetonitrile/TFA	% water/TFA
0	24	76
20	24	76
21.5	95	05
26.0	95	05
26.5	24	76
30.0	24	76

3.4.4.3 Method validation

(a) Selectivity

The selectivity of the HPLC method was determined by running different controls such as drug-free blank plasma and blank brain samples, which were processed similarly with and without any IS or RV as described in Figure 3.2 and 3.3 respectively. Processed samples were analysed by HPLC to determine the interference of the endogenous compounds at the retention time of RV and IS.

(b) Linearity

Linearity range was assessed in acetonitrile/water mixture (80:20), blank plasma, and blank brain homogenate samples. The standard or calibration curve of values ranging from 200-1000 ng/mL was prepared by adding a known amount of RV in both plasma and brain matrices.

To an aliquot of 100 µL of acetonitrile/water mixture or blank plasma or brain homogenate, a known amount of RV was added. The samples containing a mixture of RV and acetonitrile/water mixture or plasma or brain homogenate were processed similarly as described in Figure 3.2 and 3.3 respectively. All the processed samples were analyzed by HPLC with double injections. The peak area was measured for RV and IS. The standard calibration curve was constructed using known standard RV concentrations versus the ratio of peak areas of the RV to IS recorded.

(c) Recovery (Accuracy)

During the method development, a concern was to obtain the complete and reproducible recovery of RV from plasma and brain samples. Various solvents were employed to standardize the complete recovery of RV from plasma and brain matrix. The liquid-liquid extraction method for the RV was also optimized at various stages, viz. stirring time, and the volume required for successful extractions of the RV. The recovery of RV in both blank plasma and blank brain homogenate was determined by analyzing three sets of different RV concentrations (0.2, 0.5 and 1.0 µg/mL) prepared separately in both plasma and brain and extracted in as mentioned in Figure 3.2 and 3.3 respectively. All the processed samples were analyzed by HPLC with double injections. Percent RV recovery was determined by comparing analyzed concentration of RV obtained from extracted samples with the concentration of unextracted RV in acetonitrile/water (80:20).

(d) Precision

Intraday and interday precision were performed by analyzing triplicate samples of the three different sets of RV concentration. Both plasma and brain samples were spiked with three different sets of RV concentrations (0.2, 0.5 and 1.0 µg/mL) and processed similarly as mentioned in Figure 3.2 and 3.3 respectively. The final processed samples

were analyzed at three different times on day one and for two consecutive days to determine intraday and interday variability respectively. The relative standard deviation was calculated in each case. The acceptance criteria for intraday and interday precision for biological samples should be within 85-115% and precision should not be more than ±15% of the coefficient of variation except the lower limit of quantifications (US-FDA, 2013).

(e) Sensitivity

The LOD and LOQ were determined using signal noise level obtained after injecting the blank plasma and blank brain samples. Each sample was injected six times and the noise level was determined and LOD and LOQ were calculated using following formula:

$$\text{LOD} = \frac{3.0 \times \text{average noise level of six blank injection}}{\text{slope obtained from calibration curve of RV peak height against conc}}$$

$$\text{LOQ} = \frac{10.0 \times \text{average noise level of six blank injection}}{\text{slope obtained from calibration curve of RV peak height against conc}}$$

3.4.5 Method development and validation for *in-vitro* C-6 analysis

3.4.5.1 Method development

A standard solution of C-6 (20 µg/mL) in acetonitrile/water mixture (84:16) was prepared from C-6 stock solution (2 mg/mL in methanol) and used for C-6 method development.

A simple RP-HPLC-FLD method was developed to determine the C-6 content in clean *in-vitro* samples. The mobile phase used for quantitative determination of C-6 was composed of acetonitrile: milli-Q water in a ratio of 84: 16 respectively with 0.1% trifluoroacetic acid in an isocratic mode. The peak area of chromatogram was measured using fluorescence detector with excitation and emission wavelengths of 465 nm and 502 nm respectively. The flow rate employed was 1.0 mL/min. The injection volume used for analysis and validation was 50µL.

3.4.5.2 Method validation

(a) Selectivity

The selectivity of the developed RP-HPLC method for C-6 analysis was determined via observing for the interference of the matrix with the retention time of C-6. For this, the blank supernatants obtained from developed blank PLGA nanoparticulate formulations were diluted 100 times with the mobile phase and analyzed by HPLC to determine the method selectivity.

(b) Linearity

A series of C-6 concentrations ranging from 10-400 ng/mL was prepared by diluting the stock solution with the mixture of acetonitrile and water (84:16). All samples were injected on HPLC and analyzed with double injections. The standard curve was constructed using known standard C-6 concentrations versus peak area recorded.

(c) Recovery (Accuracy)

The recovery of the C-6 was carried out to determine the interference of the PLGA matrix formulation during C-6 analysis. To evaluate the accuracy of HPLC method, a

known amount of C-6 into the blank supernatant which was obtained after centrifugation of blank PLGA nanoparticulate formulation. Three sets of different concentrations of 50, 100 and 500 ng/mL of C-6 were spiked in the blank PLGA NPs supernatant and analyzed via injecting two injections of each sample. The accuracy of the developed method was determined by comparing the determined C-6 concentration with spiked concentrations.

(d) Precision

The three different concentrations of C-6 were prepared separately in a mixture of acetonitrile and water (84:16 v/v) and analyzed by six replicate injection each on HPLC to determine the precision. The average area of the C-6 and %RSD was determined for all three concentrations.

(e) Intraday and Interday repeatability

Intraday and Interday repeatability were determined by analyzing triplicate samples of the two different concentrations of C-6 (100 ng/mL and 400 ng/mL), prepared in the acetonitrile and water mixture (84:16 v/v). The prepared samples were analyzed at three different times during the same day and two consecutive days to determine intraday and interday variability respectively. The relative standard deviation was calculated in each case.

(f) Sensitivity

The LOD and LOQ were determined using noise level obtained after injecting blank supernatant solution diluted in the mobile phase. The solvent was injected six times and the average noise level was determined and LOD and LOQ were calculated using following formula:

$$\mathrm{LOD} = \frac{3.0 \times \text{average noise level of six blank injection}}{\text{slope obtained from calibration curve of RV peak height against conc}'\text{n}}$$

$$\mathrm{LOQ} = \frac{10 \times \text{average noise level of six blank injection}}{\text{slope obtained from calibration curve of RV peak height against conc}'\text{n}}$$

3.4.6 Development and Validation of analytical method for analysis of biological samples containing C-6

3.4.6.1 C-6 method development

C-6 shows high fluorescent sensitivity at excitation wavelength 465 nm and emission wavelength 502 nm, therefore, a simple, selective and sensitive method was developed and validated using a plate reader capable of measuring fluorescent signals ((EnSpire® Multimode plate reader, Perkin Elmer, Waltham, MA USA) at above mentioned wavelength for determination of C-6 in biological samples.

For the development of a method for analysis of C-6, initially, a C-6 spiked samples were prepared by adding a known amount of C-6 to a known volume of blank plasma or brain homogenate and then processed as per method described below.

Processing procedure of C-6 in biological samples

The C-6 spiked samples were treated with RIPA buffer for protein solubilization and cell lysis. In brief, to an aliquot of 200 µL of plasma or brain sample, 400 µL of RIPA buffer was added. Samples were vortex mixed for 15 min, and fluorescent tracer concentration was analyzed on the above-mentioned plate reader at excitation wavelength 465 nm and emission wavelength 502 nm. The concentration of the C-6 in unknown plasma and brain samples was determined against a calibration curve of C-6 standards. Untreated plasma and brain samples were used as controls.

3.4.6.2 C-6 method validation

(a) Recovery and senstivity

The recovery of C-6 in both plasma and brain homogenate were determined by analyzing three sets of different C-6 concentrations within the linearity range. Triplicate samples of 6.0, 12.0 and 32 ng/mL C-6 concentration were prepared by adding C-6 separately in both plasma and brain homogenate. These spiked samples were processed similarly using a processing method described above (section 3.4.6.1) to evaluate the recovery of C-6 from biological samples. The percent C-6 recovery was determined by comparing the concentration of C-6 determined from the treated samples with that of samples prepared in clean mobile phase. To determine the

sensitivity blank plasma and blank brain homogenate were also treated with RIPA buffer and analysed similarly.

(b) Linearity

C-6 linearity range was determined in milli-Q water, blank plasma and blank brain homogenate sample by plotting a calibration curve of C-6 from 1-35 ng/mL of C-6 concentration.

To an aliquot of 100 µL blank milli-Q water or blank plasma or brain homogenate, 10 µL of a known amount of C-6 was added. The samples containing a mixture of water/plasma/brain homogenate and C-6 were treated with RIPA buffer as described in sample processing method (section 3.4.6.1). The fluorescent intensity was measured by using plate reader at an excitation and emission wavelength of 465 and 502 nm respectively. All the samples were analyzed in triplicate sets on a plate reader.

3.5 Results & Discussion

3.5.1 Conversion of Rivastigmine hydrogen tartrate to RV base

Rivastigmine hydrogen tartrate was converted into RV base using an alkaline hydrolysis with potassium carbonate. The obtained RV base was clear transparent liquid in nature with more than 99.0 % purity as confirmed using ^{1}H-NMR spectrum. Figure 3.4 indicates the ^{1}H-NMR spectrum of Rivastigmine hydrogen tartrate which shows the tartaric acid peak at 4.407 ppm. The conversion of rivastigmine hydrogen tartrate into RV base was confirmed by the absence of tartrate peak in the ^{1}H-NMR spectrum. Figure 3.5 clearly indicated the absence of a tartaric acid peak in the ^{1}H-NMR spectrum of Rivastigmine base.

3.5.2 UV and Fluorescence scanning

The UV absorption maximum of RV was 214 nm and fluorescence excitation and emission were 220 nm and 305 nm, respectively, as determined by scanning a 20 µg/mL aqueous solution of RV. These wavelengths were used for analysis of RV in clean and biological samples.

The fluorescence excitation and emission 465 nm and 502 nm, respectively, as determined by scanning a 20 µg/mL methanolic solution of C-6. These wavelengths were used for analysis of C-6 *in-vitro* samples.

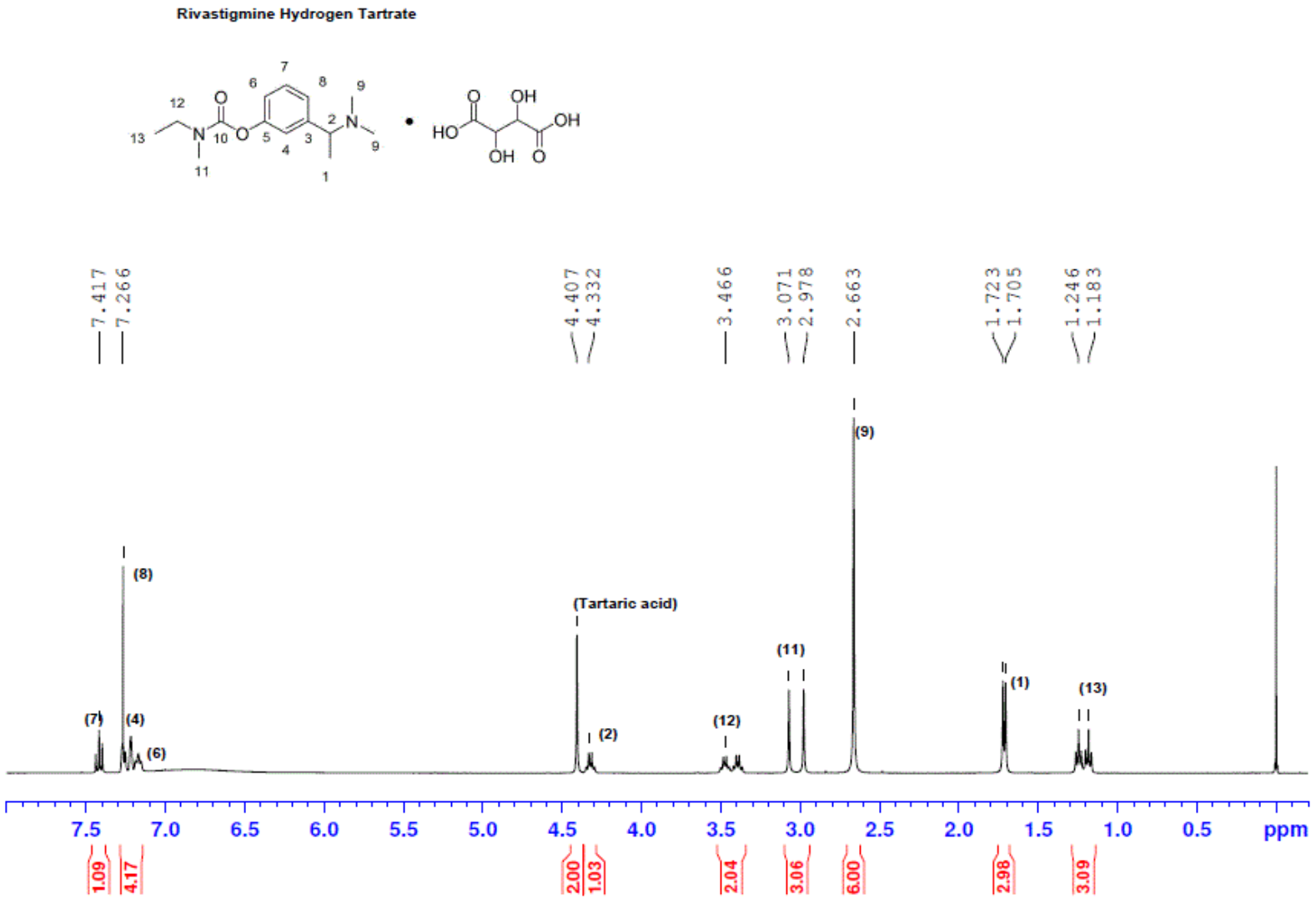

Figure 3.4: ^{1}H-NMR spectrum of Rivastigmine hydrogen tartrate in deuterated chloroform

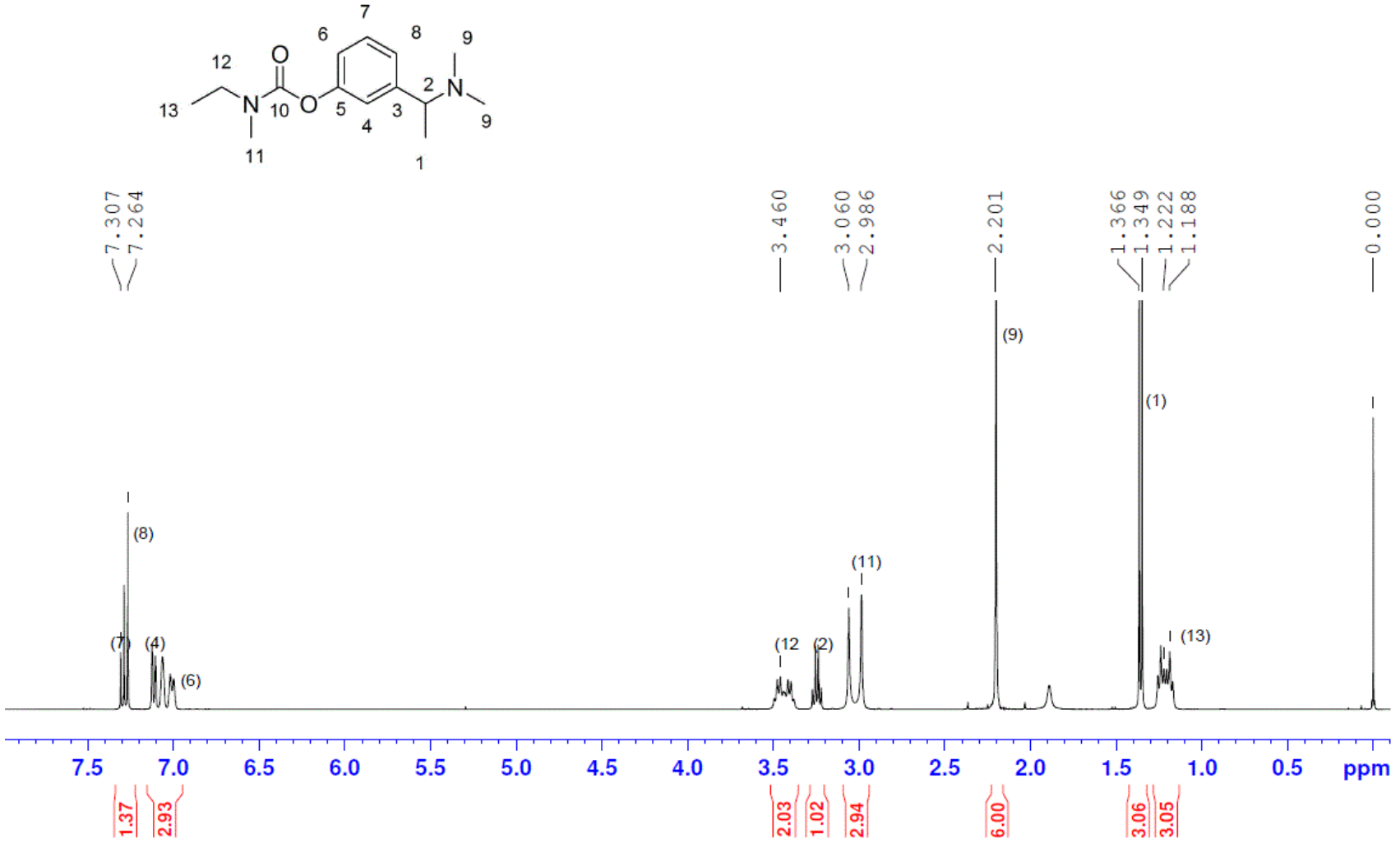

Figure 3.5: ^{1}H-NMR spectrum of Rivastigmine in deuterated chloroform

3.5.3 Forced degradation study of RV

The forced degradation study was done to determine the selectivity and stability indicating nature of a developed RP-HPLC method. The peak purity results of RV were determined using photodiode array detector and data indicating the uniformity of RV peak throughout the stress conditions. RV was stable in the mobile phase, PBS and thermal conditions both at 37°C and 60°C, however, it was unstable in basic, acidic or oxidative conditions. The typical chromatogram of RV in the mobile phase is represented in Figure 3.6.

3.5.3.1 Hydrolytic degradation

(a) Base/Acid hydrolysis

RV was unstable in alkaline conditions, even at zero hour and completely hydrolyzed in the presence of base within 24 h (Figure 3.7). The major impurity peak in alkaline conditions was found to be around 1.4 min. The non-interference of the impurity peaks with the RV peaks showed the specificity of the developed HPLC method. Our findings confirm the reported literature of RV degradation products (Thomas et al., 2012). RV was stable in acidic conditions at 60°C for 48 h. The degradation product peak was observed at 60°C after 72 hours at retention time 1.64 min (Figure 3.8).

3.5.3.2 Oxidative degradation

RV is unstable in hydrogen peroxide and formed N-oxide derivatives immediately after treatment. The formation of N-oxide was further accelerated in presence of heat (at 60°C) and completely oxidized and gives degradation peak at 7.26 min which was well separated from RV peak. (Figure 3.9).

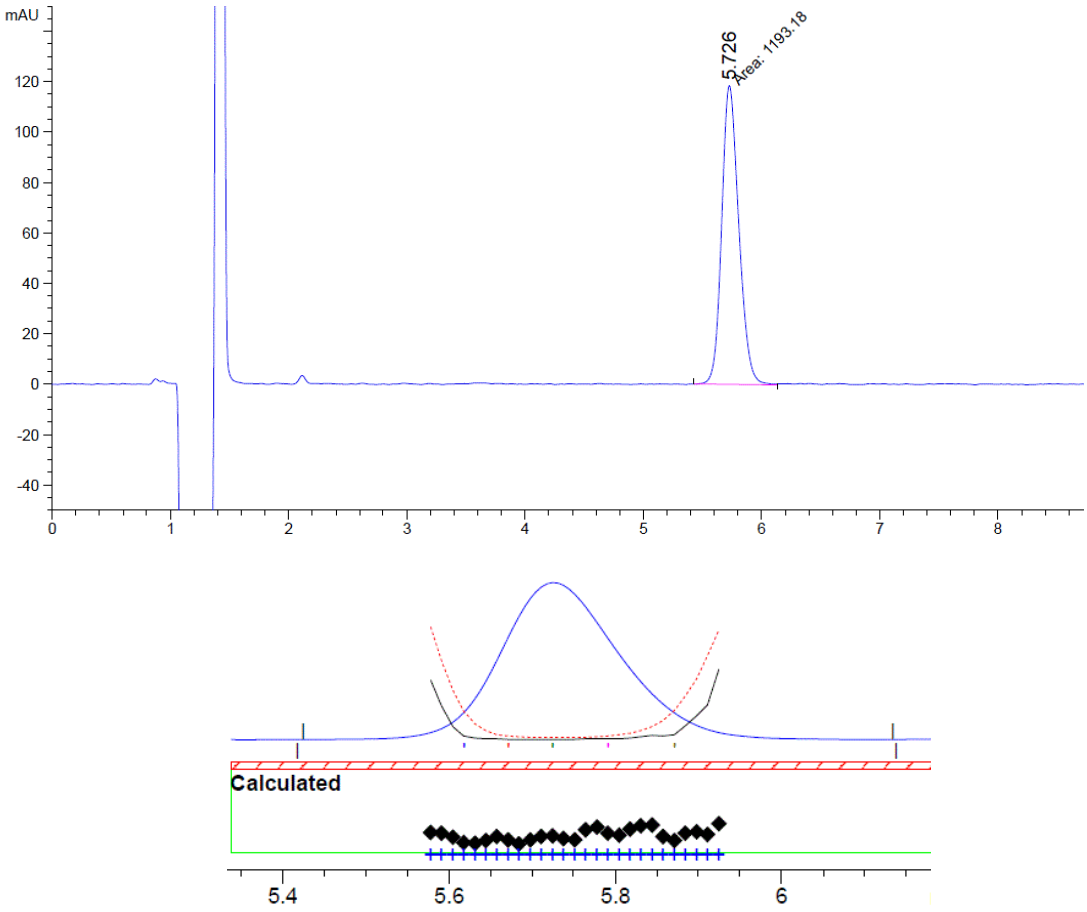

Figure 3.6: Typical HPLC chromatogram of RV prepared in a mobile phase.
The 20 µg/mL of RV was prepared in mobile phase and analysed using HPLC. The chromatogram showed RV retention time at 5.7 min with a total run time of 10 min. The purity factor was within calculated threshold limit.

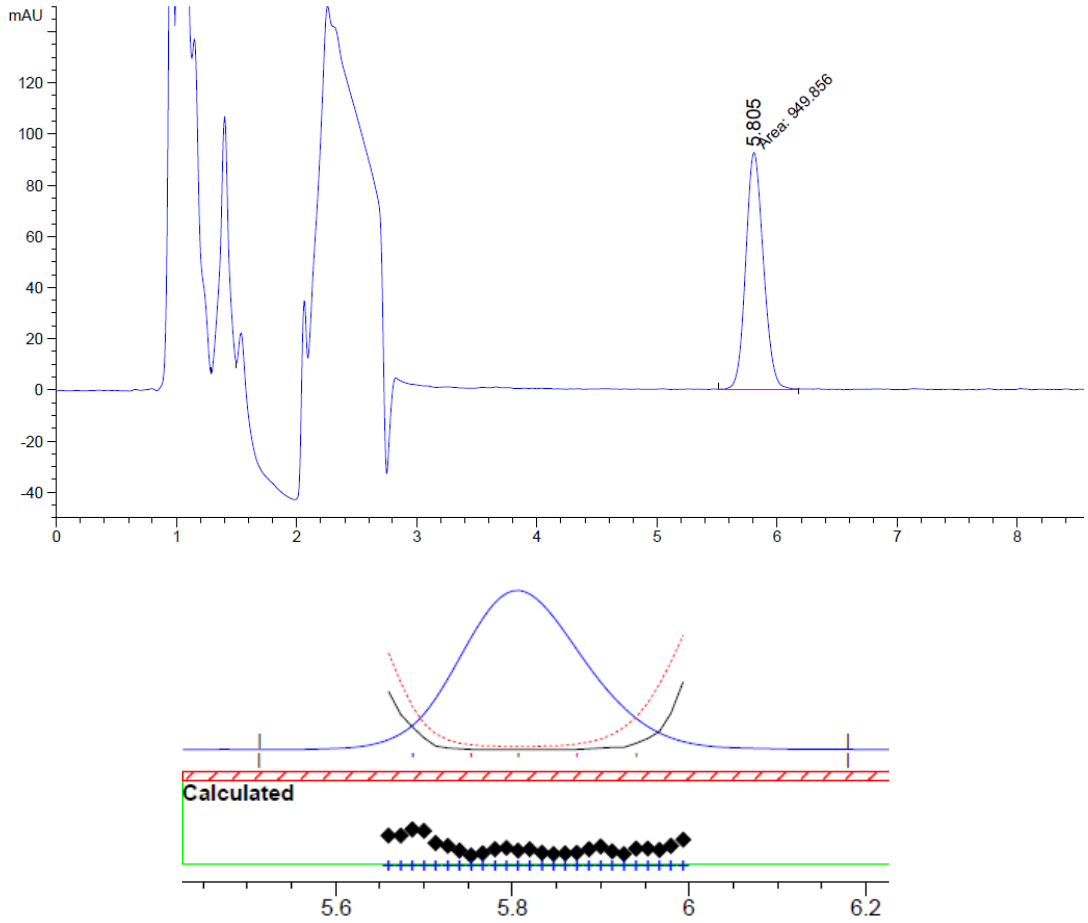

Figure 3.7: Typical HPLC chromatogram of RV obtained after hydrolysis with 1M NaOH at zero hour

The RV chromatogram showed retention time of RV at 5.8 min and RV peak is pure and free of interference from the degradation products and indicated by the facts that the peak purity was within the threshold limit.

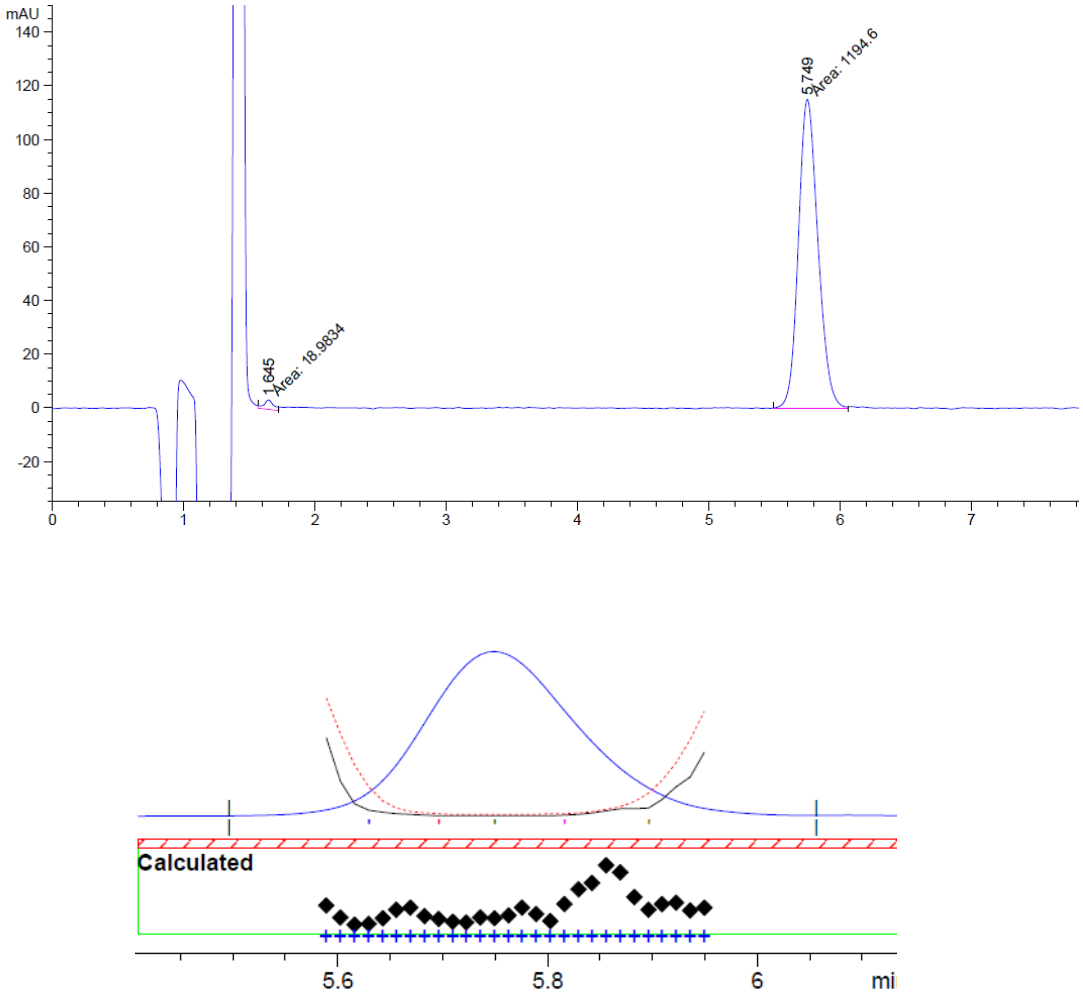

Figure 3.8: Typical HPLC chromatogram of RV after hydrolysis with 1M HCl and stored at 60°C for 72 h.

The chromatogram showed retention time of RV at 5.7 min and RV peak is pure and free of interference from the degradation products and indicated by the facts that the peak purity was within the threshold limit.

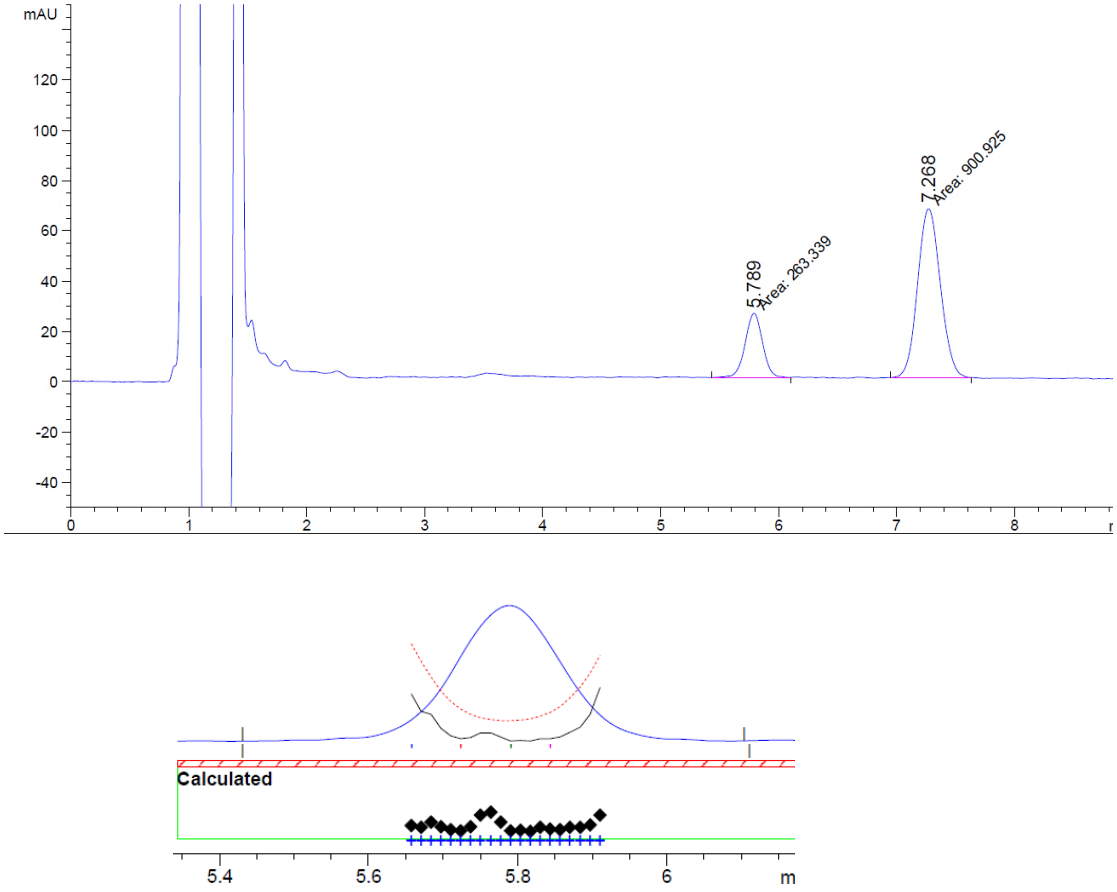

Figure 3.9: Typical HPLC chromatogram of RV obtained after oxidizing with 5% H_2O_2 at zero hour

The chromatogram showed RV retention time at 5.7 min and major degradation product peak at 7.26 min with a total run time of 10 min. RV peak is pure and free of interference from the degradation products and indicated by the facts that the peak purity was within the threshold limit.

3.5.3.3 Thermal degradation

The results obtained from the thermal degradation are represented in Table 3.1 and 3.2 which indicates that RV is stable in the mobile phase and PBS both at 37°C and 60°C for three days. No degradation peak was observed in the chromatograms of RV in the mobile phase and PBS after 72 h (Figure 3.10 and 3.11).

Table 3.1: Thermal stability of RV performed at 60°C for 3 days'

Time (h)	RV Potency (%)	
	RV in mobile phase	**RV in PBS**
0	100.0 ± 0.5	100.0 ± 1.0
1	99.8 ± 1.1	99.8 ± 1.1
2	99.8 ± 1.2	99.8 ± 0.9
4	99.8 ± 0.4	99.8 ± 0.9
6	99.4 ± 0.6	99.4 ± 1.3
8	99.5 ± 0.9	99.5 ± 1.2
24	99.4 ± 0.7	99.4 ± 0.9
48	99.3 ± 0.6	99.6 ± 0.9
72	99.2 ± 0.9	99.2 ± 1.0

Data are represented in % mean RV potency ± SD (n=2)

Table 3.2: Thermal stability of RV performed at 37°C for 3 days'

Time (h)	RV Potency (%)	
	RV in mobile phase	**RV in PBS**
0	100.0 ± 1.2	100.0 ± 0.95
2	100.4 ± 1.3	100.5 ± 1.1
8	100.7 ± 1.3	100.6 ± 0.8
24	99.9 ± 0.6	99.4 ± 0.7
48	100.1 ± 0.6	99.5 ± 0.5
72	99.6 ± 1.3	99.2 ± 0.8

Data are represented in % mean RV potency ± SD (n=2)

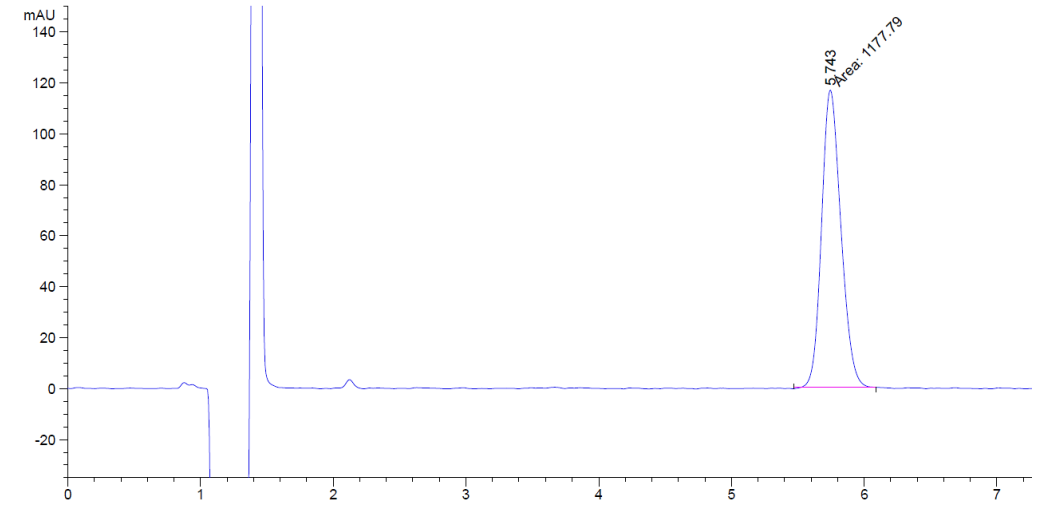

Figure 3.10: HPLC chromatogram of RV in mobile phase at 60°C for 72 h

The RV sample was prepared in the mobile phase and stored at 60°C for 72 h and analyzed by HPLC to determine the degradation product. The chromatogram indicated the retention time of RV at 5.74 min and RV peak is pure and free of the degradation products.

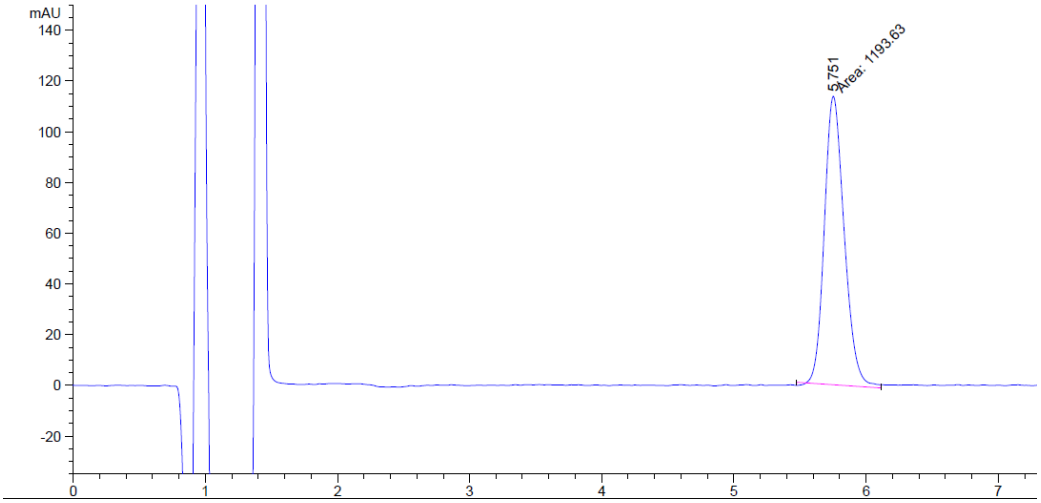

Figure 3.11: Typical HPLC chromatogram of RV in PBS at 60°C for 72 h

The RV sample was prepared in PBS and stored at 60°C after 72 h and analyzed by HPLC. The chromatogram indicated the retention time of RV at 5.8 min and RV peak is pure and free of from the degradation products.

3.5.4 Method development and validation for *in-vitro* RV analysis

Preliminary experiments were performed during the development of a stability indicating HPLC method for RV analysis. The peak shape and symmetry factor of the RV were considered as the main parameters during the method development stage. Various HPLC parameters such as flow rate, the ratio of organic to the aqueous phase, choice of buffers, pH adjustment of the mobile phase were optimized. Mobile phase with pH above the 3.0 caused peak tailing. The decrease in the pH of the mobile phase improved the peak shape and symmetry factor, therefore the pH of the mobile phase was adjusted to 2.0 using trifluoracetic acid.

3.5.4.1 Selectivity

The developed RP-HPLC method is selective for the analysis of RV in presence of PLGA nanoparticulate matrix. It didn't show any interference during the analysis of RV from NPs matrix and *in-vitro* release study samples. The chromatogram representing the selectivity of developed method is represented in Figure 3.12 and 3.13. The chromatogram indicates the selectivity of the developed RP-HPLC method for RV analysis in clean samples.

3.5.4.2 Linearity

The UV detector response for a range of RV concentrations in mobile phase (0.1-20 µg/mL) and PBS (0.1-20 µg/mL) was linear with a correlation coefficient more than 0.999. The calculated HPLC parameters were represented in Table 3.4 and Figure 8.4 (Appendix section).

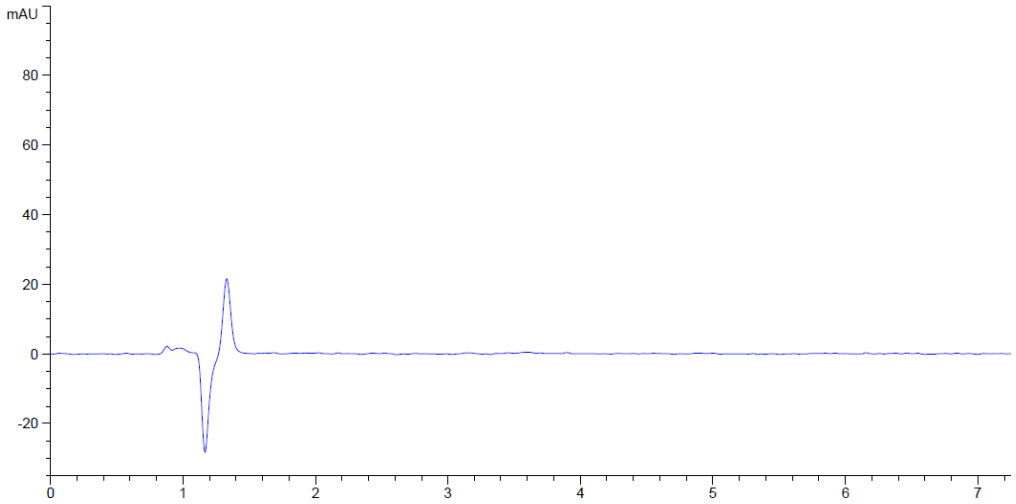

Figure 3.12: HPLC chromatogram of blank PLGA NPs supernatant.
Blank PLGA NP's supernatant was diluted 100 times with mobile phase and analyzed using developed HPLC method. HPLC chromatogram indicated the selectivity of the developed method for RV analysis in clean samples.

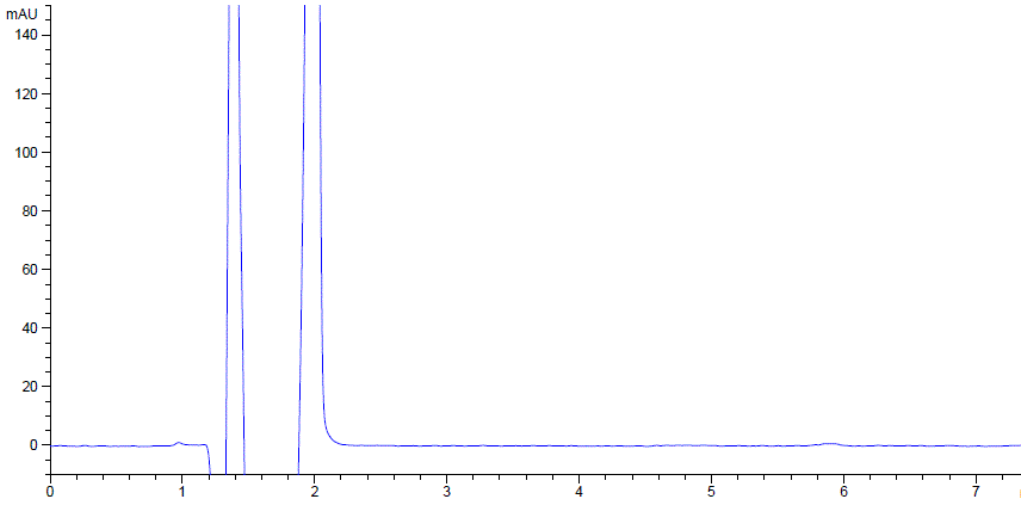

Figure 3.13: HPLC chromatogram of dialysate medium of blank PLGA NPs.
The sample obtained from dialysis of blank PLGA NPs was diluted 100 times with mobile phase to analyse by HPLC. Chromatogram indicated the selectivity of the developed method for RV analysis.

3.5.4.3 Recovery (Accuracy)

The accuracy or recovery of RV from developed PLGA nano-formulations was determined to evaluate the specificity of the developed HPLC method. RV recovery from blank PLGA matrix (Table 3.3) indicated there was no interference from the blank matrices. Recovery of RV was > 97.1 % with less than of 1.5 %RSD.

Table 3.3: RV Recovery from blank PLGA matrix

Sample No	Conc. spiked (µg/mL)	Average Conc. Recovered (µg/mL)	Recovery (%)	RSD (%)
1	2.0	1.92 ± 0.05	95.8 ± 2.3	2.4
2	4.0	3.93 ± 0.04	98.3 ± 1.0	1.1
3	8.0	7.77 ± 0.09	97.1 ± 1.0	1.1
% Average Recovery			97.1 ± 1.5	1.5

Data represented in Mean ± SD (n=3). RSD: relative standard deviation, SD is the standard deviation.

3.5.4.4 Precision

The average area of RV and %RSD was determined for all injections and tabulated in Table 3.4. The % RSD for all the samples was less than 1% and thus within the acceptable limit for the developed method to be precise (Table 8.2 and 8.3, Appendix 8).

3.5.4.5 Intraday and Interday Variation

The intraday and interday variations were conducted at different times for two consecutive days, and their %RSD calculated. %RSD for both intraday and interday variability was less than 2%, which is within an acceptable limit (Table 3.4) and (Table 8.2 and 8.3, Appendix 8).

Table 3.4: Calculated HPLC parameter for RV using developed method

Parameters	RV (Mobile phase)	RV (PBS)
R^2	0.999	0.999
Linear range (µg/mL)	0.1 - 20.0	0.1-20.0
LOD (ng/mL)	28.0	49
LOQ (ng/mL)	85.0	149
Precision (% RSD)	0.61	1.03
Intra-day R.S.D. (%)	0.58	0.46
Inter-day R.S.D. (%)	1.15	1.38

3.5.5 Development and validation of analytical method for analysis of biological samples containing RV

Successful analysis of biological samples containing RV depends upon various factors such as an efficient RV extraction from the biological samples, and adequate chromatographic separation of the analyte from plasma endogenous components interference. RV extraction from plasma and brain samples was accomplished using a combination of multiple organic solvents and buffer, viz. methyl tertbutyl ether and acetonitrile with RIPA buffer. Initially, acetonitrile was used alone as a protein precipitating agent during the RV extraction from biological samples. However, it was not suitable for the bioanalysis of RV because of extracting plasma impurities. Other protein precipitating agents such as ethyl acetate and methanol were also employed for bioanalysis of RV (Enz et al., 2004) but were not suitable for the extraction because of lower extraction efficiency (less than 60%) with high variation and a lot of interferences. To enhance the extraction efficiency, the RV extraction was performed using a mixture of tertbutyl methyl ether and acetonitrile together with RIPA buffer, which consistently showed more than 90% of RV extraction from biological samples. RIPA buffer was employed for protein solubilization and cell lysis. Preliminary experiments were performed for the development of a selective RP-HPLC-FLD method for determination of RV in biological samples. HPLC method was optimized after investigating recovery/extraction efficiency, HPLC flow rate, the ratio of organic to an aqueous phase, and pH adjustment of the mobile phase.

3.5.5.1 Selectivity

The selectivity of RV assay method was evaluated by demonstrating the absence of endogenous plasma interference at the retention time of RV and IS. Figure 3.14 (A) and (B) portrays the chromatograms obtained from blank plasma and both RV and IS spiked plasma sample respectively which indicated that RV and IS peaks are free from endogenous plasma interference. Figure 3.15 (A) and (B) shows the chromatograms of blank brain sample and both RV and IS spiked in blank brain sample respectively, which demonstrates that RV and IS peaks are free from brain endogenous interference. These results indicate that the developed HPLC method was selective for quantification of RV and IS in rat plasma and brain samples.

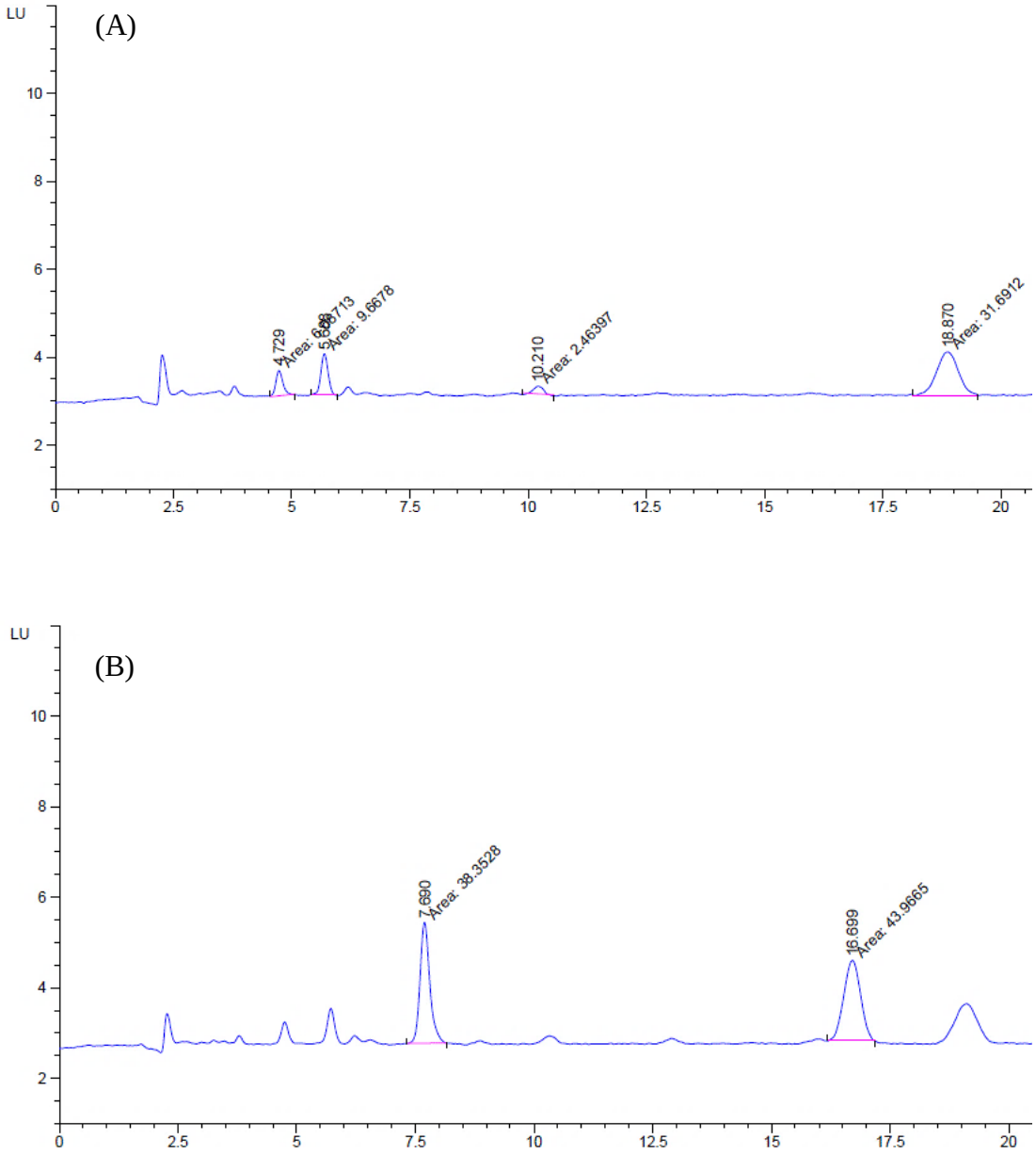

Figure 3.14: Typical HPLC-FLD chromatogram of processed samples of (A) blank plasma (control) (B) blank plasma added with RV and IS.

Blank brain tissue spiked with RV (0.02 µg) and IS (25 ng). The chromatogram in Figure-(A) indicated that no inferences at the retention time of RV and IS. The chromatogram in Figure-(B) showed a peak of RV and IS at 7.69 min and 16.6 min respectively.

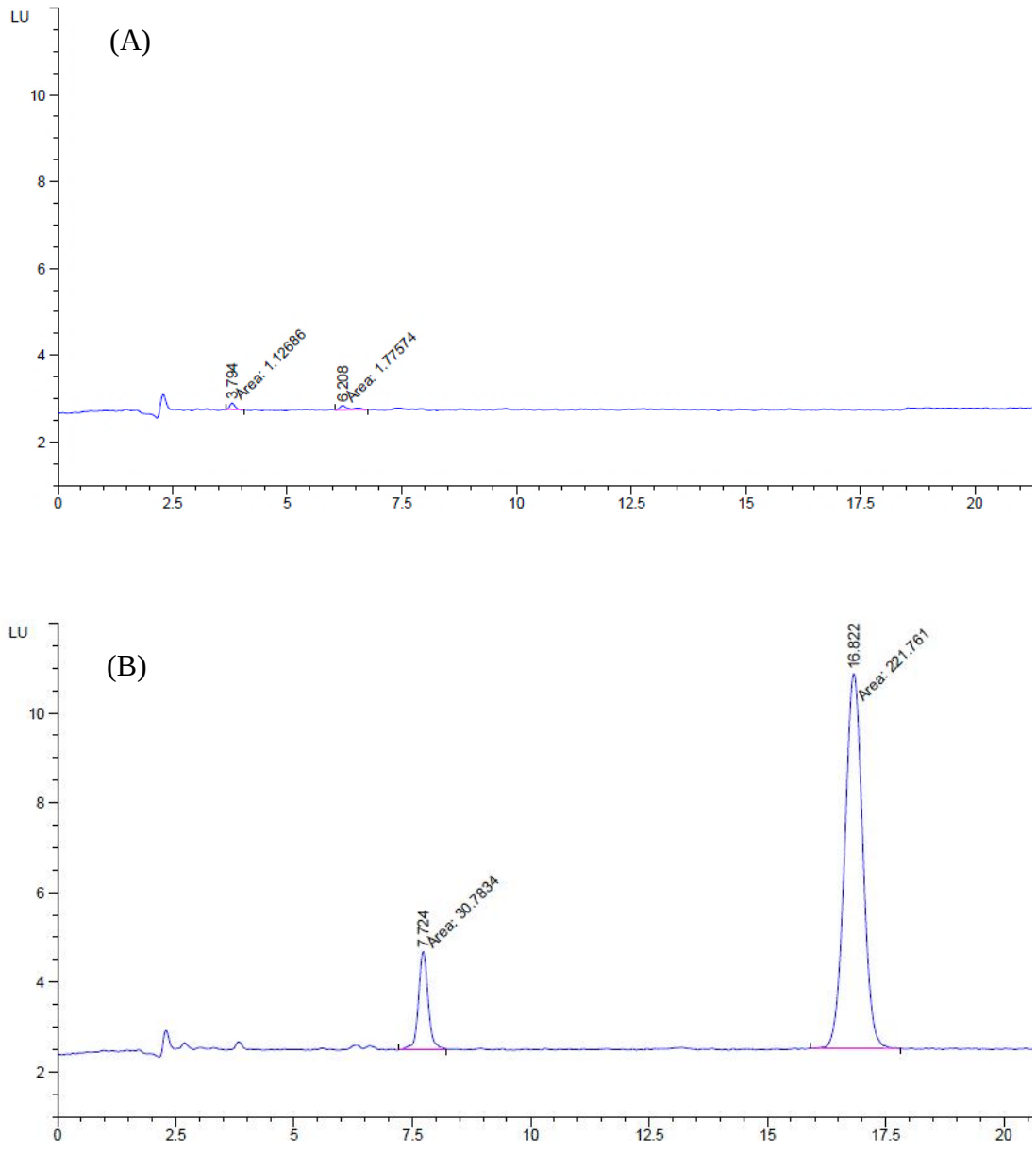

Figure 3.15: Typical HPLC-FLD Chromatogram of processed samples of (A) blank brain homogenate (B) blank brain homogenate added with RV and IS.

Blank brain tissue spiked with RV (0.02 µg) and IS (75 ng). The chromatogram in Figure-(A) indicated that no inferences at the retention time of RV and IS. The chromatogram in Figure-(B) showed a peak of RV and IS at 7.72 min and 16.8 min respectively.

3.5.5.2 Linearity

The calibration curve obtained from the ratio of peak area of RV to IS versus RV concentration prepared was linear with a r^2 value more than 0.998, in acetonitrile/water (24:76), plasma and brain matrices (Figure 8.6, Appendix section)), which was an acceptable limit for biological sample validation as per US-FDA guidelines (US-FDA, 2013).

3.5.5.3 Recovery

The mean recovery of RV from plasma and brain samples is represented in Table 3.5. A combination of acetonitrile, tertbutyl methyl ether, and RIPA buffer is the solvent of choice for the complete extraction of RV and IS from both plasma and brain matrices without any endogenous interference. The mean recovery of the RV from plasma sample was more than 97.2 ± 3.0 % with a precision of 3.3% and found to be within an acceptable limit. The mean recovery of RV from brain tissue was more than 98.3 ± 1.2 with a precision of 1.6%.

3.5.5.4 Accuracy and Precision

The intraday and interday precisions were 3.3 % and 4.0 % respectively in plasma with an accuracy of 97.2 ± 3.0 % and 93.0 ± 1.7 % (Table 3.5). However, intraday and interday precision were lower for brain samples, ranging from 1.6 % and 3.4 % respectively with 98.3 ± 1.2 and 96.7 ± 0.6 % recovery. The data indicated that the intra-day and inter-day accuracy and precision were within an acceptable range for bioanalytical method validation as per US-FDA guidelines (US-FDA, 2013).

3.5.5.5 Sensitivity

The LOD and LOQ from the developed method were calculated using the signal to noise level and slope of the calibration curve. The calculated LOD and LOQ were found to be 55.0 ng/mL and 186 ng/mL respectively in the blank plasma along with 55.0 ng/mL and 166.0 ng/mL respectively in brain samples (Table 8.7 in Appendix section).

Table 3.5: Intraday and Interday precision and accuracy data for RV in both plasma and brain samples.

Matrix/ drug	spiked concentration (ng/mL	Intraday (n=6)			Inter-day (n=6)		
		mean concentration ± SD (ng/mL)	CV (%)	Accuracy (%)	mean concentration ± SD (ng/mL)	CV (%)	Accuracy (%)
RV							
Plasma	200	187.6 ± 11.0	3.6	93.8	182.1 ± 9.7	5.4	91.0
	500	491.5 ± 16.7	3.4	98.3	472.1 ± 19.4	4.1	94.4
	1000	994.7± 27.7	2.8	99.5	936.7 ± 22.8	2.4	93.6
Average	-	-	3.3	97.2		4.0	93.0
brain	200	195.6 ± 3.9	2.0	99.6	193.2 ± 8.9	4.6	96.7
	500	486.8 ± 6.1	1.3	98.2	475.6 ± 9.0	2.8	95.7
	1000	979.5 ± 13.2	1.4	97.2	975.6 ± 26.2	2.7	97.6
Average			1.6	98.3		3.4	96.7

Data represented in Mean ±SD (n=6). CV is coefficient of variation, SD: standard deviation

3.5.6 Method development and validation for *in-vitro* C-6 analysis

3.5.6.1 Selectivity

The selectivity of C-6 assay method was evaluated by determining the peak purity using photodiode array detector and absence of nanoparticulate matrices interferences with the retention time of C-6. Figure 3.16 portrays the chromatograms obtained from analyzing the blank supernatant of PLGA NPs diluted in the mobile phase, C-6 dissolved in mobile phase which indicated that C-6 peaks at 4.4 min retention time.

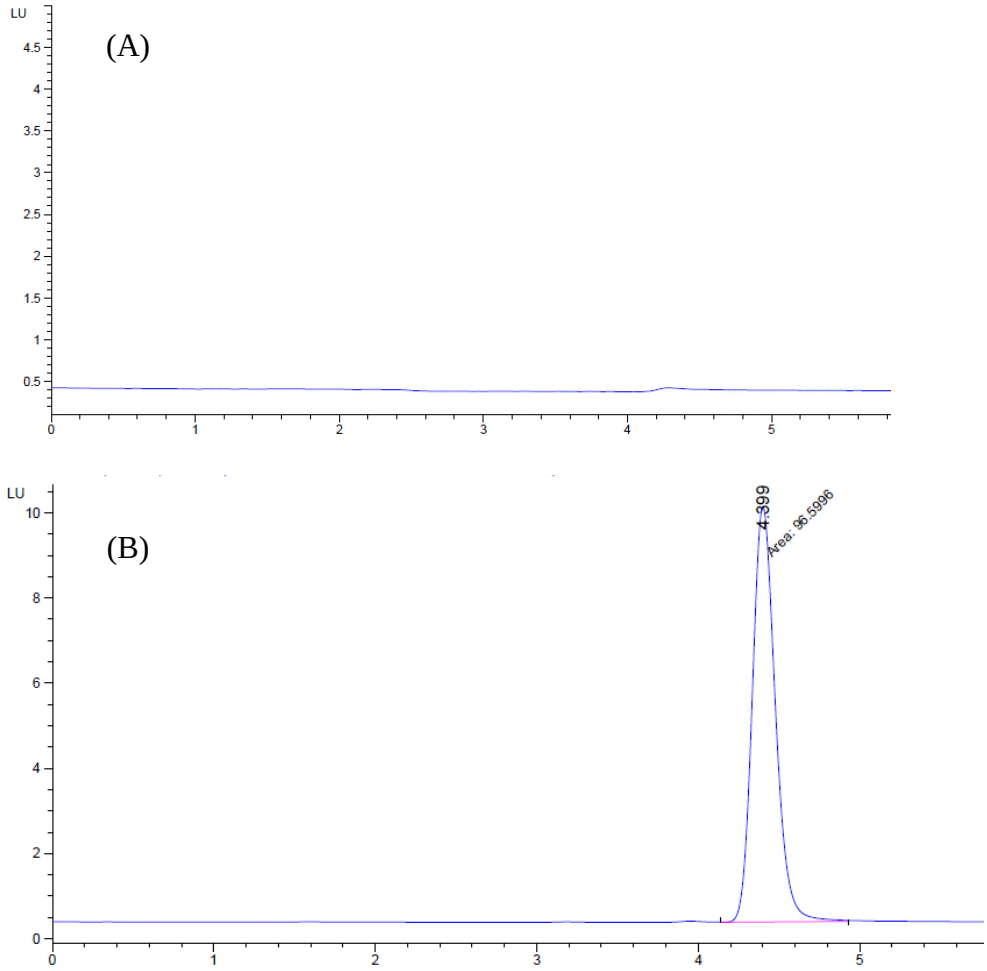

Figure 3.16: Typical HPLC chromatogram of (A) blank PLGA NP supernatant in mobile phase (B) 20 ng/mL of C-6 prepared in mobile phase
Each run was carried out for 8 min with C-6 retention time at 4.4 min.

3.5.6.2 Linearity

The fluorescent intensity detected for C-6 in mobile phase was linear within the concentration ranging from 10-400 ng/mL with a correlation coefficient more than 0.999 as indicated in Table 3.6 and Figure 8.8 in Appendix.

3.5.6.3 Recovery (Accuracy)

The accuracy or recovery of C-6 from developed PLGA nano-formulation was determined to evaluate the specificity of the developed HPLC-FLD method. The results obtained from C-6 recovery from blank PLGA matrix is tabulated in Table 3.6. The recovery test revealed that more than 98.8 ± 0.7% of C-6 recovery was achieved with less than of 0.9 %RSD.

Table 3.6: Calculated HPLC parameter for C-6 using developed method *

Parameters	C-6 (Mobile phase)	C-6 (Plasma samples)	C-6 (Brain samples)
R^2	0.999	0.999	0.999
Recovery (%)	98.8 ± 0.7	99.5 ± 0.6	99.0 ± 1.1
Linear range (ng/mL)	10 - 400	1 - 35	1 - 35
LOD (ng/mL)	0.05	4.3	5.8
LOQ (ng/mL)	0.1	-	-
Precision (% RSD)	0.9	-	-
Intra-day R.S.D. (%)	0.1	-	-
Inter-day R.S.D. (%)	0.5	-	-

* refer appendix 8 for detailed calculation of this table

3.5.7 Development and Validation of analytical method for analysis of biological samples containing C-6

Successful analysis of C-6 in biological samples was carried out in RIPA Buffer. Various preliminary experiments were performed for the development of a selective fluorescent plate reader method to determine C-6 in biological samples treated with RIPA buffer. During optimization stage, the volume of the RIPA buffer was studied to obtain complete recovery of the C-6 from biological samples. It was found that double amount of the RIPA buffer with respect to the volume of biological sample was necessary to achieve 100% recovery.

3.5.7.1 Recovery and sensitivity

Blank plasma and brain samples were also analyzed as controls and found with minimum fluorescence intensity (< 150) on a plate reader. In comparison, the plasma and brain samples spiked with 6.5 ng/mL of C-6 showed fluorescent signal more than 900 LU. An almost complete recovery (>95%) of C-6 from biological samples was achieved using RIPA buffer. The mean recovery of the C-6 from plasma and brain samples are represented in Table 3.7 The data indicated that the sample processing and assay method can produce an accurate analysis of C-6 in biological samples. Based on obtained data, we concluded that the developed method is accurate and sensitive for the analysis of C-6.

Table 3.7: Recovery of the C-6 from the plasma and brain spiked samples.

Matrix/ drug	spiked concentration (ng/mL)	mean C-6 concentration recovered ± SD (ng/mL)	Accuracy (%)
C-6			
Plasma	6.5	6.4 ± 0.06	99.1 ± 0.9
	13.0	12.9 ± 0.2	99.7 ± 1.9
	32.0	32.0 ± 0.1	99.3 ± 0.1
Average Recovery	-		99.5 %
Brain	6.5	6.4 ± 0.2	98.5 ± 3.8
	12.9	12.8 ± 0.1	99.2 ± 1.1
	32.2	32.0 ± 0.6	99.2 ± 1.9
Average Recovery			99.0 %

Data represented in Mean ± SD (n=3)

3.5.7.2 Linearity

The calibration curve obtained from average fluorescent intensity signals against C-6 concentrations was linear. The r^2 value more than 0.999 in blank milli-Q water, plasma and brain matrices which were an acceptable limit as per US-FDA guidelines for biological sample validation (US-FDA, 2013). These correlation coefficient values represent a good correlation between average intensity obtained and concentration of C-6 spiked (Figure 8.11, Appendix section).

3.6 Conclusion

The present chapter refines the development of RP-HPLC methods for the analysis of RV and C-6 in both *in-vitro* samples and biological samples. Both the methods are highly sensitive and selective in nature for the quantitative analysis of RV and C-6.

The developed and validated HPLC method for quantification of RV *in-vitro* samples was very simple and reliable in the isocratic mode. The mobile phase composition employed for analysis was easy to prepare and was not containing any buffer. The method was validated for linearity, accuracy, precision, LOD and LOQ. In addition to this, the analysis of forced degradation products demonstrated that the developed HPLC method for RV is stability indicating method. Besides this, the represented chromatograms representing the various degradation products of RV under stressed conditions. However, all degradation products were completely isolated from the peak of the RV verifying specific nature of the developed HPLC method. The method was highly sensitive with a LOD of 28.0 ng/mL and a precision of less than 2.0 %. Thus, the developed HPLC method was simple, sensitive, stability indicating, accurate and precise enough to quantify the RV in the developed nano-formulations.

The gradient method developed for the quantitative determination of RV in plasma and brain samples was simple, cost effective, and selective. The extraction method developed for extraction of RV and venlafaxine (IS) was effective as it utilized a combination of RIPA buffer and two organic solvents. The recovery of the RV from both the plasma and brain matrices was more than 97.2 ± 3.0 % and 98.3 ± 1.2 % respectively.

Likewise, RV, another simple, accurate and selective method was also developed for the *in-vitro* analysis of C-6 which was isocratic in nature. It is a short run of 8 min. The developed method was highly sensitive and able to detect the C-6 with a LOD of 0.05 ng/mL with a SD of less than 1.52%. The sample recovery of C-6 was more than 98.7 ± 0.6%, Therefore, the method for C-6 analysis was highly sensitive, accurate, selective and precise enough to quantify the C-6 in the developed nano-formulations. Simultaneously, a very fast, sensitive and accurate method was also established for the evaluation of C-6 in biological samples using RIPA buffer and plate reader. The mean recovery of the C-6 from plasma and brain sample was more than 99.0 % and well

within an acceptable limit. This high recovery is attributed to the use of RIPA buffer, direct fluorescent measurement without extraction process.

In conclusion, the developed methods are selective, accurate, highly sensitive and reproducible in nature. These developed HPLC methods are all successfully validated for quantifying the RV and C-6 separately in *in-vitro* samples, rat plasma and brain samples for pharmacokinetic study.

4. Chapter-4 Formulation and Development of Single Ligand and Dual Ligand PLGA Nanoparticles

4.1 Introduction

Brain targeting via IN route to bypass the BBB is a promising treatment approach for various neurodegenerative disorders. Although direct delivery from nose to the brain is possible, neurotherapeutic drugs still need to cross various transport barriers such as the nasal mucosa membrane, intracellular transport along the olfactory neuron, and diffusion across multiple brain compartments (Hanson & Frey, 2008; Pardeshi & Belgamwar, 2013). Biodegradable NPs with various targeting approaches such as surface chemical modification (Acharya & Reddy, 2016; Singh et al., 2016) or surface conjugation with specific targeting ligands (Bi et al., 2016; Bian et al., 2016; H. Xia et al., 2012) have been investigated to increase the nasal uptake and therapeutic efficacy of drugs in the brain. Functionalized NPs have demonstrated to be able to enhance the ability to deliver drugs specifically to the brain and sometimes can protect the drug from chemical degradation in the body.

The two most commonly used polymers for nasal drug delivery are PLGA and chitosan (or its derivatives). Both polymers are biocompatible, biodegradable and safe for preparing effective nanoparticulate drug delivery systems. As PLGA has been used for controlling drug release for decades and is approved by the U.S. FDA for parenteral use, it is an obvious choice for drug encapsulation. PLGA forms spherical particles that are normally negatively charged with a smooth surface. They can slowly release their content, based on the hydrolysis rate of the polymer (Sah et al., 2013). Whilst some promising results have been observed (Seju et al., 2011; D. Sharma et al., 2015), the use of PLGA NPs in IN drug delivery is significantly hindered due to rapid nasal mucociliary clearance, lack of mucoadhesion and short residence time in the brain region. Various efforts have been made to tackle these problems by surface modification with proper functionalization (Bi et al., 2016; L. Yan et al., 2013).

We formulated PLGA NPs containing SA-ODA for targeting neuronal cells. The SA present on the surface of the NPs will potentially interact with the SA receptor expressing cells (i.e., neuronal cells) present inside the brain and increase the drug concentration in the brain region. In addition, a mucoadhesive polymer such as GC or TGC was used to coat the surface of the NPs in order to reduce nasal mucociliary clearance and thereby increase the nasal residence time.

Mucoadhesive polymers such as chitosan and GC have been shown to enhance permeation and mucosal retention (Bernkop-Schnürch et al., 2004; Shahnaz et al., 2012). Although GC has been reported to improve the mucosal absorption of poorly soluble drugs by increasing the nasal residence time and therefore may be helpful in increasing the drug uptake (Pawar et al., 2013) but, GC has not been reported for the IN administration of NPs for brain targeting. Hence, we explored the use of thiolated GC, a water-soluble chitosan derivative for surface coating the functionalized PLGA NPs. The attachment of the thiol moiety to GC is expected to further improve its mucoadhesive properties of NPs via formation of disulfide bonds with a cysteine-rich subdomain of the mucus layer, ultimately allowing the NPs to stay longer in the nasal mucosa (Makhlof et al., 2010). The use of the TGC has not been previously reported for the brain targeting of drugs using IN pathways. Our novel formulation containing dual targeting ligands, SA-ODA and TGC, was designed to enhance the delivery of the drug into the brain via the IN route.

In addition, the use of a stabilizer is essential for the formulation of nano-sized droplets. A stabilizer plays an important role in preventing the aggregation of NPs during the emulsification process. Although many different stabilizers including surfactants have been used for the emulsification process (Cooper & Harirforoosh, 2014; Sharma et al., 2016), the biocompatibility and non-toxic nature of the stabilizer must be considered in pharmaceutical formulations. Therefore, we investigated two different types of stabilizer [Polyvinyl alcohol (PVA) and d-α-tocopheryl polyethylene glycol 1000 succinate (Vitamin E TPGS or TPGS)] for the fabrication of our NPs (Figure 4.1). PVA is the most commonly used emulsifier in the formulation of PLGA NPs (Menon et al., 2012; Murakami et al., 1999). It is widely used as a steric stabilizer for NPs and blocks the aggregation of nano-sized droplets during the emulsification process, thereby producing NPs with a low polydispersity index.

Various literature indicated that Vitamin E prevents or slows the oxidative damage of brain cells induced by β-amyloid cells (Dysken et al., 2014; Farina et al., 2012; Grundman, 2000). The idea of formulating PLGA NPs using TPGS as an emulsifier for the treatment of the brain disorder via IN route potentially would solve two purposes, stabilizing NPs and synergistically treating AD. Although in our formulation, the primary function of TPGS is functioning as an emulsifier or stabilizer.

PLGA NPs prepared with TPGS as an emulsifier may have an additional advantage is that TPGS potentially could improve cognitive disorders, which is not be possible with NPs prepared with PVA. Structurally, TPGS is amphiphilic in nature owing to the presence of the long polyethylene glycol chain and hydrocarbon chain. Due to its unique structure and property, it is miscible with both water and oil phase, which helps in improving the emulsification process during NPs fabrication (Mu & Feng, 2003a).

(A)

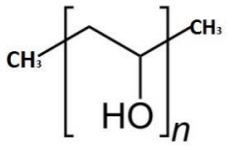

(B)

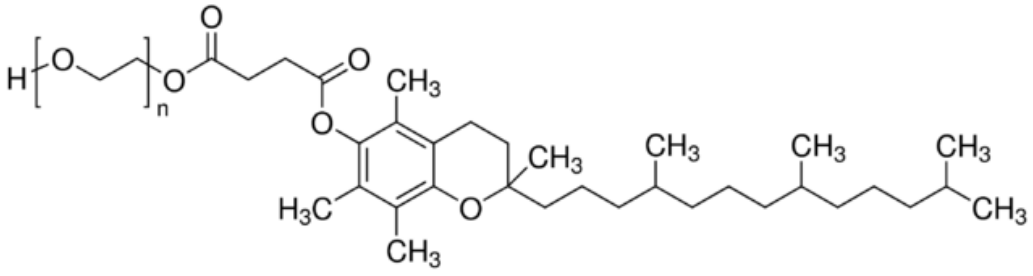

Figure 4.1 Chemical structure of (A) PVA (B) TPGS

4.2 Objective

The objective of this study was to formulate and develop biodegradable and bio-compatible RV and C-6 loaded PLGA NPs functionalized with dual targeting ligands for brain targeting. The NPs were loaded with C-6 along with the RV. C-6 has been used as a diagnostic model drug for various studies and a fluorescent marker that can be easily detected. We used the C-6 here as a marker for easy detection *in-vivo* and to assess the co-incorporation of two agents into the same NPs.

This chapter involves the formulation of three different types of nanoparticulate formulations using two separately synthesized targeting ligands, which were chosen to formulate RV loaded PLGA NPs. The first targeting ligand, GC or modified TGC polymer was employed via surface coating of the developed PLGA NPs, which aimed to provide, better mucoadhesive ability to prolong nasal residence time and promote brain uptake. A second targeting ligand, SA-ODA was incorporated into the organic phase during the formulation of PLGA NPs. Thus, this system represents a novel formulation to achieve prolonged treatment of brain disorders (Huile et al., 2011; Tosi et al., 2010). Following types of NPs were formulated and characterized:

A. RV and C-6 loaded PLGA-SA-ODA NPs (containing single ligand as SA-ODA)
B. RV and C-6 loaded PLGA-SA-ODA NPs coated with GC (containing dual ligand as SA-ODA and GC)
C. RV and C-6 loaded PLGA-SA-ODA NPs coated with TGC (containing dual ligand as SA-ODA and TGC)

4.3 Materials

Rivastigmine hydrogen tartrate (99.2%, IC-CS-146-0-140108) was purchased from Innochem Technology Co., Ltd., (Beijing, China) which was converted into RV free base before being incorporated into NP formulations. PLGA (47:53 ratio, Mw 3.5 kDa) was received as a gift sample from Durect Corporation, Birmingham, USA. PLGA (47:53 ratio, Mw 110 kDa) and PLGA (50:50 ratio, Mw 150 kDa) was purchased from Purac Biochem (Gorinchem, Germany). GC, (G7753-5g, Mw 250 kDa), PVA (80% hydrolysed; Mw: 9000-10,000, 360627 500 gm), TPGS (57668-5g) and C-6 (442631-

1G), Ellman's reagent were purchased from Sigma-Aldrich (Castle Hill NSW, Australia).

Dialysis bag (cellophane membrane, molecular weight cut off 10,000-120,00Da) was purchased from Spectrum Lab Inc (Rancho Dominguez, USA). Ultrapure Milli-Q water was used throughout all the procedures and experiments. Other chemicals used for analysis were of HPLC grade unless otherwise specified.

4.4 Methods

4.4.1 Formulation of RV loaded PLGA NPs

RV loaded PLGA NPs were prepared using oil-in-water (o/w) single emulsion solvent evaporation method using either 1% PVA or 0.3% TPGS in the external water phase as a stabilizer with slight modifications (McCall & Sirianni, 2013; Parveen & Sahoo, 2011).

General Procedure for (o/w) single emulsion solvent evaporation method

Briefly, 2 ml of ethyl acetate containing 10 mg of PLGA polymer (oil phase) and 3 mg of RV free base were added dropwise to 4.0 mL of aqueous phase (1% PVA or 0.3% TPGS), and the mixture sonicated for 90 seconds in an ice bath using a probe sonicator (UP200S, Microtip-S7, Hielscher Ultrasonics GmbH, Teltow, Germany) set with 80% amplitude and 0.4 cycle/sec. The o/w emulsion was diluted up to 20 mL of aqueous phase (1% PVA or 0.3% TPGS) and stirred at 100 rpm for 30 min using a magnetic stirrer (RW 20, Ika Laboratories, Postfach, Staufen, Germany) to harden the surface of the NPs. After 30 min, the organic solvent was evaporated at 50°C for 20 min under vacuum using a rotary evaporator (Buchi Rotavap R-200, Flawfil Switzerland) and the resultant NPs were purified by centrifugation at 35,000g (20 min, 4°C) (Allegra ™ 64R centrifuge, Backman Coulter, Inc., CA, USA) to remove free RV. After centrifugation, the supernatant was removed and PLGA NPs were resuspended into 5mL of milli-Q water and stored at 4°C for further analysis.

Blank PLGA NPs were also fabricated separately for optimization of various parameters using a similar procedure as described above.

4.4.2 Optimization of RV loaded PLGA NPs

To achieve the optimum particle size and good encapsulation efficiency (EE), RV loaded PLGA NPs were optimized for the following parameters.

4.4.2.1 Effect of aqueous phase pH

To investigate the effect of pH on EE of RV in PLGA NPs, pH of the aqueous phase was optimized. For this, milli-Q water was replaced with 1 mM HEPES Buffer (pH 9.0) as an aqueous medium. The NPs were formulated via single emulsion (o/w) solvent evaporation technique using 1% PVA (as a stabilizer) using 23.0% w/w theoretical drug loading (i.e., 3 mg of RV free base) and low molecular weight PLGA polymer (3.5 kDa). PVA was previously prepared in 1 mM HEPES buffer. PLGA NPs were formulated using the similar procedure described previously in section 4.4.1.

4.4.2.2 Effect of molecular weight of PLGA

The size of the NPs is affected by various factors, and molecular weight of the polymer is one of the most important factors. Therefore, the effect of varying molecular weight of PLGA polymer on the NP's size and EE of the drug was studied. To investigate this, PLGA NPs were prepared using 3.5 kDa, 110 kDa and 150 kDa molecular weight and 1% PVA aqueous solution as a stabilizer. Briefly, the NPs were formulated by o/w single emulsion method using a general procedure described in section 4.4.1 with 23.0% theoretical drug loading (3 mg of free RV base). The formulated NPs were characterized for nanoparticle size, EE, and experimental drug loading in order to evaluate the effect of the PLGA molecular weight on colloidal properties of the NPs.

4.4.2.3 Effect of stabilizers

A stabilizer plays an important role in facilitating the nano-emulsion formation by aligning at the o/w interface. To investigate the effect of the stabilizer, the NPs were formulated by the single emulsion (o/w) solvent evaporation method with two different types of emulsifiers: PVA (1% w/v aqueous solution) and TPGS (0.3% w/v and 1.0% w/v aqueous solution). All other parameters such as theoretical drug loading (23.0% w/v), ultra-sonication power (80% amplitude and 0.4 cycle/sec), and PLGA molecular

weight (110 kDa) were kept constant to determine the effect of stabilizer on colloidal properties of the NPs.

4.4.2.4 Effect of formulation method (single emulsion versus double emulsion)

To determine the influence of the formulation methods on physicochemical properties of the developed PLGA NPs, we compared two different methods for NPs formulation. RV loaded PLGA NPs were formulated using single and double emulsion methods as expressed in Table 4.1.

Table 4.1: Comparison of o/w and w/o/w formulation method

Name of component	Quantity used	
	Single emulsion (o/w) method	**Double emulsion (w/o/w) method**
RV (free base)	5.0 mg	5.0 mg
PLGA (110 kDA)	30 .0 mg	30.0 mg
Ethyl acetate	3.0 mL	3.0 mL
Stabilizer (0.3% TPGS)	20.0 mL	20.0 mL

(a) Single emulsion solvent evaporation method

RV loaded PLGA NPs were formulated by single emulsion solvent evaporation method following a general procedure as mentioned in section 4.4.1. Briefly, an organic phase (containing 5.0 mg of RV drug and 30.0 mg of PLGA polymer in 3.0 mL of ethyl acetate) was emulsified with 6.0 mL of 0.3% TPGS solution using a probe sonicator set with 80% amplitude and 0.4 cycle/sec. The emulsified mixture was diluted with 14.0 mL of aqueous phase (0.3% TPGS solution) and stirred at 100 rpm for 30 min to harden the surface of the NPs. RV loaded PLGA NPs were obtained by evaporating the organic solvent using rotary evaporator at 50°C and further purified by centrifugation at 35,000g (20 min, 4°C). After centrifugation, the supernatant was removed and PLGA NPs were resuspended into 5 mL of milli-Q water for further characterisation.

(b) Double emulsion solvent evaporation method

RV loaded PLGA NPs were formulated using double emulsion solvent evaporation method (w/o/w) as described following: Briefly, the primary emulsion was formed by mixing 0.5 ml of aqueous phase (5.0 mg RV dissolved in 0.3% TPGS solution) with 3 mL of ethyl acetate containing 30 mg of the PLGA polymer (oil phase). The w/o mixture was sonicated for 2 min in an ice bath using a probe sonicator set with 80% amplitude and 0.4 cycle/sec. The primary w/o emulsion was immediately transferred into 20 mL of aqueous phase (0.3% TPGS solution) and the mixture was emulsified for 2 min using the same probe sonicator under similar conditions. The w/o/w double emulsion was stirred for 30 min using a magnetic stirrer to harden the NPs surface. After 30 min, the organic solvent was evaporated at 50°C under vacuum using a rotary evaporator and the resultant PLGA NPs were purified by centrifugation at 35,000g (20 min, 4°C). After centrifugation, the supernatant was removed and RV loaded PLGA NPs were resuspended into 5mL of milli-Q water and stored at 4°C for further analysis.

4.4.2.5 Effect of theoretical RV drug loading

To achieve the maximum amount of drug loading inside the NPs, we optimized the theoretical drug loading using various amounts of RV ranging from 14.3% to 23.0% w/w of PLGA polymer. The NPs were formulated using double emulsion solvent evaporation technique as described previously in section 4.4.2.4 (b). All the batches were formulated in triplicates using 0.3% TPGS as an emulsifier and PLGA molecular weight (110 kDa) except NPs were loaded with theoretical drug loading varying from 14.3 to 23.0% w/w.

The various parameters optimized for the development of the RV loaded PLGA NPs are summarized in Table 4.2.

Table 4.2: Optimization of various formulation variables for development of PLGA NPs

Formulation Parameter	**Factors Optimized**				**Optimized conditions**
	Polymer type	**Stabilizer concentration (% w/v)**	**Aqueous phase**	**Theoretical drug loading (w/w)**	**Formulation method**	
Effect of External Aqueous phase pH						
	PLGA (3.5 kDa)	1% PVA	***1% PVA in Water***	23.0%	o/w method	***1% PVA in Water***
	PLGA (3.5 kDa)	1% PVA	***1% PVA in 1m M HEPES buffer (pH 9.0)***	23.0%	o/w method	
Effect of molecular weight of PLGA						
	PLGA (3.5 kDa)	1% PVA	1% PVA	23.0%	o/w method	
	PLGA (110 kDa)	1% PVA	1% PVA	23.0%	o/w method	***PLGA (110 kDa)***
	PLGA (150 kDa)	1% PVA	1% PVA	23.0%	o/w method	
Effect of Stabilizer						
	PLGA (110 kDa)	1% PVA	**1% PVA**	23.0%	o/w method	
	PLGA (110 kDa)	0.3% TPGS	**0.3% TPGS**	23.0%	o/w method	***0.3% TPGS***

Formulation Parameter	**Factors Optimized**				**Optimized conditions**
	Polymer type	**Stabilizer concentration (% w/v)**	**Aqueous phase**	**Theoretical drug loading (w/w)**	**Formulation method**	
	PLGA (110 kDa)	1% TPGS	**1% TPGS**	23.0%	o/w method	
Effect of formulation method						
	PLGA (110 kDa)	0.3% TPGS	0.3% TPGS	14.3%	**o/w method**	
	PLGA (110 kDa)	0.3% TPGS	0.3% TPGS	14.3%	**w/o/w method**	***w/o/w method***
Effect of theoretical drug loading						
	PLGA (110 kDa)	0.3% TPGS	0.3% TPGS	**14.3%**	w/o/w method	***14.3%***
	PLGA (110 kDa)	0.3% TPGS	0.3% TPGS	**16.6 %**	w/o/w method	
	PLGA (110 kDa)	0.3% TPGS	0.3% TPGS	**23.0%**	w/o/w method	

Various parameters were optimized to achieve the highest drug loading and EE while nanoparticulate size was kept below 250 nm and high zeta potential.

4.4.3 Optimized single ligand RV loaded PLGA-SA-ODA NPs

The naked PLGA NPs were optimized for all the formulation conditions as mentioned in Table 4.2, then these optimized conditions were employed for the formulation of single ligand modified and dual ligand modified PLGA NPs.

Single ligand RV loaded PLGA NPs were prepared using a (w/o/w) double emulsion solvent evaporation method using 0.3% TPGS as a stabilizer. Single ligand PLGA NPs were prepared by incorporating SA-ODA (neuronal cell targeting ligand) into the organic phase during formulation. SA-ODA was first synthesized by a coupling reaction between SA and octadecyl amine using EDC/NHS selective carbodiimide reaction (She et al., 2014). The synthesis and characterisation were undertaken by Nazhasan Huda (Ph.D. student, School of Pharmacy, Curtin University).

Procedure

Initially, SA-ODA conjugate formed a cloudy mixture when it was directly dispersed into the organic phase containing PLGA. Therefore, ethanol was selected as a co-solvent to dissolve SA-ODA conjugate in order to avoid aggregation with the polymer in the mixture. Briefly, the primary emulsion (w/o) was formed by mixing 0.5 ml of aqueous phase (5 mg of RV dissolved in 0.3% TPGS solution) with 3 ml of polymer solution [a mixture of 30 mg of the PLGA polymer and 3 mg of SA-ODA (previously dissolved in 120 µL of ethanol)] (oil phase). The w/o mixture was sonicated for 2 min using a probe sonicator set with 40% amplitude and 0.4 cycles over an ice bath. The primary emulsion was immediately transferred into 20 ml of aqueous phase (0.3% TPGS solution) and the mixture was emulsified for 2 min using the same probe sonicator under the same conditions over an ice bath. The w/o/w double emulsion was stirred for 30 min using a magnetic stirrer to harden the surface of NPs. After 30 min, the organic solvent was evaporated at 50°C under vacuum using a rotary evaporator and the resultant NPs were purified by centrifugation at 35,000g (20 min, 4°C) to remove the excess of free RV. After centrifugation, the supernatant was removed and RV loaded PLGA NPs were resuspended into 5mL of milli-Q water and stored at 4°C for further analysis.

4.4.4 Optimized single ligand RV+C-6 loaded PLGA-SA-ODA NPs

To evaluate the pharmacokinetic behavior and brain targeting efficiency of a developed nanoparticulate formulation, the developed single ligand PLGA NPs were also loaded with a hydrophobic fluorescent marker i.e., C-6. According to literature, 0.25 % w/w of C-6 (amount of polymer) used in the NPs was sufficient for determination its concentration in an animal brain tissue (Kulkarni & Feng, 2011), therefore, we prepared our NPs with 0.30% of C-6 loading (of the polymer's weight).

RV + C-6 loaded PLGA-SA-ODA NPs were formulated using w/o/w double emulsion solvent evaporation technique. The developed single ligand modified PLGA-SA-ODA NPs loaded with RV and C-6 was formulated using procedure described in section 4.4.3. Briefly, a known amount of C-6 was dissolved into an oily phase to achieve 0.3% theoretical C-6 loading. Oily phase consisted of a mixture of 30 mg of PLGA polymer (110 kDa), 3 mg of SA-ODA (previously dissolved in 120 µL of ethanol) and 90 µg of C-6 dissolved in 3 mL of ethyl acetate.

The primary emulsion (w/o) was formed by emulsifying an 0.5 mL of aqueous phase (5 mg of RV dissolved in 0.3% TPGS solution) with 3 ml of oily phase using a probe sonicator set with 40% amplitude and 0.4 cycles over an ice bath for 2 min. The primary emulsion was immediately diluted into 20 ml of aqueous phase (0.3% TPGS solution) and the mixture was emulsified for 2 min using the same probe sonicator under the same conditions over an ice bath. The formulated nanoparticulate suspension was stirred for 30 min using a magnetic stirrer to harden the surface of NPs. The organic solvent was evaporated at 50°C under vacuum using a rotary evaporator and the resultant NPs were purified by centrifugation at 35,000g (20 min, 4°C) to remove the excess of free RV. After centrifugation, the supernatant was removed and RV loaded PLGA NPs were resuspended into 5mL of milli-Q water and stored at 4°C for further analysis. All the components used for the final optimized formulation are represented in Table 4.4. The pictorial presentation of RV+C-6 loaded PLGA-SA-ODA NPs are shown in Figure 4.2.

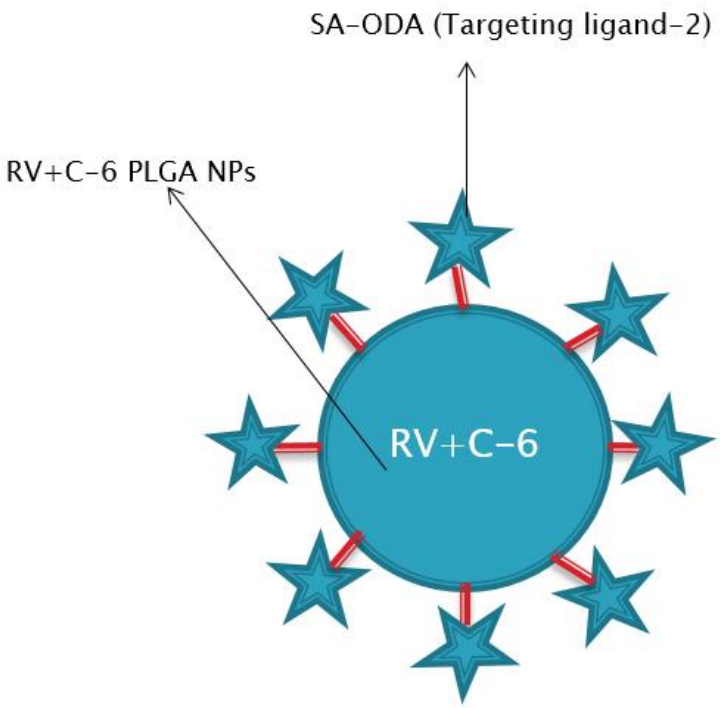

Figure 4.2: Representative image single ligand RV+C-6 loaded PLGA-SA-ODA NPs

4.4.5 Formulation and Optimization of dual ligand PLGA NPs

The developed single ligand RV+C-6 loaded PLGA-SA-ODA NPs were coated with GC/TGC in order to obtain dual ligand modified GC or TGC coated RV+C-6 loaded PLGA-SA-ODA NPs respectively. During optimization of coating, SA-ODA and C-6 was not incorporated into the loaded NPs, owing to its high cost and limited availability.

General procedure

GC or TGC coated PLGA NPs were formulated employing the double emulsion solvent evaporation method. Briefly, inner aqueous phase (5 mg of RV in 0.3% of aqueous TPGS solution) was emulsified with 3.0 mL of the organic phase (30 mg of PLGA polymer) and sonicated for 2 min using a probe sonicator set with 40% amplitude and 0.4 cycles over an ice bath. The primary emulsion was immediately transferred into 20 mL of coating polymer solution (0.2% GC or TGC dissolved in

0.3% TPGS solution) and the mixture was emulsified for 2 min using the same probe sonicator under the same conditions over an ice bath. For coating of the NPs, GC or TGC were dissolved in the outer aqueous phase. The coated NPs were purified by centrifugation at 7,168g (20 min, 4°C) to remove free RV. After centrifugation, the supernatant was removed and GC or TGC coated PLGA NPs were resuspended into 5mL of milli-Q water and stored at 4°C for further analysis.

To achieve optimum particle size and good encapsulation efficiency (EE), GC coated RV loaded PLGA NPs were optimized for the following parameters.

4.4.5.1 Effect of centrifugation speed on purification of coated NPs

During the optimization process, the size of the coated NPs was measured both before purification and after purification, as GC coated PLGA NPs were purified using centrifugation process, in order to remove the free RV drug. An increase in the size of the coated NPs was observed with higher centrifugal speed. Hence, the effect of the varying centrifugation speed for purification was investigated on the size and EE of the coated NPs.

The coated NPs were formulated following a general procedure as described in section 4.4.5 and all the other parameters such as drug loading (14.3%), ultra-sonication power and PLGA molecular weight (110 kDa), and GC coat concentration (0.2%) etc. were kept constant. NPs were purified at different centrifugation speed varying from 7000 g to 35,000 g in order to observe the effect of centrifugation speed on the colloidal characteristics of the fabricated NPs.

4.4.5.2 Effect of GC coating polymer concentration

The amount of GC polymer required for coating was optimized in order to obtain coated NPs with appropriate size and drug loading. To investigate this, GC coated PLGA NPs were prepared using double emulsion solvent evaporation method described in section 4.4.5. Various concentrations of GC (0.05% -0.4%) were dissolved in external 0.3% TPGS aqueous solution to prepare GC coated PLGA NPs. All the other formulation parameters were kept constant as mentioned in Table 4.3

Table 4.3: Formulation variables of GC coated PLGA NPs were studied

Formulation Variable	Polymer type	External phase	Theoretical drug loading (w/v)	Formulation method	GC polymer concentration (w/v) *	Centrifugation speed (in g)
Effect of centrifugal speed						
	PLGA (110 kDa)	0.3% TPGS	14.2%	w/o/w	0.2%	35,000
	PLGA (110 kDa)	0.3% TPGS	14.2%	w/o/w	0.2%	20,100
	PLGA (110 kDa)	0.3% TPGS	14.2%	w/o/w	0.2%	11,200
	PLGA (110 kDa)	0.3% TPGS	14.2%	w/o/w	0.2%	7,168
Effect of GC coating concentration						
	PLGA (110 kDa)	0.3% TPGS	14.2%	w/o/w	0.05%	7,168
	PLGA (110 kDa)	0.3% TPGS	14.2%	w/o/w	0.1%	7,168
	PLGA (110 kDa)	0.3% TPGS	14.2%	w/o/w	0.2%	7,168
	PLGA (110 kDa)	0.3% TPGS	14.2%	w/o/w	0.4%	7,168

Various parameters were optimized to achieve the highest drug loading and EE while nanoparticulate size was kept below 250 nm and high zeta potential.

* GC polymer was dissolved in 0.3% TPGS solution and used as an external aqueous to prepare the coated NPs.

4.4.6 Optimized dual ligand RV+C-6 loaded PLGA NPs coated with TGC or GC

All the optimization parameters were assessed with GC coated RV loaded PLGA NPs. The optimized conditions were used to formulate dual ligand modified RV+C-6 loaded PLGA NPs. NPs were formulated using double emulsion solvent evaporation method with both TGC or GC and SA-ODA targeting ligands.

Briefly, the inner aqueous phase (5 mg of RV in 0.5 mL of 0.3% of aqueous TPGS solution) was emulsified with 3 mL of organic phase (a mixture of 30 mg of PLGA polymer and 3 mg of SA-ODA and 0.09 mg of C-6 dissolved) sonicated for 2 min at 40% amplitude and 0.4 cycle over an ice bath. The primary emulsion was immediately transferred into 20 mL of coating polymer solution (0.2% GC or TGC dissolved in 0.3% TPGS solution) and the mixture was emulsified for 2 min using the same probe sonicator under the same conditions over an ice bath. The dual ligand coated NPs were purified by centrifugation at 7,168g (20 min, 4°C) to remove free RV. After centrifugation, the supernatant was removed and GC or TGC coated PLGA NPs were resuspended into 5mL of milli-Q water and stored at 4°C for further analysis. All the components used for the final optimized formulation are represented in Table 4.4. The pictorial presentation of dual ligand RV+C-6 loaded PLGA-SA-ODA NPs coated with GC or TGC are shown in Figure 4.2.

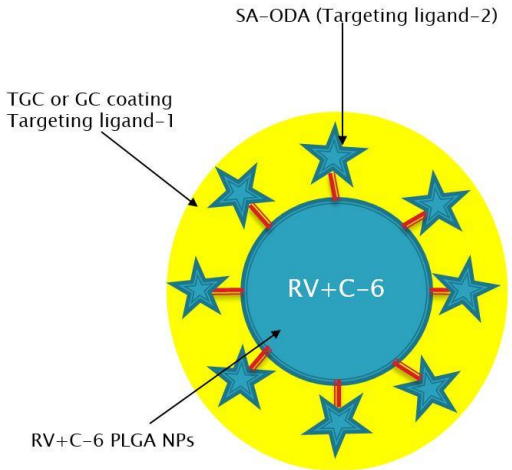

Figure 4.3: Representative image of dual ligand RV+C-6 loaded PLGA-SA-ODA NPs coated with GC or TGC

Table 4.4: Formulation of single ligand RV+C-6 loaded PLGA-SA-ODA NPs and dual ligand RV+C-6 loaded PLGA SA-ODA NPs coated with GC or TGC

Name of component	Quantity used	
	Single ligand NPs	**Dual ligand NPs**
Internal Aqueous phase		
RV (free base) dissolved in 0.3% TPGS solution	5.0 mg	5.0 mg
Oily Phase		
C-6	0.09 mg	0.09 mg
PLGA (110 kDA)	30.0 mg	30.0 mg
SA-ODA (previously dissolved in 120 μL of ethanol)	3.0 mg	3.0 mg
Ethyl acetate	3.0 mL	3.0 mL
External Aqueous phase		
Stabilizer (0.3% TPGS)	20.0 mL	20.0 mL
GC or TGC (0.2 % w/v)	-	
Sonication time and duration	4 min (2+2) 40 % amplitude and 0.4 cycles	4 min (2+2) 40 % amplitude and 0.4 cycles
Centrifugation Speed	35,000 g	7168 g
Time and temperature	for 20 min at 4°C	for 20 min at 4°C

4.4.7 Characterisation of PLGA NPs

4.4.7.1 Particle size and zeta potential measurement

The particle size, polydispersity index and surface zeta potential of NPs were determined by dynamic light scattering technique using Zetasizer Nano ZSP (Malvern Instruments Ltd., Malvern UK). All samples were measured in triplicate and results represented in mean ±SD.

4.4.7.2 HPLC analysis

RP-HPLC analysis of both RV and C-6 was carried out by using a validated method developed in Chapter 3 (section 3.4.3 and section 3.4.5 respectively).

4.4.7.3 Encapsulation efficiency and drug loading

The drug encapsulated inside the NPs was evaluated by analyzing the unloaded drug present in the supernatant obtained after centrifugation of NPs at 35,000 g (20 min, 4°C). The supernatant was diluted (X 100 times) and injected onto HPLC column following the method described in section 3.4.3 to determine the amount of free drug.

$$\text{EE}\ (\%) \quad = \frac{\text{Total drug used} - \text{free drug in supernatant}}{\text{Total drug used}} \times 100$$

$$\text{Drug Loading}\ (\%) = \frac{\text{Total drug used} - \text{free drug in supernatant}}{\text{Total NP weight}} \times 100$$

4.4.7.4 Electron microscopic studies

The surface morphological characteristics of NPs were analyzed by field emission scanning electron microscopy (FE-SEM). A sample of freeze dried NPs was mounted on a metal stub and coated with gold-palladium under vacuum using the Cressington Sputter coater (208HR, Cressington Scientific Instrument Ltd., Watford, England) and then examined on FE-SEM Zeiss NEON 40EsB, Carl Zeiss NTS (Oberkochen,

Germany) and photomicrographs were taken to determine the shape and morphological properties of the NPs.

4.4.7.5 Stability studies of NPs

Since the NPs have to be stored for certain time period at 4°C, the stability study of NPs suspension must be known. The stability study for dual ligand and single ligand PLGA NPs at 4°C was accomplished by analysing the particle size, polydispersity index, and zeta potential over a period of seven days.

The NPs used for the stability studies was Blank PLGA-SA-ODA NPs, RV+C-6 loaded PLGA-SA-ODA NPs (one ligand), RV+C-6 loaded PLGA-SA-ODA NPs coated with GC (dual ligand), and RV+C-6 loaded PLGA-SA-ODA NPs coated with TGC (dual ligand). Both single ligand and dual ligand PLGA NPs were prepared by the w/o/w method described in section 4.4.4 and section 4.4.6 using 110 kDa molecular weight of PLGA and 0.3% TPGS as an emulsifier. All four groups of NPs were stored at 4°C in the fridge for seven days and samples were withdrawn at 0, 1, 3, 5, and 7 days and analysed further for their size, PDI, and Zeta potential determined.

4.4.7.6 NPs leakage study

The NPs stored at 4°C were also evaluated for leakage of RV and C-6 for 48 h to cover the maximum time-period that NPs were likely to be stored for being used. To study the drug leaching from NPs, the two different types of NPs were produced by using w/o/w method using 110 kDa molecular weight of PLGA and 0.3% TPGS as an emulsifier. The NPs were loaded with 5 mg of RV and 0.09 mg of C-6. The prepared NPs were single ligand RV+C-6 loaded PLGA-SA-ODA NPs and dual ligand RV+C-6 loaded PLGA-SA-ODA NPs coated with TGC.

After formulation, each type of NPs was stored at 4°C, for 0 h, 6h, 24h, and 48 h. 500 µL of samples of the NPs dispersion were withdrawn and centrifuged for 15 min at 16,200 g at 4°C. The supernatant was diluted with mobile phase (X 100 times) and the percentage loss of RV and C-6 from the NPs was determined by analysing samples in HPLC (section 3.4.3 and 3.4.5 respectively).

4.4.7.7 Determination of Thiol group on NPs surface

The presence of the thiol groups on the surface of the RV+C-6 loaded TGC coated PLGA-SA-ODA NPs was determined spectrophotometrically using Ellman's reagent (5,5'-dithio-bis-2-nitro benzoic acid or DTNB) as previously described (Anitha et al., 2011; Bravo-Osuna et al., 2007; Hornof et al., 2003).

Ellman's reagent was prepared by dissolving 3.0 mg in 10 mL of 0.5 M phosphate buffer (pH 8.0). A sample of 500 µL of TGC coated NP suspension was mixed with 250 µL of phosphate buffer saline (pH 8.0) and 500 µL of Ellman's reagent. The mixture was incubated for 3h at 37°C to allow the reaction of Ellman's reagent with free sulfhydryl groups. After centrifugation at 16,200g for 15 min at 4°C, the absorbance of the supernatant was measured at 412 nm. A control sample (RV+C-6 loaded GC coated PLGA-SA-ODA NPs) was treated using the same procedure. The number of thiol group on NPs surface was determined using the following equation (Acharya & Reddy, 2016; Nobs et al., 2004).

$$n = aN[d\left(\frac{4}{3}\right)\pi r^3]$$

n is number of thiol group present per NP; a is mole of thiol determined per gram of TGC coated PLGA (which was determined using Ellman's reagent); N is Avogadro number (6.023 X 10^{23}); d is density of the NPs determined (1.65 gm/mL); r is mean radius of the NP which was determined using Zeta sizer.

4.4.7.8 *In-vitro* drug release study

The developed single ligand and dual ligand PLGA NPs were evaluated for their *in-vitro* release study. For this, 5 mL of RV loaded PLGA NPs (loaded with 1.0 mg of RV) was placed in a pre-washed dialysis tubing, immersed in 50 mL of PBS (pH 7.4) and sample was placed on shaker at 100 rpm at 37°C. In addition to release study of developed NPs, a RV control solution (1.0 mg of RV dissolved into 5 mL of milli-Q water) was placed inside the dialysis bag and immersed in 50 mL of PBS. 1 mL samples were withdrawn from the release medium at 1, 2, 3, 4, 5, 6, 7, and 24 h and replaced with an equal volume of PBS to maintain the sink conditions. All the collected samples at various time intervals were analyzed using HPLC method (section 3.3.3) to determine the mean value of % cumulative amount of RV release with respect to time. RV control solution was employed to compare the RV release from NPs against control drug solution. The RV *in-vitro* release study was performed in triplicate for each type of drug loaded NPs along with above standards.

In addition, another RV drug solution (1.0 mg free RV base dissolved in 5 mL of water) was placed in 20 mL of vial as an external standard to ensure the stability of RV at 37°C. A 200 µL of sample was withdrawn at same time intervals and diluted 100 times with mobile phase for analysis by HPLC to ensure the stability of RV.

4.4.8 Statistical analysis

All data are reported as a mean parameter determined ± standard deviation (S.D.) unless otherwise stated. The difference between the groups was determined using Student's t-test, and differences between more than two groups were determined using ANOVA method using the Graph Pad Prism Software 6.01 version (Prism, Graph Pad software Inc. Version 6.01). A P-value $\leq$ 0.05 was considered as statistically significant.

4.5 Results and Discussion

4.5.1 Formulation and optimization of PLGA NPs

4.5.1.1 Effect of the external aqueous phase pH

It is indicated in the literature that the external aqueous phase pH influences the EE of the drug in the NPs (Peltonen et al., 2004; Song et al., 1997). Evidence showed that an increase in external aqueous phase pH inhibits the ionization of a basic drug, decrease solubility in the aqueous phase and thereby increasing drug entrapment inside the NPs (Govender et al., 1999). Therefore, NPs were prepared with different aqueous medium to study the effect of the aqueous phase pH on the particle size and EE and results are indicated in Table 4.5.

NPs prepared with milli-Q water showed significantly higher EE than those prepared with HEPES buffer (Table 4.5). For example, NPs prepared in milli-Q water with 3.5 kDa PLGA molecular weight showed a much better EE 13.9 ± 4.9 % rather than 6.3 ± 0.4% EE for that prepared using HEPES buffer. Our results were different to previous literature reports (Govender et al., 1999). We speculated the reason for low EE is due to the nature of our drug and type of polymer employed in our studies. Our drug RV is amphiphilic with log P of 2.3. It has a tendency to distribute between both oily and aqueous phase during the sonication process, consequently it resulted in a low drug EE.

Particle size greatly affects the mucosal uptake and targeting efficiency. The smaller size of NPs has been shown to penetrate through the nasal mucosal membrane, whereas larger particles were localized in the nasal epithelial linings (Nafee et al., 2007; Pawar et al., 2013). Smaller NPs also have better tissue penetration across the biological membrane compared to larger NPs (Barua & Mitragotri, 2014). We found that the size of the NPs decreases with an increase in pH of an aqueous phase especially in the case of low molecular weight of PLGA. It is postulated that an increase in pH leads to greater ionization of the carboxyl group of the polymer, resulting in enhanced particle-particle repulsion, hence the smaller particle size was observed in HEPES Buffer. For example, NPs prepared with PLGA (3.5 kDa) using pH 9.0 as an aqueous phase showed 79.0±4.6 nm in size compared to 123.0±2.4 nm in water.

It can be concluded that 1mM HEPES Buffer (pH 9.0) is advantageous with regard to producing smaller particle size NPs, but drug loading and EE of NPs was also reduced. Our objective was to achieve an appropriate particle size with maximum drug loading, therefore a change of the pH was not considered necessary for optimization of NPs.

Table 4.5: Effect of the aqueous phase pH on various characteristics of RV loaded PLGA NPs.

Aqueous phase pH	PLGA Molecular weight (kDa)	Particle Size (nm)	Zeta potential (mV)	EE (%)	Drug loading (%)
Water (neutral pH)	3.5	123.0 ± 2.4	-22.8 ± 3.0	13.9 ± 4.9*	4.0 ± 1.4 *
1mM HEPES buffer (pH 9.0)	3.5	79.0 ± 4.6	-29.3 ± 3.5	6.3 ± 0.4*	1.8 ± 0.1*

Data are represented in mean ± SD (n=3). * $p<0.05$

4.5.1.2 Effect of molecular weight of PLGA

NPs size is an important parameter that influences the physical stability of the suspension, cellular uptake and biodistribution release of the drug. In general, smaller particle size provides better physical stability of NPs (De & Robinson, 2004).

When three different types of molecular weight of PLGA were assessed for their effects on size and drug EE, a trend was seen in Figure 4.4 (A). An increase in molecular weight resulted in an increase in the size of RV loaded PLGA NPs. A similar pattern was observed for blank PLGA NPs (data not shown). The possible reason for an increase in the size of the NPs could be due to the increase in viscosity of the polymer with high molecular weight that creates difficulty in the formation of nano-sized emulsion droplets (G. Mittal et al., 2007). Therefore, an increase in the NPs size with a high molecular weight of PLGA is expected which is consistent with the literature (G. Mittal et al., 2007).

Figure 4.4 (B) showed that EE did not follow a similar pattern. Initially, EE increased from 14.0% to 18.1% with an increase in molecular weight from 3.5 kDa to 110 kDa; thereafter a significant drop to 12.4% was seen with an increase in molecular weight to 150 kDa. As, the EE of the NPs is affected by both partitioning of the drug between oily and aqueous phase, and the rate of polymer solidification during the NPs formulation (G. Mittal et al., 2007) therefore, very high molecular weight which may have a very slow rate of polymer solidification because of high viscosity, showed less EE.

It is mentioned in the literature that high molecular weight of PLGA NPs may have more hydrophobic interaction between the longer molecular polymeric chain and drug molecule, which could result in an increase in viscosity of the polymeric solution and thereby hamper the solvent evaporation rate (G. Mittal et al., 2007). The slow solidification also created more opportunity for RV to continue to partitioning between oil phase and the external aqueous phase, resulting in decreased EE for 150 kDa PLGA. Based on these findings, 110 kDa molecular weight of PLGA was selected as the optimum molecular weight of PLGA polymer for making NPs. It was used for all rest studies.

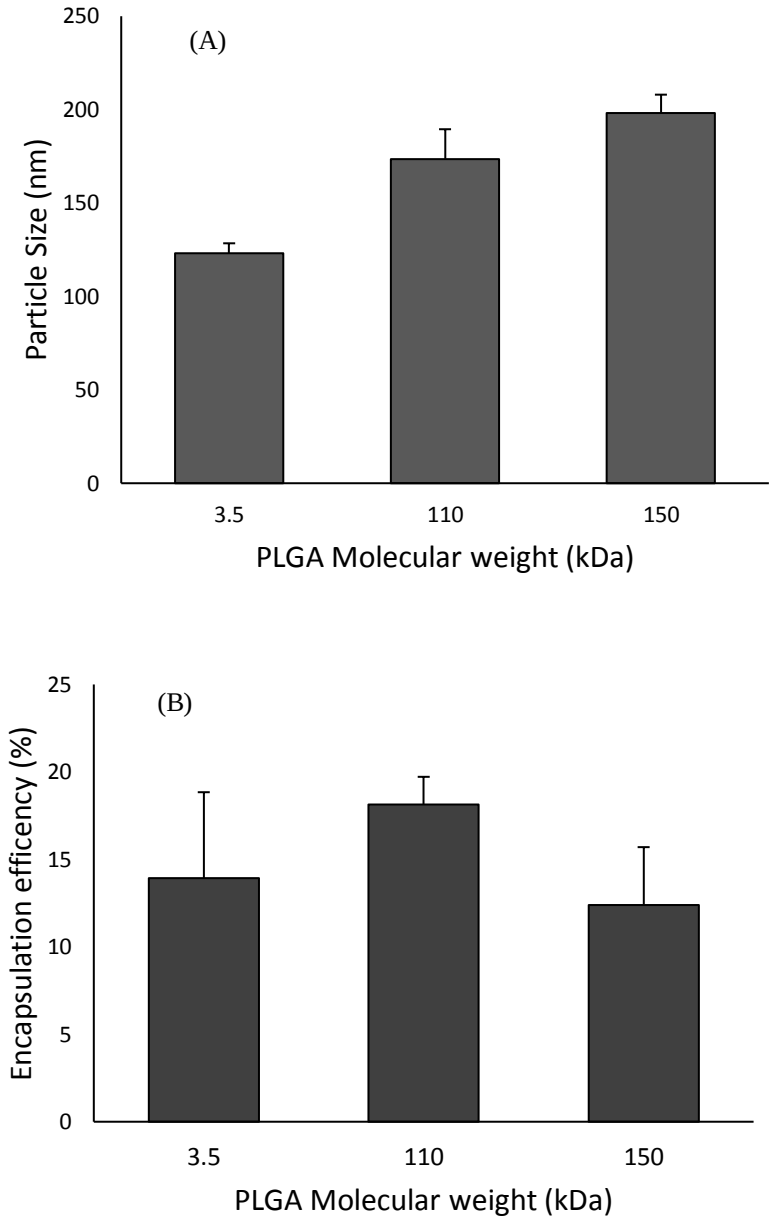

Figure 4.4: Effect of the PLGA molecular weight on (A) particles size (B) EE of the NPs

Data are represented in mean ± SD (n=3).

4.5.1.3 Effect of stabilizers

It has been reported that higher concentration of stabilizer can help to stabilize the NPs suspension and produce smaller size NPs (Patil & Surana, 2013). However, the size of the NPs also depends on other factors such as the type of the emulsifier and its concentration used. Many different types of emulsifiers (such as PVA, poloxamer, TPGS etc.) for fabricating stable nanoparticulate emulsions have been evaluated (S. S. Feng et al., 2007; McCall & Sirianni, 2013; Mu & Feng, 2003b; Patil & Surana, 2013; Turk et al., 2014; Win & Feng, 2006).

We compared two different types of non-ionic emulsifier or stabilizers to stabilize the NPs in our formulation: PVA (the most commonly used non-ionic surfactant which has been reported to produce small sized NPs with uniform particle size distribution), and TPGS (used as an emulsifier due to its amphiphilic and biodegradable nature). These are excellent emulsifiers for encapsulating both water insoluble and water soluble drugs (Turk et al., 2014). However, TPGS is believed to be less toxic and has additional therapeutic benefit as an antioxidant against inflammation (A. R. Shah & Banerjee, 2012; A. Yan et al., 2007).

The effects of various stabilizers on particles size, EE, and drug loading were determined and results are reported in Table 4.6. The results indicated that at 1% level both PVA and TPGS produced similar size and drug loading but when TPGS concentration was reduced to 0.3%, NPs size was reduced to 152.1 ± 4.1 nm and the drug loading was enhanced to 5.6 ± 0.1%. These results confirm that TPGS is an effective emulsifier, three times greater than PVA, due to its unique chemical structure to emulsify nano-emulsion and stabilize the PLGA NPs.

The mean particle size of our PLGA NPs was increased when TPGS concentration was increased to 1% level. We hypothesized that the relatively large particle size and low drug loading associated with high concentration of TPGS is related to the hydrophilic and lipophilic nature of RV. During an emulsification process, RV tends to stay in the inner oily phase but with an increase in surfactant concentration in the external aqueous phase, it may facilitate the solubilization of the drug in aqueous phase thereby promoting the drug diffusion from oil phase into the aqueous phase, leading to decrease in % EE. Our findings were in agreement with the results reported by other groups which indicate that % EE can be lower due to the solubilization effect of

emulsifier on the drug with an increased amphiphilic molecule concentration (B. Shah et al., 2015; Sharma et al., 2016).

It is concluded that 0.3% TPGS was an effective stabilizer and used further to stabilize the NPs.

Table 4.6: Effect of type of stabilizer on particle size, EE and drug loading of the RV loaded PLGA NPs.

Emulsifier used	Particle Size (nm)	EE (%)	Drug loading (%)
PVA (1%)	173.6 ± 5.8	18.2 ± 1.6	5.1 ± 0.5
Vitamin E TPGS (1%)	184.6 ± 15.0	17.4 ± 2.4	5.0 ± 0.6
Vitamin E TPGS (0.3%)	152.1 ± 4.1	20.2 ± 0.4	5.6 ± 0.1

Data are represented in mean ± SD (n=3).

4.5.1.4 Effect of formulation method

Double emulsion solvent evaporation method is most suitable for hydrophilic drugs (proteins and peptides) whereas single emulsion solvent evaporation method is more acceptable for hydrophobic (oil soluble) drugs. RV exhibits dual nature of the both hydrophilic and hydrophobic property. Therefore, the effect of the formulation method was studied on the physicochemical properties of the NPs.

In this part of optimization, we compared single emulsion method with double emulsion method. Each method was used to prepare triplicate batches of NPs. The resultant EE and drug loading are reported in Table 4.7. The double emulsion solvent evaporation (w/o/o) method yielded higher EE compared to the single emulsion method (o/w) (22.6 ± 3.2% and 17.2 ± 2.0 % respectively). It is well documented in the literature that encapsulation of amphiphilic and water soluble drugs in polymer based NPs is challenging because of the rapid partitioning of amphiphilic drugs between the oily and aqueous phases (Cohen-Sela et al., 2009; Niwa et al., 1994). The use of double emulsion method produced higher EE compared to the single emulsion method. This may be due to the presence of organic phase that is impeding the diffusion of drug droplets from the internal aqueous phase to external aqueous phase. The internal aqueous phase also acts as a drug reservoir, resulting in the increase in particle size. The slower diffusion of the RV from inner to outer aqueous phase also further explains the difference in the EE. The amphiphilic nature of RV leads to rapid diffusion from inner organic phase (high drug concentration) to outer aqueous phase (low drug concentration) in the case of single emulsion method, which was the reason for causing a decrease in the EE and drug loading.

In summary, the double emulsion method was considered more appropriate and selected as the method of choice because it showed a significantly higher drug loading (P value < 0.05) and it produced NPs different to that by single emulsion method.

Table 4.7: Physicochemical characterization of RV loaded PLGA NPs by various formulation methods.

Method	NPs size (nm)	Polydispersity Index	Zeta potential (mV)	EE (%)	Drug loading (%)
Single emulsion method	150.5 ± 10.6	0.16 ± 0.06	-37.9 ± 3.4	17.2 ± 2.0 *	2.8 ± 0.3
Double emulsion method	162.1 ± 4.2	0.17 ± 0.00	-41.4 ± 2.3	22.6 ± 3.2 *	3.6 ± 0.5

Data represented in mean ± SD (n=3) for all set of batches. * $p < 0.05$

4.5.1.5 Effect of theoretical drug loading of RV

To achieve the maximum amount of drug loading inside the NPs and better EE of the developed PLGA nano-formulations, the effect of varying theoretical drug loadings was investigated on the various properties of the NPs. The NPs were formulated using the double emulsion solvent evaporation method technique with 0.3% TPGS as an emulsifier.

The results represented in the Table 4.8 indicated that there is an increase in the drug loading from 3.6 to 5.3% w/w with an increase in theoretical drug loading, however, the EE decreased from 22.6±3.3 to 18.8±1.6 % w/w (Table 4.8; Figure 4.5). The decrease in the EE is attributed to the hydrophilic and lipophilic nature of RV which led to rapid partitioning of RV from the inner aqueous phase to the outer aqueous phase when an excess amount of RV is present thereby decreasing EE into the NPs during formulation. In addition, a limited amount of RV was expected to have a hydrophobic interaction with polymer and therefore retained in NPs.

Niwa and colleagues (Niwa et al., 1994) reported a similar pattern of low EE and increased drug loading of nafarelin acetate, a water-soluble peptide drug. These researchers concluded that decrease in EE with an increase in theoretical drug loading is due to increased drug leakage into an aqueous environment.

NPs size data showed an increase in NPs size with theoretical drug loading. The particle size of the NPs increased from 152.1±4.1 to 184.6±15.0 nm with a reduced polydispersity index, which signifies a narrow particle size distribution pattern. An increase in the drug loading in the NPs has led to an increase in NPs size. Zeta potential of the NPs decreases from -41.4 to -27.8 mV due to an increase in theoretical drug loading. This decrease in the surface negativity is due to the interaction of the carboxyl group of the polymer with a cationic drug on the particle surface. It is concluded that higher theoretical drug loading leads to lower EE and more drug wastage owing to more leakage of the drug to the external aqueous phase. Therefore, ~14% theoretical drug loading was chosen for further optimization.

Table 4.8: Effect of theoretical drug loading on the characteristics of the RV loaded PLGA NPs.

Theoretical drug loading (% w/w)	NPs size (nm)	PDI	Zeta potential (mV)	EE (%)	Drug loading (%)
0	149.3 ± 12.0	0.17 ± 0.001	-31.6 ± 4.6	-	-
14.3	162.1 ± 4.2	0.18 ± 0.02	-41.4 ± 2.3	22.6 ± 3.3	3.6 ± 0.5
16.6	165.3 ± 4.4	0.20 ± 0.03	-33.9 ± 3.4	20.7 ± 1.5	3.9 ± 0.2
23.0	184.6 ± 15.0	0.23 ± 0.03	-27.8 ± 1.1	18.8 ± 1.6	5.3 ± 0.4

Data are represented in mean ± SD (n=3).

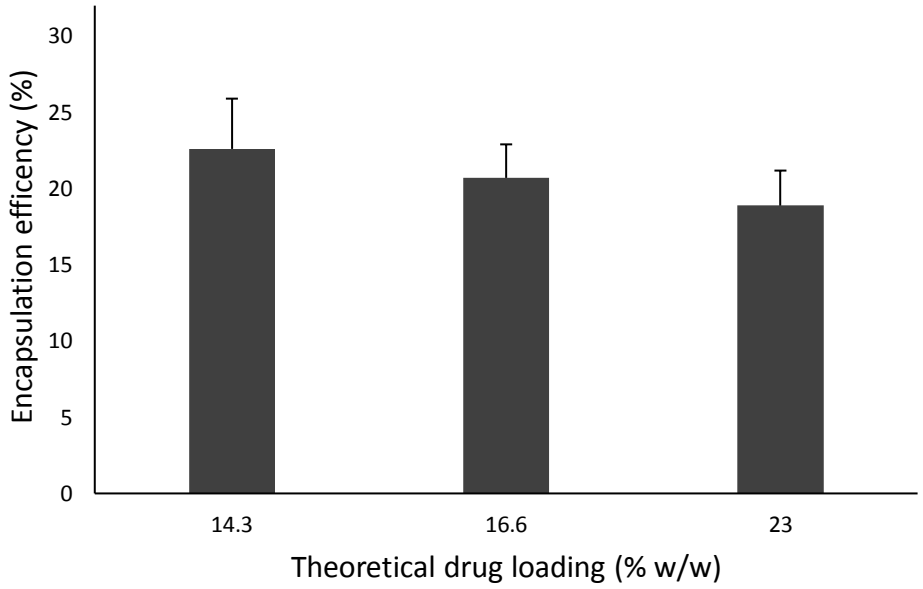

Figure 4.5: Effect of theoretical drug loading on EE of RV from PLGA NPs.
Data represented in mean ± SD (n=3) for each set of the formulation.

4.5.2 Formulation and optimization of dual ligand PLGA NPs

4.5.2.1 Effect of centrifugation speed

The size of the GC coated PLGA NPs was determined both before and after centrifugation which indicated that the size of the NPs before centrifugation was below 300 nm, however, the size after centrifugation was increased drastically (Figure 4.6). The reason was the deposition of multilayers of mucoadhesive GC on the surface of NPs during centrifugation. Hence to overcome this issue, the centrifugation speed had to be optimized. NPs were centrifuged at a different speed for purification and their size was determined.

As expected, lower the centrifugation speed, smaller the size of the NPs (Figure 4.6). Hence, lowest centrifugal speed (7168 g or 8000 rpm) was applied to separate the coated PLGA NPs from the coating solution and unloaded drug.

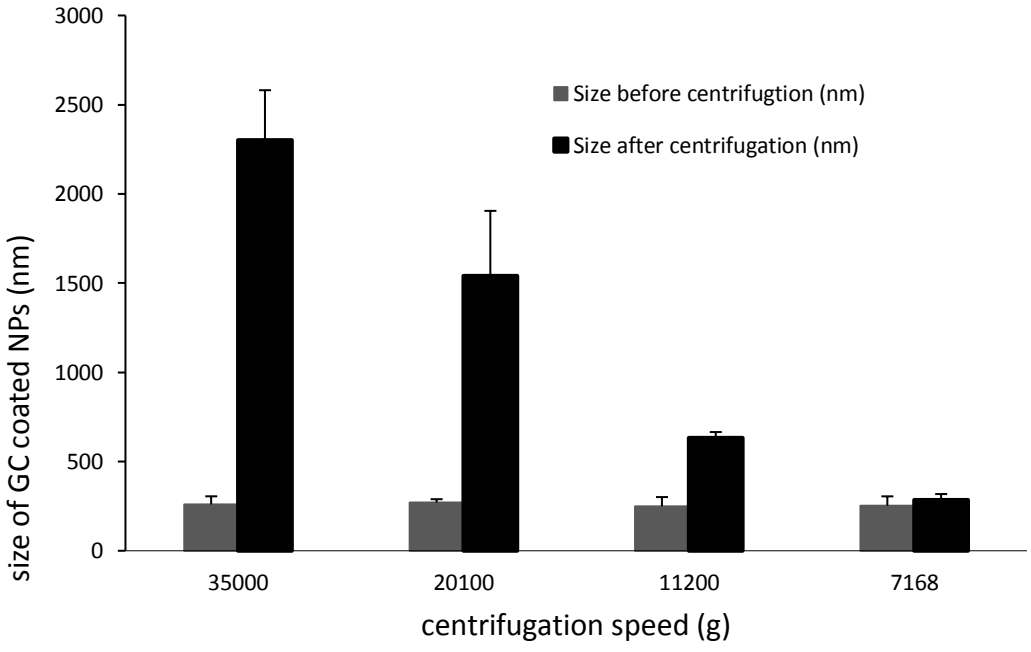

Figure 4.6: Effect of the centrifugation speed on the size of GC coated PLGA NPs. Data represented as mean ± SD (n=3) for all set of centrifugation speed.

4.5.2.2 Effect of GC coating polymer concentration

GC or TGC was used as a coating polymer to coat the PLGA NPs for obtaining GC or TGC coated PLGA NPs. To investigate the amount of the GC or TGC required to coat PLGA NPs, various coating concentrations of GC were employed for the fabrication of the GC coated PLGA NPs and results are indicated in Table 4.9. It showed NP's size increased gradually with an increase in the coating material (GC polymer) concentration, which was conspicuous at 0.4% GC concentration. The nanoparticulate formulation with 0.1% GC achieved a size of 210.6 ± 49.4 nm with zeta potential of +4.2 ± 0.0 mV, which increased to 251.4 ± 9.1 nm in size and +15.1 ± 0.2 mV in zeta potential with 0.2% GC concentration (Table 4.9). However, coating with 0.4% GC attained a size of 633.3 ± 52.2 nm with a zeta potential of +17.9 ± 3.0 mV.

The increase in the size of NPs may be due to the increased viscosity of the polymeric solution which hindered the formation of nano-sized droplets, leading to the increase in the size of NPs. Similar results were also reported by Nafee and her colleagues (Nafee et al., 2007) when they studied the effect of chitosan concentrations on the particles size and zeta potential of PLGA NPs. Both size and zeta potential of NPs increased gradually with an increase in the chitosan concentration.

As the smaller size of the NPs is correlated with better brain uptake (Saraiva et al., 2016), therefore, our aim was to produce NPs with a smaller size, and adequate positive zeta potential to stabilize nanosuspension during storage. Among these assessed NPs, NPs coated with 0.2% GC coating solution produced the appropriate size and zeta potential was acceptable. It was, therefore, decided to use 0.2% GC or TGC as the coating concentration to prepare the GC or TGC coated RV loaded PLGA-SA-ODA NPs.

Table 4.9: Effect of GC polymer concentration on colloidal properties of GC coated RV loaded PLGA NPs.

GC concentration (%)	Nanoparticle size (nm)	PDI	Zeta potential (mV)	Entrapment efficiency (%)	Drug content (%)
-	152.1 ± 4.2	0.18 ± 0.02	-41.4±2.3	22.6±3.3	3.6 ± 0.5
0.05	203.6 ± 2.6	0.23 ± 0.03	-31.4 ± 1.3	14.8 ± 2.1	2.4 ± 0.3
0.1	210.6 ± 49.4	0.3 ± 0.05	4.2 ± 0.0	18.5 ± 1.9	3.0 ± 0.3
0.2	251.4 ± 9.1	0.21 ± 0.04	15.1 ± 0.2	20.8 ± 2.1	3.4 ± 0.3
0.4	633.3 ± 52.2	0.44 ± 0.08	17.9 ± 3.0	18.3 ± 1.3	3.0 ± 0.2

Data represented in mean ± SD (n=2) for all the batches.

4.5.3 Final Formulation of PLGA NPs

After optimization of various factors, the final optimized PLGA formulation (Table 4.10) was used to produce NPs for the stability, *in-vitro* release, and *in-vivo* pharmacokinetic studies. The final formulation was used to load both RV and C-6 with two targeting ligands; SA-ODA and GC or TGC in order to obtain single ligand PLGA-SA-ODA NPs and dual ligand GC or TGC-coated PLGA-SA-ODA NPs respectively.

Both single ligand and dual ligand modified RV+C-6 loaded PLGA NPs were prepared using 0.3% TPGS as a stabilizer with double emulsion solvent evaporation method. The double emulsion (w/o/w) method was selected as an optimized method for the fabrication of the NPs on the basis of results obtained. Our results indicated that 0.3% TPGS is an effective emulsifier as compared to 1% PVA or 1% TPGS. Therefore, the optimized NPs were stabilized using 0.3% TPGS solution. In addition, 14.3% of theoretical drug loading (of polymer's weight) was chosen for loading the nanoparticulate formulation to surpass the drug wastage during the formulation. Beside this, 0.30 % theoretical drug loading of C-6 was decided to use on the basis of available literature (Kulkarni & Feng, 2011). Particles size and zeta potential are an important parameter that plays a significant role in cellular uptake efficiency of NPs during biodistribution and brain uptake study. Hence PLGA with a molecular weight of 110 kDa was selected for formulation of NPs. All the essential colloidal properties such as particle size, polydispersity index, and zeta potential were determined for the batches used later for *in-vivo* study and the results tabulated in Table 4.10.

The particle size and zeta potential for RV+C-6 loaded PLGA-SA-ODA NPs were 168.4 ± 10.3 nm and -32.4 ± 4.1 mV respectively. Figure 4.7 indicated the particles and zeta potential of single ligand RV+C-6 loaded PLGA-SA-ODA NPs determined using Zeta sizer. After coating with 0.2% GC polymer, the NP's particle size was increased to 210 ± 29.4 nm with a positive zeta potential of +15.1 ± 0.2 mV (Figure 4.8). The mean diameter of the TGC coated NPs increased to 236.0 ± 9.8 nm with a positive zeta potential of +10.4 ± 3.3 mV. The increase in the size and positive zeta potential of NPs is due to the surface deposition of the GC or TGC layer. Increasing the size of the NPs upon surface modification were also reported by Dyawanapelly

and his colleagues who modified the surface of PLGA NPs with chitosan polymer and Chitosan oligosaccharides (Dyawanapelly et al., 2016). In their study, a substantial increase in the size of the coated NPs was also reported in comparison to uncoated PLGA NPs. In addition, Tosi and colleagues also reported (Tosi et al., 2007) an increase of size of the NPs upon surface modification of glycosylated heptapeptide (G7) on PLGA polymer

Our results showed that there was slightly increase in RV drug loading and EE in RV+C6 loaded PLGA-SA-ODA NPs when compared with the only RV loaded NPs. The possible reason could be because of the hydrophobic nature of C-6, which stayed in the oil phase and formed a hydrophobic interaction with RV, further impeded the diffusion of RV from the inner aqueous phase to external aqueous phase, leading to an increase in RV EE and drug loading. A similar trend was also observed when we compared the GC coated RV loaded PLGA-SA-ODA NPs with GC coated RV+C6 loaded PLGA-SA-ODA NPs. Overall it is clear that dual loading of the RV and C-6 enhanced drug loading and EE in both the single ligand and dual ligand PLGA-SA-ODA NPs. The results presented in Table 4.10 also indicated that EE of both RV and C-6 has found to be slightly decreased after coating with TGC. We speculate this is due to the interaction of the C-6 or RV with the TGC polymer present in the external aqueous phase. Our results are in close agreement with results reported by other researchers (Dyawanapelly et al., 2016; N. Shah et al., 2009).

Shah and her colleagues (N. Shah et al., 2009) reported that the coating of Pluronic®P85 on paclitaxel loaded PLGA NPs reduces the encapsulation efficiency of the paclitaxel. The EE exhibited a slightly decreased from 76.3 % to 73.8 % after coating with P85 on paclitaxel loaded PLGA NPs. Dyawanapelly and his colleagues (Dyawanapelly et al., 2016) also reported a slight decrease in encapsulation efficiency of BSA protein from PLGA NPs upon surface coating with chitosan and its water-soluble chitosan oligosaccharides derivatives.

(A)

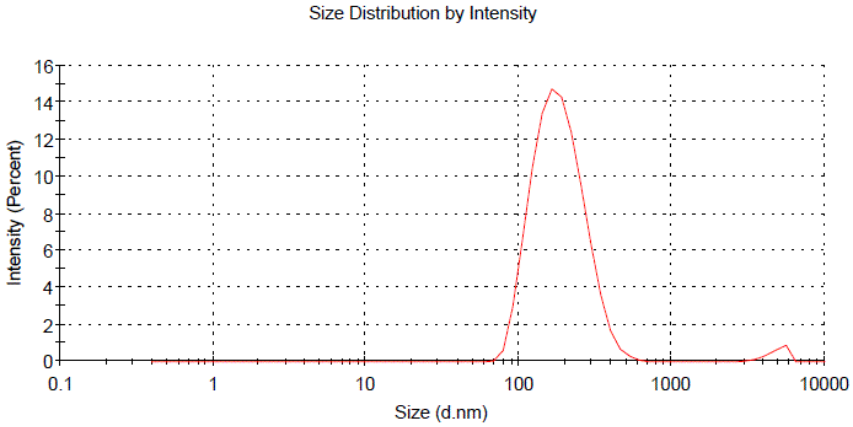

Results

			Size (d.n...	% Intensity:	St Dev (d.n...
Z-Average (d.nm):	176.5	Peak 1:	192.2	97.8	74.98
PdI:	0.187	Peak 2:	4847	2.2	729.9
Intercept:	0.927	Peak 3:	0.000	0.0	0.000
Result quality	Good				

(B)

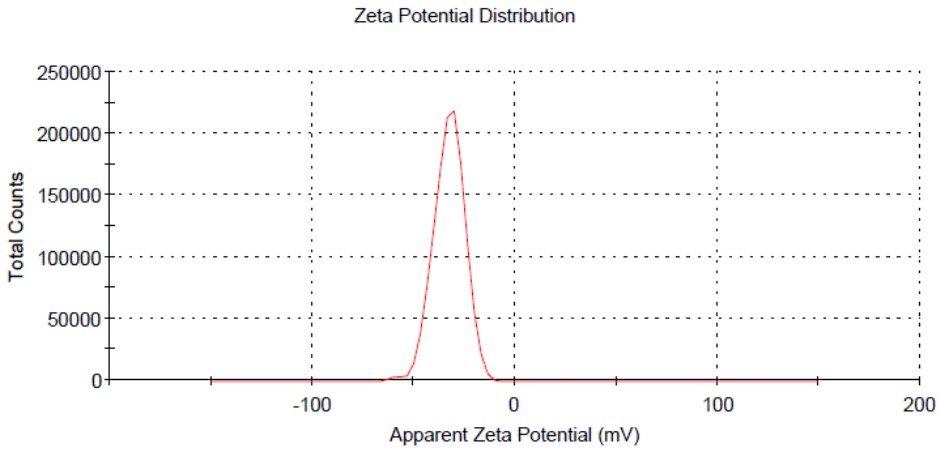

Results

			Mean (mV)	Area (%)	St Dev (mV)
Zeta Potential (mV):	-32.3	Peak 1:	-32.4	100.0	7.63
Zeta Deviation (mV):	7.33	Peak 2:	-57.8	2.5	2.90
Conductivity (mS/cm):	0.00832	Peak 3:	0.00	0.0	0.00
Result quality	Good				

Figure 4.7: Determination of (A) Particles size (B) zeta potential of single ligand modified RV +C-6 loaded PLGA-SA-ODA NPs by w/o/w method

(A)

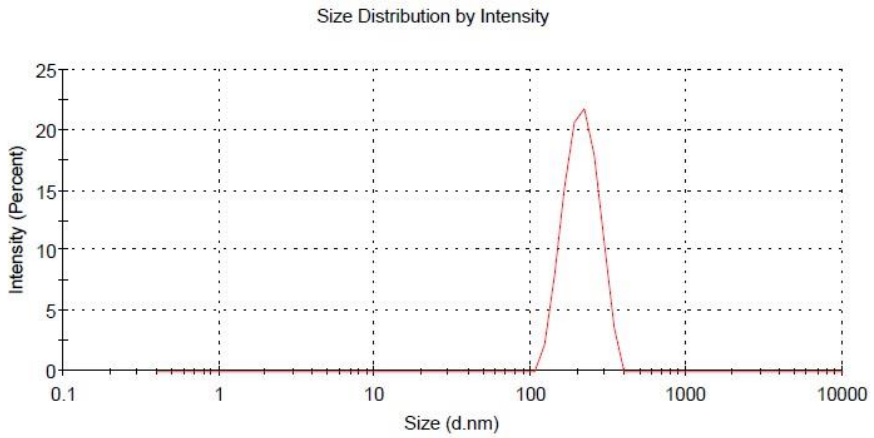

Results

		Size (d.n...	% Intensity:	St Dev (d.n...
Z-Average (d.nm): 244.8	Peak 1:	215.8	100.0	52.08
PdI: 0.387	Peak 2:	0.000	0.0	0.000
Intercept: 0.943	Peak 3:	0.000	0.0	0.000
Result quality Good				

(B)

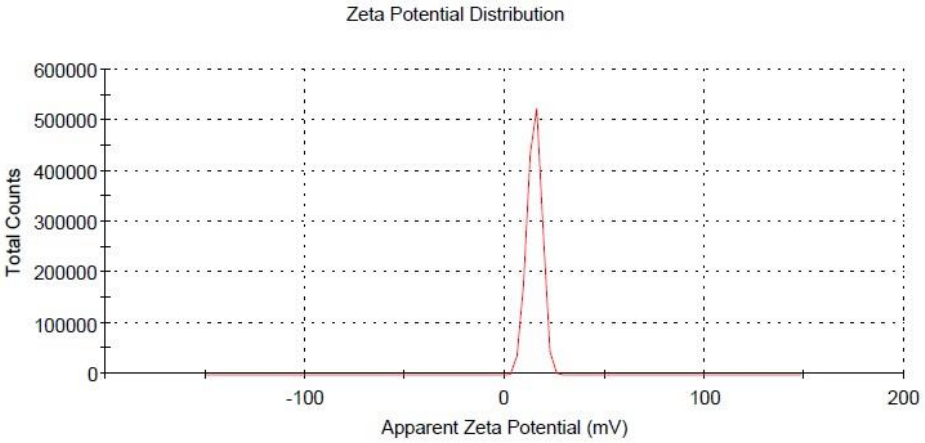

Results

		Mean (mV)	Area (%)	St Dev (mV)
Zeta Potential (mV): 14.9	Peak 1:	14.9	100.0	3.61
Zeta Deviation (mV): 3.47	Peak 2:	0.00	0.0	0.00
Conductivity (mS/cm): 0.0210	Peak 3:	0.00	0.0	0.00
Result quality Good				

Figure 4.8: Determination of (A) Particles size (B) zeta potential of dual ligand modified RV +C-6 loaded PLGA-SA-ODA NPs by w/o/w method

Table 4.10: Characterisation of single ligand and dual ligand modified-RV+C-6 loaded PLGA-SA-ODA NPs

NPs	Particle Size (nm)	Polydispersity Index	Zeta potential (mV)	RV EE (%)	RV loading (%)	C-6 EE (%)	C-6 loading (%)
Single ligand RV + C-6 loaded PLGA-SA-ODA NPs	168.4 ± 10.3	0.178 ± 0.001	-32.4 ± 4.1	23.1 ± 0.7	3.7 ± 0.7	90.4 ± 0.1	0.26 ± 0.00
Dual ligand RV + C-6 loaded PLGA-SA-ODA NPs coated with GC	210.0 ± 29.4	0.387 ± 0.001	+15.1 ± 1.2	21.4 ± 1.3	3.4 ± 0.2	92.3 ± 0.6	0.25 ± 0.01
Dual ligand RV + C-6 loaded PLGA-SA-ODA NPs coated with TGC	236.0 ± 9.8	0.387 ± 0.001	+10.4 ± 3.3	22.8 ± 0.7	3.6 ± 0.1	93.6 ± 0.05	0.28 ± 0.00

Data represents as mean ± SD (n=3) for all the formulations.

4.5.4 FE-SEM studies

FE-SEM images of single ligand modified RV loaded PLGA-SA-ODA NPs and dual ligand modified TGC coated PLGA-SA-ODA NPs confirmed the spherical shape of the developed NPs (Figure 4.9 and 4.10).

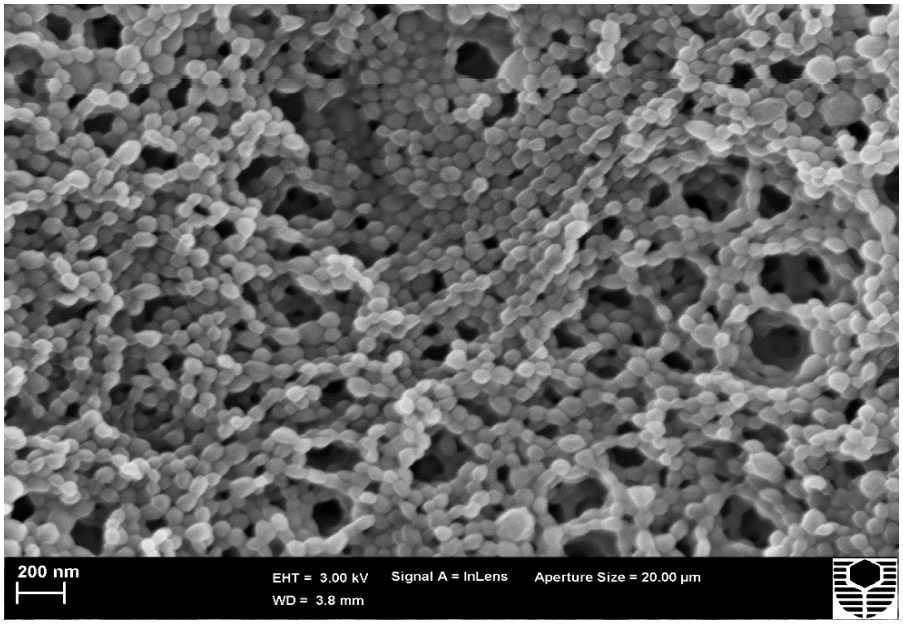

Figure 4.9: FE-SEM image of single ligand PLGA NPs.

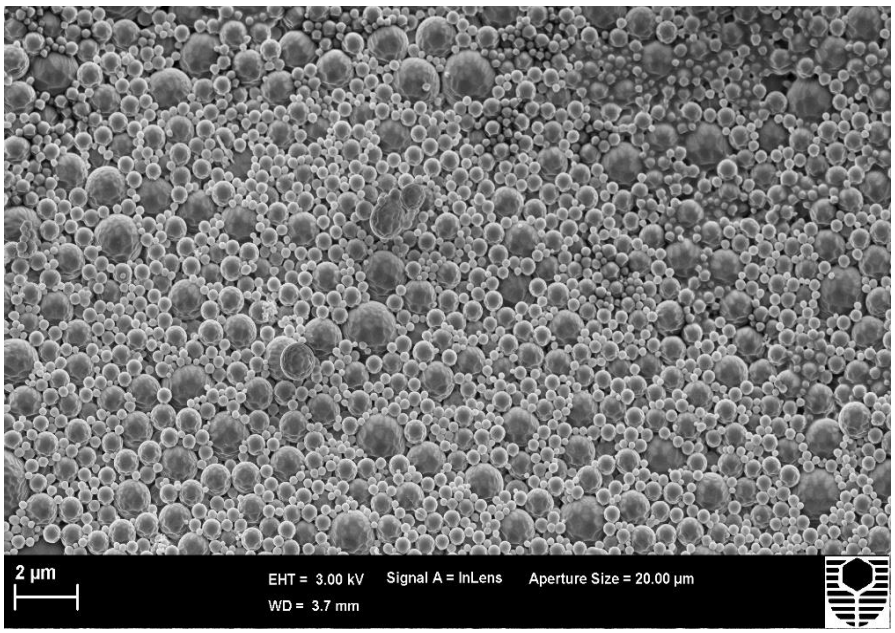

Figure 4.10: FE-SEM image of dual ligand PLGA NPs.

4.5.5 Stability studies of NPs

As the final NPs were prepared for administration and evaluation of *in-vivo* activity in animals, it is important to determine the stability of NPs in suspension form over a reasonable storage time before used for animal administration. We determined the size and surface charge of the NPs for seven days stored at 4°C.

The size of the single ligand blank PLGA-SA-ODA NPS and RV+C-6 loaded PLGA-SA-ODA NPS was consistent for seven days, whereas, the size of dual ligand PLGA NPs (both GC- and TGC-coated PLGA-SA-ODA NPs) increased over a period of time (Figure 4.11). The dual ligand PLGA NPs were stable only for one day, and their size increased constantly after 24 h. This size increase may be due to the presence of the mucoadhesive polymer on the surface of the NPs. In addition, the reduction in zeta potential of coated NPs also contributed to the instability of GC- and TGC-coated NPs.

Blank PLGA-SA-ODA NPs and RV+C-6 loaded PLGA-SA-ODA NPs exhibit negative zeta potential (-33.5 ±3.5 mV) due to the presence of ionized carboxyl group on the surface of PLGA molecule (Figure 4.12). As expected, the higher negative zeta potential of the NPs contributes to their stability. Single ligand PLGA-SA-ODA NPs were stable for seven days. The surface coating of GC and TGC leads to the inversion of the zeta potential. A positive zeta potential was observed due to the deposition of positively charged chitosan derivative on the negative surface of the PLGA NPs. Zeta potential of the single ligand NPs was almost constant, whereas dual ligand NPs showed positive zeta potential with a slightly increased value over a period of time. This change of the surface charge of dual ligand NPs was associated with an increase in the size of the NPs. The stability study suggested that dual ligand NPs should be used freshly prepared or within 24 h of preparation, while the single ligand NPs can be stored in 4°C for a longer period up to seven days, based on their physical stability.

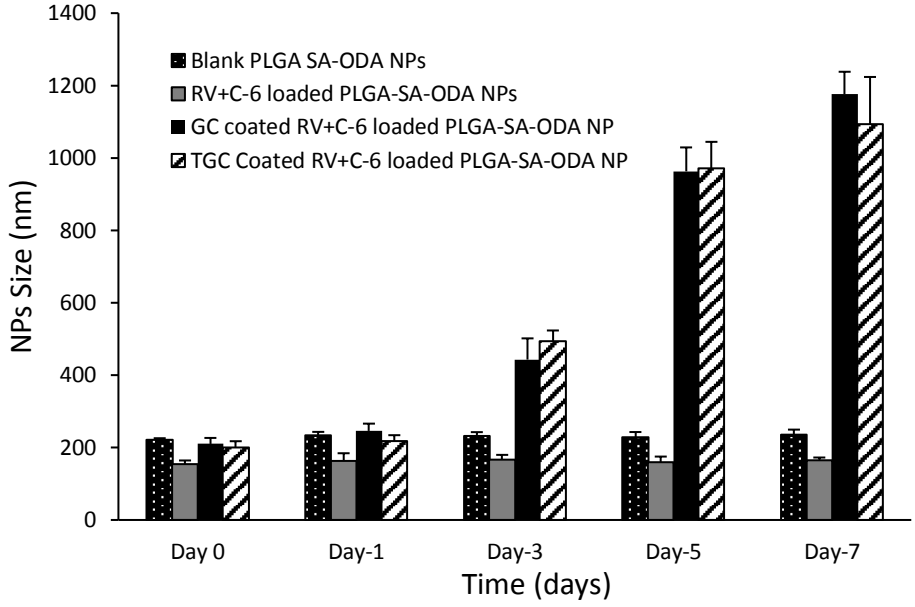

Figure 4.11: Particle size measured during the stability study for seven days for developed PLGA NPs.

Data represented as mean size ± SD (n=3) for all the formulations.

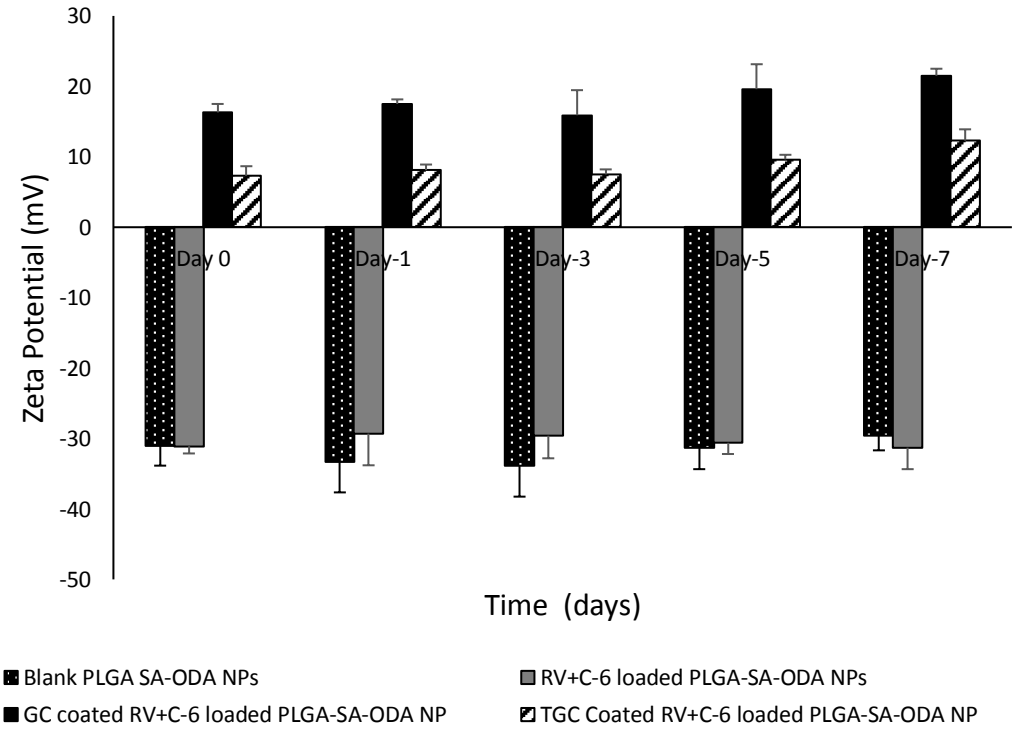

Figure 4.12: Zeta potential measured during the stability study for seven days for developed NPs.

Data represented as mean zeta potential ± SD (n=3) for all the formulations.

4.5.6 NPs Leakage study

The developed single ligand and dual ligand PLGA-SA-ODA NPs were evaluated for leakage of the RV during storage. Leak study of C-6 was also performed to further confirm that the fluorescent signal associated with *in-vivo* release study was due to the uptake of C-6 loaded PLGA-SA-ODA NPs instead of free C-6 released into the NP suspension.

4.5.6.1 RV Leakage study

Both dual ligand and single ligand PLGA-SA-ODA NPs were analyzed for % RV leached from NPs over a period of 48 h. Less than 3% of RV leaked from NPs after storing over a period of 6 h (Figure 4.13), which we attribute to the loose attachment of the RV molecule to the PLGA polymer matrix. Leaking of RV from NPs was 3.5% within 24 h, then almost 5% over a period of 48 h. In the case of dual ligand PLGA-SA-ODA NPs, the amount of the RV leaked from the NPs was less than 5% after storing of 48 h. The results suggested that once the NPs are formulated they are stable for 48 h with the RV stay inside the NPs.

4.5.6.2 C-6 leakage study

The C-6 leach study was also performed on both dual ligand and single ligand PLGA-SA-ODA NPs over a period of 48 h. Less than 2% of C-6 leaked from developed NPs within 24 h and reached to 3% after 48 h (Figure 4.14). This may be due to the hydrophobic nature of C-6 molecule which therefore remains inside in the PLGA polymer matrix for 48 h. We can be confident that the fluorescent signal acquired during our *in-vivo* study in cell or animals will be due to C-6 loaded NPs.

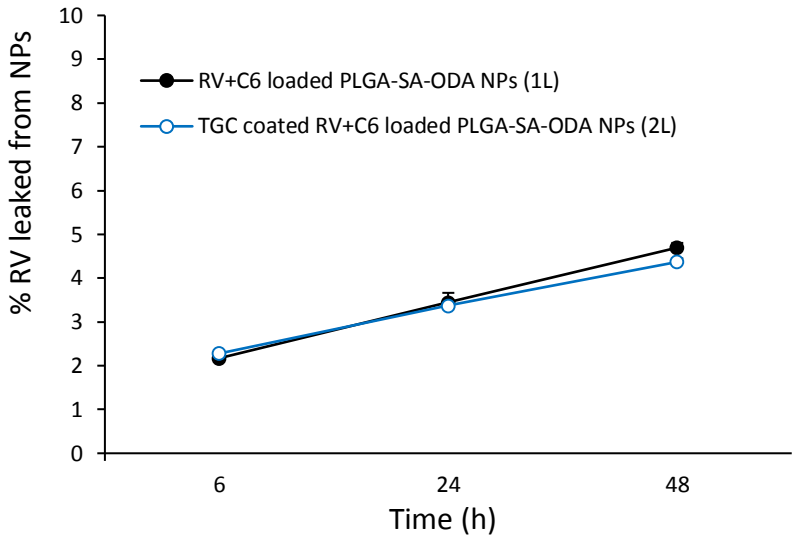

Figure 4.13: Leak study of RV from the single ligand and dual ligand RV+C-6 loaded PLGA-SA-ODA NPs over 48 h.

Data are represented as % mean RV leaked ± SD, (n=2) for each formulation

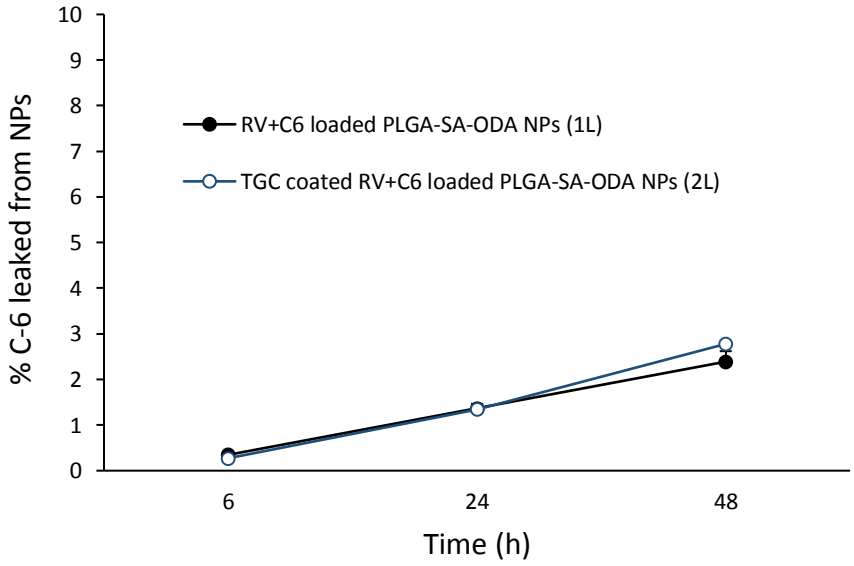

Figure 4.14: Leakage study of C-6 from the single ligand and dual ligand RV+C-6 loaded PLGA-SA-ODA NPs over 48 h.

Data are represented as % mean C-6 leaked ± SD., (n=2) for each formulation

4.5.7 Thiol group determination on NPs surface

The presence of the thiol groups on the surface of the TGC coated PLGA NPs was determined using Ellman's reagent against a standard curve constructed using thioglycolic acid solution (0.20 to 1.4 µmol/L) in the presence of GC. The calculated number of the thiol groups present on the surface of dual ligand PLGA NP was found to be 533.67 ± 94.7 (0.0608 ± 0.04 g/gm of PLGA polymer (% w/w)), which indicates the presence of the thiol moiety on the surface of the NPs.

4.5.8 *In-vitro* drug release studies of developed NPs

In-vitro drug release of RV from various types of RV loaded PLGA-SA-ODA NPs (both dual ligand and single ligand) was determined in PBS at 37°C over a period of 24 h. A biphasic release pattern with PLGA NPs, GC coated- and TGC coated-PLGA-SA-ODA NPs was obtained, which is characterized by initial burst release of RV, followed by a sustained release (Figure 4.15). The *in-vitro* release study indicated that coating of the GC and TGC did not significantly influence the release behavior of the drug over a period of 24 h.

An initial burst release of ~15% RV from NPs was observed in the first hour, followed by the relatively constant release of RV from NPs. The initial burst drug release may be due to the presence of loosely bound drug on the surface of the NPs. 54% of RV was released from the PLGA NP formulation over 24 h.

Various well-established models were applied to the *in-vitro* release study data to determine the best release kinetics from RV loaded PLGA formulation (Table 4.11 and 4.12). The model that best fitted the data for all the three types of RV loaded PLGA-SA-ODA NPs is the Higuchi model (correlation coefficient > 0.97). The best-fitted model for the nanoparticulate formulation further supports the view that the drug is uniformly dispersed in the matrix. Figure 4.16 represents the graphical representation of the Higuchi Model for the three different types of PLGA formulations. However, the RV drug solution showed a relatively better fit to the Hixson-Crowell model, which represents that dissolution occurs in the plane, and the rate of drug release was dependent on the amount of the drug solution present in the sample.

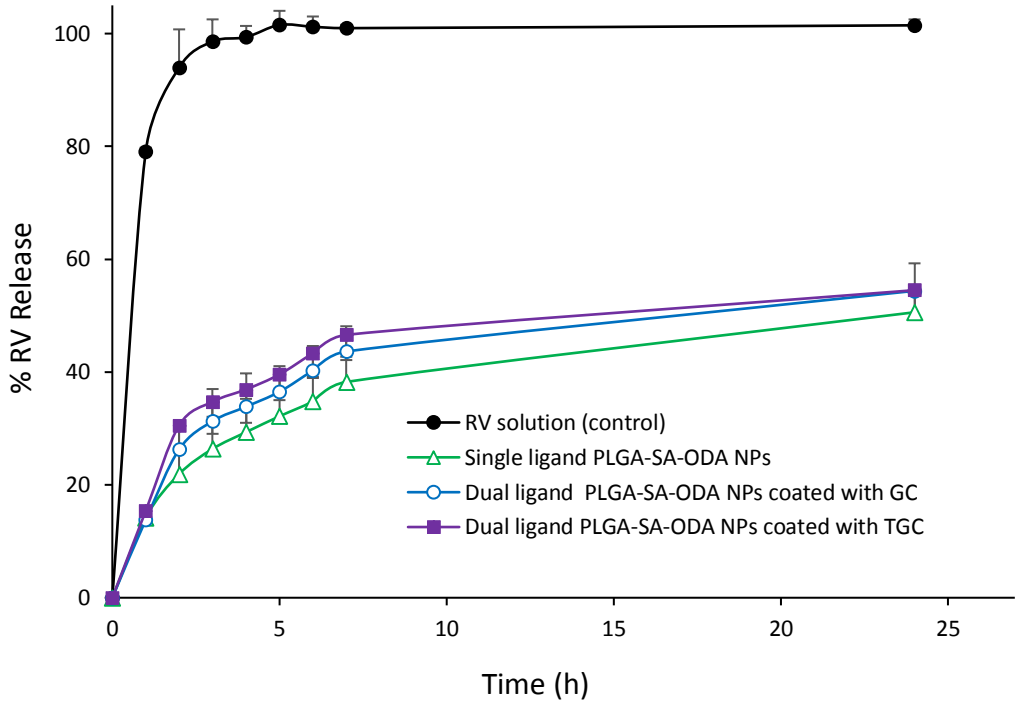

Figure 4.15: *In-vitro* drug release for RV from control drug solution and three different types of PLGA-SA-ODA NPs.
Data represented as mean ± SD (n=3) for all set of formulations

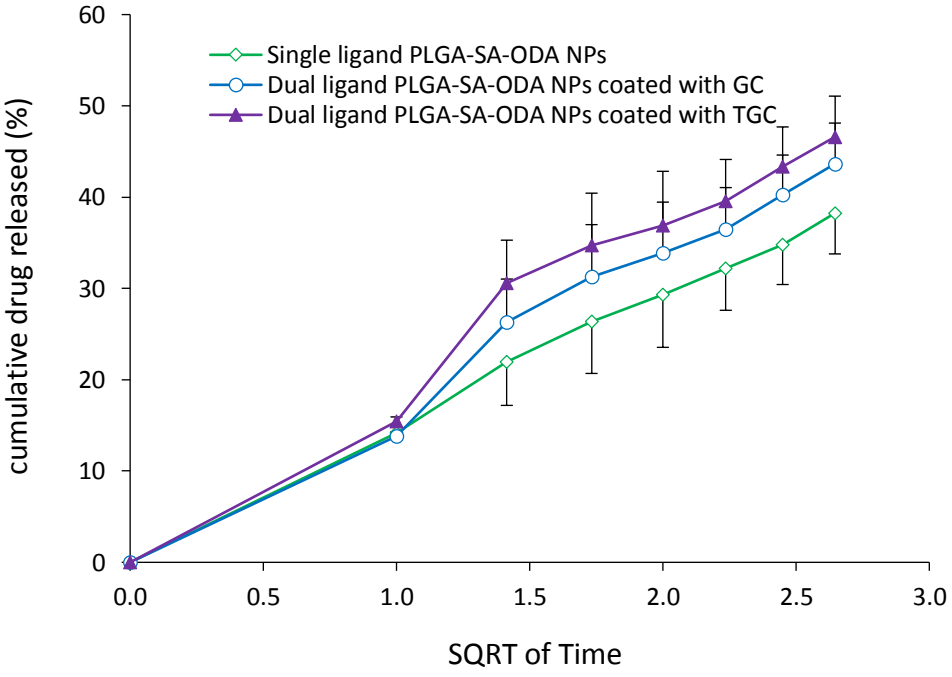

Figure 4.16: Graphical representation of Higuchi model for the three types of PLGA NPs

Table 4.11: Model fitting for the various types of the RV loaded formulations

	RV solution (control)	PLGA-SA-ODA NPs (1L)	GC coated PLGA-SA-ODA NPs (2L)	TGC coated PLGA-SA-ODA NPs (2L)
Model	r^2	r^2	r^2	r^2
Zero Order	0.490	0.892	0.878	0.843
First order	0.732	0.931	0.923	0.902
Higuchi Model	0.770	0.992	0.981	0.973
Kors-Peppas Model	0.512	0.890	0.903	0.885
Hixson and Crowell Model	0.914	0.911	0.912	0.880

r^2: square of correlation coefficient

Table 4.12: Various parameters calculated for the Higuchi Model for the different types of the RV loaded PLGA-SA-ODA NPs.

	PLGA-SA-ODA NPs	GC coated PLGA-SA-ODA NPs	TGC coated PLGA-SA-ODA NPs
Higuchi Model (r^2)	0.992	0.981	0.973
Slope of Higuchi Model	14.3	16.7	17.8
Intercept of Higuchi Model	0.5	0.1	0.9

4.6 Conclusion

The present research produced a novel formulation of single ligand and dual ligand modified C-6+RV loaded PLGA NPs using TPGS as an emulsifier. Both types of NPs were formulated using double emulsion solvent evaporation method and their various colloidal properties such as surface charge, particle size, and polydispersity index were characterized.

The effect of varying the molecular weight of the PLGA polymer indicated that the increase in the NPs size is correlated with an increase in the PLGA molecular weight. To obtain the optimum particle size and drug loading, NPs were formulated using 110kD PLGA. However, the size and loading of the NPs were also affected by the amount and type of the stabilizer used in the formulation. The use of 0.3% TPGS has improved the EE and acts as an efficient stabilizer during NPs formulation in comparison to 1% PVA and 1% TPGS. Hence the lower concentration of TPGS was considered for formulating the PLGA NPs. The present investigation suggests that EE and drug loading is correlated to the choice of the method employed for the NPs formulation. Double emulsion method produced relatively enhanced EE and drug loading compared to single emulsion method, despite their similar particle size.

The centrifugation speed employed for the purification of the GC or TGC coated NPs also govern the size and zeta potential of the NPs. Lower centrifugation speed produced smaller NPs which is advantageous for drug delivery. Therefore, dual ligand modified PLGA NPs were purified on lower centrifugation speed.

The size of fabricated single ligand formulations was < 200 nm, with a low polydispersity index. The particle size and zeta potential for RV+C-6 loaded PLGA-SA-ODA NPs were 189.3 ± 2.4 nm and -30.4±3.1 mV. In contrast to single ligand NPs, dual ligand TGC or GC coated PLGA NPs exhibited a positive zeta potential with an increase in NPs size. After attachment of another ligand (GC or TGC), the size of the NPs increased to ~250 nm. The size and zeta potential of the NPs were largely dependent on the amount of coating polymer employed. The optimized 0.2% GC or TGC concentration was successfully employed for the coating of PLGA NPs. These coated NPs were stabilized

by the electrostatic repulsion and steric force of charged hydrophilic coating polymers. The successful inversion of the zeta potential from negative to positive and detection of thiol groups on the surface of the NPs further confirmed the successful coating of NPs with TGC. Due to the chemical nature of the coating material, the coated NPs will have a positive charge and relatively lower magnitude of zeta potential, therefore they are prone to aggregation. The physical stability study indicated that the coated NPs should be used within 24 h of preparation. FE-SEM studies also revealed the spherical nature of both the dual ligand and single ligand PLGA NPs.

The NPs leakage study showed that 3.5% percent of RV and less than 2% of C-6 was released both from the single ligand and dual ligand PLGA NPs over a period of 24 h. The leak study showed that both RV and C-6 released from inside the NPs during both *in-vitro* release and *in-vivo* animal studies. The *in-vitro* drug release study showed a biphasic release pattern with an initial burst release of 13% RV in the first hour, followed by a relatively constant release of RV from NPs over 24 h. The release profile of RV loaded NPs showed best fit to Higuchi model, indicating drug release from the matrix system.

In conclusion, single ligand PLGA-SA-ODA NPs and dual ligand TGC or GC coated PLGA-SA-ODA NPs have been successfully developed and can be potentially used as a drug carrier for targeting the drug to the brain via the IN route. The latter system has the dual advantages of improved mucosal delivery resulting from both its permeation enhancement properties and mucoadhesive nature of TGC. The novel nanoparticulate technology offers a potential platform technology for the targeted delivery of a range of therapeutic molecules, thus offering a potential new approach in managing neurodegenerative disorders.

5. Chapter-5 *In-Vivo* Animal Studies of Developed Single Ligand and Dual Ligand PLGA Nanoparticles

5.1 Introduction

The intranasally administered polymeric NPs has potential to promote drug delivery into the brain bypassing the BBB (Acharya & Reddy, 2016; Mittal et al., 2016; Quintana et al., 2016; Tosi et al., 2013). Surface modification of the NPs with targeting ligands can enhance the CNS delivery of many drugs (Bi et al., 2016; Kulkarni & Feng, 2011). Bi and his colleagues (Bi et al., 2016) designed biodegradable lactoferrin modified PEG-PLGA NPs for brain delivery of rotigotine via IN route. Their surface modified NPs were able to target rotigotine to the brain more effectively than unmodified PEG-PLGA NPs, using IN administration, suggesting the importance of targeting ligands on the surface of the NPs.

The aim of this study was to evaluate whether our novel RV loaded NPs with single and dual ligands can enhance brain distribution of RV following their administration by IN route. The tested NPs were single ligand RV+C-6 loaded PLGA-SA-ODA NPs and dual ligand RV+C-6 loaded PLGA-SA-ODA NPs coated with TGC coated developed as per description in previous chapters. The purpose of the incorporating the C-6 into NPs are two folds: (i) C-6 is used as a fluorescent label for easy detection of NPs. (ii) C-6 represents hydrophobic agents, therefore, allow us to study the effectiveness of our developed NPs in delivering two drugs or a drug with a diagnostic agent with different properties into the brain.

It is our hypothesis that the effectiveness of the brain delivery of the RV-loaded NPs would be enhanced with dual targeting ligands that can target nasal mucosal membrane (by TGC) and brain neuron cells (by SA), thereby enhancing both the transport of NPS into the brain and prolonging drug concentration in the brain. To confirm that the IN route of administration is more effective for brain delivery, we compared the pharmacokinetic profile and brain uptake of RV drug solution administered by the IN and IV route.

5.2 Materials and Animals

Rivastigmine hydrogen tartrate (99.2%, IC-CS-146-0-140108) was purchased from Innochem Technology Co., Ltd., (Beijing, China) which was converted into RV free base before being incorporated into NP formulations. PLGA [(47:53 ratio), Mw 110 kDa] was purchased from Purac Biochem (Gorinchem, Germany). C-6 (442631-1G), TPGS (57668-5g), Venlafaxine (V7264-50 mg), Tertbutyl methyl ether (306975-2L) and RIPA Buffer (R0278-500mL) was purchased from Sigma-Aldrich (Castle Hill NSW, Australia).

Male Sprague-Dawley rats aged between 10-12 weeks (220-250g) were purchased from Animal Resource Centre, Perth, Australia. All the animals bought and studies were duly reviewed and approved by Animal Ethics Committee of Curtin University before the start of the animal study. The animal approval letter is attached in the appendix section.

5.3 Methods

5.3.1 Formulation of PLGA NPs for *in-vivo* studies

RV+C-6-loaded PLGA-SA-ODA NPs with single ligand and dual ligands were prepared using w/o/w double emulsion solvent evaporation technique (section 4.4.4 and 4.4.6). The developed NPs were characterized by particle size, polydispersity index, zeta potential and drug loading before being administered to animals.

5.3.2 Animal experiments

NP formulations were evaluated using Sprague-Dawley rats, a common preclinical model for efficacy, safety, toxicity and pharmacokinetic studies of drugs for both IN and IV route of administration (Katare et al., 2015). All animals were held in air-conditioned animal facility center of Curtin University and acclimatized for 4 days before the start of the animal experiment. Regular food and water ad libitum were provided to all the animals during the experiments. The animals were randomly selected and assigned into four

different treatment groups, each containing 10 rats. Each group of animals received one treatment:

Group 1: RV drug solution via IV route

Group 2: RV drug solution via IN route

Group 3: Single ligand RV + C-6 loaded PLGA-SA-ODA NPs via IN route

Group 4: Dual ligand RV + C6 loaded PLGA-SA-ODA NPs coated with TGC via IN route

Dosing and delivery of treatments

Each rat was administered a dose equivalent to 1 mg/kg RV free base (Wilson et al., 2008) and 80 µg/kg of C-6. RV drug solution/nanoparticulate formulations were dissolved/suspended in 5% dextrose solution for both IN and IV administration. The IV dosing was performed according to Curtin's standard operating procedures and RV drug solution (1 mg/kg) was injected through a syringe with a 30-gauge needle into the saphenous vein.

The IN dosing was performed following a method reported in the literature (Katare et al., 2015). Briefly, an animal was kept in an induction chamber supplied with 4-5% isoflurane in oxygen at a rate of 0.5 mL/min. Once the animal lost its righting reflex and pedal withdrawal reflex, it was removed from the chamber. The rat was placed in the supine position to administer treatments via IN route. A total 120 µL of RV solution/nanoparticle formulation per 250 gm of rat weight was administered by pipetting aliquots of 30 µL into each nostril. Each treatment was administered over 3-5 mins with 0.5-1 min intervals. Between the instillation of formulations, a dose of 1-2% isoflurane was given by inhalation route (i.e. use of a nose cone), to keep the rats sedated to prevent sneezing.

5.3.3 Pharmacokinetic study of RV and C-6

The RV and C-6 pharmacokinetic study were carried out to compare the effect of NPs formulation with that of the free drug on the drug concentration profile in the systemic circulation. After administration of RV drug solution/nanoparticulate formulations, blood samples were collected from the tail vein at designated time points, under anesthesia with

1-3% isoflurane. To ease the blood collection from a vein, the rat tail was dipped in warm water (40°C) for 5-10 seconds for vasodilation. A small incision was made with a 20G stainless steel sterile blade; 0.25 mL of blood was collected at 15, 30, 60, 90 min and 2, 3, 4, 6 and 8 h and transferred to vials with an anticoagulant (20 µL of 10% EDTA solution). The blood samples were then centrifuged at 11,370 g at 4°C for 10 min (Eppendorf Centrifuge 5415R, Australia). The supernatant plasma was collected and stored at -80°C until RV and C-6 content analysed. For analysis of RV from plasma samples, 100 µL of plasma was processed for extraction of RV using a procedure as described in Figure 3.2 and analysed by a validated HPLC-FLD method described in section 3.4.4.2. C-6 in plasma samples were analysed by treating them with double volume of RIPA buffer and fluorescent intensity was measured using a plate reader at excitation wavelength 465 nm and emission wavelength 502 nm (section 3.4.6.1). The amount of C-6 concentration at various time intervals were determined against C-6 calibration curve in HBSS buffer.

5.3.4 Brain uptake study of RV and C-6

The brain uptake of RV and C-6 loaded NP formulations was studied over 8 h following IV and IN administration. For each formulation, a set of animals (n=5) were sacrificed at 2 and 8 h of post treatment. The animals were sacrificed after deep anesthesia by isoflurane. The collection of final blood was done through a cardiac puncture. The remaining blood was flushed out by injection of saline solution into the aorta before collecting organs. The whole rat brain was harvested, washed with normal saline, made free of fluid, weighed and stored at -80°C until further analysis. The harvested whole brain was homogenized in a test tube with 3 mL of HBSS buffer using sonicator (UP200S, Microtip-S7, Hielscher Ultrasonics GmbH, Teltow, Germany) at 0.4 cycles and 40% amplitude for 3 min. The total volume of brain homogenate was recorded then an aliquot of brain sample (500 µL) was extracted as per Figure 3.3 for further analysis of RV content using the validated HPLC method (section 3.4.4.2). A known faction of the brain homogenate samples was processed for C-6 analysis using a RIPA buffer and further analysed on plate reader at an at excitation wavelength 465 nm and emission wavelength

502 nm. The amount of C-6 concentration in various samples at various time intervals were determined against C-6 calibration curve in HBSS buffer.

5.3.5 Stability study of RV and C-6 in biological samples

5.3.5.1 Stability study of RV in plasma

Since plasma samples have to be stored for a period of time before analysis, the stability of the drug in these samples must be known. The RV stability at 37°C was also conducted to mimic the body temperature conditions and to cover the worst case of the storage conditions or study conditions such as cell culture study. The plasma stability study of RV was carried out with known concentration of RV in plasma and samples exposed to conditions including 37°C, and -80°C for 48 h and 28 days respectively.

RV plasma stability at 37°C was carried for up to 48 h. Fresh rat plasma was spiked with RV at 200 ng/mL and 400 ng/mL concentration and samples were placed on a shaker at 100 rpm at 37°C. Samples were withdrawn at 0, 3, 6, 24 and 48 h and RV was extracted in the same fashion as described in Figure 3.2. The processed samples were analyzed by validated HPLC method to determine % RV remaining drug concentration.

To study RV stability in plasma at -80°C, rat plasma samples were spiked with RV at a concentration level of 3 µg/mL and 5 µg/mL. These spiked plasma samples were stored at -80℃ for up to 28 days and samples were withdrawn at 0, 7, 14, 21 and 28 days. The collected samples were processed to isolate RV following a similar method described in Figure 3.2 and further analysed by using a validated HPLC method (section 3.4.4.2).

5.3.5.2 Stability study of C-6 in plasma and the brain

C-6 fluorescence stability in plasma and brain samples was evaluated to cover various stages such as handling, extraction, and storage. As C-6 is light sensitive, all experiments were carried out in the dark and samples were stored in a dark black box.

The stability of C-6 fluorescent signals in processed plasma and brain samples were evaluated over 24 h period at room temperature. For this, 200 µL of plasma or brain

homogenate samples were spiked with a known amount of C-6 (6.5 ng/mL, 9.7 ng/mL, 13.0 ng/mL and 16.0 ng/mL) and mixed with 400 µL of RIPA buffer for cell and tissue lysis (section 3.4.6.1). These treated samples were stored at room temperature for 0, 1 h, 2 h and 24 h respectively and fluorescent intensity was measured using a plate reader (EnSpire® Multimode plate reader, Perkin Elmer, Waltham, MA USA) at excitation wavelength 465 nm and emission wavelength 502 nm. The amount of C-6 concentration at various time intervals were determined against C-6 calibration curve in HBSS buffer and calculated as percent remaining with respect to the C-6 concentration at 0 h.

The C-6 storage stability at -80℃ was studied to evaluate the stability of C-6 in actual *in-vivo* biological samples during storage. For this, 200 µL of blank plasma was spiked with a known amount of C-6 (34 ng/mL and 67 ng/mL) and stored at -80℃ for 28 days. The samples were withdrawn from -80℃ at 0, 7, 14, 21 and 28 days then thawed. The thawed samples were treated with a double amount (400 µL) of RIPA buffer and analysed using the plate reader at excitation wavelength 465 nm and emission wavelength 502 nm. The amount of C-6 concentration at various time intervals were determined against C-6 calibration curve in HBSS buffer and calculated as percent remaining with respect to C-6 concentration at 0 h.

5.3.6 Statistical analysis

All data are reported as a mean concentration ± standard error of the mean (SEM) for pharmacokinetics and brain uptake study unless otherwise stated. The difference between the groups was determined using Student's t-test, and differences between more than two groups were determined using ANOVA method using the Graph Pad Prism Software 6.01 version (Prism, Graph Pad software Inc. Version 6.01). A P-value ≤ 0.05 was considered as statistically significant. All pharmacokinetics parameters were determined using Kinetica Software Version 5 (Build 5.0.11, Thermo Fischer Scientific).

5.4 Results and Discussion

5.4.1 NPs formulation and characterization

The determined particle size of both single ligand and dual ligand modified NPs was under 250 nm with low polydispersity index which indicates that NPs suspension was monodispersed in nature (Table 5.1). Both increased size and positive zeta potential of NPs were attributed to surface deposition of the TGC layer on the NPs surface. However, the coating of NPs with the TGC did not significantly alter the NPs surface morphology and retained their original spherical shape and smooth surface (Figure 4.9 and 4.10).

5.4.2 Stability study of RV and C-6 in biological samples

5.4.2.1 Stability study of RV in plasma

RV was stable in plasma at 37°C for at least 24 h (100.6 ± 2.1 % remaining) with a 5-8% decrease in drug concentration at 48 h (Figure 5.1). This means that RV is susceptible to enzyme degradation after 24 h.

RV spiked plasma samples stored at -80°C was stable for up to 28 days (>98% remaining) [(Figure 5.2) and Table 5.2]. The results suggest that RV plasma samples obtained from the *in-vivo* animal study can be stored at -80°C for an extended period (up to 28 days) before being analyzed and the quality of the samples will not be compromised.

Table 5.1: Characterisation of single ligand and dual ligand RV+C-6 loaded PLGA-SA-ODA NPs used for *in-vivo* studies.

NPs	Particle Size (nm)	Polydispersity Index	Zeta potential (mV)	RVEE (%)	RV loading (%)	C-6 EE (%)	C-6 loading (%)
Single ligand RV + C-6 loaded PLGA-SA-ODA NPs	189.3 ± 2.4	0.169 ± 0.001	-30.4 ± 3.1	24.1 ± 0.7	3.8 ± 0.1	93.6 ± 0.01	0.26 ± 0.00
Dual ligand RV + C-6 loaded PLGA-SA-ODA NPs coated with TGC	242.6 ± 8.4	0.385 ± 0.002	+9.4 ± 4.3	22.7 ± 0.9	3.6 ± 0.2	91.3 ± 0.5	0.25 ± 0.01

Data represented as mean ± SD (n=3) for all the formulations.

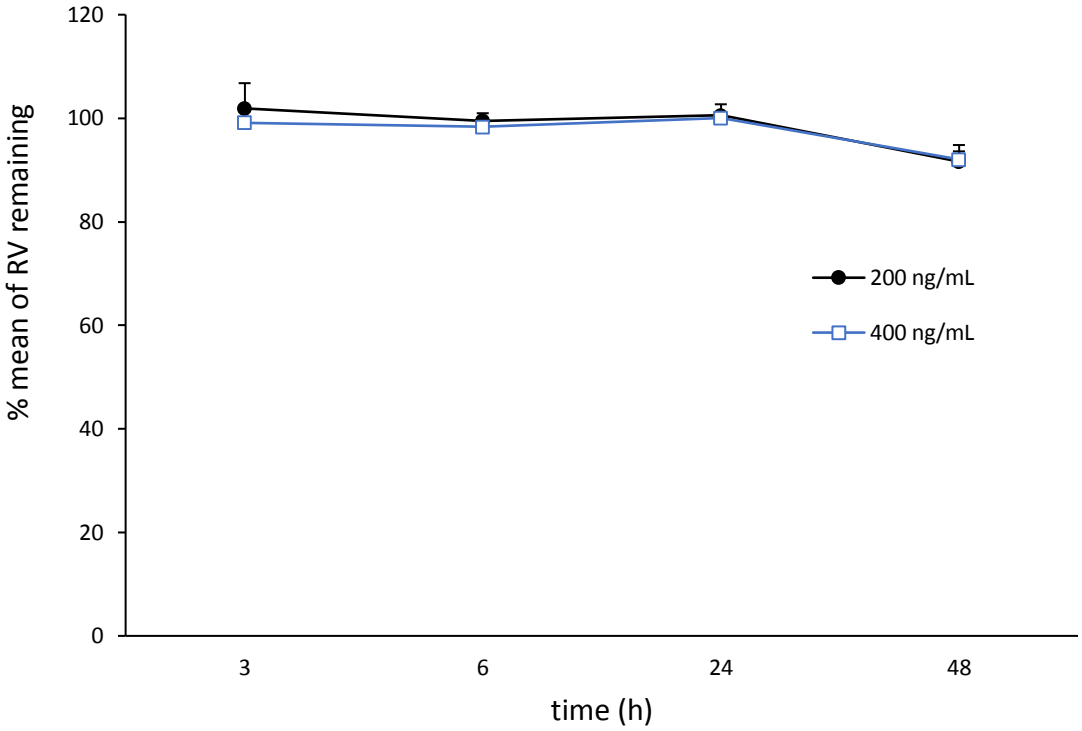

Figure 5.1: RV stability study in rats' plasma at 37°C for 48 h

Plasma samples were spiked with 200 ng/mL and 400 ng/mL RV and incubated at 37°C for 48 h. Samples were processed for RV content at predetermined time intervals (3,6, 24 and 48 h) and analyzed by validated HPLC method to determine the amount of RV remaining in rat's plasma. Data represented is the mean value of % RV remaining ± SD (n=2).

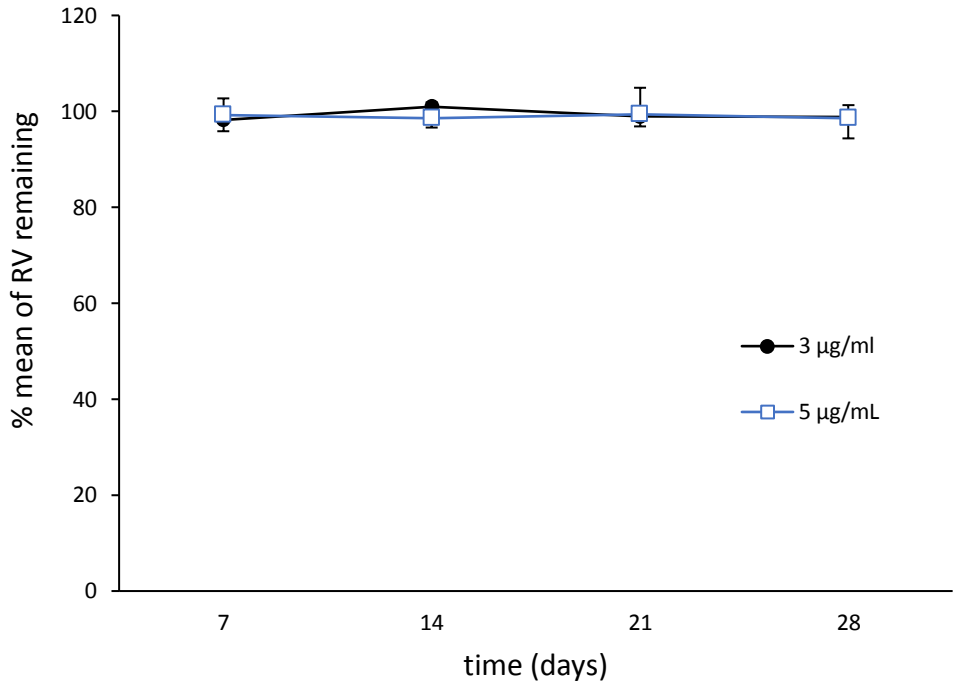

Figure 5.2: RV stability study in rats' plasma at -80°C for 28 days

Plasma samples were spiked with 3 µg/mL and 5µg/mL RV and stored at -80°C for 28 days. The samples withdrawn at 7, 14, 21 and 28 days were extracted and analyzed using the validated HPLC method for RV content. Data represented is the mean value of % RV remaining in rats' plasma ± SD (n=3).

Table 5.2: Plasma stability study of RV performed at -80°C for 28 days.

Matrix used	Condition employed for stability testing	RV concentration spiked (µg/mL)	RV concentration determined (µg/mL)	% RV remaining ± SD
Plasma	Week-0	3.0	3.0 ± 0.0	99.1 ± 1.2
		5.0	4.9 ± 0.1	98.9 ± 0.9
	Week-1	3.0	2.9 ± 0.1	98.2 ± 2.3
		5.0	4.9 ± 0.2	99.3 ± 3.4
	Week-2	3.0	3.0 ± 0.1	100.9 ± 4.3
		5.0	4.9 ± 0.1	98.6 ± 3.3
	Week-3	3.0	2.9 ± 0.1	98.9 ± 2.0
		5.0	4.9 ± 0.2	99.4 ± 5.5
	Week-4	3.0	2.9 ± 0.1	98.8 ± 4.4
		5.0	4.9 ± 0.1	98.6 ± 2.7

Data represented in mean RV concentration ± SD (n=3).

5.4.2.2 Stability study of C-6 in plasma and the brain

This study was designed to examine if there was any change of fluorescence intensity of C-6 in rats' plasma and brain tissue over the storage and when C-6 was in contact with RIPA buffer.

The fluorescence intensity signals of C-6 in plasma was stable for 24 h in processed plasma samples and 2 h in the brain tissue extracted with RIPA buffer, both at room temperature [Figure 5.3 (A) and 5.3 (B)]. This confirms that our sample process and storage will have no impact on the fluorescent analysis of C-6 sample.

Figure 5.4 showed no significant change of C-6 level in plasma stored at -80°C over 28 days which provides an evidence that C-6 present in our *in-vivo* biological samples was stable for 28 days.

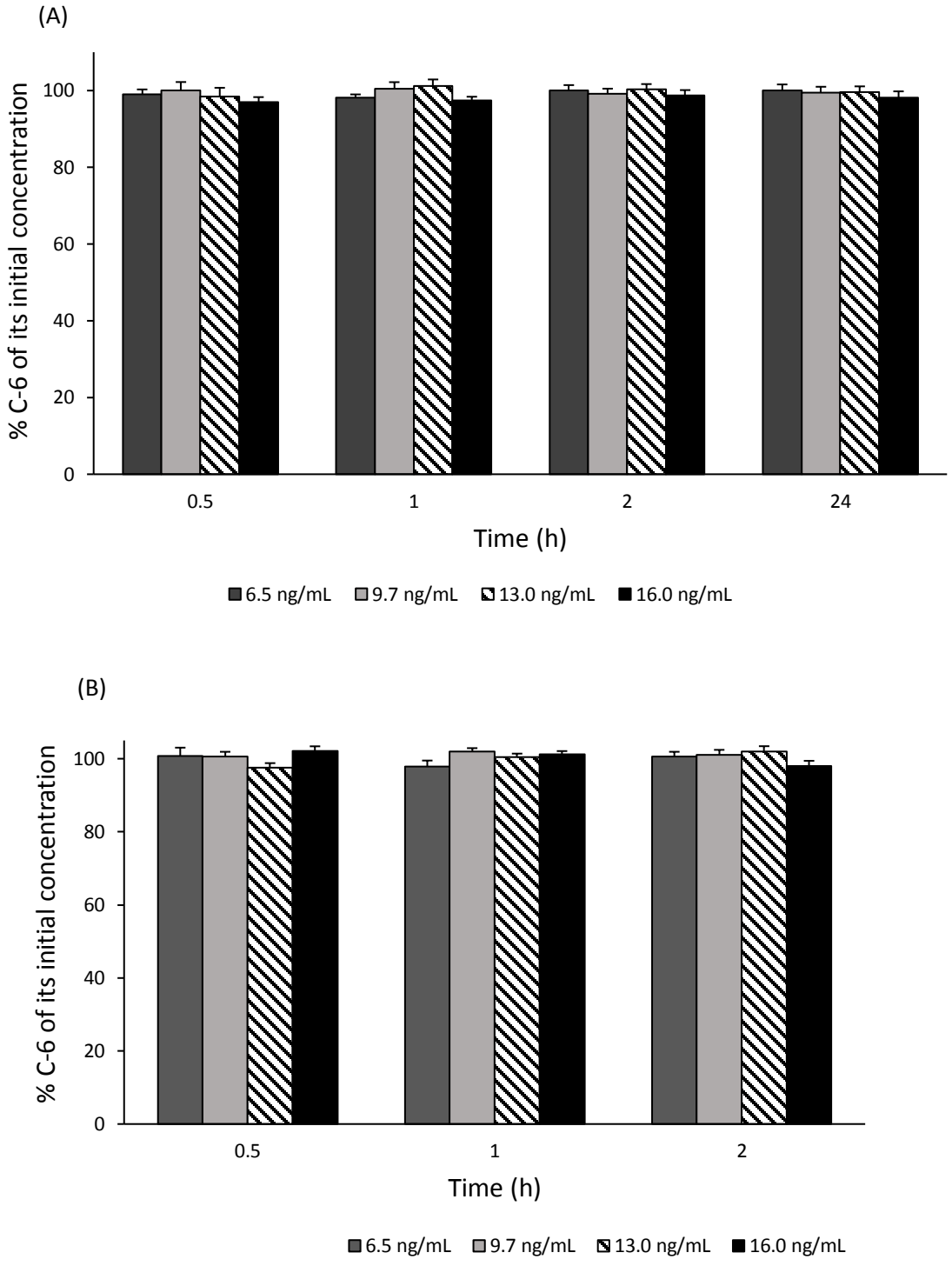

Figure 5.3: Effect of RIPA buffer on the stability of C-6 in (A) rats' plasma (B) rats' brain homogenate at room temperature.

Data is represented in the mean value of % C-6 remaining in rats' plasma ± SD (n=2).

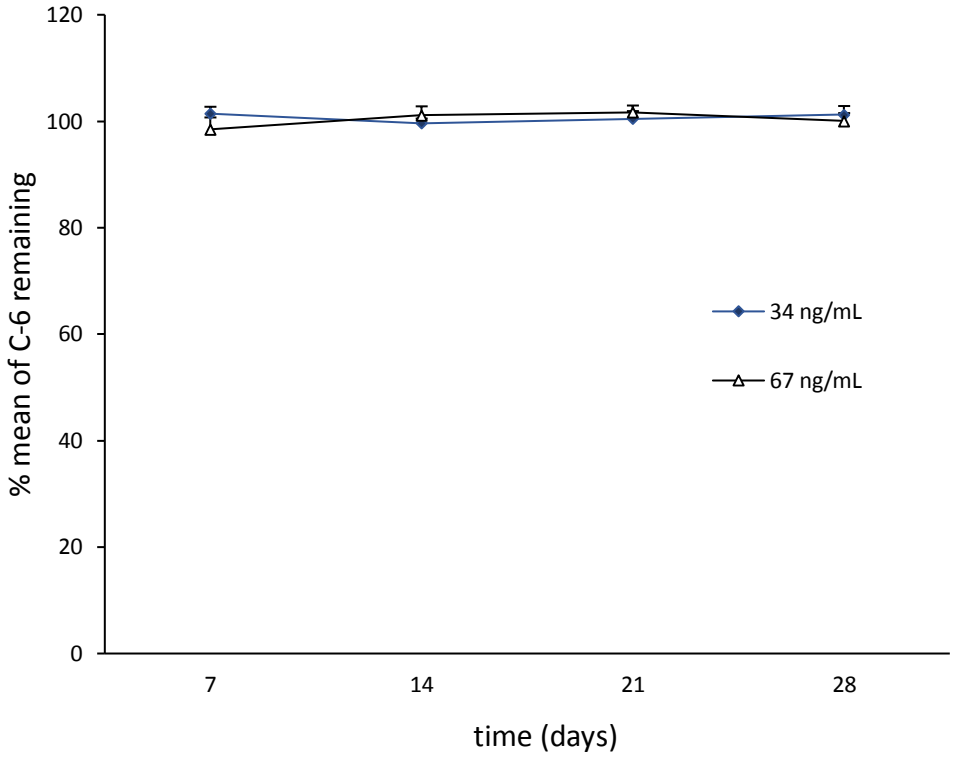

Figure 5.4: Storage stability of C-6 in rat's plasma at -80°C over 28 days.
Data was represented by the mean value of % C-6 remaining in rats' plasma ± SD (n=2).

5.4.3 Pharmacokinetics study of RV

Although the use of cell culture for evaluating cellular uptake of NPs is fast and convenient, however, it can never predict the targeting outcome in animals. Ultimately, the proof of concept study on the effectiveness of targeting ligands is the *in-vivo* animal studies. In this study, the pharmacokinetic profile of our two NPs (i.e. NPs with single and dual ligands) was compared to the free drug solution administered via IN route. A separate control, RV solution, was given by IV injection.

Figure 5.5 shows the plasma concentration-time profile of RV after administration of various NP formulations and control solutions. The RV drug solution via IN route showed a rapid increase in drug concentration from 842.0 ± 35.0 ng/mL at 15 mins post administration to the highest concentration of 1214.9 ± 103.8 ng/mL at 1 h, which suggests there was a relatively rapid and an adequate absorption of RV via the IN route. RV plasma concentration then exhibited a rapid decline in plasma concentration to 306.2 ± 79.0 ng/mL at 3 h and 75.2 ± 10.3 ng/mL at 8 h. As expected, the plasma drug concentration obtained post IV administration of free drug solution showed a continuous decline from a level of 2294 ± 438.9 ng/mL RV at 15 min to 702.2 ± 44.8 ng/mL at 2 h, due to rapid distribution and elimination. The plasma concentration of RV post IV administration finally declined to 98.5 ± 19.3 ng/mL at 8 h, similar to that post IN administration.

In contrast, the plasma profile of RV from NPs showed a much broad peak or sustained drug concentration under 8 h in a formulation dependent manner (Figure 5.5). The plasma concentration of single ligand PLGA-SA-ODA NPs was lower for the first two hours compared to both IN free RV solution and dual ligand NPs. Single ligand NPs only achieved 299.5 ± 21.5 ng/mL RV in plasma 15 min after IN administration, whereas plasma concentration of RV by IN free RV & dual ligand NPs were 842.0 ± 35.0 ng/mL and 609.5 ± 118.4 ng/mL respectively. Plasma concentration of RV by single ligand NPs then rose to 902.5 ± 144.5 ng/mL at 2 h and reached maximum 952.5 ± 61.4 ng/mL at 3h. The latter plasma concentration was approximately 2 times and 3.1 times higher than that of IV and IN of drug solution respectively at 3 h. RV plasma concentration from single ligand PLGA-SA-ODA NPs then gradually declined to 170.6 ± 14.5 ng/mL at 8 h.

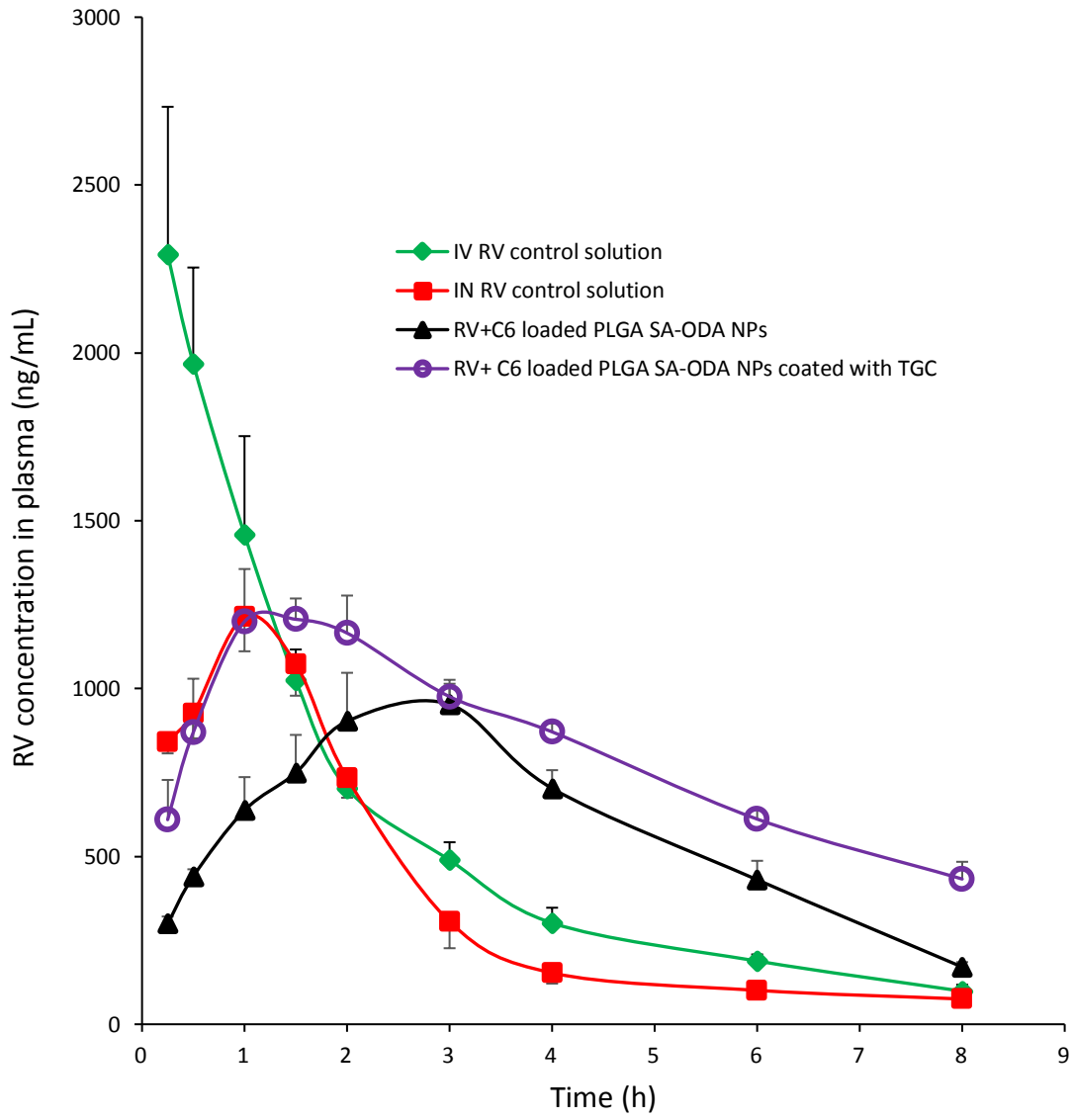

Figure 5.5: Plasma concentration-time profile of RV after administration of RV control solution, single ligand PLGA-SA-ODA NPs and dual ligand PLGA-SA-ODA NPs coated with TGC.

Both RV control solution and NPs were administered at a dose level of 1mg/Kg RV free base. Both single ligand RV=C-6 loaded PLGA-SA-ODA NPs and dual ligand RV + C=6 loaded PLGA-SA-ODA NPs were administered via IN route. The control RV solution was administered by both IV and IN route. Data are represented in mean RV concentration in plasma ± SEM (n=4) for 8 h.

Dual ligand RV+C6 loaded PLGA-SA-ODA NPs coated with TGC demonstrated the ability to produce a significantly higher drug concentration value (starting from the first-time point) along with a more sustained concentration pattern of the RV than that of single ligand RV+C6 loaded PLGA-SA-ODA NPs. Dual ligand NPs released 609.5 ± 118.4 ng/mL RV in the plasma at 15 min, with a maximum level of 1206 ± 62.1 ng/mL reached at 1.5 h. This level of RV gradually reduced to 976.0 ± 50.0 ng/mL at 3 h (Figure 5.5). RV plasma concentration from dual ligand PLGA NPs then gradually declined to 432.7 ± 51.3 ng/mL at 8 h. The prolonged high plasma concentration of RV by dual ligand NPs (1199.7-976.0 ng/mL expanding from 1 h to 3h) was in a sharp contrast to the rapid decline of the IN drug solution, indicating that the TGC coating promoted interaction and transport of the NPs in the nasal mucosal membrane, at the same time, its NPs provided continuous drug release and absorption into the systemic circulation. These results suggested that both single and dual ligands NPs were able to attain higher drug concentration in the systemic circulation for an extended period of time. This prolonged plasma concentration can also help in attaining better brain drug concentration across the BBB.

Our plasma concentration profile results were similar to that reported by Fazil and his colleagues (Fazil et al., 2012) who studied the brain delivery of RV (administered dose is 0.068 mg/kg) by IN administration of RV-loaded chitosan NPs in Wistar rats.

To minimize the dose & animal species effect, we calculated the plasma drug concentration ratio of drug solution by IN to drug solution by IV and drug-loaded NPs by IN to drug solution by IN at both 2 h and 8 h (Table 5.3). In comparison, our plasma concentration ratio of NPs by IN to drug solution by IN, at 2 h, is 1.22 for single ligand and 1.6 for dual ligand whereas CS NPs by Fazil et al (2012) showed 2.5. However, at 8h, when Fazil's group couldn't detect any drug concentration, our two NPs showed plasma drug concentration ratio of 2.26 and 5.74 for the single and dual ligand NPs respectively (Table 5.3). This means that single ligand system at 8 h produced an almost equivalent level of that CS NPs at 2 h while dual ligand at 8 h generated more than doubled the level of that of CS NPs at 2 h by Fazil et al (2012). In Table 5.3, we also compared our data to that generated by buspirone hydrochloride (BUH)-loaded thiolated chitosan (T-CS) NPs (Bari et al 2015). Plasma concentration ratio of BUH-loaded T-CS NPs by IN to BUH

solution by IN is much lower (0.55) at 2 h, indicating T-CS NPs didn't produce higher plasma concentration than its drug solution at 2 h post administration when the maximum drug concentration was detected in their study.

All of these comparisons demonstrate that our single ligand and dual ligand NPs showed a sustained release of RV over a prolonged time period and dual ligand system is more effective than that of single ligand system to produce sustained plasma concentration profile. The sustained high plasma concentration is expected to permit more drug to cross the BBB via central circulation. This also signifies the importance of our single ligand and dual ligands PLGA NPs in providing effective transport and sustained release of the drug into general circulation.

To compare the pharmacokinetics parameters for the both test formulations and controls, Thermo Kinetica Software were employed and results are presented Table 5.4. The C_{max} attained after IN administration of dual ligand PLGA NPs (1380.2±145.0, t_{max} 1.6 ± 0.2) was significantly higher than that obtained with RV (IN) drug solution (1257.1 ±106.8, t_{max} 1.1 ± 0.1) and single ligand PLGA NPs (IN) (1085.6 ± 87.9, t_{max} 2.4 ± 0.4). As Figure 5.5 indicated that the RV plasma concentration of dual ligand NPs was higher at all time points compared to single ligand NPs. Therefore, an increase in the AUC of the dual ligand NPs (9481.7 ± 749.0 ng/mL*h) compared to that of single ligand NPs (5166.0 ± 331.9 ng/mL*h) was expected. IN administration of dual ligand NPs showed ~2.61 and ~1.83 times greater $AUC_{(blood)}$ as compared to control RV (IN) solution and single ligand NPs respectively, again suggesting dual ligand NPs provides enhanced bioavailability of the drug and therefore, more drug for crossing the BBB to access the brain.

The lowest elimination rate constant was found with dual ligand NPs (0.17 ± 0.001) which was significantly lower than that of RV (IN) drug solution (0.30 ± 0.01), RV (IV) drug solution (0.31 ± 0.001) and single ligand NPs (0.30 ± 0.03) (Table 5.4). In addition, the calculated half-life of the RV was found to be 2.5 ± 0.6 h and 4.4 ±2.2 h for RV (IV) and RV (IN) in plasma respectively. The calculated RV (IN) half-life is very close to that reported by Fazil and his colleagues (Fazil et al., 2012). However, dual ligand NPs showed an increased half-life (4.5 ± 0.9 h) with an extended elimination phase.

Table 5.3: Comparative plasma drug concentration study of our developed NPs with the NPs mentioned in the literature

Drug	NPs	Plasma drug concentration ratios Time 2 h		Plasma drug concentration ratios Time 8 h		Data source
		Drug solution (IN) / Drug solution (IV)	Drug loaded NPs (IN) / Drug solution (IN)	Drug solution (IN) / Drug solution (IV)	Drug loaded NPs (IN) / Drug solution (IN)	
RHT	CS NPs [a]	0.60	2.50	N/A	N/A	(Fazil et al., 2012)
BUH	T-CS-NPs [b]	N/A	0.55	N/A	N/A	(Bari et al., 2015)
RV	Single ligand NPs [c]	1.10	1.22	0.80	2.26	Current Study
RV	Dual ligand NPs [c]	1.10	1.60	0.80	5.74	Current study

RHT: Rivastigmine hydrogen tartrate, RV: Rivastigmine; CS NP: Chitosan NPs, BUH: Buspirone hydrochloride T-CS NPs: thiolated chitosan NPs, single ligand NPs: RV +C-6 loaded PLGA-SA-ODA NPs. Dual ligand NPs: RV+C-6 loaded PLGA-SA-ODA NPs coated with TGC.

* Dose used: a: 0.068 mg/kg, b:1.6 mg/kg, c: 1 mg/Kg,

* Animals Used: a: Wistar rats, b: white albino rats, c: Sprague dawley rats.

The calculated clearance rate of the RV from plasma was found to be 195.3 ± 19.3 and 290.0 ± 28.1 L/h/kg for RV administered by IV and IN respectively. However, the clearance rate of RV from dual ligand NPs and single ligand NPs was 107.3 ± 7.5 and 200.5 ±10.9 L/h/kg respectively. The lower clearance rate of RV from both dual ligand and single ligand NPs further support less drug clearance from systemic circulation which contributes to the increase in bioavailability of RV, indicating the benefit of NPs as drug delivery system. We speculate this is the result of the combined enhanced NP transport across the mucosa membrane and sustained release of RV from NPs, which provides an opportunity for continuous delivery of the drug into the brain.

Our results are similar to that reported by Shahnaz and colleagues (Shahnaz et al., 2012) who compared thiolated chitosan-modified NPs with unmodified NPs and control IN solutions of leuprolide in Sprague-Dawley rats. They demonstrated that the thiolated chitosan-modified NPs enhanced AUC and increased mean residence time (MRT) of leuprolide as compared to unmodified NPs and control drug solutions administered by IN route. Our results also showed the enhanced MRT of both dual ligand and single ligand formulation compared to control drug solutions. The increase in the MRT of a single ligand, and mainly dual ligand formulation, further demonstrates the supremacy of our developed formulation. The prolonged residence time of dual ligand RV loaded PLGA NPs in nasal cavity may have facilitated the NPs transport and or lead to more continuous drug release, which eventually resulted in the higher drug concentration for an extended time as compared to single ligand NPs.

Table 5.4: Pharmacokinetic profiling of RV for various formulations administered the drug dose of 1 mg/kg to male Sprague-Dawley rats by IV and IN routes.

Pharmacokinetic parameters	IV RV solution	IN RV solution	RV+C6 loaded PLGA SA-ODA NPs (single ligand)	RV+ C6 loaded PLGA SA-ODA NPs coated with TGC (dual ligand)
C_{max} (ng/mL)	2439.4 ± 401.8	1257.1 ± 106.8	1085.6 ± 87.9	1380.2 ± 145.0
t_{max} (h)	0.3 ± 0.1	1.1 ± 0.1	2.4 ± 0.4	1.6 ± 0.2
AUC $_{(0-\alpha)}$ (ng/mL*h)	5269.0 ± 529.6	3559.7 ± 413.0	5166.0 ± 331.9	9481.7 ± 749.0
Ke (h^{-1})	0.31 ± 0.001	0.30 ± 0.01	0.30 ± 0.03	0.17 ± 0.001
$t_{(1/2)}$ (h)	2.5 ± 0.6	4.4 ± 2.2	3.2 ± 0.4	4.5 ± 0.9
F (%)	100	65.1 ± 3.5	94.3 ± 3.5	185.8 ± 12.6
Clearance (L/h/kg)	195.3 ± 19.3	290.0 ± 28.1	200.5 ±10.9	107.3 ± 7.5
Apparent volume of distribution (L)	194.4 ± 45.1	442.3 ± 166.6	173.8 ± 19.0	168.4 ± 17.8
MRT (h)	2.9 ± 0.4	4.4 ± 1.7	4.4 ± 0.2	7.1 ± 1.3

Data represented by a mean parameter ± SEM (n=4) for all set of formulations. C_{max}=maximum plasma drug concentration, t_{max} is the highest time of maximum drug concentration in plasma, K_e is overall elimination rate constant. AUC $_{(0-\alpha)}$ is Area under the curve from zero to infinity time, $t_{1/2}$ half-life of the drug formulation, F is systemic bioavailability of the drug, MRT is mean residence time of RV in the body.

5.4.4 Brain uptake of RV

IN drug delivery provides greater promise for delivery of drugs into the brain via an olfactory and trigeminal nerve pathway. It has been reported that RV attains the highest concentration within 2 h post IN administration. As, RV has a short half-life (1.5-2.0 h) (Fonseca-Santos et al., 2015; Hadavi & Poot, 2016), therefore, animals in this study were sacrificed at 2 h and 8 h post administration, to determine and compare RV concentration in the brain.

During the brain uptake study, the whole brain was collected, homogenized, solubilized and extracted for determination of the RV drug concentration. The use of RIPA buffer in the process to allow the tissue cells to be lysed and NPs to be solubilized to release RV drug into homogenate. Therefore, the brain drug concentration was the sum of the free and released drug in the brain as well as drug present inside the NPs which were transported to the brain from the nose.

Figure 5.6 shows the brain distribution of the RV after administration of RV solution (IV), RV solution (IN) and single ligand and dual ligand NPs. The concentration of RV is expressed in ng/gram of brain tissue. The RV brain concentration was higher with all formulations at 2 h as compared to 8 h. Additionally, the RV level of both types of NPs was significantly higher than that of the free drug solution (both IV and IN route) at all the time points.

IN administered RV drug solution (377.0 ± 24.0 ng/gm of brain tissue) showed significant better brain targeting than the IV drug solution (216.6 ± 9.0 ng/gm of brain tissue) at 2 h. Furthermore, the brain concentration of RV for both control drug solutions decreased to a comparatively similar low level at 8 h. Dual ligand RV+C-6 loaded PLGA-SA-ODA NPs coated with TGC were able to deliver the RV to the brain at a significantly higher level than the single ligand RV+C-6 loaded PLGA-SA-ODA NPs and free drug solution. The single ligand NPs increased RV concentration (1190.5 ± 104.5 ng/gm of the brain) in the brain region, which was 4.5 times and 2.2 times higher than that of IV and IN drug solution respectively at 2 h (Figure 5.6). The dual ligand NPs further enhanced brain delivery of

RV (1615.3 ± 237.0 ng/gm of the brain) showing 6.5 times and 3.3 times higher when compared to IV and IN administered control solutions respectively at 2 h.

Another interesting point worth mentioning is that the RV concentration at 8 h provided by both dual ligand and single ligand NPs showed a level similar to IN RV solution at 2 h and even significantly higher than that of IV administered RV solution at 2 h ($p < 0.01$). Hence, the data provides proof of the superiority of single and dual ligand NPs over free drug solution and furthermore the importance of the use of dual ligand NPs to further improve the drug targeting into the brain.

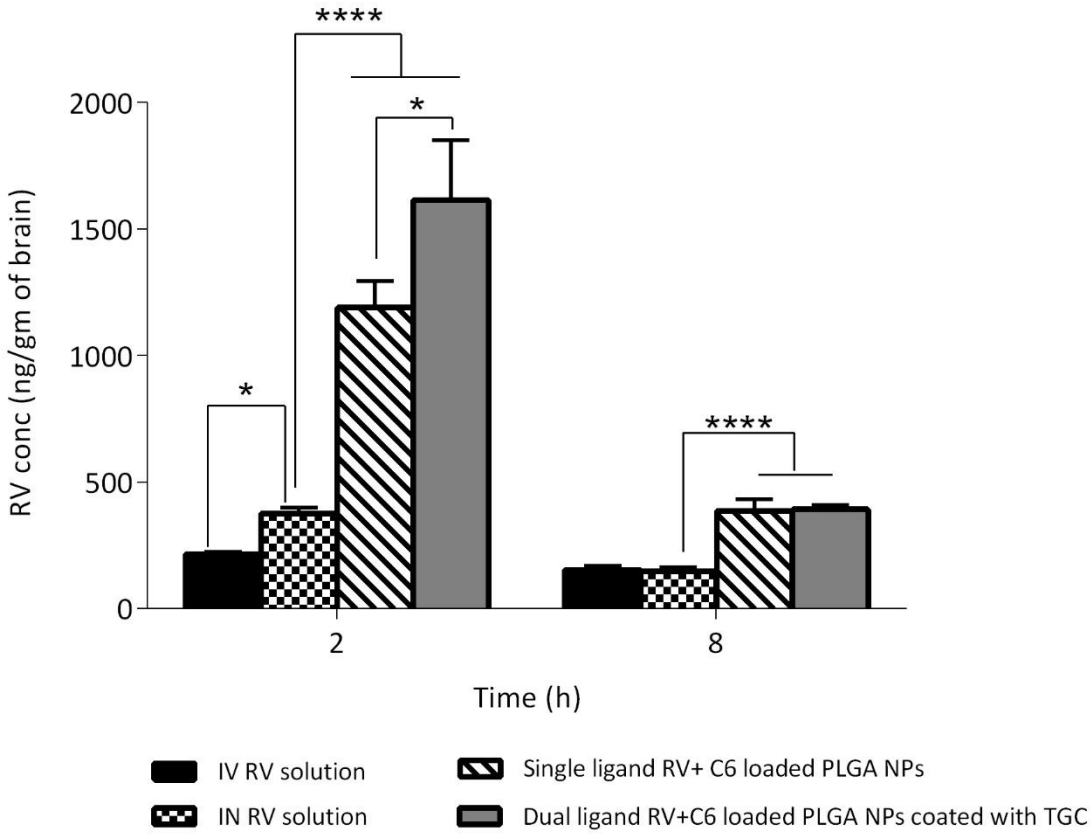

Figure 5.6: RV brain concentration after administration of various treatments
RV drug solution was administered by IN and IV route, single ligand RV+C6 loaded PLGA-SA-ODA NPs and dual ligand RV+C6 loaded PLGA-SA-ODA NPs coated with TGC via IN route. Both RV control solution and NPs were administered at a dose level of 1mg/Kg RV free base. The expressed data was represented in mean RV concentration ± SEM (ng/gm of brain) (n=5), **** $p<0.0001$, * $p<0.05$.

There are a number of plausible mechanisms for the enhanced RV delivery into the brain by both single ligand PLGA NPs and dual ligand PLGA NPs.

Firstly, thiolated polymer can interact with cysteine-rich residues forming disulphide bonds with glycoprotein layer in the nasal mucosal membrane, thereby resulting in prolonged residence time of a dual ligand NPs, owing to increased mucoadhesive nature and more importantly reducing the NPs clearance from the nasal cavity (Kast & Bernkop-Schnürch, 2001; Pawar & Jaganathan, 2016).

Secondly, there is evidence to suggest that substitution of thiol groups on the chitosan or GC polymer not only would enhance mucoadhesive properties but also increase the permeation effects of chitosan or GC polymer (Bernkop-Schnürch et al., 2004; Pawar & Jaganathan, 2016). The underlying mechanism for the increased permeation effect is due to the electrostatic interaction of the positively charge of the chitosan or GC with negatively charged cell membrane resulting in the opening of tight junctions between nasal epithelial cells (Pawar & Jaganathan, 2016; Shahnaz et al., 2012). The GC moiety present on the surface of NPs may aid opening the tight junctioned nasal epithelial cells, thereby increasing the concentration of RV in the brain. The presence of the thiolated group in GC, as expected may additionally promote opening tight junctions between the epithelial cells by inhibiting the protein tyrosine phosphatase enzyme (Bernkop-Schnürch et al., 2004; Gradauer et al., 2013). These mechanisms would enhance NPs transport via the paracellular pathway across nasal epithelial cells (Bernkop-Schnürch et al., 2004; Dyer et al., 2002; Haque et al., 2012). As a result, dual ligand PLGA NPs were expected to be able to deliver higher and prolonged RV concentration owing to its better mucoadhesive property. Meantime, the thiolated GC coating can also act as a release barrier to provide sustained release effects. These mechanisms will prolong the *in-vivo* residence time of NPs and sustain release of the drug. We don't have direct evidence to support this hypothesis, but our pharmacokinetics and biodistribution results indicated that RV concentration has significantly increased at both 2 h and 8 h, in the plasma and brain with dual ligand NPs compared to single ligand NPs and free drug solution.

Thirdly, SA-ODA synthesized derivative present in the PLGA NPs may interact with siglec (sialic acid binding immunoglobulin type lectins) family receptor cells present in

the cerebrum, resulting in the inhibition of the efflux of the NPs present inside the brain (Patel et al., 2016; Tosi et al., 2010). Our targeting ligand SA-ODA present in the NPs helped to maintain the sustained concentration of RV inside the brain for a prolonged period of the time, via formation of the complex with sialoadhesin receptor cells. Consequently, PLGA-SA-ODA NPs were able to maintain a higher RV concentration in the brain than that of the RV (IN) and RV (IV) drug solutions.

All these previously explained mechanisms eventually contributed to the high level of the RV in the brain. It is known that brain drug concentration may depend upon the several factors, including physicochemical properties of the drug and more importantly NPs, dose size, mechanism of drug and NPs transport and drug loading in the NPs. We, therefore, choose to calculate NPs drug concentration ratio over its own solution so, that the drug and dose-dependent effects can be minimized and the comparison can be made between different studies (Table 5.5).

We compared our brain targeting data with other work reported in the literature (Table 5.5). In comparison to PLGA NPs prepared by Seju et al (2011), our single ligand PLGA-SA-ODA NPs were superior in attaining higher brain drug concentration. Our single ligand NPs brain drug concentration ratio was almost 1.75 folds higher than that of the brain drug concentration ratio obtained by Seju et al (2011) at 2 h. Although, the RV brain ratio of single ligand NPs dropped at 8 h but it was still higher than that of the drug concentration ratio of PLGA NPs' prepared by Seju et al (2011) at 2 h.

Furthermore, in comparison to RV loaded chitosan NPs prepared by Fazil et al (2012), the brain drug concentration ratio of our single ligand and dual ligand NPs to that of control solution attained 1.44 folds and 2.0 folds respectively at 2 h of the ratio of chitosan NPs to their respective control solution prepared by Fazil et al (2012). The enhanced brain drug concentration ratios in comparison to the available literature data confirm the strong targeting effects of our developed single ligand and dual ligand RV+C-6 loaded PLGA NPs.

In addition, to demonstrate the effectiveness of the thiolated GC ligand in our dual ligand PLGA NPs, we compared the brain targeting data of our dual ligand NPs with the thiolated chitosan NPs prepared by Bari et al (2015). The results represented in Table 5.5 indicated

that the RV brain drug concentration ratio of our dual ligand PLGA NPs to control RV (IN) solution was 2.3 folds of that of the respective ratio of thiolated chitosan NPs to drug solution reported by Bari et al (2015) at 2 h. It was further observed that RV brain drug ratio of both single and dual ligands NPs at 8 h was still higher than that of their ratio at 2 h.

This improved brain targeting of our dual ligand NPs to control IN solution indicated that dual ligands on PLGA NPs have allowed the NPs to stay intact longer in the nasal mucosa and promote higher brain uptake of the drug, hence proving the superiority of the dual ligands modified NPs over others. At 2 h and 8 h, our dual ligand NPs are more effective than others in enhancing the drug delivery into the brain against its own solution formulation. Furthermore, the differences in plasma profile and RV brain concentrations from IN, IV solutions and IN NPs support the presence of the direct transport pathway from nose to the brain possibly via olfactory and trigeminal nerves.

Table 5.5: Comparative brain uptake study of our developed NPs with that of the IN administered NPs reported in literature

		Brain drug concentration ratio				
Drug	**NPs**	**Time 2 h**		**Time 8 h**		**Data source**
		Drug solution (IN) / Drug solution (IV)	**Drug loaded NPs (IN) / Drug solution (IN)**	**Drug solution (IN) / Drug solution (IV)**	**Drug loaded NPs (IN) / Drug solution (IN)**	
RHT	CS NPs [a]	1.83	2.18	2.00	1.71	(Fazil et al., 2012)
OZ	PLGA NPs [b]	1.36	1.79	N/A	N/A	(Seju et al., 2011)
BUH	T-CS NPs [c]	1.31	1.90	N/A	N/A	(Bari et al., 2015)
RV	Single ligand NPs [d]	1.75	3.15	0.95	2.63	Current project
RV	Dual ligand NPs [d]	1.75	4.28	0.95	2.67	Current project

* Dose used: a: 0.068 mg/kg, b:1.6 mg/kg, c: 0.26 mg/kg d: 1 mg/Kg, * Animals Used: a: Wistar rats, b: white albino rats, c: Wistar rats, d: Sprague dawley rats.
RHT: Rivastigmine hydrogen tartrate, RV: Rivastigmine; CS-NP: Chitosan NPs, BUH: Buspirone hydrochloride T-CS NPs: thiolated chitosan NPs, single ligand NPs: RV +C-6 loaded PLGA-SA-ODA NPs. Dual ligand NPs: RV + C-6 loaded PLGA-SA-ODA NPs coated with TGC.

5.4.5 Pharmacokinetics and brain uptake of C-6

To evaluate the brain targeting of developed nanoparticulate formulations for a hydrophobic drug, C-6 was incorporated at 0.3% w/w of the polymer's weight to serve as a model hydrophobic drug and a fluorescent marker, (along with RV) into NPs. The results for plasma and brain samples from the both single ligand and dual ligand PLGA NPs are presented in Figure 5.7 and Figure 5.8 respectively.

The plasma concentration profile of C-6 in Figure 5.7 indicated that though both dual ligand and single ligand NPs exhibited a similar pattern, but the dual ligand NPs attained a lower plasma concentration of C-6 than single ligand PLGA NPs at all time points. C-6 has a stronger interaction with NPs, as shown in our leach study (less than 3% of C-6 leached from NPs within 48 h: section 4.5.6.2). This may be due to the hydrophobic nature of C-6 which governs the molecule to remain in the PLGA polymer matrix thus less C-6 was released and lower plasma C-6 concentration. Furthermore, the TGC coating prevented the C-6 from diffusing out of the matrix. Therefore, less release of the C-6 over a period of time.

The mucoadhesive nature of the TGC on one hand, may cause the opening of tight junctions, leading to enhanced transportation of dual ligand RV+C-6 NPs to neuronal brain cells via the olfactory and trigeminal nerve pathway, on the other hand, dual ligand RV+C-6 NPs could stay in the nasal mucosa for a longer period of time, resulting in less available to the systemic circulation. Similar results were presented by Gao and his colleagues (Gao, Chen, et al., 2007) when they administered unmodified C-6 loaded PEG-PLA NPs and Ulex Europeus Agglutinin 1 (UEA 1) modified PEG-PLA NPs. The C_{max} and AUC of C-6 were higher in blood for the unmodified PEG-PLA NPs as compared to UEA 1 modified PEG-PLA NPs. However, in the case of the brain uptake study, the concentration and AUC was higher for the UEA 1 modified PEG-PLA NPs than that of unmodified NPs, a pattern which was also seen in our study.

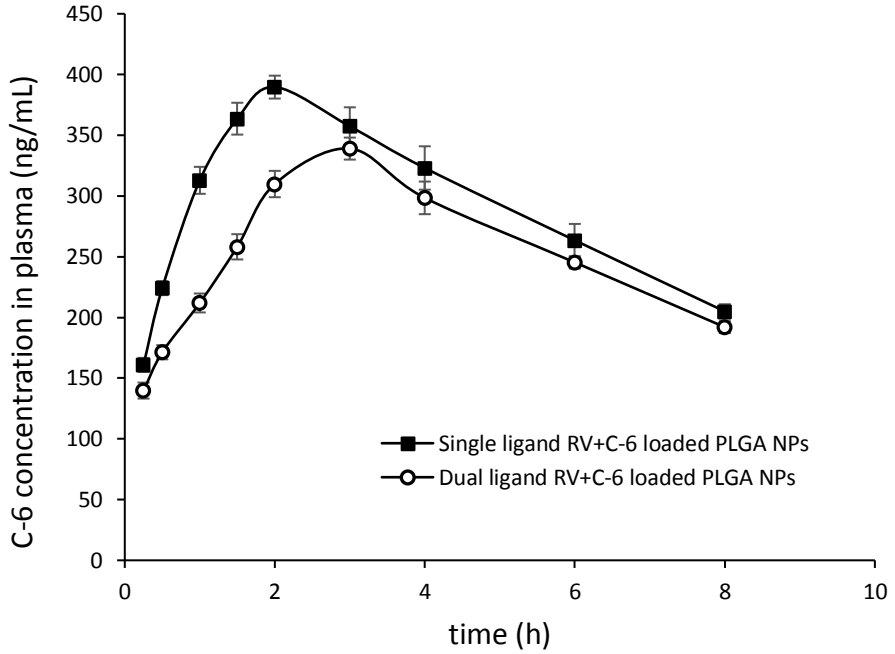

Figure 5.7: Plasma concentration-time profile of C-6 from single ligand RV+C6 loaded PLGA-SA-ODA NPs and dual ligand RV+C6 loaded PLGA-SA-ODA NPs coated with TGC.

The data was represented in mean C-6 concentration in plasma ± SEM for 8 h (n=5).

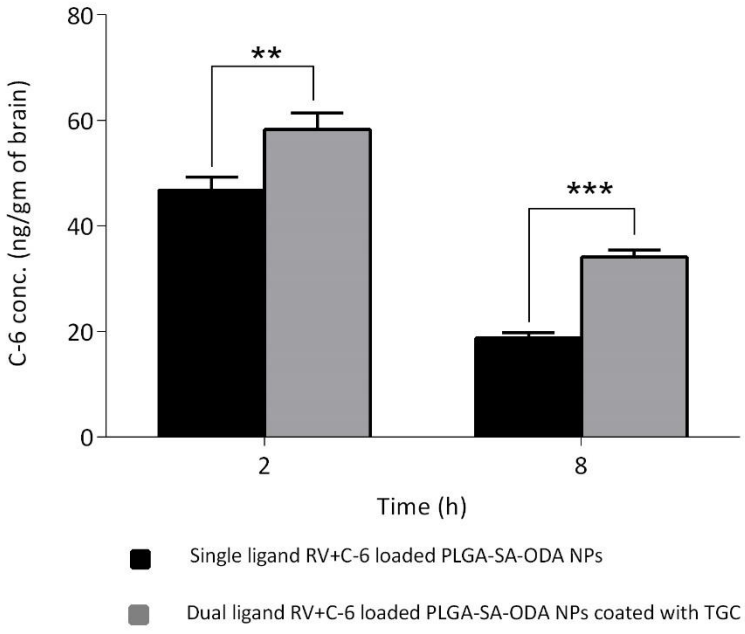

Figure 5.8: C-6 concentration in brain tissue after IN administration of single ligand RV+C6 loaded PLGA-SA-ODA NPs and dual ligand RV+C6 loaded PLGA-SA-ODA NPs coated with TGC.

Both types of NPs were administered at a dose level of 80 µg/Kg of C-6. The data represented in mean C-6 concentration in brain ± SEM (ng/gm of brain tissue) (n=5). ** $p<0.01$, *** $p<0.001$.

Various plasma pharmacokinetic parameters of C-6 by both formulations were calculated using Kinetica software (Table 5.6) Both single ligand and dual ligand NPs exhibit similar plasma concentration-time profiles. The average peak plasma concentration of single ligand NPs and dual ligand NPs was 389.6 ± 9.5 ng/mL with t_{max} 2.0 ± 0.1 h and 347.9 ± 1.7 ng/mL with t_{max} 3.0 ± 0.2 h respectively. The plasma concentration of C-6 from single ligand NPs was higher at all the times compared to dual ligand NPs (Figure 5.7). The single ligand NPs had a higher $AUC_{(0-\alpha)}$ than dual ligand NPs. The calculated $AUC_{(0-\alpha)}$ for the single ligand and dual ligand NPs was 70.7 ± 3.4 and 64.3 ± 3.1 ng/mL*h respectively, which indicated that the $AUC_{(0-\alpha)}$ of C-6 is 1.10 times higher in the case of single ligand RV+C6 loaded NPs than that of dual ligand NPs. The higher $AUC_{(0-\alpha)}$ of the single ligand NPs allows them to stay longer in the systemic circulation, which will further help to target the single ligand NPs to the brain via BBB, ultimately increasing the concentration of RV and C-6 in the brain.

Table 5.6: Pharmacokinetic parameters of C-6 following various formulations administered by IN route

Pharmacokinetic Parameters	Single ligand RV+C6 loaded PLGA NPs	Dual ligand RV+C6 loaded PLGA NPs
C_{max} (ng/mL)	389.6 ± 9.5	347.9 ± 1.7
t_{max} (in h)	2.0 ± 0.1	3.0 ± 0.2
K_e (h^{-1})	0.09 ± 0.001	0.11 ± 0.01
$t_{1/2}$ (h)	6.4 ± 0.4	6.2 ± 0.5
$AUC_{(0-\alpha)}$ (ng/mL* h)	70.3 ± 3.4	64.3 ± 3.1
Clearance (L/h/Kg)	1.1 ± 0.06	1.2 ± 0.05
Apparent volume of distribution (L)	3.3 ± 0.7	2.9 ± 0.09
MRT (h)	9.9 ± 0.5	10.0 ± 0.7

C_{max}=maximum plasma drug concentration, t_{max} is the highest time of maximum drug concentration in plasma, K_e is overall elimination rate constant. $AUC_{(0-\alpha)}$ is Area under the curve from zero to infinity time, $t_{1/2}$ half-life of the drug in a particular formulation, MRT is mean residence time of C-6 in the body.

The brain uptake concentration of C-6 was in a similar pattern as seen with RV brain uptake. The dual ligand PLGA NPs facilitated higher uptake of the C-6 fluorescent marker compared to single ligand PLGA NPs (Figure 5.8). The C-6 concentration in the brain at 2 h was 46.8 ± 2.5 ng/gm and 58.3 ± 3.1 ng/gm of brain tissue for single ligand and dual ligand NPs respectively, which reduced to 18.8 ± 0.9 ng/gm and 34.1 ± 1.3 ng/gm of brain tissue at 8 h respectively. The brain uptake of C-6 from dual ligand NP was 1.25 times of that of single ligand NPs at 2 h (similar to that of RV), and the level of C-6 concentration reached 2 times level of that of single ligand system at 8 h (better than that of RV). This suggests that dual ligand NPs can deliver significantly more C-6 from nose to brain than that of single ligand system, and was effective in delaying the clearance of C-6 from the brain. Our results were consistent with reports from other researchers (Gao, Chen, et al., 2007; Gao et al., 2006; Gao, Wu, et al., 2007).

It is interesting to note that in comparison to RV, C-6 showed a much less dramatic reduction of brain concentration at 8 h than that of 2 h, indicating the slow removal of hydrophobic C-6 from the brain. We speculate that because of the lipophilic nature of the fluorescent marker, this may have restricted the leakage and/or removal of C-6 from the brain, leading to an enhanced C-6 concentration in the brain for a prolonged period of time. In contrast, RV is hydrophilic in nature, thereby increasing its efflux from or degradation inside the brain.

In summary, TGC (targeting ligand-1), as expected, improved NPs transport from nose to the brain following IN administration, possibly by multiple mechanisms as described previously. SA-ODA (targeting ligand-2) were thought to provide a function of maintaining a higher concentration of NPs near the neuronal cells in the brain via interacting with sialic acid receptor cells. The combined effect of the targeting ligands 1 and 2 has dramatically improved the delivery of the drug and fluorescent marker into the brain as demonstrated in our studies. This study indicates the success of our dual ligand NPs as a platform technology potentially for transport of other brain drugs.

5.5 Conclusion

The present research involved the development of a dual ligand nanoparticulate delivery system for RV that has a unique affinity to the nasal mucosal membrane and neuron cells in the brain. Both single and dual ligand PLGA-SA-ODA NPs were loaded with RV and C-6, administered through the IN route and their brain targeting ability was compared with IN and IV RV drug solutions. Our RV plasma stability study indicated that RV was stable in plasma at 37°C for 24 h and at -80°C for 28 days which suggests that plasma samples can be stored for 28 days prior to analysis. In addition, the plasma stability study results of C-6 demonstrate that C-6 was also stable in plasma for 28 days while stored in a black box at -80°C. Relevant stability study results also confirm that our plasma and brain tissue samples were stable during the extraction and processing.

Our *in-vivo* experiments demonstrate that both dual ligand and single ligand RV formulations successfully increased the brain targeting of RV compared to drug solution, proving the superiority of developed NPs over free drug solution. Both dual ligand and single ligand NPs were retained in the brain longer than that of control RV drug solutions. The dual ligand and single ligand PLGA NPs provided 3.3 and 2.2 times higher RV concentration in the brain at 2 h than that of IN RV drug solution. We also showed that dual ligand PLGA-SA-ODA NPs coated with TGC provided 1.4 and 1.3 times higher brain concentration of RV and C-6 respectively as compared to single ligand PLGA-SA-ODA NPs, indicating the pre-eminence of the TGC allowing enhanced nose to the brain delivery of drug-loaded NPs. The bioavailability of RV by dual ligand NPs was higher than that of both single ligand NPs and control IN drug solution which may also contribute to higher concentration in the brain. It was concluded that dual ligand NPs showed better brain targeting ability compared to single ligand NPs, possibly via their strong mucoadhesive property, tight junction opening ability, sustained release properties and interaction with siglect family receptor cells in the brain which facilitated the NPs transport and continuous drug release inside the brain. All these leads to a higher drug and C-6 concentration for an extended time in the brain as compared to single ligand NPs. Successful incorporation and delivery of two molecules with opposing properties by the same NPs allowed us

to demonstrate the versatility of our NP formulation and its potential multiple functions.

This study has ultimately revealed that an optimal formulation and route of administration are important for successful delivery of treatment of AD using RV. Both single ligand and dual ligand PLGA NPs can act as an effective carrier for targeting the drugs from the nose to the brain, ultimately enhancing the drug concentration in the brain tissue.

6. Chapter-6 General Discussion and Conclusion

6.1 General Discussion

Drug delivery to the brain is challenging due to the BBB, which restricts the entry of the more than 98% of hydrophilic drug molecules. There are a number of alternative modes of drug delivery potentially available to achieve enhanced drug concentrations in the brain for the treatment of neurodegenerative disorders (NDs) (Lu et al., 2014). A feasible and non-invasive approach is to deliver the drugs through the IN route which provides drug transport to the brain via the olfactory pathway, bypassing the BBB. RV is a parasympathomimetic drug that has been approved as a safe, first line drug for the treatment of mild to moderate AD. RV undergoes extensive first pass metabolism, primarily via acetylcholinesterase enzyme-mediated hydrolysis, to a decarbamylated phenolic metabolite (NAP 226-90) (Amini & Ahmadiani, 2010; Polinsky, 1998). This phenolic derivative has approximately 10% activity of the parent compound and 2.5 to 4 h plasma half-life. RV has limited ability across the BBB due to its hydrophilic nature and rapid metabolism, therefore it is difficult to attain a high drug concentration in the brain to treat AD. There is a need to increase the RV concentration in the brain and extend its retention in the brain to improve RV therapy.

The overall objective of this Ph.D. thesis was to develop a novel nano-formulation to improve the delivery of therapeutic drug molecules, such as RV, into the brain through IN administration. RV loaded PLGA NPs with two targeting ligands were prepared using double emulsion solvent evaporation technique. The first targeting ligand, modified TGC or GC, increases the mucosal retention of the NPs and second targeting ligand, SA-ODA, targets the neuronal cells present in the cerebrum. This developed dual ligand NPs were loaded with C-6 as a diagnostic model molecule and a fluorescent marker. The developed NPs were then evaluated for their pharmacokinetics and brain targeting efficacy administered IN route to Sprague-Dawley rats.

TGC and mPEG-TAT (PEGylated TAT) polymer were synthesized and characterized as potential targeting ligands. (i). SA-ODA was synthesized and characterized by another member of our research group.

TGC was successfully synthesized by conjugating the thioglycolic acid to the surface of the GC using selective carbodiimide reaction. Amide bond formation was confirmed qualitatively by FT-IR spectroscopy and quantitatively using Ellman's reagent. The

presence of amide bands at 1627 cm^{-1} (Amide-I band) and 1519 cm^{-1} (Amide-II band) in FT-IR spectra and number of thiol group determined on the GC using Ellman's reagent confirmed the successful attachment of thiol moiety on GC polymer.

The mPEG-TAT-conjugated polymer was synthesized via two-step reaction: (i) selective oxidation of hydroxyl group of mPEG using potassium permanganate in the presence of potassium hydroxide; (ii) coupling of activated mPEG-COOH with TAT peptide using selective carbodiimide reaction. Several factors were optimized during the reaction to improve the conjugation efficiency between mPEG-COOH and TAT peptide. Purification of PEGylated products mixture from unreacted starting materials, reactants used in excess, products of their degradation and by-products of the reaction was achieved. The product of the reaction was rather heterogeneous as the PEGylation process resulted in PEGylated peptide conjugates of different composition alongside unreacted PEG molecule. We utilized two commonly used purification methods for the reaction mixtures: (i) dialysis technique and (ii) SEC. The conjugate undergoes the hydrolysis in water during dialysis purification due to the instability of the newly formed amide bond between mPEG-COOH and TAT peptide. This technique was also unable to separate the mono-PEGylated peptide conjugate from the di- and tri-PEGylated peptides, thereby limiting its utility. SEC was therefore adopted as an alternative method for the purification of the PEGylated TAT peptide from the reaction mixture components according to their difference in size. However, we could not achieve better separation with limited resources. A number of purification methods were attempted to extract the conjugated mPEG-TAT polymer from the unreacted components of the reaction mixture. An accurate and reproducible quantification of TAT peptide tagged mPEG polymer was a challenging exercise throughout the process development. The mPEG-TAT approach had to be abandoned due to unstable and extreme low yield. TGC was used instead.

The second part of this project provides the insights about the analytical methods developed for the analysis of RV and C-6 in both clean *in-vitro* and *in-vivo* biological samples. The quantitative RP-HPLC method for RV analysis in clean *in-vitro* samples was developed using diode array detector. The developed method employed the use of acetonitrile and water mixture (20:80) with 0.1% trifluoroacetic acid in an isocratic mode. The developed method was highly selective, linear, sensitive, précised and stability indicating in nature. All the degradation products were completely isolated

from the peak of the RV representing the specific nature of the developed method. The developed method was highly sensitive in nature and able to identify the RV with a LOD of 28.0 ng/mL in the mobile phase. In addition, the gradient method was developed for analysis of RV in biological samples using fluorescent detector. The developed method was simple, cost effective and selective in nature. A novel extraction method was developed for the isolation of RV from the biological samples utilizing the combination of organic solvents and RIPA buffer. The recovery of the RV from both plasma and brain samples was more than 97.2 %. The developed gradient method was highly sensitive in nature and able to quantify the RV with a LOD of 55.0 ng/mL both in plasma and brain matrices.

A simple, selective, précised and accurate RP-HPLC method using fluorescence detector was also developed for C-6 analysis in clean *in-vitro* samples. The method was highly sensitive in nature and able to detect C-6 with a LOD of 0.05 ng/mL with a recovery of more than 98.7 ± 0.6 %. The C-6 analysis of biological samples was evaluated using RIPA buffer and a plate reader. The mean recovery from biological samples was more than 99.0% and found to be within an acceptable limit. These all developed method were employed for the determination of RV and C-6 in clean samples and rat plasma and brain samples from animal studies.

The third part of this project involved the formulation, optimization and *in-vitro* evaluation of the biodegradable RV+C-6 loaded PLGA NPs modified with two different targeting ligands. A large number of published data investigated the effect of various in-process formulation factors on the physicochemical characteristics of PLGA NPs (Joshi et al., 2010; McCall & Sirianni, 2013; Mu & Feng, 2003a; Patil & Surana, 2013). Based on preliminary literature research, it was found that particle size and EE of PLGA NPs is significantly affected by various process variables such as polymer molecular weight and its concentration, emulsifier type and its concentration, a method of formulation, etc. These parameters were optimized to achieve the NPs with optimum size and drug loading. The literature suggested that increase in the external aqueous phase pH also influences the drug EE inside the NPs by inhibiting the ionization of the basic drug (Peltonen et al., 2004; Song et al., 1997). Our results are contrary due to dual lipophilic and hydrophilic nature of RV, which causes easy distribution between the oily and aqueous phase during the sonication process, resulting in a nullifying effect of pH on drug EE.

In the present study, we reported the use of the two types of the stabilizers (PVA and TPGS) for the formulation of PLGA NPs. Our results confirm that 0.3% TPGS is the best among these tested emulsifiers due to its unique chemical structure for stabilizing PLGA NPs. PLGA molecular weight was indicated having a direct correlation with a particle size of the NPs. An increase in the PLGA molecular weight from 3.5 kDa to 150 kDa, lead to an increase in the size of the NPs from 123 nm to 195 nm, whereas the EE did not follow a similar pattern. Initially, its EE increased from 14.0% to 18.1% with an increase in molecular weight from 3500 Da to 110,000 Da; thereafter a significant drop to 12.4% was seen with an increase in molecular weight to 150,000 Da. The fluctuating EE of RV in PLGA NPs is due to increase in the viscosity of the polymeric solution with an increase in the polymeric molecular weight which might hamper the solvent evaporation rate with reduced stirring, ultimately increased EE. Achieving high drug loading and encapsulation efficiency of hydrophilic drugs in polymeric NPs is challenging. Our formulations showed a low RV encapsulation efficiency in both single ligand and dual ligand nano-formulations. Approaches such as pH adjustment and use of free base drug were tried but failed to increase the drug entrapment efficiency. Other strategies such as inclusion of ion-pairing agent in the polymer phase may worth further investigation to improve the drug encapsulation. The selection of proper surfactants for multiple emulsions may be another avenue for investigation.

The developed PLGA-SA-ODA NPs were finally optimized for the GC coating concentration in order to obtain the optimum size of GC coated PLGA-SA-ODA NPs. The increase in the coating concentration leads to bigger NPs size owing to increased viscosity of the coating polymer solution which hampered the formation of the nanoformulation. It was observed that 0.2% GC coating concentration was the optimum to obtain NPs with an appropriate size and zeta potential. The developed single ligand and dual ligand-RV+C-6 loaded PLGA-SA-ODA NPs were in size of 168.4 ± 10.4 nm and 236.0 ± 9.8 nm respectively with more than 3.5 % of RV drug loading. The positive surface charge on the NPs and presence of thiol group confirmed the deposition of the TGC as a polymer coat, on the surface of the PLGA-SA-ODA NPs. The *in-vitro* release study of both dual ligand and single ligand NPs showed an initial burst drug release (15%) due to the presence of loosely bound RV on the NPs surface. NPs showed up to 54% release in 24 h. The model fitting indicated that

Higuchi Model was the best fit model for the all three types of the nanoparticulate formulation with a correlation coefficient > 0.97.

In the final part of this project, the developed PLGA NPs were evaluated for RV pharmacokinetic profile delivered by single and dual ligand NPs and their effectiveness in brain targeting via IN pathway. The pharmacokinetic profile and brain targeting efficiency of single ligand and dual ligand NPs were compared to the control drug solution administered by IN and IV route. The plasma stability study suggested that RV was stable in plasma both at 37°C for 24 h and -80°C for 28 days. In addition, C-6 was also stable in plasma for 28 days while stored in a black box at -80°C. Both RV and C-6 stability study results prove that our plasma and brain tissue samples were stable during the extraction of the drug, handling, and storage of samples.

The plasma profile of RV from NPs showed a higher drug concentration in the systemic circulation for 8 h in a formulation dependent manner. Dual ligand RV+C6 loaded PLGA-SA-ODA NPs coated with TGC exhibited a significantly higher plasma level along with a more sustained concentration pattern of the RV than that of single ligand RV+C6 loaded PLGA-SA-ODA NPs. Both single and dual ligand NPs showed a slower clearance of drug compared to drug solution given by either IN or IV route. These result indicated that both single and dual ligands NPs were able to attain higher drug concentration in the systemic circulation for an extended period of time. This extended plasma concentration can also help in achieving better brain drug targeting across the BBB.

The brain distribution study performed at 2 h and 8 h indicated that the RV brain drug concentration was higher in all formulations at 2 h as compared to 8 h. Both dual ligand and single ligand NPs are retained in the brain longer than that of control RV drug solutions. The dual ligand and single ligand PLGA NPs provided 3.3 and 2.2 times higher RV concentration in the brain at 2 h than that of IN RV drug solution. This increase RV drug concentration in the brain region was owing to the mucoadhesive nature of the TGC and SA-ODA as targeting ligands. TGC may cause the opening of tight junctions, leading to enhanced transportation of dual ligand RV+C-6 NPs to neuronal brain cells via a nasal pathway. Also, the coated TGC polymer further helps to reduce the mucociliary clearance via forming disulfide bonds with mucus layer. The presence of the SA-ODA, which interacts with the sialic acid receptor cells present in

the brain further allowed the NPs to remain for longer duration in the brain region, resulting in the constant availability of drugs in the brain region. The comparative study suggested that both our single ligand and dual ligand PLGA NPs were able to achieve higher plasma and brain drug levels than that of the existing NPs.

The brain uptake concentration of C-6 was in a similar pattern as seen with RV brain uptake concentration. The dual ligand PLGA NPs enabled higher uptake of the C-6 fluorescent marker compared to single ligand PLGA NPs. Hence, our data provides proof of the superiority of dual ligand NPs over single ligand NPs and free drug solution for delivery of RV into the brain.

In summary, IN route provides great promise for the effective delivery of the drugs via nose to the brain, however, the bioavailability of drugs administered through nasal route is restricted due to rapid enzymatic degradation and nasal mucociliary clearance. The incorporation of the drugs into nanoparticulate carriers is a promising strategy to protect drugs from nasal enzymatic degradation and facilitate the transport of the drug from nose to brain.

6.2 Conclusion

RV+C-6 loaded PLGA-SA-ODA NPs were formulated by using double emulsion solvent evaporation techniques. The size of the developed PLGA NPs was under 250 nm for both dual ligand and single ligand NPs. Preliminary studies were conducted to evaluate the impact of each factor on the quality of the developed NPs. After optimization, RV+ C-6 loaded NPs with dual-functionalized ligands were formulated with an appropriate size and improved EE using TPGS as an emulsifier. The *in-vivo* pharmacokinetics and biodistribution study indicated the sustained release of the RV from the developed formulation with the brain targeting efficiency. The increase in the drug targeting efficiency of the developed formulation is due to the presence of the targeting ligands. The functionalised TGC and SA-ODA were capable of targeting the nasal mucosal membrane and brain neuron cells respectively will enhance and prolong drug concentration in the brain. The route of administration, IN or IV can have an influence on the level of drug targeting into the brain by the same formulation. IN drug delivery is more effective in this regard.

In summary, as shown by the present study that delivery of RV into the brain can be enhanced by the dual ligand NPs, this may be effective in the treatment of Alzheimer's disease. These formulations still require further development and clinical studies to prove their efficacy in humans. The developed nanoparticulate formulations have the potential to be used as a nanoparticle platform technology to deliver drugs into the brain and its adaptation to deliver a range of clinically relevant drug molecules.

6.3 Future work

Although a significant amount of the work has been done in this project to formulate single ligand and dual ligand functionalized PLGA NPs and evaluated the brain targeting efficacy of the developed formulations, there is scope for further research work to address the following issues.

1. The PLGA NPs were successfully formulated with dual functionalised targeting ligands, however, the method of determination of the level of SA in the single and dual ligand PLGA NPs needs to be developed to fully understand the effect of SA on the performance of NPs *in vitro* and *in vivo.*

2. The developed dual ligand decorated PLGA NPs indicated the stability for a limited time therefore, further techniques such as lyophilization with cryoprotectant should be employed for increasing storage stability and reconstituted later. However, various parameters such as size, zeta potential, encapsulation efficiency and experimental drug loading need to be evaluated prior to execute *in-vivo* studies.
3. The cell uptake of both single ligand and dual ligand PLGA NPs by neuronal cells needs to be studied. *In-vitro* cell experiments may be considered to evaluate the effectiveness of SA-ODA ligand and its impact on the RV and NPs cellular uptake. The cytotoxicity effects of the two ligands towards neuronal cells should be studied too.

4. The present *in-vivo* study conducted on Sprague-Dawley rats has revealed the optimum brain targeting efficacy of the developed nano-formulations along with the importance of the IN route. In the future, more *in-vivo* experiments on RV uptake by the brain should be investigated with time points between 2-8 hrs and 10- 24hrs In addition, RV biodistribution study in other organs such as lungs, liver, heart and intestine should be carried out too to obtain about drug distribution in other organs.

5. There is scope to further compare the brain uptake study of the developed NPs administered via different routes such as IV route.

7. References

Acharya, S. R., & Reddy, P. R. V. (2016). Brain targeted delivery of paclitaxel using endogenous ligand. *Asian Journal of Pharmaceutical Sciences, 11*(3), 427-438.

Al-Ghananeem, A. M., Saeed, H., Florence, R., Yokel, R. A., & Malkawi, A. H. (2010). Intranasal drug delivery of didanosine-loaded chitosan nanoparticles for brain targeting; an attractive route against infections caused by AIDS viruses. *Journal of Drug Targeting, 18*(5), 381-388.

Alistair, B., & Steve, I. (2009). Alzheimer's disease. *The BMJ, 338*.

Alzheimer's-Association. (2016). Overview of Alzheimer's Disease Facts and Figures *Alzheimer's & Dementia, 12*(4).

Alzheimer's-Australia. (2017). *Alzheimer's Disease Key facts and statistics 2017*. Retrieved from

Amini, H., & Ahmadiani, A. (2010). High-Performance Liquid Chromatographic Determination of Rivastigmine in Human Plasma for Application in Pharmacokinetic Studies. *Iranian Journal of Pharmaceutical Research, 9*(2), 115-121.

Anitha, A., Deepa, N., Chennazhi, K. P., Nair, S. V., Tamura, H., & Jayakumar, R. (2011). Development of mucoadhesive thiolated chitosan nanoparticles for biomedical applications. *Carbohydrate Polymers, 83*(1), 66-73.

Arumugam, K., Chamallamudi, M. R., Mallayasamy, S. R., Mullangi, R., Ganesan, S., Jamadar, L., . . . Udupa, N. (2011). High Performance Liquid Chromatographic Fluorescence Detection Method for the Quantification of Rivastigmine in Rat Plasma and Brain: Application to Preclinical Pharmacokinetic Studies in Rats. *Journal of Young Pharmacists : JYP, 3*(4), 315-321.

Bae, D. G., Gho, Y. S., Yoon, W. H., & Chae, C. B. (2000). Arginine-rich anti-vascular endothelial growth factor peptides inhibit tumor growth and metastasis by blocking angiogenesis. *The Journal of Biological Chemistry, 275*(18), 13588-13596.

Bari, N. K., Fazil, M., Hassan, M. Q., Haider, M. R., Gaba, B., Narang, J. K., . . . Ali, J. (2015). Brain delivery of buspirone hydrochloride chitosan nanoparticles for the treatment of general anxiety disorder. *International Journal of Biological Macromolecules, 81*, 49-59.

Barrera, C., Herrera, A., Zayas, Y., & Rinaldi, C. (2009). Surface modification of magnetite nanoparticles for biomedical applications. *Journal of Magnetism and Magnetic Materials, 321*(10), 1397-1399.

Barua, S., & Mitragotri, S. (2014). Challenges associated with Penetration of Nanoparticles across Cell and Tissue Barriers: A Review of Current Status and Future Prospects. *Nano today, 9*(2), 223-243.

Bernkop-Schnürch, A., Hornof, M., & Guggi, D. (2004). Thiolated chitosans. *European Journal of Pharmaceutics and Biopharmaceutics, 57*(1), 9-17.

Bhatt, J., Subbaiah, G., Kambli, S., Shah, B., Nigam, S., Patel, M., . . . Yadav, G. (2007). A rapid and sensitive liquid chromatography-tandem mass spectrometry (LC-MS/MS) method for the estimation of rivastigmine in human plasma. *Journal of Chromatography. B: Analytical Technologies in the Biomedical and Life Sciences, 852*(1-2), 115-121.

Bi, C., Wang, A., Chu, Y., Liu, S., Mu, H., Liu, W., . . . Li, Y. (2016). Intranasal delivery of rotigotine to the brain with lactoferrin-modified PEG-PLGA nanoparticles for Parkinson's disease treatment. *International journal of nanomedicine, 11*, 6547-6559.

Bian, J., Yuan, Z., Chen, X., Gao, Y., Xu, C., & Shi, J. (2016). Preparation of surface multiple-coated polylactide acid drug-loaded nanoparticles for intranasal delivery and evaluation on its brain-targeting efficiency. *Drug Delivery, 23*(1), 269-276.

Birks, J. (2006). Cholinesterase inhibitors for Alzheimer's disease. *Cochrane Database Syst Rev*(1), CD005593.

Blessy, M., Patel, R. D., Prajapati, P. N., & Agrawal, Y. K. (2014). Development of forced degradation and stability indicating studies of drugs-A review. *Journal of Pharmaceutical Analysis, 4*(3), 159-165.

Bodor, N., Prokai, L., Wu, W. M., Farag, H., Jonalagadda, S., Kawamura, M., & Simpkins, J. (1992). A strategy for delivering peptides into the central nervous system by sequential metabolism. *Science, 257*(5077), 1698-1700.

Bondioli, L., Ruozi, B., Belletti, D., Forni, F., Vandelli, M. A., & Tosi, G. (2011). Sialic acid as a potential approach for the protection and targeting of nanocarriers. *Expert Opinion on Drug Delivery, 8*(7), 921-937.

Bondioli., Lucia, Costantino, L., Ballestrazzi, A., Lucchesi, D., Boraschi, D., . . . Vandelli, M. A. (2010). PLGA nanoparticles surface decorated with the sialic acid, N-acetylneuraminic acid. *Biomaterials, 31*(12), 3395-3403.

Born, J., Lange, T., Kern, W., McGregor, G. P., Bickel, U., & Fehm, H. L. (2002). Sniffing neuropeptides: a transnasal approach to the human brain. *Nature Neuroscience, 5*(6), 514-516.

Boulton, M., Flessner, M., Armstrong, D., Mohamed, R., Hay, J., & Johnston, M. (1999). Contribution of extracranial lymphatics and arachnoid villi to the clearance of a CSF tracer in the rat. *American Journal of Physiology, 276*(3 Pt 2), R818-823.

Boulton, M., Young, A., Hay, J., Armstrong, D., Flessner, M., Schwartz, M., & Johnston, M. (1996). Drainage of CSF through lymphatic pathways and arachnoid villi in sheep: measurement of 125I-albumin clearance. *Neuropathology and Applied Neurobiology, 22*(4), 325-333.

Brambilla, D., Le Droumaguet, B., Nicolas, J., Hashemi, S. H., Wu, L.-P., Moghimi, S. M., . . . Andrieux, K. (2011). Nanotechnologies for Alzheimer's disease: diagnosis, therapy, and safety issues. *Nanomedicine: Nanotechnology, Biology and Medicine, 7*(5), 521-540.

Bravo-Osuna, I., Teutonico, D., Arpicco, S., Vauthier, C., & Ponchel, G. (2007). Characterization of chitosan thiolation and application to thiol quantification onto nanoparticle surface. *International Journal of Pharmaceutics, 340*(1–2), 173-181.

Brooks, H., Lebleu, B., & Vives, E. (2005). Tat peptide-mediated cellular delivery: back to basics. *Advanced Drug Delivery Reviews, 57*(4), 559-577.

Casettari, L., & Illum, L. (2014). Chitosan in nasal delivery systems for therapeutic drugs. *Journal of Controlled Release, 190*, 189-200.

Chaturvedi, M., Kumar, M., & Pathak, K. (2011). A review on mucoadhesive polymer used in nasal drug delivery system. *Journal of Advanced Pharmaceutical Technology & Research, 2*(4), 215-222.

Cheng, K. K., Yeung, C. F., Ho, S. W., Chow, S. F., Chow, A. H., & Baum, L. (2013). Highly stabilized curcumin nanoparticles tested in an in vitro blood-brain barrier model and in Alzheimer's disease Tg2576 mice. *AAPS J, 15*(2), 324-336.

Cho, Y.-W., Cho, Y.-N., Chung, S.-H., Yoo, G., & Ko, S.-W. (1999). Water-soluble chitin as a wound healing accelerator. *Biomaterials, 20*(22), 2139-2145.

Cohen-Sela, E., Teitlboim, S., Chorny, M., Koroukhov, N., Danenberg, H. D., Gao, J., & Golomb, G. (2009). Single and double emulsion manufacturing techniques of an amphiphilic drug in PLGA nanoparticles: formulations of mithramycin and bioactivity. *Journal of Pharmaceutical Sciences, 98*(4), 1452-1462.

Cooper, D. L., & Harirforoosh, S. (2014). Effect of Formulation Variables on Preparation of Celecoxib Loaded Polylactide-Co-Glycolide Nanoparticles. *PloS One, 9*(12), e113558.

Cui, Y., Zhang, M., Zeng, F., Jin, H., Xu, Q., & Huang, Y. (2016). Dual-Targeting Magnetic PLGA Nanoparticles for Codelivery of Paclitaxel and Curcumin for Brain Tumor Therapy. *ACS Applied Materials & Interfaces, 8*(47), 32159-32169.

De, S., & Robinson, D. H. (2004). Particle size and temperature effect on the physical stability of PLGA nanospheres and microspheres containing Bodipy. *AAPS PharmSciTech, 5*(4), e53.

Dhuria, S. V., Hanson, L. R., & Frey, W. H., 2nd. (2010). Intranasal delivery to the central nervous system: mechanisms and experimental considerations. *Journal of Pharmaceutical Sciences, 99*(4), 1654-1673.

Doggui, S., Dao, L., & Ramassamy, C. (2012). Potential of drug-loaded nanoparticles for Alzheimer's disease: diagnosis, prevention and treatment. *Therapeutic Delivery, 3*(9), 1025-1027.

Dyawanapelly, S., Koli, U., Dharamdasani, V., Jain, R., & Dandekar, P. (2016). Improved mucoadhesion and cell uptake of chitosan and chitosan oligosaccharide surface-modified polymer nanoparticles for mucosal delivery of proteins. *Drug delivery and translational research, 6*(4), 365-379.

Dyer, A. M., Hinchcliffe, M., Watts, P., Castile, J., Jabbal-Gill, I., Nankervis, R., . . . Illum, L. (2002). Nasal delivery of insulin using novel chitosan based formulations: a comparative study in two animal models between simple chitosan formulations and chitosan nanoparticles. *Pharmaceutical Research, 19*(7), 998-1008.

Dysken, M. W, Guarino, P. D., Vertrees, J. E., Asthana, S., Sano, M., . . . Vatassery, G. (2014). Vitamin E and memantine in Alzheimer's disease: clinical trial methods and baseline data. *Alzheimers & Dementia: the journal of the Alzheimer's association, 10*(1), 36-44.

Emoto, K., Harris, J. M., & Van Alstine, J. M. (1996). Grafting Poly(ethylene glycol) Epoxide to Amino-Derivatized Quartz: Effect of Temperature and pH on Grafting Density. *Analytical Chemistry, 68*(21), 3751-3757.

Enz, A., Chappuis, A., & Dattler, A. (2004). A simple, rapid and sensitive method for simultaneous determination of rivastigmine and its major metabolite NAP 226-90 in rat brain and plasma by reversed-phase liquid chromatography coupled to electrospray ionization mass spectrometry. *Biomedical Chromatography, 18*(3), 160-166.

Farina, N., Isaac, M. G., Clark, A. R., Rusted, J., & Tabet, N. (2012). Vitamin E for Alzheimer's dementia and mild cognitive impairment. *Cochrane Database Syst Rev, 11*, Cd002854.

Fazil, M., Md, S., Haque, S., Kumar, M., Baboota, S., Sahni, J. k., & Ali, J. (2012). Development and evaluation of rivastigmine loaded chitosan nanoparticles for brain targeting. *European Journal of Pharmaceutical Sciences, 47*(1), 6-15.

Feng, S.-S., & Chien, S. (2003). Chemotherapeutic engineering: Application and further development of chemical engineering principles for chemotherapy of cancer and other diseases. *Chemical Engineering Science, 58*(18), 4087-4114.

Feng, S. S., Zeng, W., Teng Lim, Y., Zhao, L., Yin Win, K., Oakley, R., . . . Pan, S. (2007). Vitamin E TPGS-emulsified poly(lactic-co-glycolic acid) nanoparticles for cardiovascular restenosis treatment. *Nanomedicine (Lond), 2*(3), 333-344.

Fernandes, C., Soni, U., & Patravale, V. (2010). Nano-interventions for neurodegenerative disorders. *Pharmacological Research, 62*(2), 166-178.

Folch, J., Petrov, D., Ettcheto, M., Abad, S., #xe1, nchez-L, . . . Camins, A. (2016). Current Research Therapeutic Strategies for Alzheimer's Disease Treatment. *Neural Plasticity, 2016*, 15.

Fonseca-Santos, B., Gremião, M. P. D., & Chorilli, M. (2015). Nanotechnology-based drug delivery systems for the treatment of Alzheimer's disease. *International journal of nanomedicine, 10*, 4981-5003.

Frankfort, S. V., Ouwehand, M., van Maanen, M. J., Rosing, H., Tulner, L. R., & Beijnen, J. H. (2006). A simple and sensitive assay for the quantitative analysis of rivastigmine and its metabolite NAP 226-90 in human EDTA plasma using coupled liquid chromatography and tandem mass spectrometry. *Rapid Communications in Mass Spectrometry, 20*(22), 3330-3336.

Gao, X., Chen, J., Tao, W., Zhu, J., Zhang, Q., Chen, H., & Jiang, X. (2007). UEA I-bearing nanoparticles for brain delivery following intranasal administration. *International Journal of Pharmaceutics, 340*(1–2), 207-215.

Gao, X., Tao, W., Lu, W., Zhang, Q., Zhang, Y., Jiang, X., & Fu, S. (2006). Lectin-conjugated PEG–PLA nanoparticles: Preparation and brain delivery after intranasal administration. *Biomaterials, 27*(18), 3482-3490.

Gao, X., Wu, B., Zhang, Q., Chen, J., Zhu, J., Zhang, W., . . . Jiang, X. (2007). Brain delivery of vasoactive intestinal peptide enhanced with the nanoparticles conjugated with wheat germ agglutinin following intranasal administration. *Journal of Controlled Release, 121*(3), 156-167.

Gill, S. S., Anderson, G. M., Fischer, H. D., Bell, C. M., Li, P., Normand, S. L., & Rochon, P. A. (2009). Syncope and its consequences in patients with dementia receiving cholinesterase inhibitors: a population-based cohort study. *Archives of Internal Medicine, 169*(9), 867-873.

Gilman, S., Koller, M., Black, R. S., Jenkins, L., Griffith, S. G., Fox, N. C., . . . Orgogozo, J. M. (2005). Clinical effects of Abeta immunization (AN1792) in patients with AD in an interrupted trial. *Neurology, 64*(9), 1553-1562.

Gottwald, M. D., & Rozanski, R. I. (1999). Rivastigmine, a brain-region selective acetylcholinesterase inhibitor for treating Alzheimer's disease: review and current status. *Expert opinion on investigational drugs, 8*(10), 1673-1682.

Govender, T., Stolnik, S., Garnett, M. C., Illum, L., & Davis, S. S. (1999). PLGA nanoparticles prepared by nanoprecipitation: drug loading and release studies of a water soluble drug. *Journal of Controlled Release, 57*(2), 171-185.

Grabarek, Z., & Gergely, J. (1990). Zero-length crosslinking procedure with the use of active esters. *Analytical Biochemistry, 185*(1), 131-135.

Gradauer, K., Barthelmes, J., Vonach, C., Almer, G., Mangge, H., Teubl, B., . . . Prassl, R. (2013). Liposomes coated with thiolated chitosan enhance oral peptide delivery to rats. *Journal of Controlled Release, 172*(3), 872-878.

Grundman, M. (2000). Vitamin E and Alzheimer disease: the basis for additional clinical trials. *American Journal of Clinical Nutrition, 71*(2), 630s-636s.

Hadavi, D., & Poot, A. A. (2016). Biomaterials for the Treatment of Alzheimer's Disease. *Frontiers in Bioengineering and Biotechnology, 4*, 49.

Hanson, L. R., & Frey, W. H. (2008). Intranasal delivery bypasses the blood-brain barrier to target therapeutic agents to the central nervous system and treat neurodegenerative disease. *BMC Neuroscience, 9*(3), 1-4.

Haque, S., Md, S., Fazil, M., Kumar, M., Sahni, J. K., Ali, J., & Baboota, S. (2012). Venlafaxine loaded chitosan NPs for brain targeting: Pharmacokinetic and pharmacodynamic evaluation. *Carbohydrate Polymers, 89*(1), 72-79.

Heimann, U., & Vögtle, F. (1980). Hydrophile Fette. *Liebigs Annalen der Chemie, 1980*(6), 858-862.

Hock, C., Konietzko, U., Papassotiropoulos, A., Wollmer, A., Streffer, J., von Rotz, R. C., . . . Nitsch, R. M. (2002). Generation of antibodies specific for beta-amyloid by vaccination of patients with Alzheimer disease. *Nature Medicine, 8*(11), 1270-1275.

Hock, C., Konietzko, U., Streffer, J. R., Tracy, J., Signorell, A., Muller-Tillmanns, B., . . . Nitsch, R. M. (2003). Antibodies against beta-amyloid slow cognitive decline in Alzheimer's disease. *Neuron, 38*(4), 547-554.

Hong, S., Lee, D., Zhang, H., Zhang, J. Q., Resvick, J. N., Khademhosseini, A., . . . Karp, J. M. (2007). Covalent immobilization of p-selectin enhances cell rolling. *Langmuir, 23*(24), 12261-12268.

Hornof, M. D., Kast, C. E., & Bernkop-Schnurch, A. (2003). In vitro evaluation of the viscoelastic properties of chitosan-thioglycolic acid conjugates. *European Journal of Pharmaceutics and Biopharmaceutics, 55*(2), 185-190.

Huile, G., Shuaiqi, P., Zhi, Y., Shijie, C., Chen, C., Xinguo, J., . . . Yu, H. (2011). A cascade targeting strategy for brain neuroglial cells employing nanoparticles modified with angiopep-2 peptide and EGFP-EGF1 protein. *Biomaterials, 32*(33), 8669-8675.

Human Metabolome Database NIH. (2012). Rivastigmine. (HMDB15124). Retrieved 2017-05-02, from Wishart Research Group, University of Alberta National Centre for biotechnology information

Illum, L. (2000). Transport of drugs from the nasal cavity to the central nervous system. *European Journal of Pharmaceutical Sciences, 11*(1), 1-18.

Illum, L. (2003). Nasal drug delivery—possibilities, problems and solutions. *Journal of Controlled Release, 87*(1–3), 187-198.

Jann, M. W. (2000). Rivastigmine, a new-generation cholinesterase inhibitor for the treatment of Alzheimer's disease. *Pharmacotherapy, 20*(1), 1-12.

Jayakumar, R., Chennazhi, K. P., Muzzarelli, R. A. A., Tamura, H., Nair, S. V., & Selvamurugan, N. (2010). Chitosan conjugated DNA nanoparticles in gene therapy. *Carbohydrate Polymers, 79*(1), 1-8.

Johnson, N. J., Hanson, L. R., & Frey, W. H. (2010). Trigeminal pathways deliver a low molecular weight drug from the nose to the brain and orofacial structures. *Molecular Pharmaceutics, 7*(3), 884-893.

Johnston, M., Zakharov, A., Papaiconomou, C., Salmasi, G., & Armstrong, D. (2004). Evidence of connections between cerebrospinal fluid and nasal lymphatic vessels in humans, non-human primates and other mammalian species. *Cerebrospinal Fluid Research, 1*, 2-2.

Joshi, S. A., Chavhan, S. S., & Sawant, K. K. (2010). Rivastigmine-loaded PLGA and PBCA nanoparticles: preparation, optimization, characterization, in vitro and pharmacodynamic studies. *European Journal of Pharmaceutics and Biopharmaceutics, 76*(2), 189-199.

Kabanov, A. V., & Gendelman, H. E. (2007). Nanomedicine in the diagnosis and therapy of neurodegenerative disorders. *Progress in Polymer Science, 32*(8–9), 1054-1082.

Kale, M. N. (2014). Development of validated RP-HPLC method for quantitative estimation of rivastigmine hydrogen tartarate in transdermal drug delivery system *International Journal of Pharmaceutical sciences and research, 5 (5)*, 1892-1902.

Kaliner, M., Shelhamer, J. H., Borson, B., Nadel, J., Patow, C., & Marom, Z. (1986). Human respiratory mucus. *American Review of Respiratory Disease, 134*(3), 612-621.

Karthik, A., Subramanian, G. S., Surulivelrajan, M., Ranjithkumar, A., & Kamat, S. B. (2008). Fluorimetric determination of rivastigmine in rat plasma by a reverse phase--high performance liquid chromatographic method. Application to a pharmacokinetic study. *Arzneimittel-Forschung, 58*(5), 205-210.

Kast, C. E., & Bernkop-Schnürch, A. (2001). Thiolated polymers-thiomers: development and in vitro evaluation of chitosan–thioglycolic acid conjugates. *Biomaterials, 22*(17), 2345-2352.

Katare, Y. K., Daya, R. P., Sookram Gray, C., Luckham, R. E., Bhandari, J., Chauhan, A. S., & Mishra, R. K. (2015). Brain Targeting of a Water Insoluble Antipsychotic Drug Haloperidol via the Intranasal Route Using PAMAM Dendrimer. *Molecular Pharmaceutics, 12*(9), 3380-3388.

Khawli, L. A., & Prabhu, S. (2013). Drug Delivery across the Blood–Brain Barrier. *Molecular Pharmaceutics, 10*(5), 1471-1472.

Kida, S., Pantazis, A., & Weller, R. O. (1993). CSF drains directly from the subarachnoid space into nasal lymphatics in the rat. Anatomy, histology and immunological significance. *Neuropathology and Applied Neurobiology, 19*(6), 480-488.

Kobayashi, H., Ohnishi, T., Nakagawa, R., & Yoshizawa, K. (2016). The comparative efficacy and safety of cholinesterase inhibitors in patients with mild-to-moderate Alzheimer's disease: a Bayesian network meta-analysis. *International Journal of Geriatric Psychiatry, 31*(8), 892-904.

Kotze, A. F., Thanou, M. M., Luessen, H. L., de Boer, B. G., Verhoef, J. C., & Junginger, H. E. (1999). Effect of the degree of quaternization of N-trimethyl chitosan chloride on the permeability of intestinal epithelial cells (Caco-2). *European Journal of Pharmaceutics and Biopharmaceutics, 47*(3), 269-274.

Kubota, N., Tatsumoto, N., Sano, T., & Toya, K. (2000). A simple preparation of half N-acetylated chitosan highly soluble in water and aqueous organic solvents. *Carbohydrate Research, 324*(4), 268-274.

Kulkarni, S. A., & Feng, S. S. (2011). Effects of surface modification on delivery efficiency of biodegradable nanoparticles across the blood-brain barrier. *Nanomedicine (Lond), 6*(2), 377-394.

Kumar, M., Misra, A., Mishra, A. K., Mishra, P., & Pathak, K. (2008). Mucoadhesive nanoemulsion-based intranasal drug delivery system of olanzapine for brain targeting. *Journal of Drug Targeting, 16*(10), 806-814.

La Porte, S. L., Bollini, S. S., Lanz, T. A., Abdiche, Y. N., Rusnak, A. S., Ho, W.-H., . . . Pons, J. (2012). Structural Basis of C-terminal β-Amyloid Peptide Binding by the Antibody Ponezumab for the Treatment of Alzheimer's Disease. *Journal of Molecular Biology, 421*(4–5), 525-536.

Li, W., Zhou, Y., Zhao, N., Hao, B., Wang, X., & Kong, P. (2012). Pharmacokinetic behavior and efficiency of acetylcholinesterase inhibition in rat brain after

intranasal administration of galanthamine hydrobromide loaded flexible liposomes. *Environmental Toxicology and Pharmacology, 34*(2), 272-279.
Lochhead, J. J., & Thorne, R. G. (2012). Intranasal delivery of biologics to the central nervous system. *Advanced Drug Delivery Reviews, 64*(7), 614-628.
Lu, C. T., Zhao, Y. Z., Wong, H. L., Cai, J., Peng, L., & Tian, X. Q. (2014). Current approaches to enhance CNS delivery of drugs across the brain barriers. *International journal of nanomedicine, 9*, 2241-2257.
Makhlof, A., Werle, M., Tozuka, Y., & Takeuchi, H. (2010). Nanoparticles of glycol chitosan and its thiolated derivative significantly improved the pulmonary delivery of calcitonin. *International Journal of Pharmaceutics, 397*(1-2), 92-95.
Malhotra, M., Tomaro-Duchesneau, C., & Prakash, S. (2013). Synthesis of TAT peptide-tagged PEGylated chitosan nanoparticles for siRNA delivery targeting neurodegenerative diseases. *Biomaterials, 34*(4), 1270-1280.
McCall, R. L., & Sirianni, R. W. (2013). PLGA nanoparticles formed by single- or double-emulsion with vitamin E-TPGS. *J Vis Exp*(82), 51015.
Md, S., Khan, R. A., Mustafa, G., Chuttani, K., Baboota, S., Sahni, J. K., & Ali, J. (2012). Bromocriptine loaded chitosan nanoparticles intended for direct nose to brain delivery: Pharmacodynamic, Pharmacokinetic and Scintigraphy study in mice model. *European Journal of Pharmaceutical Sciences, 48*(3), 393-405.
Mehta, M., Adem, A., & Sabbagh, M. (2012). New Acetylcholinesterase Inhibitors for Alzheime's Disease. *International Journal of Alzheimer's Disease, 2012*, 8.
Menon, J. U., Kona, S., Wadajkar, A. S., Desai, F., Vadla, A., & Nguyen, K. T. (2012). Effects of surfactants on the properties of PLGA nanoparticles. *J Biomed Mater Res A, 100*(8), 1998-2005.
Mistry, A., Stolnik, S., & Illum, L. (2009). Nanoparticles for direct nose-to-brain delivery of drugs. *International Journal of Pharmaceutics, 379*(1), 146-157.
Mittal, D., Md, S., Hasan, Q., Fazil, M., Ali, A., . . . Ali, J. (2016). Brain targeted nanoparticulate drug delivery system of rasagiline via intranasal route. *Drug Delivery, 23*(1), 130-139.
Mittal, G., Carswell, H., Brett, R., Currie, S., & Kumar, M. N. V. R. (2011). Development and evaluation of polymer nanoparticles for oral delivery of estradiol to rat brain in a model of Alzheimer's pathology. *Journal of Controlled Release, 150*(2), 220-228.
Mittal, G., Sahana, D. K., Bhardwaj, V., & Ravi Kumar, M. N. (2007). Estradiol loaded PLGA nanoparticles for oral administration: effect of polymer molecular weight and copolymer composition on release behavior in vitro and in vivo. *Journal of Controlled Release, 119*(1), 77-85.
Modi, G., Pillay, V., Choonara, Y. E., Ndesendo, V. M. K., du Toit, L. C., & Naidoo, D. (2009). Nanotechnological applications for the treatment of neurodegenerative disorders. *Progress in Neurobiology, 88*(4), 272-285.
Mourya, V. K., & Inamdar, N. N. (2008). Chitosan-modifications and applications: Opportunities galore. *Reactive and Functional Polymers, 68*(6), 1013-1051.
Mu, L., & Feng, S. S. (2003a). A novel controlled release formulation for the anticancer drug paclitaxel (Taxol): PLGA nanoparticles containing vitamin E TPGS. *Journal of Controlled Release, 86*(1), 33-48.
Mu, L., & Feng, S. S. (2003b). PLGA/TPGS nanoparticles for controlled release of paclitaxel: effects of the emulsifier and drug loading ratio. *Pharmaceutical Research, 20*(11), 1864-1872.

Murakami, H., Kobayashi, M., Takeuchi, H., & Kawashima, Y. (1999). Preparation of poly(DL-lactide-co-glycolide) nanoparticles by modified spontaneous emulsification solvent diffusion method. *International Journal of Pharmaceutics, 187*(2), 143-152.

Murrey, H. E., & Hsieh-Wilson, L. C. (2008). The Chemical Neurobiology of Carbohydrates. *Chemical Reviews, 108*(5), 1708-1731.

Nafee, N., Taetz, S., Schneider, M., Schaefer, U. F., & Lehr, C.-M. (2007). Chitosan-coated PLGA nanoparticles for DNA/RNA delivery: effect of the formulation parameters on complexation and transfection of antisense oligonucleotides. *Nanomedicine: Nanotechnology, Biology and Medicine, 3*(3), 173-183.

Nagpal, K., Singh, S. K., & Mishra, D. N. (2013). Optimization of brain targeted chitosan nanoparticles of Rivastigmine for improved efficacy and safety. *International Journal of Biological Macromolecules, 59*(0), 72-83.

Nazem, A., & Mansoori, G. A. (2008). Nanotechnology solutions for Alzheimer's disease: advances in research tools, diagnostic methods and therapeutic agents. *Journal of Alzheimer's Disease, 13*(2), 199-223.

Nazem, A., & Mansoori, G. A. (2011). Nanotechnology for Alzheimer's disease detection and treatment. *Insciences Journal, 1*(4), 169-193.

Nicoll, J. A., Wilkinson, D., Holmes, C., Steart, P., Markham, H., & Weller, R. O. (2003). Neuropathology of human Alzheimer disease after immunization with amyloid-beta peptide: a case report. *Nature Medicine, 9*(4), 448-452.

Niwa, T., Takeuchi, H., Hino, T., Kunou, N., & Kawashima, Y. (1994). In vitro drug release behavior of D,L-lactide/glycolide copolymer (PLGA) nanospheres with nafarelin acetate prepared by a novel spontaneous emulsification solvent diffusion method. *Journal of Pharmaceutical Sciences, 83*(5), 727-732.

Nobs, L., Buchegger, F., Gurny, R., & Allémann, E. (2004). Poly(lactic acid) nanoparticles labeled with biologically active Neutravidin™ for active targeting. *European Journal of Pharmaceutics and Biopharmaceutics, 58*(3), 483-490.

Noetzli, M., Ansermot, N., Dobrinas, M., & Eap, C. B. (2012). Simultaneous determination of antidementia drugs in human plasma: Procedure transfer from HPLC–MS to UPLC–MS/MS. *Journal of Pharmaceutical and Biomedical Analysis, 64–65*, 16-25.

Pardeshi, C. V., & Belgamwar, V. S. (2013). Direct nose to brain drug delivery via integrated nerve pathways bypassing the blood–brain barrier: an excellent platform for brain targeting. *Expert Opinion on Drug Delivery, 10*(7), 957-972.

Pardridge, W. M. (2007). Blood-brain barrier delivery. *Drug Discovery Today, 12*(1-2), 54-61.

Parekh, J. M., Sanyal, M., Yadav, M., & Shrivastav, P. S. (2014). Systematic evaluation of plasma phospholipids for reliable and precise determination of dronedarone and desbutyldronedarone by LC–MS/MS. *Bioanalysis, 6*(19), 2635-2650.

Parveen, S., & Sahoo, S. K. (2011). Long circulating chitosan/PEG blended PLGA nanoparticle for tumor drug delivery. *European Journal of Pharmacology, 670*(2–3), 372-383.

Patel, H. K., Gajbhiye, V., Kesharwani, P., & Jain, N. K. (2016). Ligand anchored poly(propyleneimine) dendrimers for brain targeting: Comparative in vitro and in vivo assessment. *Journal of Colloid and Interface Science, 482*, 142-150.

Patil, G. B., & Surana, S. J. (2013). Fabrication and statistical optimization of surface engineered PLGA nanoparticles for naso-brain delivery of ropinirole

hydrochloride: in-vitro-ex-vivo studies. *Journal of Biomaterials Science, Polymer Edition, 24*(15), 1740-1756.

Pawar, D., & Jaganathan, K. S. (2016). Mucoadhesive glycol chitosan nanoparticles for intranasal delivery of hepatitis B vaccine: enhancement of mucosal and systemic immune response. *Drug Delivery, 23*(1), 185-194.

Pawar, D., Mangal, S., Goswami, R., & Jaganathan, K. S. (2013). Development and characterization of surface modified PLGA nanoparticles for nasal vaccine delivery: Effect of mucoadhesive coating on antigen uptake and immune adjuvant activity. *European Journal of Pharmaceutics and Biopharmaceutics, 85*(3, Part A), 550-559.

Pelaz, B., del Pino, P., Maffre, P., Hartmann, R., Gallego, M., Rivera-Fernandez, S., . . . Parak, W. J. (2015). Surface Functionalization of Nanoparticles with Polyethylene Glycol: Effects on Protein Adsorption and Cellular Uptake. *ACS Nano, 9*(7), 6996-7008.

Peltonen, L., Aitta, J., Hyvonen, S., Karjalainen, M., & Hirvonen, J. (2004). Improved entrapment efficiency of hydrophilic drug substance during nanoprecipitation of poly(l)lactide nanoparticles. *AAPS PharmSciTech, 5*(1), E16.

Pires, A., Fortuna, A., Alves, G., & Falcao, A. (2009). Intranasal drug delivery: how, why and what for? *Journal of Pharmacy & Pharmaceutical Sciences, 12*(3), 288-311.

Polinsky, R. J. (1998). Clinical pharmacology of rivastigmine: a new-generation acetylcholinesterase inhibitor for the treatment of Alzheimer's disease. *Clinical Therapeutics, 20*(4), 634-647.

Pommier, F., & Frigola, R. (2003). Quantitative determination of rivastigmine and its major metabolite in human plasma by liquid chromatography with atmospheric pressure chemical ionization tandem mass spectrometry. *Journal of Chromatography. B: Analytical Technologies in the Biomedical and Life Sciences, 784*(2), 301-313.

Quintana, D. S., Guastella, A. J., Westlye, L. T., & Andreassen, O. A. (2016). The promise and pitfalls of intranasally administering psychopharmacological agents for the treatment of psychiatric disorders. *Molecular Psychiatry, 21*(1), 29-38.

Quintana., D., S., Alvares, G. A., Hickie, I. B., & Guastella, A. J. (2015). Do delivery routes of intranasally administered oxytocin account for observed effects on social cognition and behavior? A two-level model. *Neuroscience and Biobehavioral Reviews, 49*, 182-192.

Rao, M, B., Srinivasu, M. K., Kumar, K. P., Bhradwaj, N., Ravi, R., . . . Kumar, P. R. (2005). A stability indicating LC method for rivastigmine hydrogen tartrate. *Journal of Pharmaceutical and Biomedical Analysis, 37*(1), 57-63.

Rao, J. P., & Geckeler, K. E. (2011). Polymer nanoparticles: Preparation techniques and size-control parameters. *Progress in Polymer Science, 36*(7), 887-913.

Robert-Egge. (2015). *Researching Alzheimer's Medicines: Setbacks and Stepping Stones, Summer 2015*. Retrieved from USA:

Ross, T. M., Martinez, P. M., Renner, J. C., Thorne, R. G., Hanson, L. R., & Frey Ii, W. H. (2004). Intranasal administration of interferon beta bypasses the blood–brain barrier to target the central nervous system and cervical lymph nodes: a non-invasive treatment strategy for multiple sclerosis. *Journal of Neuroimmunology, 151*(1–2), 66-77.

Sah, H., Thoma, L. A., Desu, H. R., Sah, E., & Wood, G. C. (2013). Concepts and practices used to develop functional PLGA-based nanoparticulate systems. *International journal of nanomedicine, 8*, 747-765.

Sahni, J. K., Doggui, S., Ali, J., Baboota, S., Dao, L., & Ramassamy, C. (2011). Neurotherapeutic applications of nanoparticles in Alzheimer's disease. *Journal of Controlled Release, 152*(2), 208-231.

Saraiva, C., Praça, C., Ferreira, R., Santos, T., Ferreira, L., & Bernardino, L. (2016). Nanoparticle-mediated brain drug delivery: Overcoming blood–brain barrier to treat neurodegenerative diseases. *Journal of Controlled Release, 235*, 34-47.

Seju, U., Kumar, A., & Sawant, K. K. (2011). Development and evaluation of olanzapine-loaded PLGA nanoparticles for nose-to-brain delivery: in vitro and in vivo studies. *Acta Biomater, 7*(12), 4169-4176.

Sforza, C., Grandi, G., De Menezes, M., Tartaglia, G. M., & Ferrario, V. F. (2011). Age- and sex-related changes in the normal human external nose. *Forensic Science International, 204*(1-3), 205 e201-209.

Shah, A. R., & Banerjee, R. (2012). Development and evaluation of anti-oxidant and anti-inflammatory drugs loaded lung surfactants. *Soft Matter, 8*(47), 11911-11922.

Shah, B., Khunt, D., Bhatt, H., Misra, M., & Padh, H. (2015). Application of quality by design approach for intranasal delivery of rivastigmine loaded solid lipid nanoparticles: Effect on formulation and characterization parameters. *European journal of pharmaceutical sciences : official journal of the European Federation for Pharmaceutical Sciences, 78*, 54-66.

Shah, N., Chaudhari, K., Dantuluri, P., Murthy, R. S., & Das, S. (2009). Paclitaxel-loaded PLGA nanoparticles surface modified with transferrin and Pluronic (R) P85, an in vitro cell line and in vivo biodistribution studies on rat model. *Journal of Drug Targeting, 17*(7), 533-542.

Shahnaz, G., Vetter, A., Barthelmes, J., Rahmat, D., Laffleur, F., Iqbal, J., . . . Bernkop-Schnurch, A. (2012). Thiolated chitosan nanoparticles for the nasal administration of leuprolide: bioavailability and pharmacokinetic characterization. *International Journal of Pharmaceutics, 428*(1-2), 164-170.

Sharma, Navneet, Madan, P., & Lin, S. (2016). Effect of process and formulation variables on the preparation of parenteral paclitaxel-loaded biodegradable polymeric nanoparticles: A co-surfactant study. *Asian Journal of Pharmaceutical Sciences, 11*(3), 404-416.

Sharma, D., Sharma, R. K., Sharma, N., Gabrani, R., Sharma, S. K., Ali, J., & Dang, S. (2015). Nose-To-Brain Delivery of PLGA-Diazepam Nanoparticles. *AAPS PharmSciTech*.

She, Z., Zhang, T., Wang, X., Li, X., Song, Y., Cheng, X., . . . Deng, Y. (2014). The anticancer efficacy of pixantrone-loaded liposomes decorated with sialic acid-octadecylamine conjugate. *Biomaterials, 35*(19), 5216-5225.

Simon, A., Amaro, M. I., Healy, A. M., Cabral, L. M., & de Sousa, V. P. (2016). Comparative evaluation of rivastigmine permeation from a transdermal system in the Franz cell using synthetic membranes and pig ear skin with in vivo-in vitro correlation. *International Journal of Pharmaceutics, 512*(1), 234-241.

Singh, D., Rashid, M., Hallan, S. S., Mehra, N. K., Prakash, A., & Mishra, N. (2016). Pharmacological evaluation of nasal delivery of selegiline hydrochloride-loaded thiolated chitosan nanoparticles for the treatment of depression. *Artificial Cells, Nanomedicine, and Biotechnology, 44*(3), 865-877.

Song, C. X., Labhasetwar, V., Murphy, H., Qu, X., Humphrey, W. R., Shebuski, R. J., & Levy, R. J. (1997). Formulation and characterization of biodegradable nanoparticles for intravascular local drug delivery. *Journal of Controlled Release, 43*(2–3), 197-212.

Temussi, F., Passananti, M., Previtera, L., Iesce, M. R., Brigante, M., Mailhot, G., & DellaGreca, M. (2012). Phototransformation of the drug rivastigmine: Photoinduced cleavage of benzyl-nitrogen sigma bond. *Journal of Photochemistry and Photobiology A: Chemistry, 239*, 1-6.

Thomas, S., Shandilya, S., Bharati, A., Paul, S. K., Agarwal, A., & Mathela, C. S. (2012). Identification, characterization and quantification of new impurities by LC–ESI/MS/MS and LC–UV methods in rivastigmine tartrate active pharmaceutical ingredient. *Journal of Pharmaceutical and Biomedical Analysis, 57*, 39-51.

Thorne, R. G., Pronk, G. J., Padmanabhan, V., & Frey Ii, W. H. (2004). Delivery of insulin-like growth factor-I to the rat brain and spinal cord along olfactory and trigeminal pathways following intranasal administration. *Neuroscience, 127*(2), 481-496.

Torchilin, V. P. (2008). Tat peptide-mediated intracellular delivery of pharmaceutical nanocarriers. *Advanced Drug Delivery Reviews, 60*(4-5), 548-558.

Tosi, G., Costantino, L., Rivasi, F., Ruozi, B., Leo, E., Vergoni, A. V., . . . Forni, F. (2007). Targeting the central nervous system: in vivo experiments with peptide-derivatized nanoparticles loaded with Loperamide and Rhodamine-123. *Journal of Controlled Release, 122*(1), 1-9.

Tosi, G., Ruozi, B., Belletti, D., Vilella, A., Zoli, M., Vandelli, M. A., & Forni, F. (2013). Brain-targeted polymeric nanoparticles: in vivo evidence of different routes of administration in rodents. *Nanomedicine (Lond), 8*(9), 1373-1383.

Tosi, G., Vergoni, A. V., Ruozi, B., Bondioli, L., Badiali, L., Rivasi, F., . . . Vandelli, M. A. (2010). Sialic acid and glycopeptides conjugated PLGA nanoparticles for central nervous system targeting: In vivo pharmacological evidence and biodistribution. *Journal of Controlled Release, 145*(1), 49-57.

Trapani, A., Sitterberg, J., Bakowsky, U., & Kissel, T. (2009). The potential of glycol chitosan nanoparticles as carrier for low water soluble drugs. *International Journal of Pharmaceutics, 375*(1–2), 97-106.

Turk, C. T., Oz, U. C., Serim, T. M., & Hascicek, C. (2014). Formulation and optimization of nonionic surfactants emulsified nimesulide-loaded PLGA-based nanoparticles by design of experiments. *AAPS PharmSciTech, 15*(1), 161-176.

Ugwoke, M. I., Exaud, S., Van Den Mooter, G., Verbeke, N., & Kinget, R. (1999). Bioavailability of apomorphine following intranasal administration of mucoadhesive drug delivery systems in rabbits. *European Journal of Pharmaceutical Sciences, 9*(2), 213-219.

US-FDA. (2003). *Memantine HCl* USA: US-FDA.

US-FDA. (2013). Guidance for Industry Bioanalytical Method Validation *U.S. Department of Health and Human Services, Center for Drug Evaluation and Research (CDER)*.

US-National-Library-of-Medicine. (2005). Rivastigmine. from National Center for Biotechnology Information. PubChem Compound Database; CID=77991,(accessed Mar. 16, 2017).

Van Delden, C. J., Bezemer, J. M., Engbers, G. H. M., & Feijen, J. (1997). Poly(ethylene oxide)-modified carboxylated polystyrene latices -

immobilization chemistry and protein adsorption. *Journal of Biomaterials Science, Polymer Edition, 8*(4), 251-268.

Walter, B. A., Valera, V. A., Takahashi, S., Matsuno, K., & Ushiki, T. (2006). Evidence of antibody production in the rat cervical lymph nodes after antigen administration into the cerebrospinal fluid. *Archives of Histology and Cytology, 69*(1), 37-47.

Wang, X., Chi, N., & Tang, X. (2008). Preparation of estradiol chitosan nanoparticles for improving nasal absorption and brain targeting. *European Journal of Pharmaceutics and Biopharmaceutics, 70*(3), 735-740.

Wazawa, T., Ishizuka-Katsura, Y., Nishikawa, S., Iwane, A. H., & Aoyama, S. (2006). Grafting of poly(ethylene glycol) onto poly(acrylic acid)-coated glass for a protein-resistant surface. *Analytical Chemistry, 78*(8), 2549-2556.

Wielgat, P., & Braszko, J. J. (2012). The participation of sialic acids in microglia–neuron interactions. *Cellular Immunology, 273*(1), 17-22.

Wilcock, D. M., & Colton, C. A. (2008). Anti-amyloid-beta immunotherapy in Alzheimer's disease: relevance of transgenic mouse studies to clinical trials. *Journal of Alzheimer's Disease, 15*(4), 555-569.

Wilson, B., Samanta, M. K., Muthu, M. S., & Vinothapooshan, G. (2011). Design and evaluation of chitosan nanoparticles as novel drug carrier for the delivery of rivastigmine to treat Alzheimer's disease. *Therapeutic Delivery, 2*(5), 599-609.

Wilson, B., Samanta, M. K., Santhi, K., Kumar, K. P. S., Paramakrishnan, N., & Suresh, B. (2008). Poly(n-butylcyanoacrylate) nanoparticles coated with polysorbate 80 for the targeted delivery of rivastigmine into the brain to treat Alzheimer's disease. *Brain Research, 1200*(0), 159-168.

Wilson, B., Samanta, M. K., Santhi, K., Kumar, K. P. S., Ramasamy, M., & Suresh, B. (2010). Chitosan nanoparticles as a new delivery system for the anti-Alzheimer drug tacrine. *Nanomedicine: Nanotechnology, Biology and Medicine, 6*(1), 144-152.

Win, K. Y., & Feng, S. S. (2006). In vitro and in vivo studies on vitamin E TPGS-emulsified poly(D,L-lactic-co-glycolic acid) nanoparticles for paclitaxel formulation. *Biomaterials, 27*(10), 2285-2291.

Xia, Huimin, Gao, X., Gu, G., Liu, Z., Zeng, N., . . . Chen, H. (2011). Low molecular weight protamine-functionalized nanoparticles for drug delivery to the brain after intranasal administration. *Biomaterials, 32*(36), 9888-9898.

Xia, H., Gao, X., Gu, G., Liu, Z., Hu, Q., Tu, Y., . . . Chen, H. (2012). Penetratin-functionalized PEG-PLA nanoparticles for brain drug delivery. *International Journal of Pharmaceutics, 436*(1-2), 840-850.

Xia., H., Gao, X., Gu, G., Liu, Z., Zeng, N., . . . Chen, H. (2011). Low molecular weight protamine-functionalized nanoparticles for drug delivery to the brain after intranasal administration. *Biomaterials, 32*(36), 9888-9898.

Yan, A., Von Dem Bussche, A., Kane, A. B., & Hurt, R. H. (2007). Tocopheryl Polyethylene Glycol Succinate as a Safe, Antioxidant Surfactant for Processing Carbon Nanotubes and Fullerenes. *Carbon, 45*(13), 2463-2470.

Yan, L., Wang, H., Jiang, Y., Liu, J., Wang, Z., Yang, Y., . . . Huang, Y. (2013). Cell-penetrating peptide-modified PLGA nanoparticles for enhanced nose-to-brain macromolecular delivery. *Macromolecular Research, 21*(4), 435-441.

Yang, Z. Z., Zhang, Y. Q., Wang, Z. Z., Wu, K., Lou, J. N., & Qi, X. R. (2013). Enhanced brain distribution and pharmacodynamics of rivastigmine by liposomes following intranasal administration. *International Journal of Pharmaceutics, 452*(1-2), 344-354.

Yasir, M., & Sara, U. V. S. (2014). Solid lipid nanoparticles for nose to brain delivery of haloperidol: in vitro drug release and pharmacokinetics evaluation. *Acta Pharmaceutica Sinica B, 4*(6), 454-463.

Zaki, N. M., Awad, G. A., Mortada, N. D., & Abd Elhady, S. S. (2007). Enhanced bioavailability of metoclopramide HCl by intranasal administration of a mucoadhesive in situ gel with modulated rheological and mucociliary transport properties. *European Journal of Pharmaceutical Sciences, 32*(4-5), 296-307.

Zalipsky, S. (1995). Functionalized Poly(ethylene glycols) for Preparation of Biologically Relevant Conjugates. *Bioconjugate Chemistry, 6*(2), 150-165.

Zhang, C., Wan, X., Zheng, X., Shao, X., Liu, Q., Zhang, Q., & Qian, Y. (2014). Dual-functional nanoparticles targeting amyloid plaques in the brains of Alzheimer's disease mice. *Biomaterials, 35*(1), 456-465.

Zhang, Q.-Z., Zha, L.-S., Zhang, Y., Jiang, W.-M., Lu, W., Shi, Z.-Q., . . . Fu, S.-K. (2006). The brain targeting efficiency following nasally applied MPEG-PLA nanoparticles in rats. *Journal of Drug Targeting, 14*(5), 281-290.

Every reasonable effort has been made to acknowledge the owners of copyright material. I would be pleased to hear from any copyright owner who has been omitted or incorrectly acknowledged.

8. Appendix

Chapter-2 Appendix

8.1 Determination of the Percent yield of TGC

$$Percent\ (\%)\ Yield = \frac{Actual\ Yield}{Theoretical\ Yield} * 100$$

Actual Yield of TGC obtained = 410 mg or 0.00163 mmol

$$Theoretical\ Yield\ of\ TGC\ = \frac{Amount of\ GC\ used}{Molecular\ weight\ of\ GC} * Molecular\ weight\ of\ TGC$$

$$Theoretical\ Yield = \frac{500\ mg\ of\ GC\ used}{250{,}000\ Da} * 250092 = \ 500.184\ mg\ or\ 0.002\ mmol$$

$$\%\ Yield = \frac{410.0\ mg}{500.184\ mg} * 100 = 82\ \%$$

Results: The calculated yield for TGC synthesized conjugated polymer was 82.0 %.

8.2 Determination of thiol group in synthesized TGC polymer

Standard Curve of thioglycolic acid

Various concentration of thioglycolic acid was prepared in milli-Q water from the stock solution of thioglycolic acid (20 mM). To 1.0 mL of each concentration of thioglycolic acid solution was mixed with 1 mL of PBS (pH 8.0) and 2.0 mL of Ellman's reagent. The mixture was incubated for 3 h at 37°C in dark to allow the reaction of free sulfhydryl groups with Ellman's reagent and absorbance was measured at 412 nm. The blank used for the calibration curve is mixture of 1.0 mL of milli-Q water, 1.0 mL of PBS and 2.0 mL of Ellman's reagent. The absorbance of the standard concentrations of thioglycolic acid was measured and plotted against concentration. The calibration curve is represented in Figure 8.1.

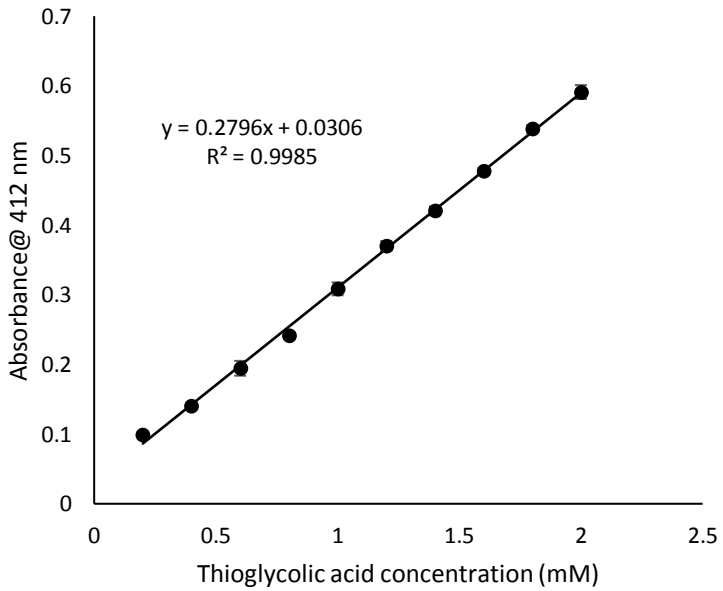

Figure 8.1: Standard curve of thioglycolic acid

Procedure for determination of Thiol group in synthesized TGC polymer: Briefly, 2 mg/mL of TGC polymer solution was prepared in milli-Q water. To 1.0 mL of the TGC solution (containing 2.0 mg of TGC polymer), 1.0 mL of phosphate buffer saline (pH 8.0) and 2.0 mL of Ellman's reagent was added. The mixture was incubated for 3 h at 37°C in dark to allow the reaction of free sulfhydryl groups with Ellman's reagent and absorbance was measured at 412 nm. A control sample (GC) of the same concentration was also incubated using the same procedure with similar concentration (2 mg/mL GC solution in milli-Q water). The blank sample used was for this is mixture of milli-Q water, PBS and Ellman's reagent in same volume. The number of thiol groups present in the synthesized TGC polymer was determined from a standard curve constructed from 0.20 to 2.0 mM of thioglycolic acid in water after subtracting absorbance of the control samples.

Table 8.1: Determination of concentration of thiol group in synthesized TGC sample

1	**2**	**3**	**4**	**5**	**6**	**7**	**8**	**9**
Sample name	Actual Abs	Abs after subtraction of control	concentration (mM or mmol/L)	Concentration (mmol/mL)	Amount of -SH group in polymer (mmol/gm of polymer)	Amount of -SH group in polymer (µmol/gm of polymer)	Average	SD
TGC	0.591	0.532	1.792	1.792×10^{-3}	0.896	896.04	881.14	21.33
TGC	0.588	0.529	1.781	1.781×10^{-3}	0.891	890.68		
TGC	0.569	0.510	1.713	1.713×10^{-3}	0.857	856.70		
Blank	0							

Column-1 sample were all made to the equivalent molar concentration.
Column-2 UV absorbance obtained from the samples at 412 nm.
Column-3 Calculated absorbance after subtraction of GC control absorbance
Column-4 Calculated concentration using the standard curve represented in Figure 8.1.
Column-5 is the concentration in mmol/mL
Column-6 is the amount of the -SH group present in the polymer

$$\frac{Amount\ of\ SH\ group(mmol)}{gm\ of\ polymer} = \text{Concentration of sample (mmol/mL)/Weight of the polymer (in g)}$$

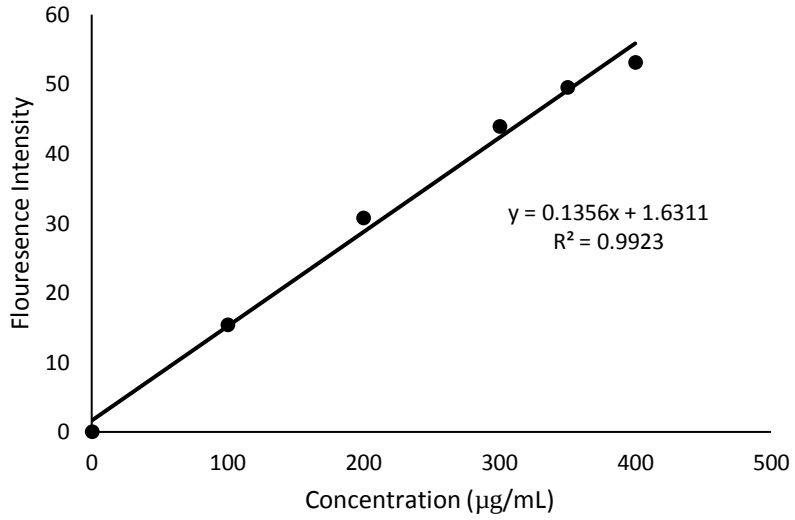

Figure 8.2: Calibration curve of TAT peptide (0-400 µg/mL) in presence of mPEG-COOH using fluorescamine assay method

8.3 HPLC Chromatograms and Validated Parameters for RV and C-6

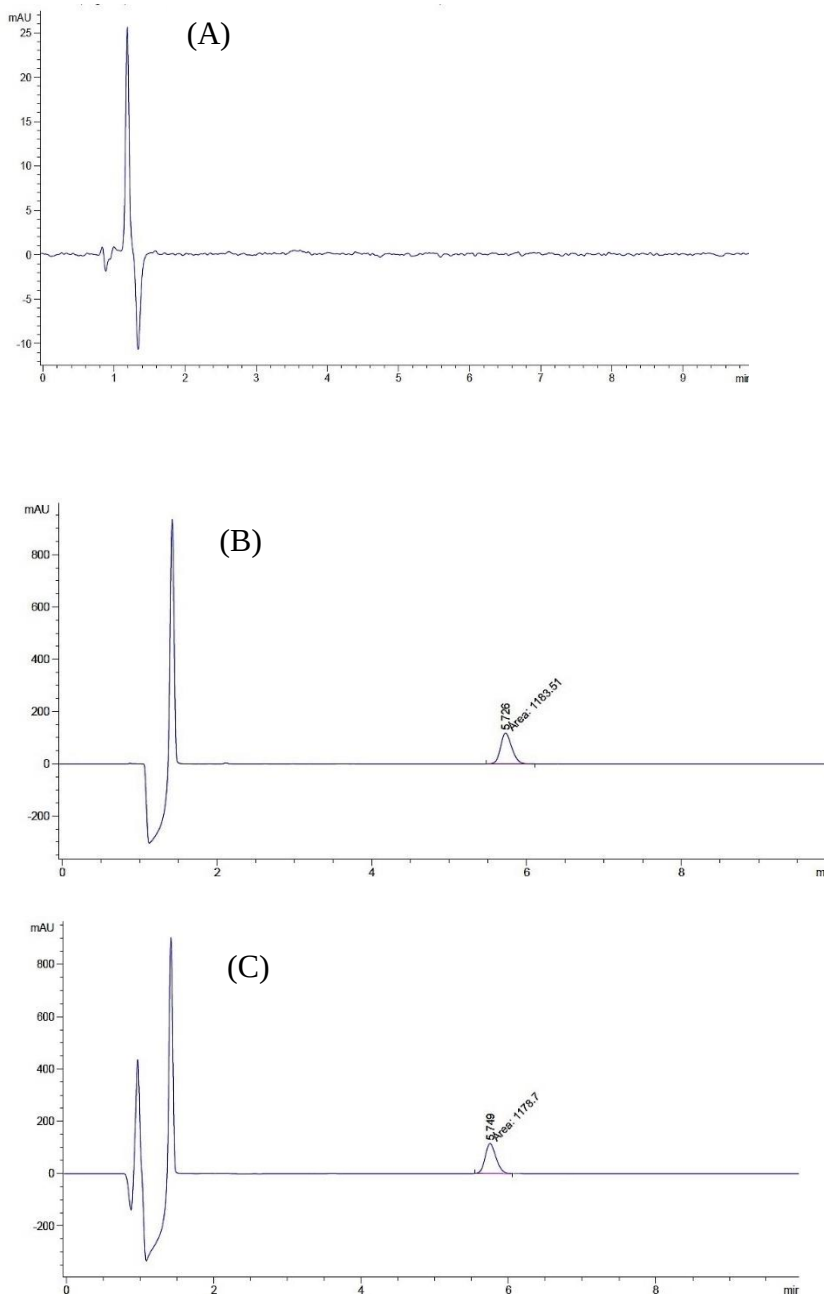

Figure 8.3: Typical HPLC chromatogram of (A) blank mobile phase (B) 20 µg/mL of RV prepared in mixture of acetonitrile and water (20:80 v/v) (C) 20 µg/mL of RV prepared in PBS.

The prepared samples were analysed using a developed and validated HPLC method for clean *in-vitro* samples. Each run was carried out for 10 min with RV retention time at 5.72 min.

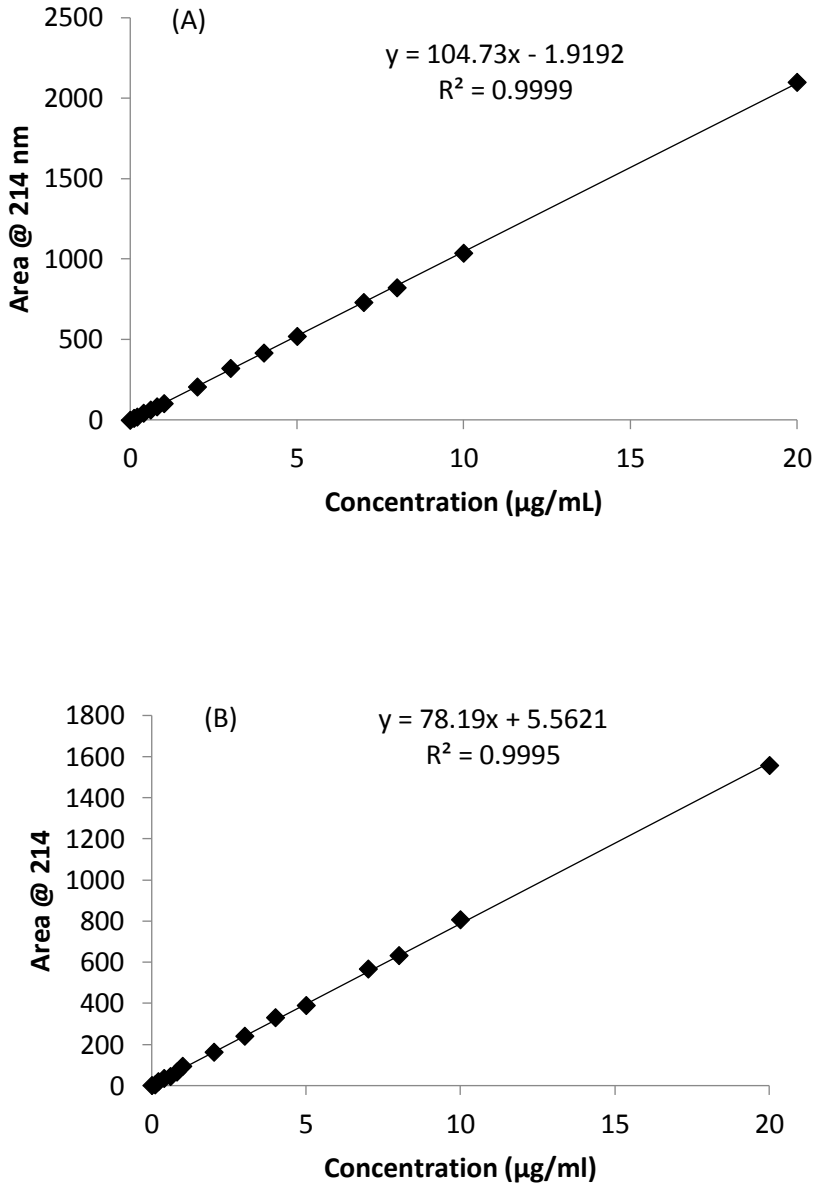

Figure 8.4: Standard curve of RV in (A) acetonitrile/water mixture (B) PBS

Table 8.2: Precision of developed HPLC method for determination of RV in mixture of acetonitrile/water

Area Obtained of various concentration			
Injection no.	1 µg/mL	4 µg/mL	8 µg/mL
1	100.8	414.2	823
2	100.2	422.4	833.4
3	100.9	422.4	833.1
4	100.6	419.3	829.2
5	100.2	420.2	828.4
6	101.4	419.4	819.6
Average area	100.68	419.65	827.78
SD	0.46	3.01	5.51
RSD (%)	0.45	0.72	0.67

Table 8.3: Precision of HPLC method for determination of RV in PBS

Area Obtained of various concentration			
Injection no.	2 µg/mL	5 µg/mL	10 µg/mL
1	164.3	384.2	812.3
2	160.5	392.1	819.8
3	164.5	387.5	821
4	161.3	389.6	809.7
5	165.9	382.3	805.9
6	164.4	381.3	815.3
Average area	163.48	386.17	814.00
SD	2.10	4.27	5.85
RSD	1.28	1.11	0.72

Table 8.4:Intraday and Interday variation of RV in acetonitrile/water (20:80, v/v)

RV Concentration Prepared (µg/mL)	Intra-day R.S.D.[b] (%)	Inter-day R.S.D.[c] (%)
1.0	0.42	1.32
4.0	0.74	0.91
Average	0.58	1.15

[a] n=6 for each sample concentration, triplicate samples were prepared for two different concentrations.
[b] each sample of RV were analysed at 0, 3 and 6 hours in the same day and RSD was calculated using all the data.
[c] each sample of RV was analysed for two consecutive days and % RSD was calculated using all the data.

Table 8.5: Intraday and Interday variation of RV in PBS

RV Concentration Prepared [a] (µg/mL)	Intra-day R.S.D. [b] (%)	Inter-day R.S.D. [c] (%)
2.0	0.53	1.81
5.0	0.40	0.96
Average	0.46	1.38

[a] n=6 for each sample concentration, triplicate samples were prepared for two different set of concentrations.
[b] each sample of RV were analysed at 0, 3 and 6 hours in the same day and RSD was calculated using all the data.
[c] each sample of RV was analysed for two consecutive days and % RSD was calculated using all the data.

Table 8.6: Determination of height of noise level in mobile phase and PBS for calculation of LOD and LOQ

Blank Injection #	Noise level in mobile phase	Noise level in PBS
1	0.08	0.08
2	0.09	0.10
3	0.10	0.08
4	0.10	0.09
5	0.10	0.08
6	0.07	0.09
Average noise	0.10	0.09
Slope	10.57	5.80
LOD (ng/mL)	28.0	49.0
LOQ (ng/mL)	85.14	149.0

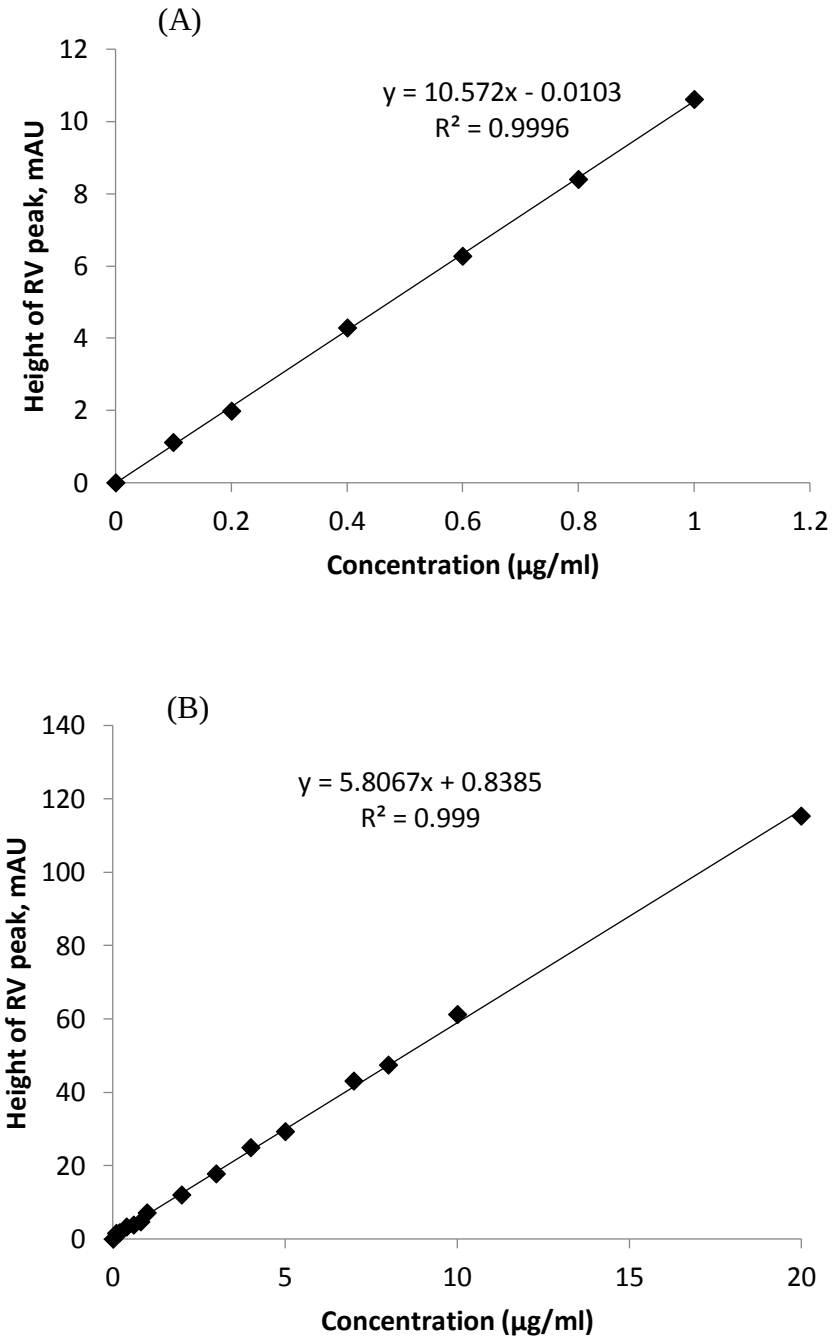

Figure 8.5: Standard curve between height of peak obtained of the RV sample versus RV concentration prepared in (A) acetonitrile/water mixture (B) PBS

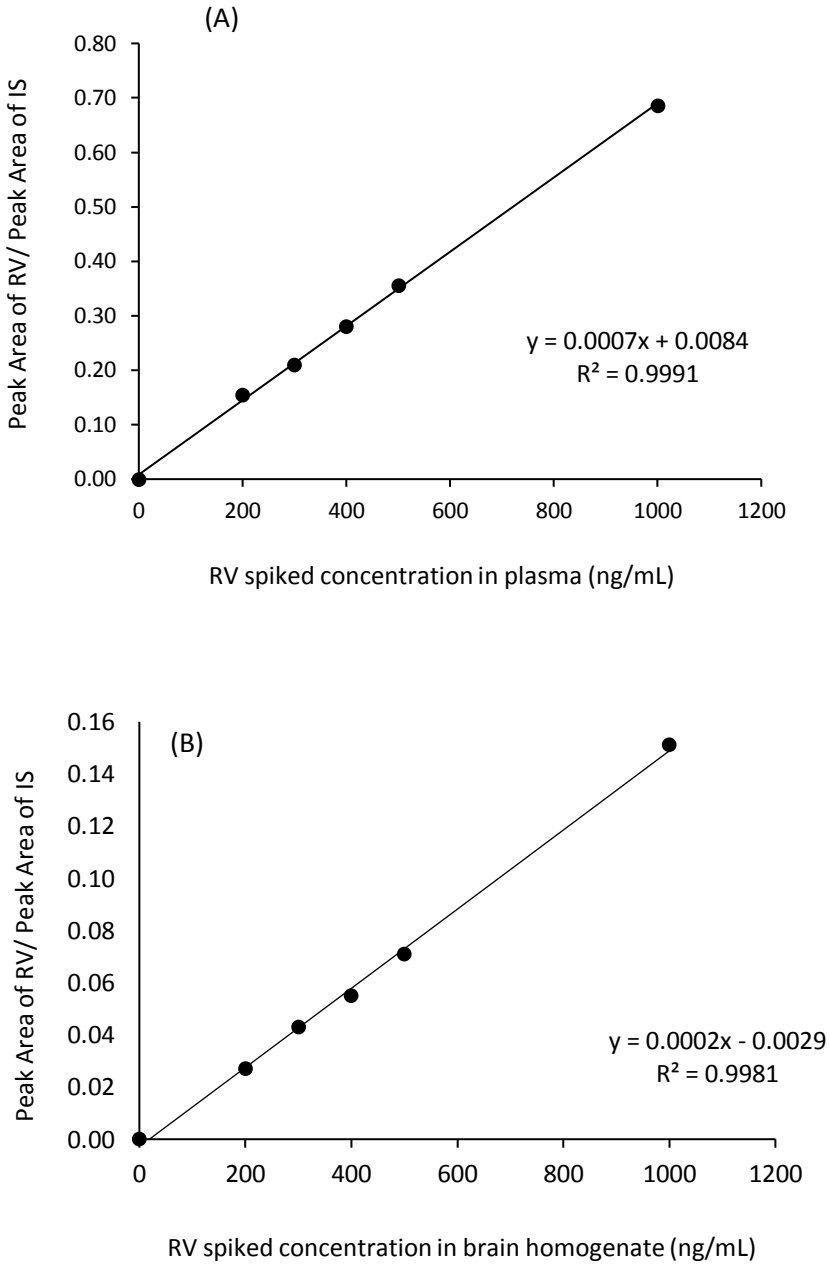

Figure 8.6: Linearity ranges of RV in (A) blank plasma (B) blank brain matrices

Table 8.7: Determination of Noise level, LOD and LOQ assessment in plasma and brain homogenates using developed RP-HPLC method for analysis of RV using fluorescence detector

Blank Injection #	Noise level in Blank Plasma	Noise level in blank brain homogenate
1	0.04	0.06
2	0.05	0.05
3	0.03	0.06
4	0.03	0.08
5	0.02	0.03
6	0.02	0.08
Average noise	0.03	0.05
Slope	0.0017	0.003
LOD (ng/mL)	55.0	55.0
LOQ (ng/mL)	186	166.0

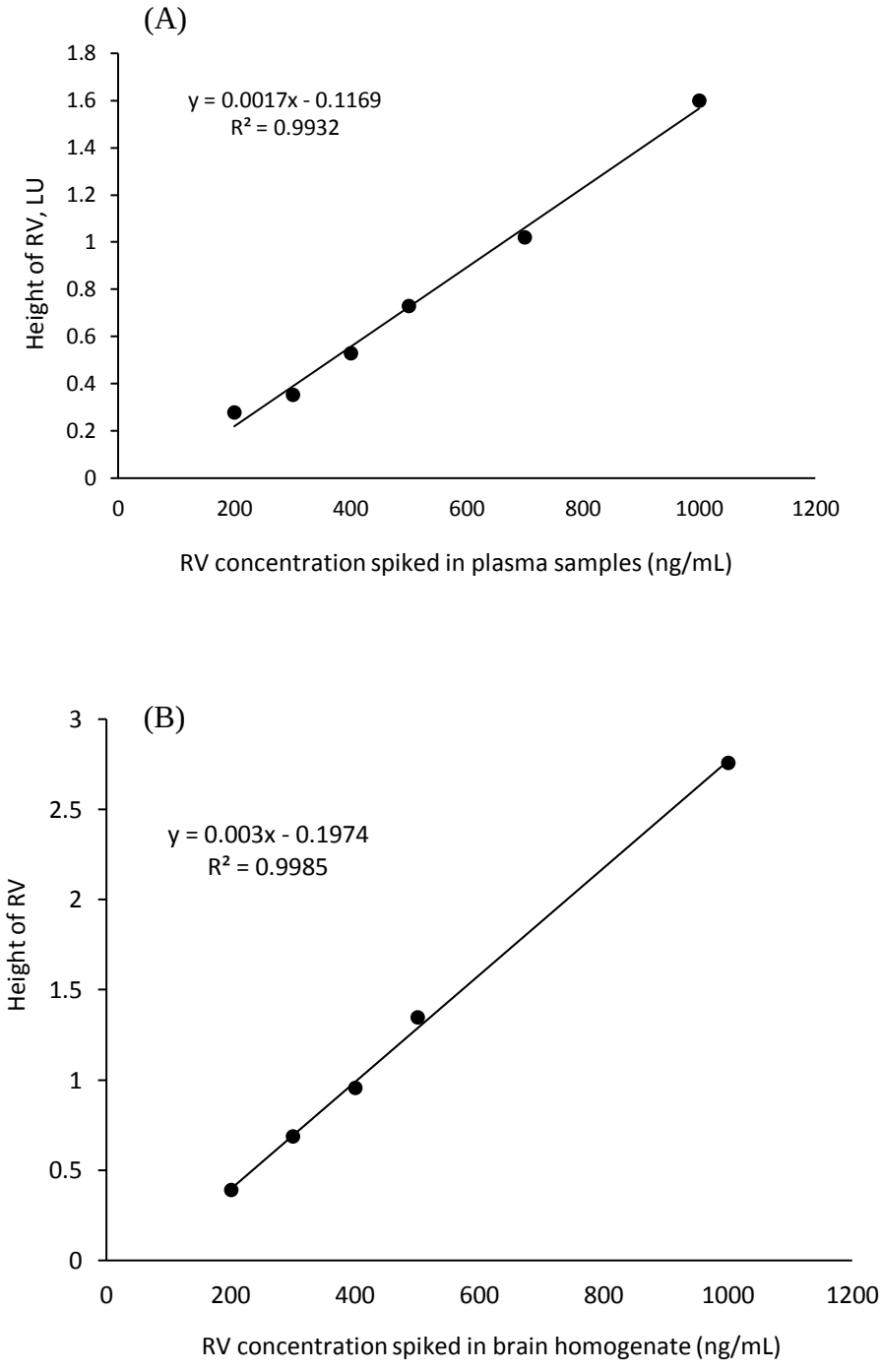

Figure 8.7: Calibration curve plotted between height of RV obtained from sample versus RV concentration spiked in (A) plasma sample (B) brain homogenate samples

Table 8.8: Recovery of C-6 from blank PLGA matrix with developed HPLC method

Sample No	Conc. spiked (ng/mL)	Average conc. recovered (ng/mL)	Mean recovery (%)	RSD (%)
1	50	49.1 ± 0.3	98.1	0.3
2	100	98.9 ± 0.9	98.9	0.9
3	500	496.5 ± 1.6	99.3	1.6
	% Mean Recovery		98.8 ± 0.7	0.9

Data represented in % Mean Recovery ± S.D (n=3). RSD: relative standard deviation, S.D is standard deviation.

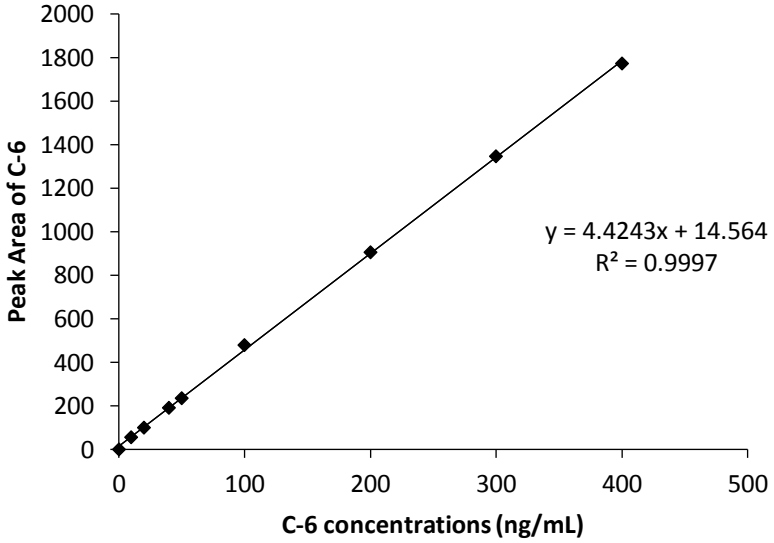

Figure 8.8: Calibration curve plotted between area and C-6 concentration prepared in mixture of acetonitrile/water mixture (84: 16)

Table 8.9: Precision of HPLC method for determination of C-6 in acetonitrile/ water (84:16, v/v)

Area of C-6 obtained			
Injection no.	20 ng/mL	100 ng/mL	400 ng/mL
1	96.4	473.6	1761.8
2	96.4	474.8	1756.6
3	99.2	474.8	1766.1
4	99.7	470.6	1758.7
5	97.8	481.1	1770
6	96.5	479.2	1773
Average	97.67	475.6	1764.3
SD	1.49	3.83	6.45
RSD (%)	1.52	0.81	0.37

Table 8.10: Intraday and interday variation of C-6 in acetonitrile/water mixture

C-6 Concentration Prepared [a] (ng/mL)	**Intra-day R.S.D. [b] (%)**	**Inter-day R.S.D. [c] (%)**
100	0.19	0.66
400	0.07	0.27

[a] n=6 for each sample concentration, triplicate samples were prepared for two different concentrations.

[b] each sample of C-6 were analyzed at 0, 3 and 6 h in the same day and RSD was calculated using all the data.

[c] each sample of C-6 was analysed for two consecutive days and % RSD was calculated using all the data.

Table 8.11: Noise level, LOD an LOQ determination in mobile phase mixture for C-6 using developed RP-HPLC-FLD method

Blank Injection #	Noise level in Blank
1	0.0140
2	0.0065
3	0.0035
4	0.0035
5	0.0045
6	0.0100
Average noise	0.01
Slope	0.45
LOD (ng/mL)	0.05
LOQ (ng/mL)	0.15

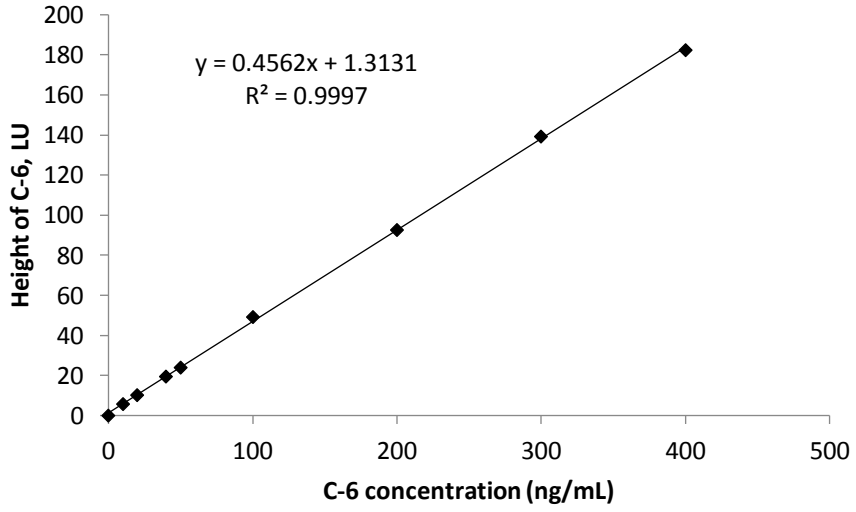

Figure 8.9: Calibration curve between height of C-6 versus C-6 concentration prepared in mixture of acetonitrile/water mixture (84: 16)

8.4 Determination of thiol group on the surface of the PLGA NPs

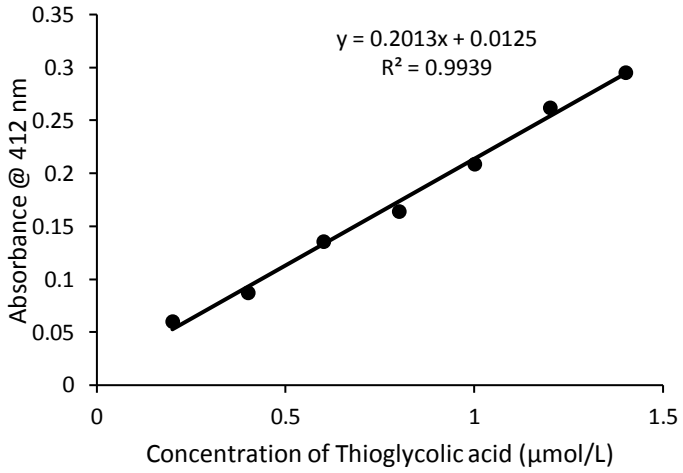

Figure 8.10: Standard curve of Thioglycolic acid used for determination of Thiol content

Table 8.12: Determination of thiol groups on TGC coated NPs surface

Sample name	Absorbance noted	conc (µmol/L)	conc (mmol/mL)	Dilution factor	conc (mmol/ 500 uL or 0.5 mL)	Thiol group (a) (mmol/gm of PLGA)	Thiol group/PLGA NPs	Average Thiol Group	SD
TGC coated PLGA NPs	0.083	0.351	0.000000351	1.40299E-06	7.01493E-07	**4.67662E-08**	428	533.67	94.733
TGC coated PLGA NPs	0.105	0.460	0.000000460	1.8408E-06	9.20398E-07	**6.1359E-08**	562		
TGC coated PLGA NPs	0.115	0.510	0.000000510	2.0398E-06	1.0199E-06	**6.79934E-08**	611		

Measurements was performed with 500 µL of NPs dispersions which contains 15 mg of TGC coated PLGA NPs

$$n = aN[d\left(\frac{4}{3}\right)\pi r^3]$$

n is number of thiol group present per NP; a is mole of thiol determined per gram of TGC coated PLGA (which was determined using Ellman's reagent); N is Avogadro number ($6.023 \text{ X } 10^{23}$); d is density of the NPs determined (1.5 gm/mL); r is mean radius of the NP which was determined using Zeta sizer.

For calculating n

$$n = a * 6.023 * 1E + 23\ [\ 1.65\left(\frac{4}{3} * \frac{22}{7} * \frac{130}{10000000} * \frac{130}{10000000} * \frac{130}{10000000}\right)]$$

$$n = a * 91659985187.54$$

$$n = 4.676E - 08 * 91659985187.54$$

8.5 Method for calculation of EE of NPs using HPLC data

$$\text{EE}\ (\%) \quad = \frac{\text{Total drug used} - \text{free drug in supernatant}}{\text{total drug used}} \times 100$$

$$\text{Drug Loading}\ (\%) = \frac{\text{Total drug used} - \text{free drug in supernatant}}{\text{total NP weight}} \times 100$$

Sample preparation:

2 batches of NP prepared on 16-07-2016 with High molecular weight of PLGA (110 KDa) and 0.3% Vitamin E

1) Supernatant was collected after centrifugation

2) it was further diluted 100 times with mobile Phase before injecting on HPLC

Mobile phase: 80: 20; Water : ACN with 0.1% TFA

volume injected	40	uL
External STD	**2**	**ugm/mL**
External Area	**125**	

Conc'n of RV in supernatant

Batch #	RV added (in mg)	Area of supernatant @40uL	RV conc in Sup (ugm/mL)	DF (100 *)	RV conc (mg/mL)	Total RV conc'n in 20 mL of Sup (mg)	Amt went into NP (mg)	PLGA added (mg)	% RV loading in NP	Theoretical Drug loading	%EE
1	5	129.3	2.0688	206.88	0.20688	4.1376	0.8624	30	2.794339	14.30	17.248
2	5	125.1	2.0016	200.16	0.20016	4.0032	0.9968	30	3.215816	14.30	19.936

vitamin E used		TDL(%)	Drug added in NP (In mg)	PLGA added (in mg)	%RV exp. Loading in NP	% EE
0.30%	n=2	14.3	5	30	3.005077	18.592

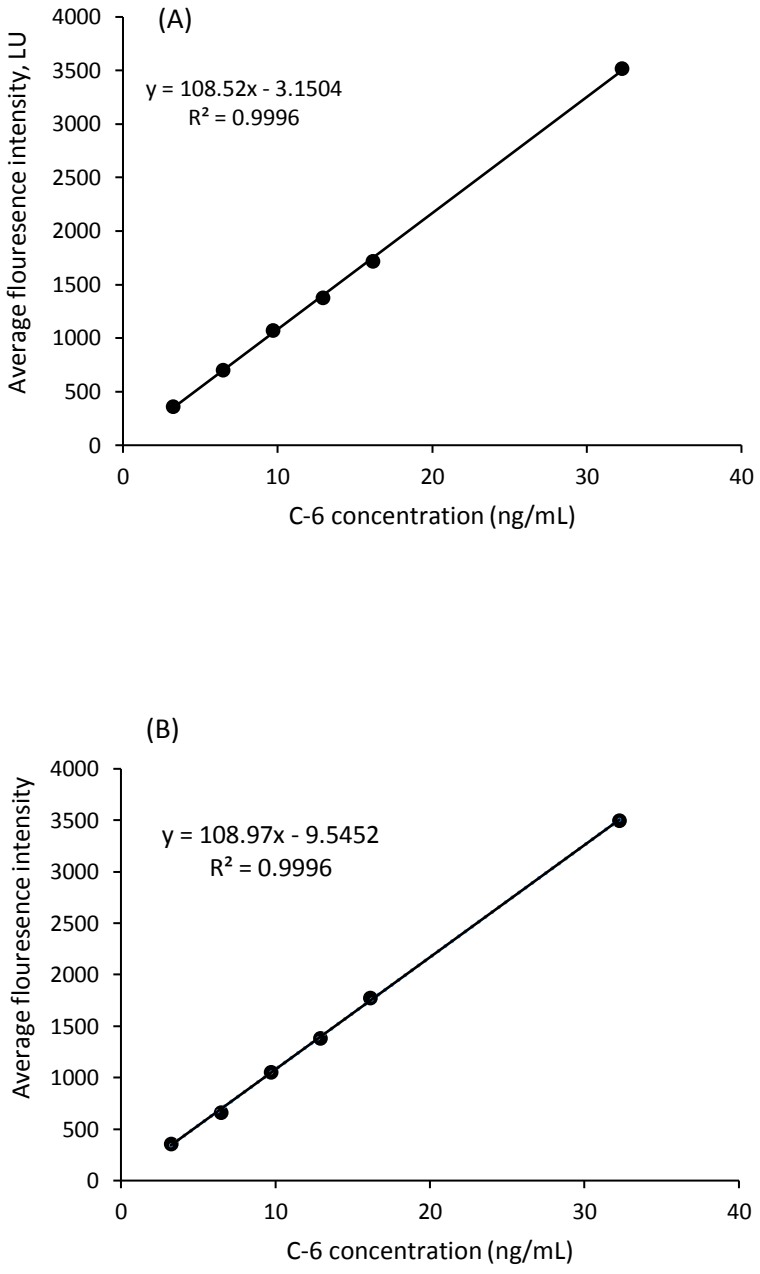

Figure 8.11: Determination of linearity ranges of C-6 in (A) blank plasma (B) blank brain matrices

Table 8.13: Determined percent RV drug concentration recovered during stability study of RV in plasma samples at 37°C for 48 h

Time (h)	Percent mean RV concentration determined in plasma samples	
	200 ng/mL	**400 ng/mL**
3	101.3 ± 2.3	99.1 ± 0.7
6	99.5 ± 0.5	98.3 ± 2.6
24	100.6 ± 2.1	100.0 ± 0.6
48	91.6 ± 2.0	92.0 ± 2.7

Data represented in % mean of RV concentration remaining in rats' plasma ± SD (n=2)

8.6 Extraction and calculation of RV from plasma samples

1. Take 100 µL of plasma sample, add 15 µL of IS (1000 ng/mL) and vortex for 2 min.
2. Added 100 µl of Acetonitrile +20µL of RIPA Buffer + and 880 µL of Tert-butyl methyl ether (TBME).
3. Vortex for 10 min and then stir for 20 min on shaker.
4. Centrifuge mixture at 16,200 g for 15 min at 4°C.
5. Take out 900 µL of Supernatant and transfer it into another centrifuge tube.
6. Added another 900 µL of TBME into the remaining pellet and vortex it for 10 min and stir for 20 min. Centrifuge the mixture again at 16,200 g for 15 min at 4°C. Take out 900 µL of Supernatant and combine it with previous organic layer in the above centrifuge tube. Total supernatant collected was 1.8 mL.
7. Evaporate the both organic layer to dryness and reconstitute further with 200 µL of mobile phase and inject 70 µL.

Total aqueous phase volume=135µL; organic phase =880+100+900=1880

real plasma conc=C after taking into consideration of EDTA dilution $C_{plasm}*(0.2/1.8)*(1.88/0.1)$

final $C=C^* Vol_{(total\ blood\ collected)}/(Vol_{(total\ blood\ collected)}-20\mu L EDTA)$

Table 8.14: Plasma concentration time data of RV obtained after administration of RV standard drug solutions administered by IV and IN route, single ligand and dual ligand NPs administered by IN route

Time (in h)	IV RV control solution	IN RV control solution	RV+C6 loaded PLGA-SA-ODA NPs (single ligand NPs)	RV+ C6 loaded PLGA-SA-ODA NPs coated with TGC (dual ligand NPs)
0.25	2294.1 ± 438.9	842.0 ± 35.0	299.5 ± 21.5	609.5 ± 118.4
0.50	1968.1 ± 286.2	926.5 ± 74.9	440.6 ± 21.1	869.8 ± 159.6
1.00	1458.4 ± 293.6	1214.9 ± 103.8	637.5 ± 98.7	1199.7 ± 156.4
1.50	1024.2 ± 92.3	1073.4 ± 94.6	749.1 ± 112.9	1206.0 ± 62.1
2.00	702.1 ± 44.7	733.9 ± 59.1	902.5 ± 144.8	1165.2 ± 111.9
3.00	489.0 ± 53.2	306.2 ± 79.4	952.9 ± 61.5	976.0 ± 50.0
4.00	301.7 ± 45.5	153.0 ± 31.7	702.6 ± 54.3	871.0 ± 25.3
6.00	188.3 ± 19.6	101.0 ± 11.2	430.6 ± 56.3	611.2 ± 28.5
8.00	98.5 ± 19.3	75.2 ± 10.3	170.6 ± 14.5	432.7 ± 51.3

Data represented in mean RV concentration (ng/mL of plasma) ± SEM (n=4) for 8 h

8.7 Extraction and calculation of RV from Brain samples

1. Take 500 µL of brain homogenate sample, add 50 µL of IS (1500 ng/mL previously determined concentration using HPLC) and vortex for 2 min.
2. Added 100 µl of Acetonitrile +50µL of RIPA Buffer + and 800 µL of Tertbutyl methyl ether (TBME).
3. Vortex for 10 min and then stir for 20 min on shaker.
4. Centrifuge mixture at 16,200 g for 15 min at 4°C.
5. Take out 900 µL of Supernatant and transfer it into another centrifuge tube.
6. Added another 900 µL of TBME into the remaining pellet and vortex it for 10 min and stir for 20 min. Centrifuge the mixture again at 16,200 g for 15 min at 4°C. Take out 900 µL of Supernatant and combine it with previous organic layer in the above centrifuge tube.
7. Evaporate the both organic layer to dryness and reconstitute further with 200 µL of mobile phase and inject 70 uL.

Total aqueous phase volume=135µL;

Total organic phase =900+100+900=1900 µL

Total withdrawn organic layer = 1800 µL

Total Brain homogenate volume = 4.2 mL

real brain conc=C $C_{plasm}*(0.2/1.8)*(1.9)*(4.2/0.5)$

Table 8.15: Determined RV concentration in brain after administration of RV drug solution by IN and IV route and single ligand RV+C-6 loaded PLGA-SA-ODA NPs and dual ligand RV+C-6 loaded PLGA-SA-ODA NPs coated with TGC via IN route.

Formulation	Time (h)	
	2	**8**
RV solution (IV)	216.6 ± 9.0	154.0 ± 15.8
RV solution (IN)	377.0 ± 24.0	146.6 ± 18.1
Single ligand NPs (IN)	1190.5 ± 104.5	386.0 ± 46.3
Dual ligand PLGA NPs (IN)	1615.3 ± 237.0	393.0 ± 16.0

The data expressed in mean RV concentration ± SEM (ng/gm of brain tissue) (n=5),

Table 8.16: Freeze-thaw stability studies of RV in plasma

Matrix used	Condition employed for stability testing	RV concentration spiked (µg/mL)	RV concentration determined (µg/mL)	% RV remaining ± SD
Plasma	Freeze-Thaw Cycle	2.0	2.0 ± 0.1	101.0 ± 2.8
Plasma	(3 cycles, -80°C)	4.0	3.9 ± 0.1	99.1 ± 3.5

Data represented in mean concentration ± SD (n=3)

Table 8.17: Plasma concentration time data of C-6 obtained after administration of single ligand RV+C-6 loaded PLGA-SA-ODA NPs and dual ligand RV+C-6 loaded PLGA-SA-ODA NPs coated with TGC

Time (h)	Single ligand RV+C-6 loaded PLGA-SA-ODA NPs	Dual ligand RV+C-6 loaded PLGA-SA-ODA NPs coated with TGC
0.25	160.9 ± 5.8	139.7 ± 6.6
0.50	224.3 ± 5.9	171.3 ± 5.8
1.00	312.8 ± 11.1	211.8 ± 7.8
1.50	363.6 ± 13.1	258.1 ± 10.5
2.00	389.6 ± 9.5	309.8 ± 10.8
3.00	357.3 ± 15.6	338.9 ± 9.1
4.00	323.0 ± 17.8	298.4 ± 13.4
6.00	263.4 ± 13.5	245.3 ± 5.0
8.00	204.9 ± 5.9	191.9 ± 4.8

Data represented in mean C-6 concentration (in ng/mL) ± SEM (n=5) for 8 h

Table 8.18: C-6 brain concentration determined after administration of single ligand RV+C-6 loaded PLGA-SA-ODA NPs and dual ligand RV+C-6 loaded PLGA-SA-ODA NPs coated with TGC via IN route.

NPs formulation	Time (in h)	
	2	8
Single ligand RV + C6 loaded PLGA-SA-ODA NPs	46.8 ± 2.5	18.8 ± 0.9
Dual ligand RV + C6 loaded PLGA-SA-ODA NPs coated with TGC	58.3 ± 3.1	34.1 ± 1.3

Data represented in mean C-6 concentration (in ng/gm of brain tissue) ± SEM (n=5) for 8 h

8.8 Animal Ethical Approval Letter

Curtin Universit

13 November 2015

Office of Research and Developm

Building 100 Level 1 West
Dumas Road
Bentley Western Australia 6102

GPO Box U1987
Perth Western Australia 6845

Telephone +61 8 9266 7863
Facsimile +61 8 9266 3793
Web research.curtin.edu.au

Animal Ethics Committee

Telephone +61 8 9266 2784
Facsimile +61 8 9266 3793
Email aec@curtin.edu.au

Dr Yan Chen
Pharmacy
Curtin University

Dear Yan,

Animal Ethics

Approval Number: AEC_2015_37
Project Title: *Development and Evaluation of Nanoparticulate Formulations for Enhanced Transport of Rivastigmine into the Brain (Application Number 42-2015)*

Thank you for providing additional information for the project titled "*Development and Evaluation of Nanoparticulate Formulations for Enhanced Transport of Rivastigmine into the Brain*". The information you have provided has satisfactorily addressed the queries raised by the Committee.

The application has now been **approved** and the relevant approval number is **AEC_2015_37** and the period of the project approval is from **12/11/2015** to **31/12/2015.** Your approval is automatically revoked if an annual progress report is not provided by **31 December 2015** and year end in subsequent years.

Approval of this project is for the period **12/11/2015 to 31/12/2016.**

Species Approved	Code	No
Rat (Rattusnorvegicus)	100 RatOutbred Sprague Dawley	166

OTHER REQUIREMENTS/NOTES

Should any animal(s) experience an adverse or unexpected outcome resulting from the experimentation, the AEC is to be notified in writing immediately.

Please note that it is the policy of the Animal Ethics Committee to give approval up to end of the current year only. Should the project be continuing in the following year, an application for renewal must be submitted for approval by the AEC. An application for renewal may be made three years running, after which a 'new' application form, providing comprehensive details, must be submitted.

You are reminded that it is your responsibility to maintain your own animal records and to report annually to the Committee.

Please ensure that you quote the Animal Ethics Committee approval number whenever you order animals for this project. Note also that an AEC approval number must be displayed on the cage(s)/aquaria etc used to house/maintain animals during an approved activity.

If the results of this research will be published, citations should state: "All experiments were performed according to the Australian Code of Practice for the care and use of animals for scientific purposes".

Regards

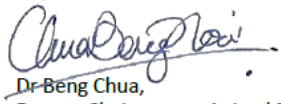

Dr Beng Chua,
Deputy Chairperson, Animal Ethics Committee
cc: Bhawna Gauri
Nazhasan Huda Pharmacy

8.9 List of Abstracts and Presentations

❖ Oral Presentation

1. B Gauri, A. V. Dolzhenko, H. A. E Benson and Y. Chen. 2015 "An efficient and rapid synthesis of carboxylic acid functionalized Poly (ethylene glycol) derivatives" Oral Presentation in Mark Liveris Research Seminar Organized by Curtin University, Perth Western Australia

❖ Posters Presented

1 B Gauri, A. V. Dolzhenko, H. A. E Benson and Y. Chen. 2014 "Synthesis and Characterization of α-methoxy-ω-methyl ester mPEG derivative by Williamson etherification method." Poster Presentation in Mark Liveris Research Seminar Organized by Curtin University, Perth Western Australia.

2 B Gauri, A. V. Dolzhenko, H. A. E Benson and Y. Chen 2015 "Development of functionalized methoxy polyethylene glycol polymer for targeted nanoparticle delivery" CRS, Organized by Drug Delivery Australia.

3 B Gauri, A. V. Dolzhenko, H. A. E Benson and Y. Chen. 2016 "Formulation and Characterization of mucoadhesive thiolated glycol chitosan coated poly-(lactic-co-glycolic acid) nanoparticles for brain targeting of Rivastigmine" Poster Presentation in Mark Liveris Research Seminar Organized by Curtin University, Perth Western Australia.

Permission for Figure used in this thesis

by publisher or by CCC) as provided in CCC's Billing and Payment terms and conditions. If
full payment is not received on a timely basis, then any license preliminarily granted shall be
deemed automatically revoked and shall be void as if never granted. Further, in the event that you breach any of these terms and conditions or any of CCC's Billing and Payment terms and conditions, the license is automatically revoked and shall be void as if never granted. Use of materials as described in a revoked license, as well as any use of the materials beyond the scope of an unrevoked license, may constitute copyright infringement
and publisher reserves the right to take any and all action to protect its copyright in the materials.
9. Warranties: Publisher makes no representations or warranties with respect to the licensed
material.
10. Indemnity: You hereby indemnify and agree to hold harmless publisher and CCC, and their respective officers, directors, employees and agents, from and against any and all claims arising out of your use of the licensed material other than as specifically authorized pursuant to this license.
11. No Transfer of License: This license is personal to you and may not be sublicensed, assigned, or transferred by you to any other person without publisher's written permission.
12. No Amendment Except in Writing: This license may not be amended except in a writing
signed by both parties (or, in the case of publisher, by CCC on publisher's behalf).
13. Objection to Contrary Terms: Publisher hereby objects to any terms contained in any purchase order, acknowledgment, check endorsement or other writing prepared by you, which terms are inconsistent with these terms and conditions or CCC's Billing and Payment

terms and conditions. These terms and conditions, together with CCC's Billing and Payment
terms and conditions (which are incorporated herein), comprise the entire agreement between you and publisher (and CCC) concerning this licensing transaction. In the event of
any conflict between your obligations established by these terms and conditions and those established by CCC's Billing and Payment terms and conditions, these terms and conditions
shall control.
14. Revocation: Elsevier or Copyright Clearance Center may deny the permissions described
in this License at their sole discretion, for any reason or no reason, with a full refund payable
to you. Notice of such denial will be made using the contact information provided by you. Failure to receive such notice will not alter or invalidate the denial. In no event will Elsevier
or Copyright Clearance Center be responsible or liable for any costs, expenses or damage

incurred by you as a result of a denial of your permission request, other than a refund of the
amount(s) paid by you to Elsevier and/or Copyright Clearance Center for denied permissions.
LIMITED LICENSE
The following terms and conditions apply only to specific license types:
15. Translation: This permission is granted for nonexclusive
world English rights only
unless your license was granted for translation rights. If you licensed translation rights you
may only translate this content into the languages you requested. A professional translator must perform all translations and reproduce the content word for word preserving the integrity of the article.
16. Posting licensed content on any Website: The following terms and conditions apply as
follows: Licensing material from an Elsevier journal: All content posted to the web site must
maintain the copyright information line on the bottom of each image; A hypertext must be
included to the Homepage of the journal from which you are licensing at
http://www.sciencedirect.com/science/journal/xxxxx or the Elsevier homepage for books at
http://www.elsevier.com; Central Storage: This license does not include permission for a scanned version of the material to be stored in a central repository such as that provided by
Heron/XanEdu.
Licensing material from an Elsevier book: A hypertext
link must be included to the Elsevier
homepage at http://www.elsevier.com . All content posted to the web site must maintain the
copyright information line on the bottom of each image.
Posting licensed content on Electronic reserve: In addition to the above the following clauses are applicable: The web site must be passwordprotected
and made available only to
bona fide students registered on a relevant course. This permission is granted for 1 year only.
You may obtain a new license for future website posting.
17. For journal authors: the following clauses are applicable in addition to the above:
Preprints:
A preprint is an author's own writeup
of research results and analysis, it has not been peerreviewed,
nor has it had any other value added to it by a publisher (such as formatting,
copyright, technical enhancement etc.).
Authors can share their preprints anywhere at any time. Preprints should not be added to or
enhanced in any way in order to appear more like, or to substitute for, the final versions of

articles however authors can update their preprints on arXiv or RePEc with their Accepted Author Manuscript (see below).
If accepted for publication, we encourage authors to link from the preprint to their formal publication via its DOI. Millions of researchers have access to the formal publications on ScienceDirect, and so links will help users to find, access, cite and use the best available version. Please note that Cell Press, The Lancet and some societyowned
have different
preprint policies. Information on these policies is available on the journal homepage.
Accepted Author Manuscripts: An accepted author manuscript is the manuscript of an article that has been accepted for publication and which typically includes authorincorporated
changes suggested during submission, peer review and editorauthor
communications.
Authors can share their accepted author manuscript:
immediately

via their noncommercial
person homepage or blog
by updating a preprint in arXiv or RePEc with the accepted manuscript
via their research institute or institutional repository for internal institutional
uses or as part of an invitationonly
research collaboration workgroup
directly by providing copies to their students or to research collaborators for
their personal use
for private scholarly sharing as part of an invitationonly
work group on
commercial sites with which Elsevier has an agreement
After the embargo period
via noncommercial
hosting platforms such as their institutional repository
via commercial sites with which Elsevier has an agreement
In all cases accepted manuscripts should:
link to the formal publication via its DOI
bear a CCBYNCND
license this
is easy to do
if aggregated with other manuscripts, for example in a repository or other site, be
shared in alignment with our hosting policy not be added to or enhanced in any way to appear more like, or to substitute for, the published journal article.
Published journal article (JPA): A published journal article (PJA) is the definitive final record of published research that appears or will appear in the journal and embodies all valueadding
publishing activities including peer review coordination,
copyediting,
formatting, (if relevant) pagination and online enrichment.
Policies for sharing publishing journal articles differ for subscription and gold open access

articles:
Subscription Articles: If you are an author, please share a link to your article rather than the
fulltext.
Millions of researchers have access to the formal publications on ScienceDirect,
and so links will help your users to find, access, cite, and use the best available version.
Theses and dissertations which contain embedded PJAs as part of the formal submission can
be posted publicly by the awarding institution with DOI links back to the formal publications on ScienceDirect.
If you are affiliated with a library that subscribes to ScienceDirect you have additional private sharing rights for others' research accessed under that agreement. This includes use
for classroom teaching and internal training at the institution (including use in course packs
and courseware programs), and inclusion of the article for grant funding purposes.
Gold Open Access Articles: May be shared according to the authorselected
enduser
license and should contain a CrossMark logo, the end user license, and a DOI link to the formal publication on ScienceDirect.
Please refer to Elsevier's posting policy for further information.
18. For book authors the following clauses are applicable in addition to the above:
Authors are permitted to place a brief summary of their work online only. You are not allowed to download and post the published electronic version of your chapter, nor may you
scan the printed edition to create an electronic version. Posting to a repository: Authors are
permitted to post a summary of their chapter only in their institution's repository.
19. Thesis/Dissertation: If your license is for use in a thesis/dissertation your thesis may be
submitted to your institution in either print or electronic form. Should your thesis be published commercially, please reapply for permission. These requirements include permission for the Library and Archives of Canada to supply single copies, on demand, of
the complete thesis and include permission for Proquest/UMI to supply single copies, on demand, of the complete thesis. Should your thesis be published commercially, please reapply for permission. Theses and dissertations which contain embedded PJAs as part of the formal submission can be posted publicly by the awarding institution with DOI links back to the formal publications on ScienceDirect.
Elsevier Open Access Terms and Conditions
You can publish open access with Elsevier in hundreds of open access journals or in nearly 2000 established subscription journals that support open access publishing. Permitted third

party reuse
of these open access articles is defined by the author's choice of Creative